1999

Sediment-Air Partitioning of Hydrophobic Organic Chemicals.

Guilhem De seze
Louisiana State University and Agricultural & Mechanical College

INFORMATION TO USERS

This manuscript has been reproduced from the microfilm master. UMI films the text directly from the original or copy submitted. Thus, some thesis and dissertation copies are in typewriter face, while others may be from any type of computer printer.

The quality of this reproduction is dependent upon the quality of the copy submitted. Broken or indistinct print, colored or poor quality illustrations and photographs, print bleedthrough, substandard margins, and improper alignment can adversely affect reproduction.

In the unlikely event that the author did not send UMI a complete manuscript and there are missing pages, these will be noted. Also, if unauthorized copyright material had to be removed, a note will indicate the deletion.

Oversize materials (e.g., maps, drawings, charts) are reproduced by sectioning the original, beginning at the upper left-hand corner and continuing from left to right in equal sections with small overlaps. Each original is also photographed in one exposure and is included in reduced form at the back of the book.

Photographs included in the original manuscript have been reproduced xerographically in this copy. Higher quality 6" x 9" black and white photographic prints are available for any photographs or illustrations appearing in this copy for an additional charge. Contact UMI directly to order.

UMI

A Bell & Howell Information Company
300 North Zeeb Road, Ann Arbor MI 48106-1346 USA
313/761-4700 800/521-0600

SEDIMENT-AIR PARTITIONING OF HYDROPHOBIC ORGANIC CHEMICALS

A Dissertation

Submitted to the Graduate Faculty of the
Louisiana State University and
Agricultural and Mechanical College
in partial fulfillment of the
requirements for the degree of
Doctor of Philosophy

in

The Department of Chemical Engineering

by
Guilhem de Seze
M.S., Ecole Nationale Supérieure des Industries Chimiques (Nancy, France), 1994
May 1999

Acknowledgements

I would like to thank Drs. Kalliat T. Valsaraj and Danny D. Reible for their guidance during my research. I am thankful to them for giving me the opportunity to carry out this project and allowing me to work in an atmosphere of trust and freedom. I also appreciated comments and suggestions from other members in my committee, Drs Cartledge, Price, Sajo and Thibodeaux. I also want to thank Dr. Reible for his irreplaceable help in dealing with administrative matters. He greatly simplified my life as a student.

My research would not have been possible without the help of the student workers in the group. I want to express my gratitude to three of them in particular, Sonal Agrawal, Dan Dippery and Shawn Short. Their ability and dedication greatly contributed to this project.

I also enjoyed the stimulating interaction with other group members. My appreciation specially goes to Brian Cunningham and Raghunathan Ravikrishna. My research largely benefited from their ideas and help.

Finally, I wish to thank the Hazardous Substance Research Center (South and Southwest), which supported this research through grant R819165-01.

Table of Contents

List of Tables

List of Figures

Abstract

Contaminated sediments that become exposed to the air as a result of dredging or water receding are potential sources of emissions of toxic compounds to the atmosphere. Exposure models are currently being developed to assess the risk associated with this pathway of contaminant release and to design efficient remediation techniques. A critical parameter in these emission models is the equilibrium partition coefficient of the contaminant between the sediment and the air.

In this study, the sediment-air equilibrium partitioning of a polynuclear aromatic hydrocarbon (phenanthrene) and a heterocyclic aromatic hydrocarbon (dibenzofuran) was investigated. Both classes of compounds are commonly found in contaminated sediments and are known carcinogens. A gas saturation technique was used to study the influence of ambient temperature and sediment moisture content on the partition coefficient of the contaminants. The primary factor affecting the partitioning is the sediment moisture content (mc). Its variation from about 0% to 6% causes the partition coefficient to decrease by up to three orders of magnitude. Determination of phenanthrene's heat of sorption in dry (mc=0.3%) and wet (mc>6.0%) sediments indicates that different mechanisms of sorption exist in each moisture range. In the dry range, the contaminant is mainly adsorbed on the mineral surfaces of the sediment. When the moisture content increases, the competitive adsorption of water progressively displaces the contaminant from the mineral adsorption sites. Finally, in the wet range, the contaminant is mainly associated with the sediment organic matter.

In addition, the physical state of water in the sediment as a function of moisture content was characterized by comparing the isotherm of water sorption to the pore-volume distribution. This permitted the estimation of the respective contributions of the various sorption mechanisms to the overall sediment-air partitioning process. A model of the sediment-air partition coefficient is proposed that accurately accounts for the observed variations resulting from changes in sediment moisture content.

Chapter 1
Introduction and Objectives

1.1 Effects of PAHs and related compounds

1.1.1 Toxicity

Polynuclear aromatic hydrocarbons (PAHs) and heterocyclic aromatic hydrocarbons represent a wide range of molecular sizes and structural types. Figure 1.1 shows the molecular structure of the two PAHs (pyrene and phenanthrene) and the heterocyclic aromatic hydrocarbon (dibenzofuran) used in this study. Both classes of compounds are ubiquitous in the human environment. This is of concern since some PAHs such as 7,12-dimethylbenz[a]anthracene are among the most carcinogenic substances known (Harvey, 1997). The carcinogenic activity of dibenz[a,h]anthracene and benzo[a]pyrene (5-ring PAHs) was first established in the early 1930's. Since then, several other PAHs have been shown to induce tumors in laboratory animals.

1.1.2 Bioaccumulation

PAHs are classified as bioaccumulative contaminants of concern (BCCs), along with other compounds such as polychlorinated biphenyls (PCBs), pesticides (DDT), butyltins and metals (mercury, lead) (Bridges et al., 1996). Some PAHs, because of their high hydrophobicity, have the potential to biomagnify, i.e., their concentrations increase in the tissues of the species higher in the food chain.

1.2 Sources of PAHs

1.2.1 Generation

A wide variety of pyrolytic processes release polynuclear aromatic hydrocarbons into the environment. Fossil fuel combustion, solid waste incineration and coke ovens are

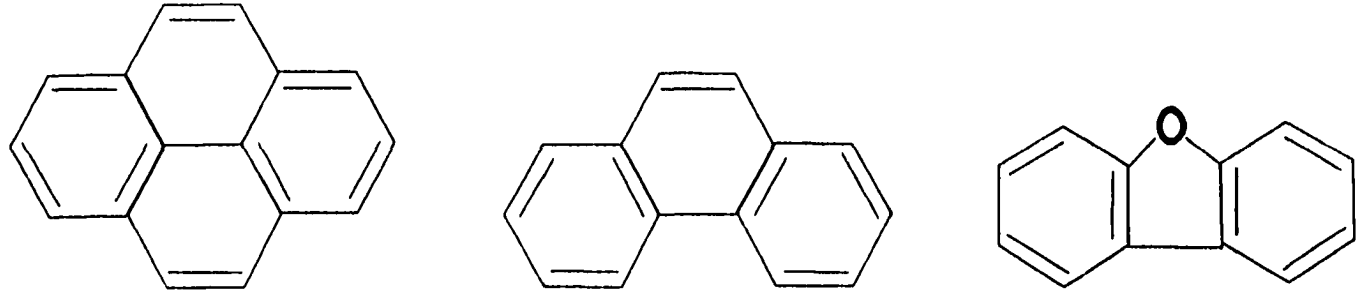

Pyrene Phenanthrene Dibenzofuran

Figure 1.1 Molecular structures of the studied polyaromatic and heterocyclic hydrocarbons

responsible for more than 50% of the emission of benzo[a]pyrene in the United States (Harvey, 1997). Exhaust from vehicles are thought to account for 35% of the total emissions (Bjorseth and Ramdahl, 1985, cited in Harvey, 1997). Harvey, 1991 reports that an estimated 1300 tonnes of benzo[a]pyrene alone are released annually into the atmosphere of the United States. Natural events such as volcanic activity or forest fires are also sources of PAHs although of less significance.

1.2.2 Transport

Due to their high boiling points, PAHs present in combustion gases condense on fly ash particles as they cool (Bidleman and Foreman, 1987). They can then be airborne over long distances (Aamot et al., 1996). Eventually, atmospheric deposition (washout) transfers PAHs to the ground. In fact, soils are thought to be a major repository of PAHs in the environment (Wild and Jones, 1995). However, part of the PAHs subsequently drain from surface soils and urban structures to water bodies. Ollivon et al., 1995 estimated that storm discharges resulted in a colloid-bound PAH concentration of about 60 ng/L in the river Seine downstream from Paris, France. PAHs can have long lifetimes in water. Mackay et al., 1992 report values of up to 69 days for phenanthrene in surface water and up to 40 months for benzo[b]fluoranthene in ground water. Furthermore, because of their high organic content, sediments show a great affinity for PAHs and accumulate them over time.

1.2.3 Confined disposal facilities

Sediments from navigable waterways or those presenting a threat to the environment must be dredged. Approximately 19 to 23 million cubic meters of contaminated sediments require special handling annually (US EPA, 1996).

Contaminated sediments are often placed in confined disposal facilities (CDFs). CDFs are structures designed to retain dredged materials. They are used either as a remediation method or as a temporary facility where the sediment is left to dewater before further treatment. Although CDFs are designed to isolate contaminated sediment from the environment, to some extent, they act as sources of PAHs. A schematic of a CDF is shown in Figure 1.2. Release of contaminants occur via:

- Uptake by plants and animals living or feeding in the CDF (bioaccumulation).
- Surface runoff or seepage through the bottom or through the dikes of the CDF.
- Volatilization into the atmosphere.

Volatilization has been determined to be the main transport pathway (US EPA, 1996). The present study is concerned about this specific problem.

1.2.4 Air emissions from exposed sediments

As a result of volatilization from exposed sediments or soils, humans, animals and plants are exposed to contaminants through inhalation, direct contact (dermal exposure) and ingestion (bioaccumulation). In order to find means of reducing emissions as well as to make exposure and risk assessments, theoretical models of the phenomenon are currently being developed (Valsaraj et al., 1999). The emission of PAHs from exposed sediments involves desorption from the sediment particles and the subsequent diffusion through the vapor phase in the pore space to the sediment surface.

The transport is described by a Fickian diffusion model modified to account for the porosity and tortuosity of the diffusion pathways and for the sorption phenomena in the porous medium:

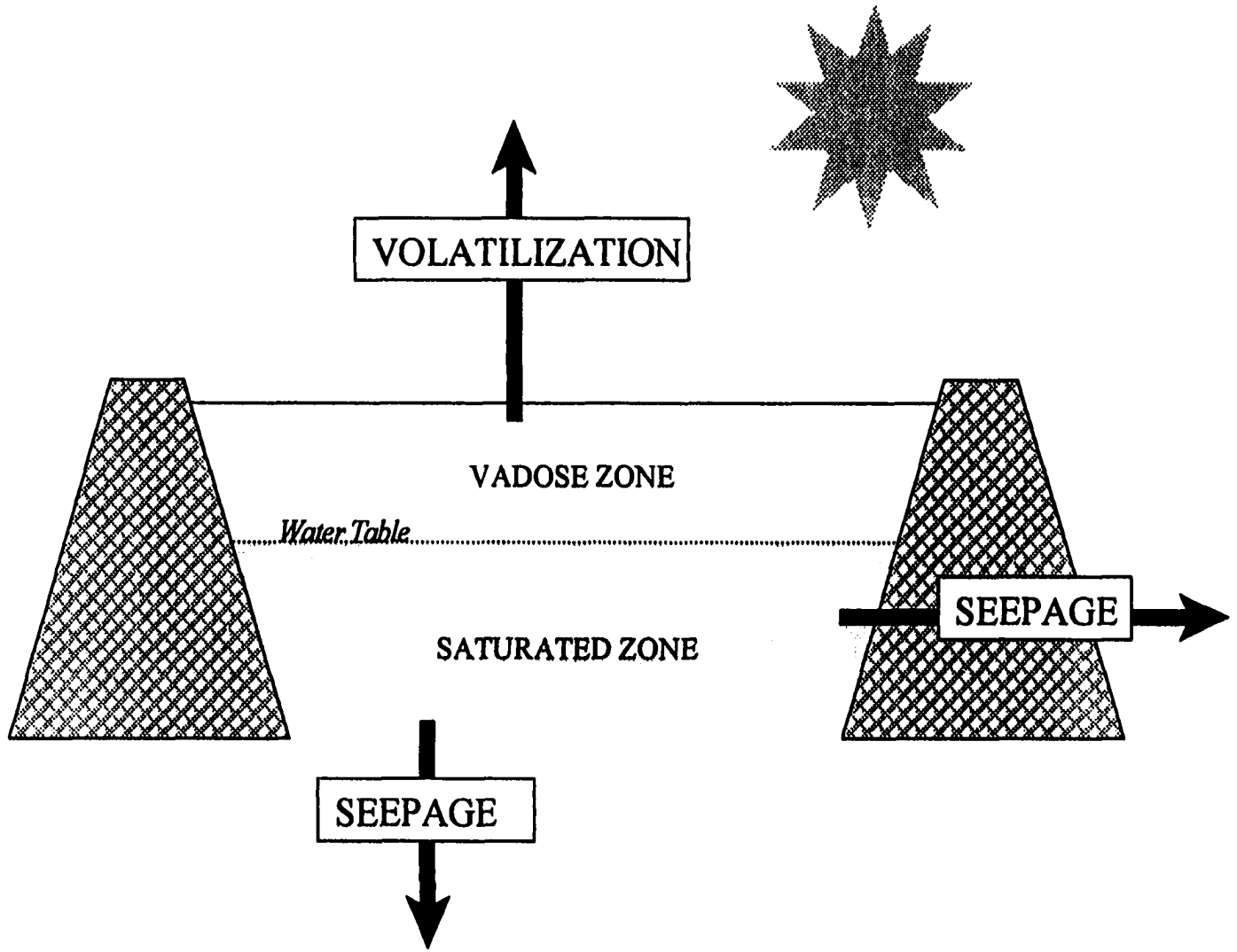

Figure 1.2 Release pathways in a confined disposal facility.

$$\frac{\partial C_g}{\partial t} = \frac{D_{eff}}{\varepsilon R_F} \frac{\partial^2 C_g}{\partial z^2} \quad (1.1)$$

Where:

- C_g is the concentration of contaminant chemical in the sediment pore space.
- D_{eff} is the effective air diffusivity of the compound in the porous sediment:

$$D_{eff} = \frac{\varepsilon D}{\tau} \quad (1.2)$$

(τ and ε are respectively the tortuosity and the air-filled porosity of the sediment)

- R_F is the retardation factor that accounts for the equilibrium partitioning of the pollutant in the sediment, in all the phases in which it may be present (mineral, organic, aqueous). It is defined by:

$$R_F = 1 + \frac{(1-\varepsilon)}{\varepsilon} \rho K_s \quad (1.3)$$

Where ρ is the bulk density of the sediment and K_s is the sediment-air equilibrium partition constant. K_s is the ratio of the concentration of chemical in the sediment phase, C_s over the concentration in the air phase, C_g: $K_s = C_s/C_g$.

R_F can be seen as the ratio of the total amount of chemical in a given volume of sediment over the amount present in the air-filled porosity of this volume.

The sediment-air partition coefficient is the most significant parameter in modeling the flux from the sediment.

1.3 Objectives of the study

1.3.1 Development of emission models

There are several environmental variables that impact the magnitude of K_s for a given compound. The most important ones are sediment moisture, air relative humidity, sediment specific surface area, ambient temperature and sediment organic matter content. The effect of sediment moisture is of importance since cyclic variations in air relative humidity, air temperature and evaporation/drainage of soil-water can lead to significant differences in surface moisture contents in sediments and soils. Scarce experimental data exist for PAHs in soils with high moisture content (mc>5% on a mass basis) (Hippelein and McLachlan, 1998). Unfortunately, no data on dryer soils (mc<2%) could be found in the literature. This prevents the accurate assessment of volatilization models. It is thus the primary objective of this study to measure the sediment-air partition coefficient of selected polynuclear and heterocyclic aromatic hydrocarbons over a wide range of sediment moisture content.

1.3.2 Modeling K_s

Several models and correlations have been proposed to account for the effect of various environmental parameters on the soil-air partitioning of synthetic organic compounds. It is another goal of this research to develop and validate by experimental data a model for the partition coefficient of PAHs in sediment. Such a model is a prerequisite to the development of a versatile model able to evaluate the volatilization of the various PAH found in contaminated soils and sediments.

1.3.3 Understanding sorption mechanisms

Further understanding of the partitioning mechanisms of PAHs is also of significance in two other fields of environmental engineering:

- It makes possible the estimation of exchange rates of PAHs between the atmosphere and surface soils. These exchange rates are a key element in the description of PAHs lifecycle in the terrestrial environment.
- PAHs and heterocyclic aromatic compounds are present in the atmosphere as vapor and attached to atmospheric particles. An accurate description of PAHs particle-air partitioning is important (i) to estimate their removal from the atmosphere by washout and dry deposition and (ii) to design air pollution equipment.

Chapter 2
Sorption of Hydrophobic Organic Chemicals in Unsaturated Sediments and Soils: Literature Review

In the literature reviewed, very little information was found on the soil-air equilibrium partitioning of polynuclear aromatic hydrocarbons (PAHs). Insight on this subject had to be gained mainly from three sources:

- There is an abundant literature in physical chemistry journals on the use of pyrene as a fluorescence probe to study adsorption sites on a variety of synthetic surfaces. This is an interesting source of information that does not seem to have been exploited in the environmental field. These studies are thus reviewed here for the enlightenment they bring on the microscopic mechanisms of PAH adsorption.
- Most studies of the soil-air partitioning found in the literature focus on volatile organic compounds (VOCs) and pesticides. The partitioning of PAHs is expected to show some similarities. Therefore, the main characteristics of VOCs sorption in soils are summarized here.
- Finally the particle-air partitioning of PAH has been investigated by researchers studying SVOCs transport by airborne particles. There are two limitations to using these studies: (i) the solid phase is fairly different from a soil solid phase (higher carbon content) and (ii) in many field studies particles are not even characterized. However, this is the most abundant source of information on solid-air quantitative partitioning of PAHs.

First, in this chapter, the different components of soils and sediments are briefly described, focusing on their potential uptake of synthetic organic compounds. In section

2.2, studies highlighting the microscopic mechanisms of PAHs sorption are reviewed. Finally, in section 2.3 quantitative studies of the sediment-air partitioning of HOCs are presented and implications for PAHs are discussed.

2.1 Soil and sediment matrix

Soils or sediments have complex compositions. In the most general case, in the unsaturated zone, three phases compose the medium. A simplified representation of the sediment matrix is shown in Figure 2.1.

2.1.1 Air phase

The relative volume of air phase in a dry soil is measured by its porosity, ε. ε is the ratio of the air volume, V_{air} to the bulk volume, V_{bulk} in a soil: $\varepsilon=V_{air}/V_{bulk}$. Common values of ε are in the range of 0.4 to 0.7.

2.1.2 Water phase

Water is condensed in pores and adsorbed on the mineral solids. This water contains:

- Dissolved components: cations (Ca^{2+}, Mg^{2+}, Na^{+}) and anions (NO^{3-}, HCO^{3-}) from the mineral phase, and soluble soil organic matter (SSOM), which has a composition similar to humic acid.
- Organic or mineral colloidal particles.

A few centimeters from the exposed surface of the sediment, the moisture content (mc) is usually higher than 10%.

2.1.3 Solid phase

The solid phase is made of mineral and organic materials that are often tightly bound together.

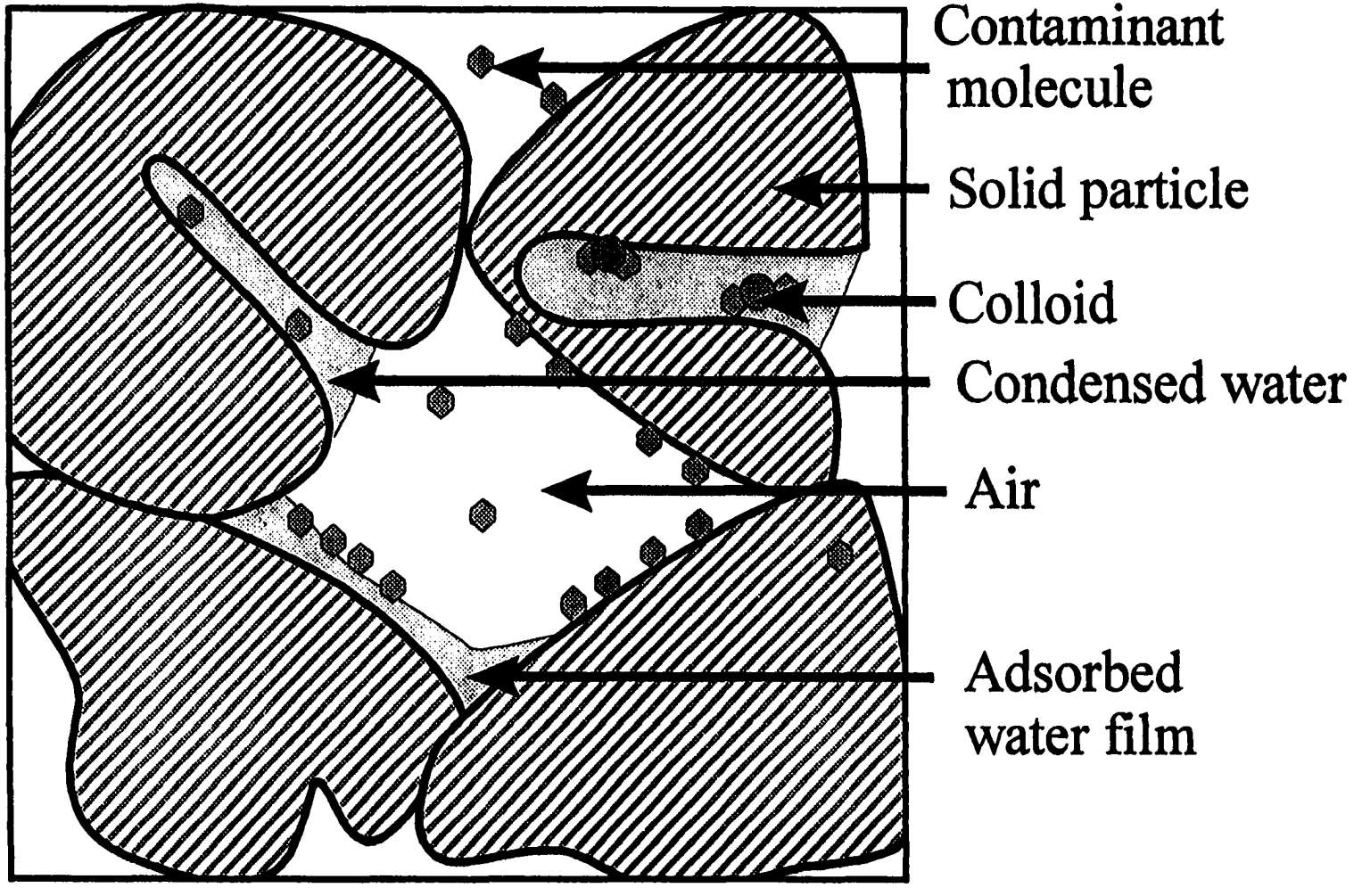

Figure 2.1 Schematic of soil phases and contaminant sorption locations.

2.1.3.1 Organic phase

Stevenson, 1994 classifies soil organic matter into three main fractions:

- Litter and "light fraction" (decomposing plants and animal residues).
- Microorganisms.
- Large polymers resulting from the degradation of plant remains (lignin).

Organic matter polymers such as humic and fulvic acids, have molar mass from 20,000 up to 200,000. They have no specific structural formula but exhibit a large variety of functional groups. Most of the organic polymers are bound to clay surfaces by forces such as electrostatic and Van der Waals forces or hydrogen bonds.

2.1.3.2 Mineral phase. Clay fraction and phyllosilicate minerals

The mineral phase is composed of crystalline (e.g., quartz) and amorphous (e.g., insoluble carbonate salts) minerals. Soil minerals are usually classified according to their size into four fractions, as shown in Table 2.1.

Table 2.1 Soil mineral fractions.

Particles size	Fraction name
> 2 mm	Gravel
50 μm – 2 mm	Sand
2 – 50 μm	Silt
< 2 μm	Clay

The study of adsorption onto soils mineral fraction should focus on particles having the highest specific surface area. These particles are found in the clay fraction.

A. Chemical composition of the clay fraction minerals. Most of the minerals found in the clay fraction are built from two types of molecular structural units (Sposito, 1984):

- Polymeric sheets of the octahedral complex $MX_6^{(a-b)-}$, where M^{a+} is a metal cation and X^{b-} an anion.
- Polymeric sheets of silica tetrahedron, SiO_4^{4-}.

The octahedral sheet structure is the form taken by metal oxides, hydroxides and oxihydroxides. For instance, goethite (α-FeOOH) and gibbsite (γ-$Al(OH)_3$) are two very common soil minerals having this structure. Hydroxyl functional groups are expected at their surface. Silica tetrahedral sheets bound to $MX_6^{(a-b)-}$ octahedral sheets form the class of phyllosilicate minerals. Kaolinite, illite and montmorillonite, commonly found in soils, are examples of phyllosilicates. Because of the layer structure, particles of the clay fraction are assumed to be plate-like shaped. Thus, when stacking up on one another, particles create parallel-walls pores (Sposito, 1984). Figure 2.2 shows such a pore structure.

B. Adsorptive properties of phyllosilicate minerals. Phyllosilicates made of two silica sheets for one metal octahedral sheet (2:1 structure) often bear a global negative charge caused by the substitution of metal cations of lower valence in the octahedral sheet. A surface electrical field results that gives clays some of their characteristic adsorptive properties.

Phyllosilicates particles also expose functional groups at their surface that can create specific physical bonds with adsorbing molecules. The two main kinds are:

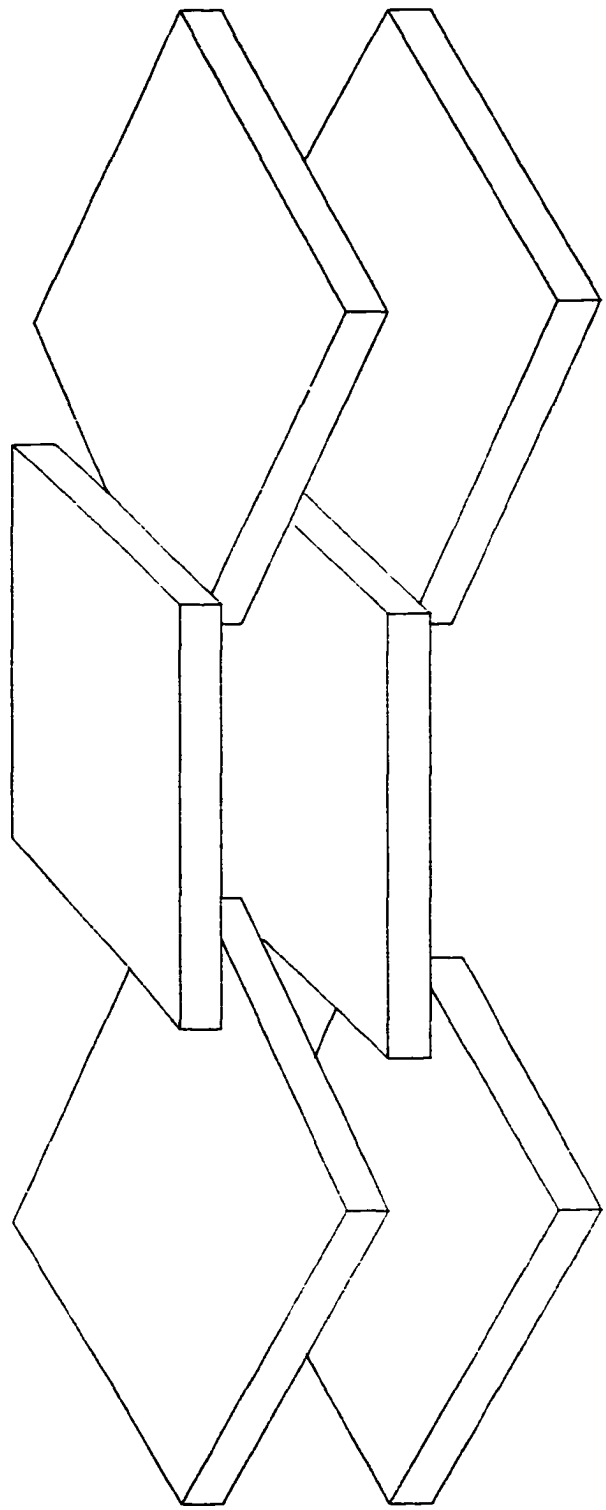

Figure 2.2 Pore structure created by clay particles.

- Siloxane goup. The tetrahedral silica sheet is bound by an outer plane of oxygen atoms called siloxane surface. The functional group associated with this surface is the cavity formed by six corner-sharing silica tertrahedra (Sposito, 1984). Siloxane groups are thus located on the exposed plane surfaces of clay particles. This group behaves as a Lewis base. In a phyllosilicate structure the strength of the Lewis base depends on the isomorphic cation substitutions of the underlying octahedral sheet.
- Hydroxyl group. This group is found on the edges of broken clay crystallites (Liu and Thomas 1991). It may be bound to a metal atom of the octahedral sheet or, more often, to a silcon atom (silanol group). The importance and characteristics of silanol groups are discussed in more details in section 2.2.2.

2.2 Qualitative studies of PAHs sorption

Fluorescence spectroscopy is a powerful technique to study the mechanisms of PAH sorption. The principle of the fluorescence process is briefly recalled in Appendix A. In this section the fluorescence properties of pyrene are outlined. Then characteristics of the silica gel surface are described and its value as a model for natural surfaces is argued. Finally studies using pyrene as a molecular probe to investigate sorption mechanisms are reviewed.

2.2.1 Pyrene as molecular probe

Pyrene has been widely used as a fluorescence probe to characterize heterogeneous systems because of the following interesting photophysical properties:

- High quantum yield of fluorescence in the adsorbed state. In particular, its fluorescence quantum yield when adsorbed on a dry or wet silica gel surface is higher

than most other PAHs (of lighter as well as heavier molecular formula) (Liu et al., 1993).

- Intensities of the first (I_0) and third (I_2) vibrational bands of emission are sensitive to the microenvironment polarity. The ratio of the two intensities (I_0/I_2) has been measured in solvents of various polarities. Thus, by measuring this ratio, one can characterize pyrene's microenvironment.
- Because of its long excited state lifetime, formation of an excited state dimer (excimer) is relatively easy. This property gives information on the proximity of adsorbed molecules and their mobility. (The dimer formed by unexcited adsorbed pyrene is referred to as ground state dimer).

Pyrene has been used to study the adsorption sites of surfaces like silica (Bauer et al., 1982), alumina (Tro et al., 1989)) and synthetic smectite clay (Labbé et al., 1988).

2.2.2 Silica gel as a model surface

Silica gel is a commonly used adsorbent. Therefore, a great number of studies in the literature relate the use of pyrene and other molecular probes to investigate its surface. Although it is a synthetic material, studies of pyrene adsorption onto silica gel are a valuable source of information on the mechanisms of adsorption onto soils mineral fraction for two reasons:

- As in natural clays, siloxane and silanol groups are the functional groups present at the surface of silica gel.
- The weathering of soil minerals causes the transformation of the original surface functional groups into hydroxyl groups (Sposito, 1984). In fact, natural quartz

particles are usually covered by an amorphous surface layer believed to be very similar to silica gel (Kiselev,1957 cited in Storey et al., 1995).

Silica gel is often produced by the polycondensation of orthosilicic acid and has the general formula: $SiO_2.xH_2O$. Depending on the synthesis method, silica gel can have a variety of amorphous forms. It always consists of a disordered lattice of SiO_4^{4-} tetrahedra forming globules on the surface of which hydroxyl groups are present. The spatial arrangement of silicon atoms on which hydroxyl groups are bonded leads to four types of silanol groups (Oscik and Jaroslaw, 1982):

- Isolated. The distance between two adjacent hydroxyl groups is too large to permit the creation of hydrogen bonds between them.
- Bonded. Two hydroxyl groups belonging to neighboring silicon atoms are linked by a double hydrogen bond. This type of silanol group is not effective in binding.
- Active. Two hydroxyl groups belonging to neighboring silicon atoms are linked by a single hydrogen bond. Thus, the hydrogen that does not take part in a hydrogen bond is more reactive than the hydrogen of an isolated silanol group.
- Geminal. Two hydroxyl groups are linked to a single silicon atom.

The average distribution of silanol groups at the surface of silica is about 5 per $100Å^2$ (Bauer et al., 1982). A pyrene molecule having a surface area of 150-170 $Å^2$ (Bauer et al., 1982; Hara et al., 1980), a pyrene adsorption site is certainly made of more than one silanol group.

2.2.3 Adsorption of pyrene onto silica gel and clay

Pyrene has been widely used as a molecular probe to study the surface properties of mineral surfaces such as silica gels and clays. Most studies focus on the adsorbent

properties for applications in the fields of heterogeneous catalysis and chemical separation (chromatography, purification). It is interesting to look at such studies to get information not only on adsorption sites at the surface of synthetic mineral surfaces but also on pyrene behavior as an adsorbate.

In the literature reviewed, reported pyrene concentrations that were not expressed in monolayer coverage percentage were converted to this scale. For the sake of environmental comparison it is worth relating the surface coverage, θ to an equivalent sediment concentration, C_s: $C_s = (\theta AM)/(\sigma N)$. In this expression, A is the specific surface area of the sediment, σ is the surface area occupied by one adsorbed molecule, N is the Avogadro number and M is the molar mass of the compound. The value of A for the sediment studied in this work is determined in section 3.5.2: 7.9m^2/g. Literature values of σ for pyrene were reported in section 2.2.2: 150-170 $Å^2$. Therefore, 1% monolayer coverage by pyrene corresponds to a mass concentration of about 17 mg/kg.

2.2.3.1. Adsorption on dry surfaces

It is well established that silanol groups bind to aromatic hydrocarbons by establishing hydrogen bonds to the aromatic π-system, resulting in adsorption in a flat configuration (Galkin et al., 1963; Pohle, 1982). Bauer et al., 1982, 1983 observed that at low surface coverage, pyrene molecules adsorb selectively onto the silanol groups. Silanols provide the adsorption sites of highest energy at the silica gel surface. Also, pyrene molecules alone on the surface occupy heterogeneous adsorption sites. This heterogeneity is probably caused by the heterogeneous distribution of silanol groups over the surface (vicinal, geminal). Furthermore, the overall environment of adsorbed pyrene molecules is highly polar. The I_0/I_2 ratio for pyrene adsorbed on dry silica gel was

determined to be 1.8. As shown in Table 2.2 this value is similar to those observed for pyrene in aqueous solution. Labbé and Reverdy, 1988 investigated the adsorption of pyrene onto laponite, a synthetic smectite clay, at a concentration corresponding to 7% coverage. Similarly, they reported that on samples dried under vacuum, the environment of adsorbed pyrene was very polar (I_0/I_2=1.8). Liu and Thomas, 1991 determined that pyrene adsorption sites at the surface of laponite activated at 115°C were not homogeneously distributed but formed clusters. This is compatible with the structure of clay crystallites, displaying localized areas of high concentration of hydroxyl groups on their edges.

2.2.3.2 Adsorbed dimers and microcrystals

Hara et al., 1980 observed that pyrene or naphthalene molecules are adsorbed on the surface of activated silica gel as dimers as well as monomers. Similarly, Labbé and Reverdy, 1988 observed that pyrene adsorbed at 7 and 12% coverage on air dry laponite, was present as a monomer as well as a dimer. Bauer et al., 1982 observed the presence of pyrene dimers adsorbed on silica gel at a concentration as low as 0.2% of monolayer coverage. Francis et al., 1983 using a two-site kinetic model of fluorescence decay, estimated the proportion of adsorption sites occupied by dimers and monomers for pyrene adsorbed on silica gel. At 1.3% surface coverage, they calculated that monomers occupied 83% of the sites and ground state dimers 17%. Fujii et al., 1988 determined that in the range of 0.1% to 7.6% coverage, the proportion of ground state dimeric pyrene at the surface of activated silica gel increased with the total amount adsorbed.

Bauer et al., 1982 determined that a more vigorous activation of the silica gel increased the proportion of dimers. This supports the hypothesis that silanol groups play a

Table 2.2 Intensity ratio of the first and third peaks of pyrene fluorescence emission spectrum in different environments.

PYRENE ENVIRONMENT	I_0/I_2	Reference
Solvated in:		
Cyclohexane	0.65	Bauer et al., 1982
	0.58	Labbé and Reverdy, 1988
	0.58	Dong and Winnik, 1982
Ether	1.08	Hara and Ware, 1980
Benzene	1.13	Labbé and Reverdy, 1988
	1.05	Dong and Winnik, 1982
Dioxane	1.32	Bauer et al., 1982
Ethanol	1.32	Bauer et al., 1982
Methanol	1.56	Bauer et al., 1982
	1.35	Labbé and Reverdy, 1988
	1.35	Dong and Winnik, 1982
Water	1.74	Labbé and Reverdy, 1988
	1.87	Dong and Winnik, 1982
Acetonitrile	2.00	Bauer et al., 1982
Dimethylformamide	2.04	Bauer et al., 1982
Adsorbed on:		
Laponite (room temperature, atmospheric humidity)	1.05	Liu and Thomas, 1991
	0.9	Labbé and Reverdy, 1988
Laponite (activated at 115C)	1.14	Liu and Thomas, 1991
Laponite (activated at 350C)	1.35	Liu and Thomas, 1991
Laponite (progressively dehydrated at room temperature under vacuum)	1.8	Labbé and Reverdy, 1988
Silica gel (hydrated over 5% of surface)	1.35 to 1.60	Bauer et al., 1984
Silica gel (activated)	1.72 to 1.80	Bauer et al., 1984
	1.72	Krasnansky and Thomas, 1994

role in the formation of ground state pyrene dimers. From the study of pyrene adsorption onto porous glass beads (amorphous silica structure with silanol groups) they determined that dimer formation was high even on hydrated silanol sites. Bauer et al., 1983 observed that an increase of temperature decreased the proportion of pyrene dimers. Formation of ground state dimer is favored on silanol sites. On siloxane planes, pyrene is more mobile and forms less dimers.

Labbé and Reverdy, 1988 observed pyrene microcrystals on laponite samples at a concentration of pyrene corresponding to about 30% coverage. Lochmueller and Wenzel, 1990 argue that at surface coverage lower than 3%, pyrene is adsorbed on silica gel solely as a monomer. At surface coverage higher than 3%, pyrene forms microcrystals that are adsorbed along with the monomers. The proportion of the two varieties depends on the total amount adsorbed. They argue that demonstration of the existence of a ground state dimer by Bauer et al., 1982, 1983 is not conclusive. Presence of microcrystals could explain equally the experimental observations substantiating the existence of a ground state dimer.

2.2.3.3 Effect of the coadsorption of hydrophilic molecules

Hydrophilic molecules, by establishing hydrogen bonds with silanol groups, decrease their binding capacity (Galkin et al., 1964). Thus, they are expected to affect pyrene adsorption on mineral surfaces.

Bauer et al., 1982, 1983 report that addition of a hydrophilic molecule like glycerin or 1-decanol onto the surface of silica causes pyrene molecules originally adsorbed to strong silanol sites to migrate to the weaker, more homogeneous and much less polar siloxane sites. This effect was visible even at very low coverage by the

competing molecule. 1-Decanol at a surface coverage as low as 1.5% was able to displace pyrene adsorbed at a coverage of about 2%. Adsorption of decanol-1 at a coverage of 50% resulted in a decreases of the I_0/I_2 ratio from 1.80 to 1.32. The polarity of pyrene's environment was thus similar to ethanol or dioxane.

Bauer et al., 1984 studied the effect of water competition with pyrene for silica adsorption sites. At a pyrene surface coverage of 0.05%, addition of increasing amounts of water caused pyrene molecules to progressively migrate from silanol to siloxane adsorption sites. Labbé and Reverdy, 1988 investigated the adsorption of pyrene onto laponite. The clay was not activated. Samples were dried in air at room temperature and studied in open air. They observed that pyrene originally present as microcrystals in a moist clay paste (at concentration corresponding to 7% coverage) was progressively adsorbed as a monomer with restricted mobility as the clay was drying in air, down to about 10% moisture content. This phenomenon was reversible. Remoisturizing the clay caused pyrene to desorb and microcrystals to reform. Observations were similar at concentration corresponding to 12% coverage. In both cases pyrene adsorbed on air dried laponite formed ground state dimers. Further drying of the sample under vacuum caused the environment of adsorbed pyrene to become less homogeneous and much more polar. Liu and Thomas, 1991 demonstrated that on laponite dried in air at 20°C (8.8% moisture content), only few adsorption sites for pyrene were present. (Uptake from a pyrene-pentane solution in excess was limited to an amount corresponding to 0.5% coverage). Air-drying of the clay at 115°C prior to adsorption removed the water molecules adsorbed on the outer and lateral surfaces as well as some of the interlayer water (Walker, 1961). This had three consequences:

- Laponite's adsorption capacity for pyrene was dramatically increased. 99% of the pyrene contained in a pentane solution was adsorbed by the clay, representing about 2.5% coverage.
- Pyrene was adsorbed on much more polar sites.
- Pyrene mobility was restricted.

Liu and Thomas, 1991 observed that, as for silica gel, exposure to water of a sample of activated laponite causes pyrene molecules to migrate from silanol to siloxane sites.

2.2.3.4 Conclusions

The adsorption of pyrene on mineral surfaces presents the following qualitative characteristics:

- On dry surfaces, pyrene is preferentially adsorbed on the hydrophilic silanol groups. The polarity of pyrene's environment is similar to the one of water. At low surface coverage, the most abundant form of pyrene is the monomer. However, pyrene is also present in one other state. It is not clear weather it is the dimer or the crystal. The proportion of this second form of pyrene increases with the surface coverage.
- Hydrophilic molecules (water and hydrophilic groups of natural organic polymers) displace pyrene from the silanol sites.
- In the presence of hydrophilic molecules, pyrene adsorbs on the weaker siloxane groups. At sufficient surface coverage, microcrystals can be formed.
- Adsorption sites made of silanol groups are heterogeneously distributed on mineral surfaces. Thus, only a small fraction of a dry mineral surface offers high energy adsorption sites.

2.2.4 Sorption of PAHs in soil organic matter

Morra et al., 1990 studied naphthalene and 1-naphthol interactions with soil extracted humic acid in water solution. They proposed that cage-like entities are present along the constituent chains of humic acid. Naphthalene and 1-naphthol are solubilized in the hydrophobic environment of the micelle-like environment. Even though the fluorescent molecules are in contact with the humic acid, they are mobile within the non-polar environment. Engeretson and Wandruszka, 1994 came to similar conclusions by studying five different humic acids using pyrene as the molecular probe.

Fluorescence spectroscopy has also been used to get insight into the mechanisms of PAHs sorption in wet soils. Ganaye et al., 1997 used the technique to evaluate quantitatively the polarity of soil organic matter. They determined the I_0/I_2 ratio of the fluorescence spectrum specifically emitted by pyrene associated with organic matter. Values of 0.6 and 1.1 were found for two different soils. Furthermore, they observed that pyrene in an aqueous suspension of organic free montmorillonite did not partition at all and remained in the water phase. For such a sample, the I_0/I_2 ratio was close to the literature value for pyrene in aqueous solution (Table 2.2). Thus it seems possible to use Table 2.2 to assess pyrene microenvironment in soil organic matter. Pyrene was sorbed in a very non polar environment. The polarity was similar to cyclohexane in the first soil and similar to ether or benzene in the second one.

2.3 Quantitative studies of hydrophobic organic compounds sorption

2.3.1 The partition coefficient

2.3.1.1 Definition

The soil-air (or sediment-air) sorption isotherm of a contaminant may adopt a variety of different shapes. The soil-air partition coefficient, K_s is defined as the slope near the origin of the isotherm. In the range of linear partitioning, K_s may be defined by:

$$K_s = \frac{C_s}{C_g} \tag{2.1}$$

Where C_s and C_g are respectively the sediment and air concentrations in contaminant. In this study, K_s is expressed in liters of air per kilograms of sediment.

2.3.1.2 Multimechanistic approach of soil-air partitioning

The soil moisture content is decisive in determining the air-soil partitioning of organic compounds. The plot of the partition coefficient of most VOCs and pesticides in soil pore air, as a function of the soil water content exhibits three characteristic zones as shown in Figure 2.3. (Spencer et al., 1969; Spencer and Cliath, 1974). This leads to the distinction of three types of soil regimes, depending on the range of moisture content. Valsaraj and Thibodeaux, 1988 refer to these three types as dry, damp and wet. Usually, a dry soil contains less than 1 to 2% of water and a wet soil contains more than 5 to 7%. Soils in between these two limits are said damp. Different mechanisms of contaminant sorption are operative in each moisture range and must be considered individually in order to understand the overall contaminant partitioning into the soil. The mechanisms of sorption and the expression of K_s in the three ranges of moisture conditions are presented below.

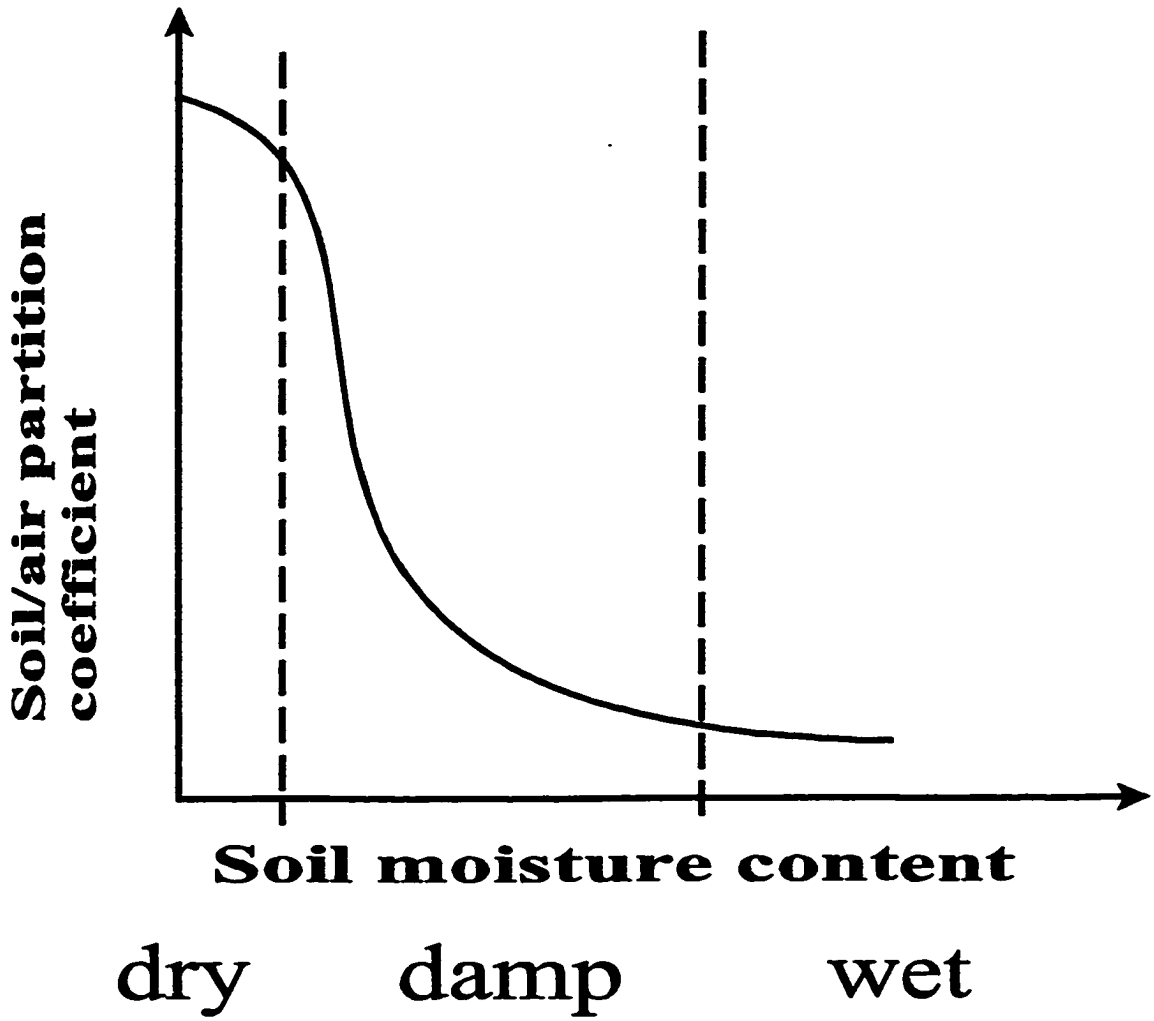

Figure 2.3 Influence of the soil moisture content on the partitioning of hydrophobic organic chemicals between the soil and air phases.

2.3.2 Dry soil

2.3.2.1 Characteristics of VOCs adsorption

Thibaud-Erkey et al., 1995 reviewed about 30 studies on the adsorption of VOCs on soils and soil constituents. For dry soils, the main conclusions relevant to this study were the following:

- Adsorption of slightly polar and non-polar VOCs by the soil mineral phase accounts for most of the uptake. Organic matter has a much smaller role in dry soils due to the relatively low surface area it offers to non-polar and slightly polar molecules (Pennel et al., 1992). Organic matter may even decrease the soil adsorption capacity for a contaminant, by competing with the hydrophobic organic contaminant for the stronger adsorption sites.
- Adsorption of VOCs is described by a Brunauer-Emmet-Teller (BET) isotherm of type II (see Appendix B). This indicates that the heat of adsorption in the first layer is more negative than the heat of condensation of the compound. In other words, the physical bonds between the molecule and the soil are stronger than intermolecular bonds. This explains the large mass of compound that can be adsorbed at partial pressures much smaller than the saturation vapor pressure.
- Polar molecules are more strongly adsorbed by soils than non-polar ones. This is compatible with the surface characteristics of clay minerals (see section 2.1.3.2). Polar groups such as silanols make stronger bonds with polar molecules. Also, the electrical field at the surface of 2:1 smectite particles is favorable to polar molecules subject to field-dipole interactions.

- The adsorption capacity of smectite clays for small polar molecules (ethanol, water) is greater than for non-polar molecules. This is explained by the capacity of small polar molecules to penetrate the silicate sheet interlayers, hence increasing the available adsorption surface area. (It is well known that the surface area of smectite clays is significantly larger when determined by adsorption of ethylene glycol rather than nitrogen.) Non-polar molecules such as alkylbenzenes have no access to the interlayer surface. Thus, the adsorption of large non-polar molecules (such as PAHs) will be restricted to the outer surface of soil particles.

2.3.2.2 SVOCs adsorption on soil mineral surfaces

Pankow, 1997 analyzed the approaches used by different authors (Junge, 1977, Yamasaki, 1982 and Bidleman and Foreman, 1987) to describe partitioning of SVOCs between the gas and aerosol particulate phases. The BET or Langmuir equation (see Appendix B) can be simplified when the partial pressure of chemical in the air phase, P, is very small compared to its saturated vapor concentration, P^{sat} (as in the case of trace contamination of a sediment by SVOCs). In this case, the ratio X ($=P/P^{sat}$) is very small and the equation becomes:

$$\frac{W}{W_m} = XB \qquad (2.2)$$

Where:

- W is the mass of contaminant adsorbed on the soil.
- W_m is the mass of an adsorbed monomolecular layer of contaminant covering the entire surface.

- $B=\exp[(\Delta H_{ads}-\Delta H_{vap})/RT]$, with ΔH_{ads} and ΔH_{vap} being respectively the heat of adsorption on the surface and the heat of vaporization of the compound.

Assuming that the gas phase behaves as an ideal gas, the latter expression can be used to approximate the partition coefficient between the mineral surface of a particle and air,

$$K_s = \frac{W}{C_g} = RT\frac{W_m B}{P^{sat}} \tag{2.3}$$

Where:

- C_g is the air phase concentration of the contaminant.
- R is the ideal gas constant.
- T is the temperature.

A. Influence of the saturated vapor pressure, P^{sat} in equation (2.3). The saturated vapor pressure is known for most compounds. However, for low vapor pressures, values determined in independent studies often vary significantly.

Most SVOCs are solids in the range of temperatures in which environmental adsorption is studied. Several authors studying SVOCs partitioning in the environment have recommended the use of the subcooled liquid saturated vapor pressure, P_L^{sat} for P^{sat}. Discussion of this point is presented in Appendix B. Storey et al., 1995 studied the adsorption of SVOCs (six n-alkanes from C_{17} to C_{23} and five 3 and 4-ring PAHs) on quartz surface at low humidity. Unfortunately, they warn that at 0.36% relative humidity, the quartz surface may not have been as free of adsorbed water as expected. Nevertheless, their data give information on a fairly dry mineral surface. At this humidity, for both sets of compounds (alkanes and PAHs), the partition coefficient on a surface area basis, κ_m

(L/m^2) was well correlated by the equation: $\log(\kappa_m)=m\log(P_L^{sat})+b$ ($r^2 = 0.998$ and $r^2 = 0.974$, respectively). The slopes for the alkane and PAHs sets were respectively m=-1.1 and m=-1.2 which are close to the value m=-1 that is expected from equation (2.3). According to equation (2.3), the existence of such a correlation indicates that the term W_mB is fairly constant within a family of compounds. In fact, as argued in Appendix B, both B and W_m taken individually are expected to be fairly constant for compounds of similar structure and size.

B. Influence of the heat of adsorption in equation (2.3). The energetic term B can be calculated using literature value of the heat of condensation and experimentally determined value of the heat of adsorption on the soil or estimate thereof.

Storey and Pankow, 1991 reanalyzed the data of Niessner and Wilbring, 1989 using the theory developed by Pankow, 1991. The original experimental study focused on the partitioning of seven 4 and 5-ring PAHs between dry nitrogen and model airborne particles (graphitic carbon, sodium chloride, alumina and silica). The authors express some reservation about the quality of the experimental data, weakened by poor characterization of the solid particles. However, their analysis indicates that the heats of adsorption on a given surface increase with increasing molecular size. This is compatible with the observation reported in section 2.2.3 that multiple sites are involved in the binding of pyrene to a silica gel surface. As an example, the value determined for chrysene heat of adsorption on the various surfaces were:

-120 kJ/mol on sodium chloride

-111 kJ/mol on graphitic carbon

-108 kJ/mol on alumina

-91 kJ/mol on silica

All the other PAHs studied followed this trend. Because of the concern about the data quality, these results have to be taken cautiously. Nevertheless, they give a range of magnitude for the heat of adsorption. The high value of the heat of adsorption on sodium chloride, if confirmed, would demonstrate the importance of surface electric field and PAHs polarizability in the adsorption process. This would thus give great importance to the cation exchange capacity of the soil.

C. Influence of the soil monolayer capacity, W_m in equation (2.3). The soil monolayer adsorption capacity for the compound is more difficult to estimate than other parameters used in (2..3). Based on Langmuir theory, Pankow, 1987 proposed the general expression:

$$W_m = AN_s \qquad (2.4)$$

Where:

- A is the surface area of the sediment available for adsorption.
- N_s is the molar site concentration at the sediment surface.

This expression calls for two remarks:

- A is the surface area available to the particular adsorbing molecule. As mentioned in 2.3.2.1, A may be different from the surface area determined by any of the conventional methods.
- An adsorption site is defined here as either (i) a portion of adsorbent surface having the area of an adsorbed molecule (non-specific adsorption) or (ii) a set of surface functional groups in a particular configuration that binds to one adsorbate molecule (specific adsorption).

Valsaraj and Thibodeaux, 1987 proposed an expression to estimate W_m for spherical molecules, based on the classical expression used to determine surface area from BET adsorption isotherms (Smith, 1981):

$$W_m = 0.917 \cdot F \cdot A \cdot \left(\frac{\rho^2 M}{N} \right)^{1/3} \qquad (2.5)$$

Where:

- The numerical factor is the projection factor relating the cross sectional area of the molecule to its projected surface area in two-dimensional hexagonal packing.
- A is the surface area of the soil (m^2/g).
- ρ is the density of the adsorbed chemical (g/m^3).
- M is the molar mass of the chemical (g).
- N is the Avogadro number.
- F is the fraction of surface area actually occupied by adsorbed molecules when full coverage is achieved. More attention is given to F in Appendix C. In this Appendix, results presented in two experimental studies are also reanalyzed to gain insight on F.

In summary, estimation of W_m hinges on relating the size of a molecule to the portion of mineral surface necessary to accommodate it in the adsorbed state. Parameters to evaluate this relationship (N_s, F) are difficult to estimate *a priori*.

2.3.3 Damp soil

2.3.3.1 Adsorption on mineral phase

Mineral sites, responsible for most of soil adsorption capacity in the dry range, are favorable to polar molecules like water. Therefore, as the moisture content of the soil increases, polar water molecules compete with non-polar organic molecules for

adsorption sites and are preferentially adsorbed. A schematic representation of competitive adsorption is shown in Figure 2.4. The competition with water causes the desorption of the organic molecules and thus a higher partial pressure in the air phase. The competitive adsorption is observed as long as some adsorption sites remain available for the contaminant. Several authors have observed that competitive adsorption ceases when the soil moisture content corresponds to the amount of water needed to cover the whole external surface area by a monomolecular water film.

Models have been developed to describe the simultaneous adsorption of two gaseous species on the solid phase. Starting from the BET theory, Hill, 1946a, 1946b derived an equation for multimolecular layer adsorption of a mixture of gases on a solid surface. In order to describe competitive adsorption on soils, Valsaraj and Thibodeaux, 1988 added some assumptions to Hill's model. Their main assumption is that the influence of the solid surface dies out as the number of layers increases and hence multimolecular adsorption on these layers is equivalent to condensation of vapors of A and B. The final model for competitive adsorption on soils is:

$$\frac{W_A}{W_{mA}} = \frac{X_A\left[B_A(1-X_B)+X_B B_B\right]}{(1-X_A-X_B)\left[1+X_A(B_A-1)+X_B(B_B-1)\right]} \qquad (2.6)$$

Where:

- Subscripts A and B relate respectively to the organic compound and to water.
- B, W, W_m and X have the same significance as in (2.2).

Furthermore, they argued that for environmental situations, high values of B_A and B_B and low values of X_A and X_B are expected, so that adsorption can be described by the

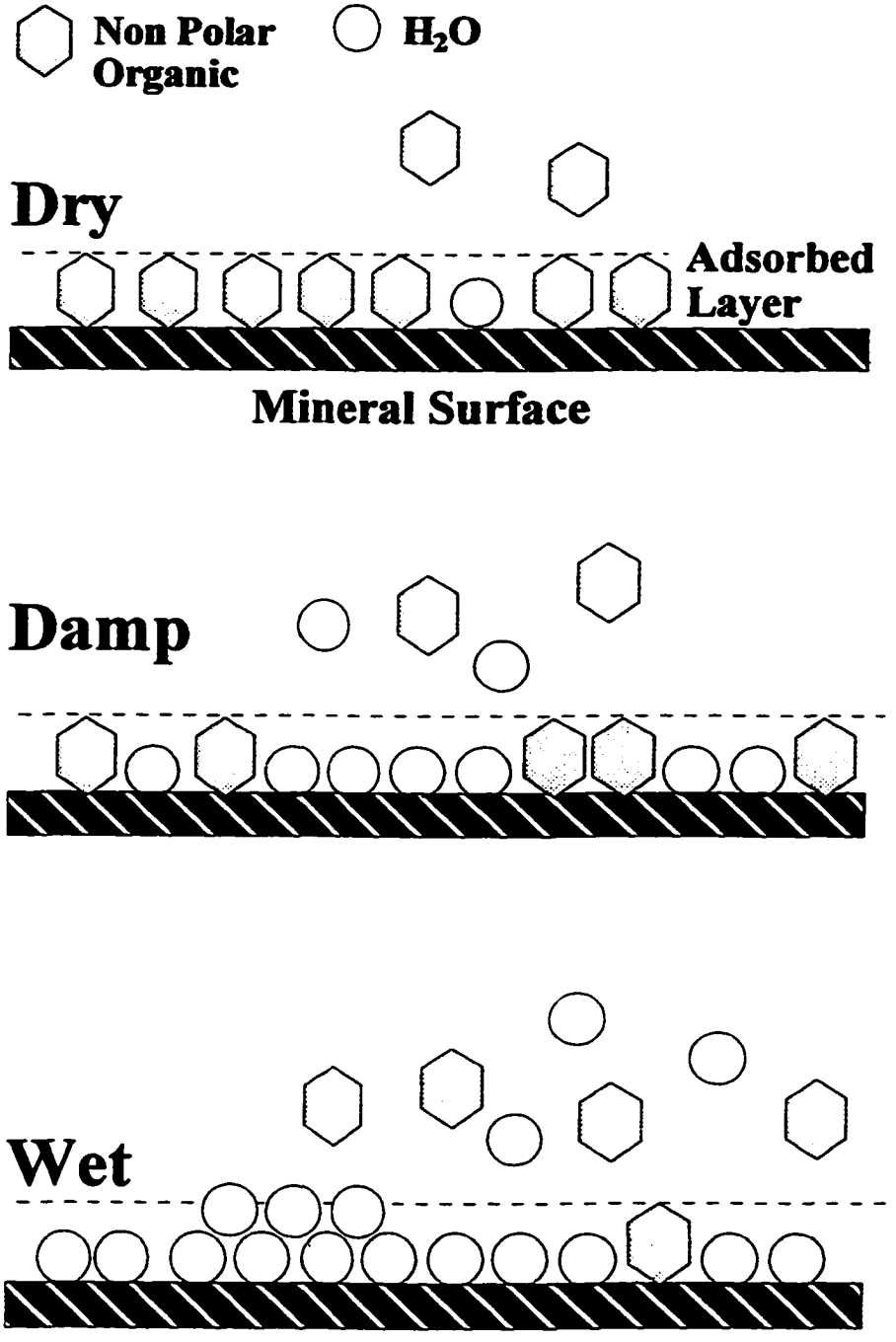

Figure 2.4 Competitive adsorption of water and contaminant molecules on sediment mineral surface.

Langmuir model. With these assumptions, using (2.6) and the symetrical expression for W_B/W_{mB}, they derived an expression for P_A:

$$P_A = \frac{P_A^{sat}}{B_A}\left[\frac{W_A/W_{mA}}{1-(W_A/W_{mA}+W_B/W_{mB})}\right] \tag{2.7}$$

It is to be noted that (2.7) can also be obtained from the Langmuir model of competitive adsorption.

One more simplification can be made to equation (2.7). In the concentration range where the coverage by A is negligible compared to the monolayer coverage ($W_A/W_{ma}<<1$), it is possible to obtain an expression for K_m:

$$K_m = RT\frac{B_A W_{mA}}{P_A^{sat}}\left(1-\frac{W_B}{W_{mB}}\right) \tag{2.8}$$

Or, with the notation used in this document:

- The subscript A is dropped.
- The moisture content, W_B is renamed mc.
- The monolayer moisture content, W_{mB} is renamed mc_m.

(2.8) becomes:

$$K_m = RT\frac{BW_m}{P^{sat}}\left(1-\frac{mc}{mc_m}\right) \tag{2.9}$$

In summary, this expression for K_m can be seen as resulting from a simple model based on three assumptions:

- (i) Water adsorbs onto the sediment preferentially to the contaminant.

- (ii) The contaminant adsorbs subsequently on the remaining water-free surface (and not on the water film nor on already adsorbed contaminant molecules).

These two assumptions lead to a general model:

$$K_m = RT\frac{B\,W_m}{P^{sat}}\Theta(mc) \qquad (2.10)$$

Where Θ(mc) is the fraction of water-free surface area. Θ(mc) is defined by the model chosen to describe water adsorption.

- (iii) The third assumption is that water adsorbs only onto the solid mineral surface and not on the already adsorbed water film (Langmuir model). This is equivalent to stating that: $\Theta(mc)=1-(mc/mc_m)$.

As a consequence of the third assumption, knowledge of the soil moisture content allows the determination of the sediment surface area fraction covered by adsorbed water. Thus, it is straightforward to calculate the fraction of surface available for organic molecule adsorption. Moreover, it is interesting to note that this simple model predicts a linear decrease in K_m as the moisture content increases in the damp range.

Finally, it is easy to see how a water adsorption model different from the Langmuir model could be used in (2.10) i.e. $\Theta(mc)\neq(1-mc/mc_m)$. In some cases, this could allow a more accurate description of water adsorption and thus, a more accurate description of organic contaminants adsorption on mineral surfaces. In other words, understanding water behavior in damp sediments is a prerequisite to estimating the magnitude of organic contaminant adsorption on mineral surfaces.

2.3.3.2 Adsorption on water film

Water occupying a number of adsorption sites creates a molecular film on soil particles surface. In some cases, adsorption at the interface between the air and this water film is an important mechanism of organic sorption (Valsaraj, 1988a, 1988b). Pennel et al., 1992 estimated that adsorption at the air-water interface was responsible for 50% of the uptake of p-xylene by a soil at 90% air relative humidity (RH). Hoff et al., 1993 determined that adsorption at the water surface accounted for 33 to 52% of the uptake of alkanes (pentane to octane) by an aquifer material at about 90% RH.

A. VOCs adsorption. Goss, 1992, 1993 studied the adsorption of a variety of volatile hydrophobic chemicals on water films supported by silica, sand and clay surfaces. For each compound, the heat of adsorption was found to be less negative than the heat of condensation. Similarly, Dorris and Gray, 1981 reported that the adsorption of alkanes (n-heptane up to n-decane) on water coated silica was less favorable than condensation of the pure substance resulting in adsorption isotherms of the BET Type III. They found that the free energy of adsorption per methylene group was the same for all alkanes investigated. Thus, for a compound, the partitioning at the air-water interface decreased with an increase in vapor pressure. Similarly, Goss, 1992, 1993 found that the partition constant for volatile aromatic compounds, naphthalene and cyclohexane, is a decreasing function of the vapor pressure.

Dorris and Gray, 1981 also found that the free energy of adsorption per methylene group decreases with the water loading until it reaches 8 water layers. Many other authors have observed a decrease of the partition constant, even after monolayer coverage is achieved. Goss, 1992, 1993 found that for the compounds he studied, the decrease was an

inverse exponential function of the relative humidity. The water molecules are polarized by the underlying mineral surface. This phenomenon favors the adsorption of non-polar molecules by creating dipole-induced dipole interactions. As the relative humidity increases, the water film gets thicker and the influence of the mineral surface decreases. This results in the water surface being less attractive to non-polar molecules.

Dorris and Gray, 1981 report that above a water coverage of 8 layers, the free energy of adsorption per methylene group and therefore, the partition constant at the air-water interface remains constant, indicating that the water film behaves as bulk water. At 100% RH, Goss, 1992, 1993 estimated that the solids he studied were covered by 5 to 10 layers of water, which is the generally accepted limit after which an electrically neutral solid surface cannot influence the air-water interface. Accordingly, he found that for quartz sand and kaolinite, the adsorption of hydrophobic compounds extrapolated to 100% RH was similar to the adsorption on bulk water reported in the literature.

For bentonite clay, however, the adsorption extrapolated to 100% RH was still higher than the adsorption on bulk water. Goss concluded that the difference in behavior was due to the residual valence present at the surface of bentonite but not at the surface of sand and kaolinite. Cations present at the surface of bentonite to balance the residual valence form a stronger electrostatic double layer than in the case of sand and kaolinite. This electrostatic double layer might influence the water surface even for film thickness above 5 to 10 monolayers. Furthermore, Goss observed that for quartz sand and kaolinite, the adsorption on the water film depends on the surface area of the solid but not on its nature. This was not the case for bentonite. The difference was also attributed to the influence of the electrostatic double layer.

Finally, Goss, 1994 found that the dependence of the partition constant on the air humidity (above one monolayer coverage) was best predicted by a set of four parameters characterizing the organic molecule:

- The saturated vapor pressure at 25°C.
- The molar refraction (measure of the polarizability).
- The hydrogen bond acceptor (measure of the ability to form hydrogen bonds).
- The dipole moment (measure of the polarity).

B. SVOCs adsorption. Storey et al., 1995 studied the adsorption of SVOCs (six n-alkanes from C_{17} to C_{23} and five 3 and 4-ring PAHs) on quartz atmospheric particles at relative humidity between 30 and 75%. They calculated that over this range of humidity from 1 to 4 layers of water are adsorbed on the quartz surface. They determined the partition coefficient for the compounds between the air and the air-water interface, on a surface area basis: $\kappa_{a/w}$ (L/m^2). At any relative humidity tested, $\kappa_{a/w}$ for either set of compounds could be described by a correlation similar to the one observed in the case of adsorption on a dry surface: $\log\kappa_{a/w}=m\log P_L^{sat}+b$ ($r^2>0.96$). The slope of the line showed no relation to humidity; for PAHs the value was $-1.2>m>-1.3$, which is not too different from the value m=-1 predicted by the BET adsorption model. Using the data obtained by Goss, 1992 for the adsorption of volatile compounds, the authors showed that at any humidity there was an excellent linear relation between $\log\kappa_{a/w}$ and $\log P_L^{sat}$ in each family (aromatic/polyaromatic compounds and alkanes) over a wide range of volatility. As observed by Goss, 1992, $\log\kappa_{a/w}$ was found to decrease linearly with increasing humidity. Slope for the alkanes and the PAHs were calculated to be, respectively, -0.020 and –0.025. For eight non polar VOCs (benzene, naphthalene), Goss, 1992, obtained a

slope of about –0.03. This consistency is remarkable, considering the difference in volatility of the compounds studied. It indicates that the effect of increasing humidity (and thus water layer thickness) on the strength of non polar organic adsorption is independent of the nature of the compound.

Pankow, 1996 extrapolated the results by Storey et al., 1995 to RH=100 % in order to evaluate the partition coefficient associated with adsorption on a bulk water surface. Correlations by these two authors are in good agreement with the one developed by Goss, 1994. They predict that the partition coefficient decreases by about two orders of magnitude between adsorption on the first monomolecular water layer and a bulk water surface.

C. Overall partitioning to the sediment water film. The partition coefficient between the air and the air-water interface, on a sediment mass basis, is $K_{a/w}$:

$$K_{a/w} = A_{a/w} K_{a/w} \tag{2.11}$$

Where $A_{a/w}$ is the free surface of water film per mass of dry sediment. It is thus necessary to be able to determine $A_{a/w}$ as a function of sediment moisture content in order to estimate the sorption of organic chemical in the sediment. However, $A_{a/w}$ is not always easy to determine. In fact, researchers have noticed that the surface area of the water film adsorbed on the solid particles can be dramatically modified by phenomena such as:

- Adsorption on the inner surface of smectite type particles (Goss, 1993)
- Condensation in small diameter pores of the solid particles occurring at RH below saturation (Hoff et al., 1993)

In conclusion, it is necessary to obtain a realistic picture of water behavior in damp sediments in order to estimate the adsorption of organic contaminant on both the dry mineral surface and the water film.

2.3.4 Wet soil

When the soil moisture content increases above that required for monolayer coverage (~1-2%), virtually all the adsorption sites are occupied by polar water molecules. There is no more mineral surface available for contaminant adsorption. The uptake of organic compounds is then usually explained by the following mechanisms.

2.3.4.1 Adsorption on the water film

As reviewed above, heat of adsorption of non-polar compounds on the water film decreases as the water film thickens. Furthermore, in porous media such as soils and sediments the increasing air humidity will provoke water condensation in pores, thus decreasing the water film surface and its adsorption capacity. Thus, both effects contribute to decrease the importance of the adsorption on the water film in the wet region.

2.3.4.2 Dissolution in water

Under environmental conditions, concentrations of organic compounds are usually low and the dissolution of organic substance in the adsorbed water phase can be quantified by Henry's law: $C_g = H. C_w$

Where:

- C_g is the air phase concentration of the organic compound above the water
- C_w is the concentration of the organic contaminant in water
- H is Henry's law constant

The mass of contaminant in the water phase of the sediment, on a sediment mass basis is: $W_w=C_w mc$, where mc is the sediment moisture content. Thus, the coefficient of partition between the air and the aqueous phase of the sediment, on a sediment mass basis, is K_w:

$$K_w = \frac{C_w mc}{C_g} = \frac{mc}{H} \tag{2.12}$$

This mechanism is obviously significant only for fairly soluble compounds.

2.3.4.3 Partitioning in the organic matter of the soil

Non polar compounds have a much greater affinity for the organic matter of the soil than for the polar air-water interface. Therefore, in soils that have a high organic content, the amount of non-polar organic compounds adsorbed on the water surface is small compared to the amount sorbed in the organic matter (Hoff et al., 1993). The air-sediment partitioning is thus believed to occur by the following process: (i) dissolution in the water layer around the sediment particle, followed by (ii) partitioning from the water to the organic matter. The amount of compound sorbed in the organic phase, W_{oc} is thus calculated by:

$$W_{oc} = f_{oc} \cdot K_{oc} \cdot C_w = \frac{f_{oc} \cdot K_{oc}}{H} \cdot C_g \tag{2.13}$$

Where:

- K_{oc} is the partition constant of the compound between water and the organic carbon fraction of the soil.
- f_{oc} is the fraction of organic carbon in the sediment.

From (2.12), an expression for the partition coefficient between the sediment organic matter and the air, K_{org} is obtained:

$$K_{org} = \frac{W_{oc}}{C_g} = \frac{f_{oc} K_{oc}}{H} \tag{2.14}$$

The partitioning of organic compound between water and the soil organic matter is similar to the partitioning of those compounds between a polar, protic solvent (water) and a non-polar, non-protic solvent (octanol). Several correlations have been developed to predict K_{oc} as a function of K_{ow}, the octanol-water partition constant of the compound. Hippelein and McLachlan, 1998 observed that the soil-air partition coefficient of various PCBs and two PAHs was independent on moisture content as long as the soil was in equilibrium with a water saturated air phase. Furthermore, for all SVOCs tested, K_s was proportional to K_{ow}/H, indicating that sorption in the soil organic matter was the principal partitioning mechanism.

2.3.5 Closure

Soils and sediments offer a variety of different compartments in which synthetic organic chemicals can be sorbed. A realistic evaluation of the partitioning of pollutants between exposed sediments and the air must consider each of them. From the individual partition coefficients, an expression for the overall partition coefficient between the sediment and the air phase can be obtained:

$$K_s = K_m + K_{a/w} + K_{org} + K_w \tag{2.15}$$

The individual partition coefficients can be replaced by their respective expressions: (2.10), (2.11), (2.12) and (2.14). This gives the general expression:

$$K_s = \left[\left(RT\frac{BW_m}{P^{sat}}\right)\Theta(mc)\right] + \left[\kappa_{a/w}A_{a/w}\right] + \left[\frac{K_{oc}f_{oc}}{H}\right] + \left[\frac{mc}{H}\right] \qquad (2.16)$$

Thus the evaluation of the sediment-air partition coefficient requires the determination of three sets of parameters:

A. Physico-chemical properties of the contaminant. P^{sat}, H and K_{oc}. Values of these parameters are available in the literature. However, the values reported are sometimes fairly different from one study to another. Due to its importance to estimate the partition coefficient in dry and damp sediments, the saturated vapor pressures of the investigated contaminants has to be experimentally determined.

B. Sediment characteristics. the fraction of organic carbon, f_{oc} and the characterization of water behavior in the sediment. An accurate model of water sorption in the sediment would allow the determination of $A_{a/w}$ and Θ(mc) at any sediment moisture content or air relative humidity. Such a model has to be developed based on the experimental study of water partitioning between the air and the sediment.

C. Parameters describing the contaminant-sediment interaction: W_m and B. The determination of W_m requires the measurement of the sediment specific surface area, A and the estimation of the fraction of this surface area, F that is available for adsorption. The parameter B can be determined experimentally by measuring the heat of adsorption of the contaminant on dry sediment.

Chapter 3
Materials and Methods

In the first section of this chapter, the different experimental methods used to investigate contaminant sorption in soils and sediments are critically reviewed. Based on this review, the choice of the gas saturation technique is justified. In section 3.2, a model is developed to assist in the design of the experimental method. The set-up that was constructed to implement the gas saturation technique is then described in section 3.3. The preparation procedure and the characterization of the sediment that is used in this project is presented in section 3.4 and 3.5. Finally, section 3.6 features the analytical procedures.

3.1 Choice of an experimental method

Measurement of the equilibrium partial pressure of semi-volatile organic compounds (SVOCs) in contact with contaminated soils and sediments presents two analytical difficulties:

- SVOCs have low saturated vapor pressures and the equilibrium partial pressures expected above contaminated sediments are even lower.
- In soils or sediments containing a substantial amount of organic matter, the SVOC of concern is likely to be mixed in the air phase with natural semi-volatile organic chemicals such as terpenes or azepins.

Methods used in the literature to study the soil-air equilibrium of anthropogenic chemicals are hereafter reviewed, and their capability to overcome the above-mentioned difficulties is assessed.

3.1.1 Static batch equilibriation method

In static equilibration methods, the sediment and the vapor phases are brought into contact in a closed vessel and allowed to equilibrate. The vapor is then directly sampled and analyzed. The sediment concentration is subsequently determined by mass balance or direct analysis. Such batch experiments have been successfully used to investigate the soil-air partitioning of volatile organic compounds (Rao et al., 1989; Gan and Dupont, 1989; Ong and Lion, 1991). Unfortunately direct analysis of the vapor phase is limited to high partial pressures of contaminant. The detection limit of a Flame Ionization Detector for instance, is about 1 ng of organic chemical. This corresponds to the amount of phenanthrene found in about 10 L of air in equilibrium with a dry sediment contaminated at 100mg/kg.

Static experiments are thus inappropriate to the study the sediment-air partitioning of SVOCs.

3.1.2 Chromatographic methods

In chromatographic methods, the sediment studied is the stationary phase of a packed column and air is the carrier gas. The partition coefficient is derived from observations made on the characteristics of the contaminant transport through the sediment bed.

3.1.2.1 Pulse input chromatography

In classical pulse input chromatography, the partition constant of a compound is back calculated from its retention time. Several authors have used this method to study the adsorption of VOCs onto (i) dry soils with low organic content (Bohn et al., 1980) or (ii) water films supported by various materials (Karger et al., 1971; Okamura and

Sawyer, 1973; Doris and Gray, 1981; Goss, 1993). However, application of this method to the present study would be complicated by three factors:

- The chromatographic process relies on the condition of instantaneous equilibrium between the gas and the stationary phases. This condition is certainly fulfilled in the case of adsorption at the air/water interface. However it is probably not the case for sorption into natural media in which equilibrium may be very slow to establish (Hoff et al., 1993).
- When studying the partitioning equilibrium at relatively high concentrations, the assumption of linear isotherm is no longer valid. However, Hoff et al., 1993 have used the method to study non linear isotherms but in this case the sediment loading has to be calculated based on the envelope profile of the peaks obtained by injection of different amounts of chemicals. This leads to uncertainty, since peak shape does not depend solely on the type of the sorption isotherm.
- Finally, Goss, 1992, found the method limited to fairly volatile compounds (naphthalene) having relatively short retention time because of base line drifting. This problem is expected to be exacerbated when studying materials with high organic matter content such as sediments, probably subject to column bleeding.

3.1.2.2 Frontal analysis chromatography

Another method based on chromatography is sometimes used to study VOC partitioning. It is referred to as frontal analysis chromatography. In this method, monitoring of the break-through and elution curves resulting from a step input of feed containing the contaminant permits the determination of the amount of compound sorbed (Thibaud et al., 1992, 1993; Grathwohl and Reinhard, 1993; Thibaud-Erkey, 1996). This

method is also reserved to fairly low partitioning coefficients since the time required for saturating even a small amount of sediment with a SVOC would be prohibitive.

3.1.3 Flow adsorption experiment

In this method, a stream of air containing a given concentration of contaminant is passed through an initially clean sediment. After equilibrium is reached, the sediment is analyzed (Chiou and Shoup, 1985; Pennel et al., 1992a, 1992b; Rhue et al., 1993). This is the same principle as the one used in the determination of BET isotherms by nitrogen adsorption. This method cannot be used in the present study because the time to saturate even a very small amount of sediment would be prohibitive.

3.1.4 Gas saturation technique

The gas saturation technique appears to be the most suitable for this study. This technique, as defined in ASTM method E 1194-87 (1993), is a reference technique to measure saturated vapor pressures and has been widely used to this effect (Wasik, 1983). It has also been used to measure partial pressures of various chemicals in soils such as: dieldrin (Spencer et al., 1969), lindane (Spencer and Cliath, 1970a,1970b), DDT (Spencer and Cliath, 1972), trifluralin (Spencer and Cliath, 1974), parathion (Spencer et al., 1969) chlorinated VOCs, (Farrell and Reinhard, 1994; Werth and Reinhard, 1997), PAHs and PCBs (Hippelein and Mc Lachlan, 1998). The principle behind this technique is shown in Figure 3.1. A stream of clean gas is passed through a column loaded with the sediment containing the chemical of interest at a known concentration. As the gas progresses through the column, it becomes concentrated with the chemical until it reaches equilibrium with the sediment. Analysis of the effluent gas allows the determination of one point on the desorption isotherm. Using this method, Spencer and Cliath, 1972

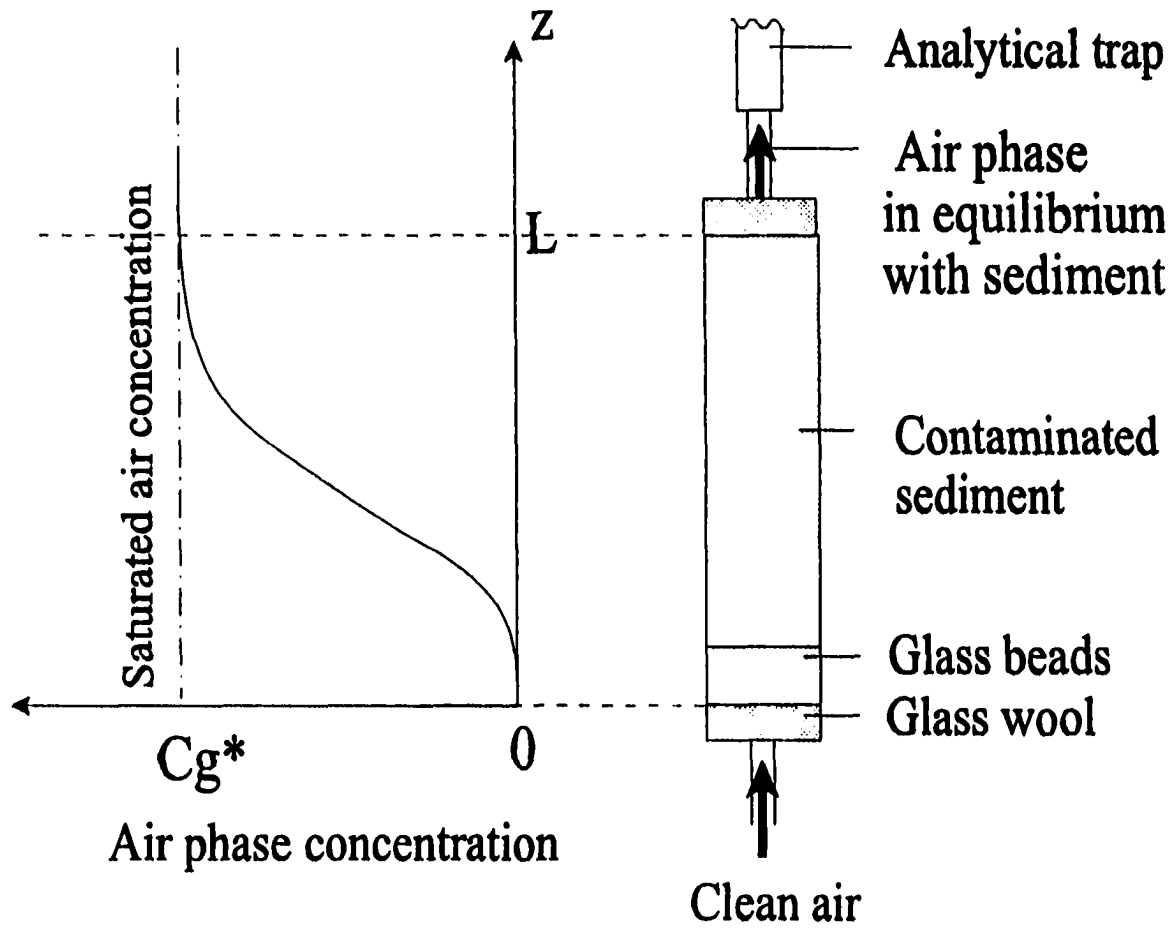

Figure 3.1 Principle of the gas saturation technique.

measured concentrations of insecticide in the air phase of a dry soil as low as 90 pg/L. In this project, improvements listed in Table 3.1 were made to the gas saturation set-up used by Spencer and Cliath, 1969.

Table 3.1 Improvements made in this study to the gas saturation set-up used by Spencer and Cliath, 1969.

	Spencer and Cliath, 1969	This project
Outlet gas trapping method	bubbling through hexane in a gas washing bottle. This pobably causes losses of contaminant (i) by adsorption onto structural parts of the set-up between the outlet of the column and the gas washing bottle and (ii) during hexane concentration before analysis.	Use of a trap specifically design for analyzing PAHs air concentrations (see section 3.7.2.1)
Humid air flow control	Valves that do not allow a sensitive control of the flow, which automatically leads to an imprecision on the total volume of air that flew through the column and thus on the calculation of the air concentration.	Mass flow controllers (see section 3.3.1.2)

Because of the possible presence of natural semi-volatile compounds in the air phase, analysis should be specific to the compound investigated. Non specific on-line analytical techniques such as FID or IR analysis of the CO_2 produced by combustion are not suitable. Techniques based on measuring weight change of a collection trap should also be avoided. In this study, determination of the air phase concentration is achieved by using collection traps that are subsequently desorbed using a solvent and analyzed by Liquid Chromatography.

3.2 Design of a gas saturation column

3.2.1 General model

The transport phenomena occurring in a gas saturation column are the same as that in a packed bed absorption tower. Thus, the modeling of both units is identical. Only

the boundary conditions are different. The physical model of a gas saturation column is presented here, based on the analysis of a packed bed absorber by Bird et al., 1960. The conceptual model is represented in Figure 3.2. The variables and parameters featured are summarized in Table 3.2.

To formulate the mass balances over a differential element of the column, it is assumed that:

- The diffusion of PAHs through the solid phase of the sediment is negligible.
- The interstitial gas velocity, V, is uniform over the cross-section of the column and constant along its z-axis.

For the solid phase, the continuity equation is :

$$\left(\frac{\partial((1-\varepsilon)C_s)}{\partial t}\right) = k_g a(1-\varepsilon)(C_g - C_g^*) \tag{3.1}$$

and for the gas phase:

$$\varepsilon S dz\left(\frac{\partial C_g}{\partial t}\right)_z = -k_g a(1-\varepsilon)(C_g - C_g^*)Sdz - \left(\frac{\partial(QC_g)}{\partial z}\right)_t dz + S\frac{\partial}{\partial z}\left(\varepsilon D\frac{\partial C_g}{\partial z}\right)_t \tag{3.2}$$

If the extra assumptions are made that:

- The dispersion coefficient is constant along the axis of the column.
- The porosity ε is uniform over the bed volume and constant in time.
- The pressure drop is negligible along the column and thus, the interstitial gas velocity, V, is constant along the axis of the column.

(3.1) and (3.2) become respectively:

$$\left(\frac{\partial Cs}{\partial t}\right)_z = k_g a(Cg - Cg^*) \tag{3.3}$$

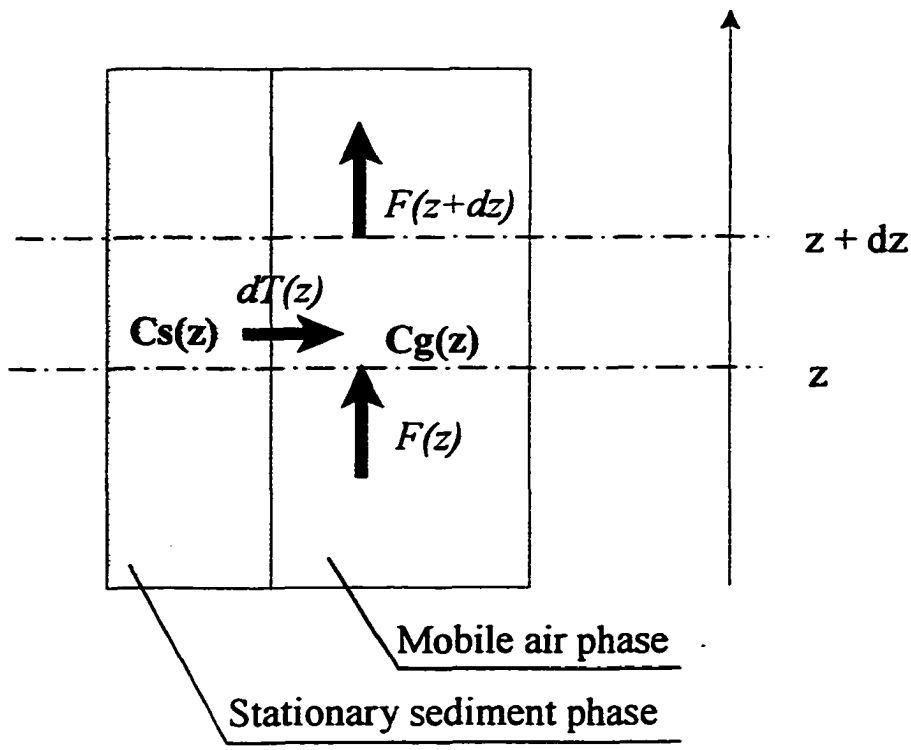

Figure 3.2 Model of contaminant mass transfer in a gas saturation column.

Table 3.2 Variables and parameters involved in the modeling of a gas saturation column.

A	Particle surface area of the sediment; (m^{-1})
β	Phase ratio: $\beta = \varepsilon / (1-\varepsilon)$; (-)
C_g	Chemical concentration in the sediment air phase; ($\mu g / m^3$)
C_g^*	Chemical air concentration in equilibrium with the sediment; ($\mu g / m^3$)
C_s	Overall chemical concentration in the sediment; ($\mu g/kg$)
C_s^i	Initial (thus uniform) chemical concentration in the column sediment bed; ($\mu g/kg$)
D	Dispersion coefficient of the chemical in the air phase of the column bed; (m^2/s). D is the sum of the effective and eddy diffusivities.
D_m	Air molecular diffusivity of the chemical; (m^2/s)
ε	Porosity (or void fraction) of the sediment ; (-)
K_s	Equilibrium partition constant of the chemical between the sediment and air. $K_s = C_s / C_g^*$; (m^3/kg)
k_g	Chemical air-side global mass transfer coefficient ; (m/s)
k_s	Chemical sediment-side global mass transfer coefficient ; (m/s)
Pe	Peclet number. $Pe = L \cdot V/D$
Q	Air flow-rate through the column ; (m^3/s)
R_F	Retardation factor; (-)
ρ	Sediment bulk density; (kg/m^3)
S	Cross sectional area of the column ; (m^2)
Sh	Sherwood number. $Sh = (L^2 \cdot k_g \cdot a)/D$
St_{AB}	Stanton number. $St_{AB} = k_g/V$
τ	Tortuosity of the sediment; (-)
V	Air interstitial velocity through the column. $V = Q/S \cdot \varepsilon$; (m/s)

$$\left(\frac{\partial C_g}{\partial t}\right) = -V\left(\frac{\partial C_g}{\partial z}\right)_t + D\left(\frac{\partial^2 C_g}{\partial z^2}\right)_t + \frac{1-\varepsilon}{\varepsilon} k_g a\left(C_g^* - C_g\right) \tag{3.4}$$

In addition, the partition coefficient is defined:

$$C_g^* = \frac{C_s}{K_s} \tag{3.5}$$

(3.3) through (3.5) are system of three equations with three unknowns. The following boundary conditions are used:

- The gas stream is clean before entering the column. Hence, C_g=0 for z=0.
- The concentration in the gas stream is finite and thus C_g must be finite for z tending to infinity.

This set of boundary conditions describes an ideal plug-flow reactor with no axial dispersion. It is thus not perfectly adapted to the stated problem. Wehner and Wilhelm, 1956 presented a detailed analysis of the boundary conditions for a steady-state flow reactor with axial diffusion. They show that more accurate boundary conditions should take into account outward diffusion at the entrance and at the outlet of the bed. However, the boundary conditions chosen here give a simple solution that is not significantly different from the one obtained with more elaborate boundary conditions, provided that the Peclet number is reasonably large.

3.2.2 SVOC desorption

3.2.2.1 Modeling

A very important simplification can be made when modeling SVOC desorption. Due to the very low saturated vapor pressure and the relatively short duration of an

experiment, the total amount of SVOC volatilized is insignificant compared to the initial loading of the sediment. Therefore, the depletion of the sediment with time is negligible and the volatilization is at quasi-steady state. It should be noted that this simplification is perfectly correct in the modeling of a gas saturation column loaded with the pure compound.

With this assumption, (3.4) becomes:

$$\frac{\partial^2 C_g}{\partial z^2} - \frac{V}{D}\frac{\partial C_g}{\partial z} - \frac{(1-\varepsilon)}{\varepsilon}\frac{k_g a}{D} C_g = -\frac{(1-\varepsilon)}{\varepsilon}\frac{k_g a}{D} C_g^* \qquad (3.6)$$

(3.6) can be modified by introducing the dimensionless variables ζ and X defined by: $\zeta = z / L$ and $X = 1 - (Cg / Cg^*)$, where L is the total length of the column.

$$\frac{\partial^2 X}{\partial \zeta^2} - \frac{LV}{D}\frac{\partial X}{\partial \zeta} - \frac{(1-\varepsilon)}{\varepsilon}\frac{L^2 k_g a}{D} X = 0 \qquad (3.7)$$

Furthermore, by introducing the dimensionless numbers, α, Pe and Sh, (3.7) gives:

$$\frac{\partial^2 X}{\partial \zeta^2} - Pe\frac{\partial X}{\partial \zeta} - \alpha Sh X = 0 \qquad (3.8)$$

This second order homogeneous linear differential equation has a solution of the form:

$$X = \lambda e^{Pe(1+\gamma)\zeta} + \mu e^{Pe(1-\gamma)\zeta} \qquad (3.9)$$

where γ is defined by:

$$\gamma = \sqrt{1 + \frac{4\beta Sh}{Pe^2}} \tag{3.10}$$

Finally, the boundary conditions are used to determine λ and μ:

- The concentration in the gas stream is finite and thus X must be finite for ζ tending to infinity. This imposes $\lambda = 0$.
- The gas stream is clean before entering the column, i.e. X=1 for ζ=0. This imposes μ=1.

The solution is:

$$X = \exp\left(Pe \cdot (1-\gamma)\zeta\right) \tag{3.11}$$

In dimensional form, the final model is:

$$C_g = C_g^* \cdot \left[1 - \exp\left(-Pe \cdot (\gamma - 1) \cdot \frac{z}{L}\right)\right] \tag{3.12}$$

3.2.2.2 Mass transfer and dispersion coefficients

In order to plot the concentration profile in the gas phase of the column, one must estimate D and k_g.

A. Dispersion coefficient. Several correlations have been developed for the determination of the axial dispersion coefficient in packed beds. Unfortunately they either apply to (i) particles larger than soil particles (Ruthven, 1984) or (ii) flow rates higher than the ones applied in this study (Thibaud-Erkey et al., 1996). As a result, all the correlations tested predicted values of the dispersion coefficient smaller than the

molecular diffusivity. Thus, D was conservatively estimated by taking one hundred times the molecular diffusivity.

B. Mass transfer coefficient. Similar remarks apply to correlations developed to estimate the mass transfer coefficient. However, Wilkins et al., 1994 developed a correlation to predict k_g for the evaporation of Non Aqueous Phase Liquids (NAPLs) from a soil packed in an experimental column. The range of flowrate in which the correlation is applicable is compatible with this study. However, contaminant molecules sorbed in the sediment matrix are expected to be subject to sediment-side mass transfer resistance unlike NAPLs entrapped in sediment. Thus, a value of kg equal to one hundredth of the one predicted by the correlation was picked.

A concentration profile using these conservative estimates of D and k_g is plotted in Appendix C. Based on this profile, the column dimensions were chosen as:

- radius = 3.5 cm
- length = 40 cm (In order to get a bed length of 30cm)

For the determination of the vapor pressures, due to the absence of solid-side mass transfer resistance, smaller column dimensions were chosen:

- radius = 0.75 cm
- length = 20 cm (In order to get a bed length of 10cm)

3.2.3 Water equilibration

3.2.3.1 Desorption

When modeling more volatile chemicals like water, it is necessary to take into account the progressive depletion occuring in the sediment because of the chemical evaporation. Lapidus and Amundson, 1952 presented an analytical solution to the system

of coupled differential equations (3.3), (3.4) and (3.5) that takes into account both the resistance to mass transfer at the air-sediment interface and the dispersion in the air flow. Unfortunately, this solution has a complicated form that makes it difficult to use. Approximate solutions have been found by neglecting either the mass transfer resistance (Lapidus and Amundson, 1952) or the dispersion in the air flow (Rosen, 1952; Bird, et al., 1960). The latter approach is presented hereafter.

It is convenient to define a modified time variable, t':

$$t' = t - \frac{z}{V} \tag{3.13}$$

t'(z) may be interpreted as the time elapsed since the carrier gas first reached the point of altitude z. The relations between t, z and t' are:

$$\left(\frac{\partial C_g(t',z)}{\partial z}\right)_t = \left(\frac{\partial t'}{\partial z}\right)_t \cdot \left(\frac{\partial C_g}{\partial t'}\right)_z + \left(\frac{\partial C_g}{\partial z}\right)_{t'} \tag{3.14}$$

$$\left(\frac{\partial t'}{\partial z}\right)_t = -\frac{1}{V} \tag{3.15}$$

$$\left(\frac{\partial t'}{\partial t}\right)_z = 1 \tag{3.16}$$

Equation (3.4), without the dispersion term, is simplified by introducing t':

$$\varepsilon \cdot \left(\frac{\partial C_g}{\partial t'}\right)_z = -(1-\varepsilon) \cdot k_g \cdot a \cdot (C_g - C_g^*) - V \cdot \varepsilon \cdot \left[-\frac{1}{V}\left(\frac{\partial C_g}{\partial t'}\right)_z + \left(\frac{\partial C_g}{\partial z}\right)_{t'}\right] \tag{3.17}$$

(3.17) simplifies further:

$$\left(\frac{\partial C_g}{\partial z}\right)_{t'} = -\frac{1-\varepsilon}{\varepsilon}\cdot\frac{k_g \cdot a}{V}\cdot\left(C_g - C_g^*\right) \qquad (3.18)$$

Similarly, by introducing t', (3.3) simplifies to:

$$\left(\frac{\partial C_g}{\partial t'}\right)_z = k_g \cdot a \cdot \left(C_g - C_g^*\right) \qquad (3.19)$$

It should be noted that equation (3.5) which describes a linear isotherm is not valid for the adsorption of water. Nevertheless, it is used here to obtain qualitative information on the evaporation of water from the sediment.

Here again, simplified boundary conditions are used:

- Before the carrier gas reaches the altitude z in the column, the concentration of the sediment above this altitude is C_s^i :

  for $t \leq z / V$ and for any z, $\quad C_s(z) = C_s^i \qquad (3.20)$

- Before entering the column, the carrier gas is free of chemical :

  For $z \leq 0$ and for any t, $\quad C_g = 0 \qquad (3.21)$

It is then convenient to introduce the following dimensionless variables:

- Dimensionless time, τ:

$$\tau = \frac{t - \frac{z}{V}}{\theta} \qquad \text{with} \quad \theta = \frac{K_s}{k_g \cdot a} \qquad (3.22)$$

- Dimensionless altitude, ζ:

$$\zeta = \frac{z}{\delta} \qquad with \quad \delta = \frac{\varepsilon}{1-\varepsilon} \cdot \frac{V}{k_g \cdot a} \left(= \frac{1}{a} \cdot \frac{\varepsilon}{1-\varepsilon} \cdot St_{AB} \right) \tag{3.23}$$

- **Dimensionless gas concentration:**

$$X = C_g \cdot \left(\frac{K_S}{C_S^i} \right) \tag{3.24}$$

- **Dimensionless sediment concentration:**

$$Y = \frac{C_S}{C_S^i} \tag{3.25}$$

In terms of these variables, the system of equations can be rewritten as:

$$\left(\frac{\partial X}{\partial \zeta} \right)_\tau = Y - X \tag{3.26}$$

$$\left(\frac{\partial Y}{\partial \tau} \right)_\zeta = X - Y \tag{3.27}$$

with the boundary conditions:

- for $\tau \leq 0$ and for any ζ, $Y = 1$ (3.28)
- for $\zeta \leq 0$ and for any τ, $X = 0$ (3.29)

Solution to this system is inferred from the solution given by Bird et al., 1960 for a packed bed absorber:

$$X(\tau,\zeta) = \int_0^{\zeta} \exp(-\tau - z) J_o\left(i\sqrt{4\tau z}\right) dz \tag{3.30}$$

$$Y(\tau,\zeta) = 1 - \int_0^{\tau} \exp(-t - \zeta) J_o\left(i\sqrt{4t\zeta}\right) dt \tag{3.31}$$

where J_0 is the zero-order Bessel function of the first kind. J_0 can be expressed as an infinite series or as an integral:

$$\forall x \in C \qquad J_o(x) = \sum_0^{\infty} \frac{(-1)^k \cdot \left(\frac{x}{2}\right)^{2k}}{(k!)^2} \qquad \rightarrow \qquad J_o\left(i\sqrt{4tz}\right) = \sum_0^{\infty} \frac{(tz)^k}{(k!)^2} \tag{3.32}$$

or

$$\forall x \in C \quad J_o(x) = \frac{1}{\pi}\int_0^{\pi} \cos(x \cdot \sin\theta) d\theta \rightarrow J_o\left(i\sqrt{4tz}\right) = \frac{1}{2\pi}\int_0^{2\pi} \exp\left(2\sqrt{tz}\sin\theta\right) d\theta \tag{3.33}$$

Using the integral expression of the Bessel function (3.33) in equations (3.30) and (3.31) and regrouping the exponential functions, expressions suited to computer calculations are obtained:

$$X(\tau,\zeta) = \frac{1}{2\pi}\int_0^{\zeta}\left(\int_0^{2\pi} \exp\left(-\tau - z + 2\sqrt{\tau z}\sin\theta\right) d\theta\right) dz \tag{3.34}$$

$$Y(\tau,\zeta) = \frac{1}{2\pi}\int_0^{\tau}\left(\int_0^{2\pi}\exp\left(-t-\zeta+2\sqrt{t\zeta}\sin\theta\right)d\theta\right)dt \qquad (3.35)$$

These two dimensionless concentration profiles are plotted in Appendix D for different times. The qualitative evolution with time of the air concentration profile is also shown in Figure 3.3. The general shape of the solution would not be changed by taking into account the dispersion term. Both resistance to mass transfer and dispersion cause a spreading of the S-shaped curve. Spreading caused separately by either resistance to mass transfer or dispersion is additive due to the system being linear.

3.2.3.2 Adsorption

The modeling of water adsorption from a water saturated air stream to a relatively dry sediment is symmetrical to the problem just treated. Solutions to (3.3), (3.4) and (3.5) have been given by Bird et al., 1960:

$$X(\tau,\zeta) = 1 - \int_0^{\zeta}\exp(-\tau - z)J_o\left(i\sqrt{4\tau z}\right)dz \qquad (3.36)$$

$$Y(\tau,\zeta) = \int_0^{\tau}\exp\left(-t-\zeta\right)J_o\left(i\sqrt{4t\zeta}\right)dt \qquad (3.37)$$

However, water sorption in soils is known to exhibit hysteresis. Thus, adsorption and desorption equilibrium may not be identical. Consequently, in equation (3.36), value of the equilibrium partition constant used to define the dimensionless variables τ and X is *a priori* different from the value it had in (3.34).

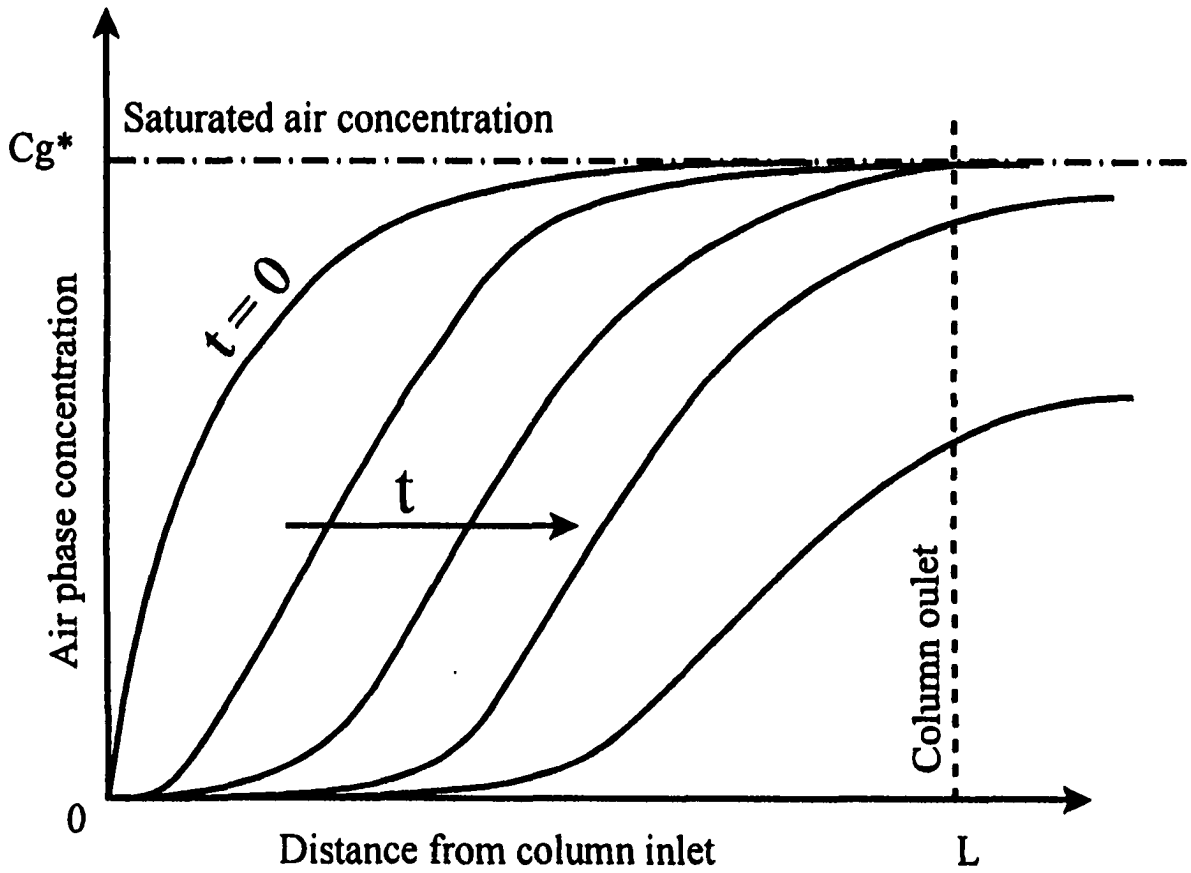

Figure 3.3 Qualitative concentration profile in the air phase of a gas saturation column for a volatile chemical.

3.2.4 Conclusions on column design

The model was used to determine the dimensions of the gas saturation columns using conservative values of the dispersion and mass transfer coefficients. In addition, the model also suggests methods to assess the outlet air phase equilibrium.

3.2.4.1 Assessing air phase equilibrium

A. Variation of the bed length. The analytical expression of the air concentration at the outlet of a gas saturation column suggests a method to ascertain that the chemical (water or contaminant) has reached equilibrium with the solid phase (sediment or pure compound). Given the characteristic shape of the exponential function, if the outlet stream is far from equilibrium, a change in bed length will noticeably modify the outlet concentration. Conversly, if a change of bed length has only a negligible influence on the outlet concentration this demonstrates that the outlet stream is close to equilibrium. This is easily seen in Figure 3.3. Thus, monitoring the effect resulting from a bed length variation is a reliable method to assess the outlet concentration.

B. Variation of the air flow rate. Studies featuring the gas saturation technique found in the literature rely solely on variations of the air flow-rate through the column to check the outlet concentration (ASTM method E 1194-87). While more convenient than varying the bed length, this approach is not systematically valid. Equation (3.12) shows that the air velocity can influence the outlet concentration only if it affects the factor k_gD/V^2. Thus, if the product k_gD is proportional to V^2, V will have no effect on the concentration of the outlet stream, whether it is at equilibrium or not. As a matter of fact, several correlations predict that both the air-side mass transfer coefficient and the axial dispersion coefficient are proportional to V^n with n equal or close to 1 (Hougen and

Marshall, 1947; Wilke and Hougen, 1945, Langer et al., 1978, Ruthven, 1984). Furthermore, volatilization from a pure compound is essentially air-side controlled. Thus, equation (3.12) predicts that the air velocity should have no or only very little influence on the outlet concentration in such a case. Therefore, varying the air flow rate is not a reliable way to ascertain the equilibrium of the outlet stream. However, in a sediment loaded column, the mass transfer coefficient, because it accounts for sediment-side resistance should not be proportional to V and the method should be valid.

3.2.4.2 Breakthrough time

There is yet another experimental concern when investigating sorption of a fairly volatile compound like water by the gas equilibration technique. Plots of equation (3.33) shown in Appendix D indicate that the water transfer resulting from the equilibration of the air stream humidity results in a significant change in sediment moisture content. With time, the moisture content changes from the bottom of the column toward the top and eventually perturbs the outlet air humidity. It is thus important that an experiment not be pursued after the critical breakthrough time.

3.3 Experimental set-up

A set-up was constructed to implement the gas saturation technique. A schematic is shown in Figure 3.4.

3.3.1 Partition coefficient determination

3.3.1.1 Temperature control

The set-up is kept thermostated in an insulated chamber. This chamber consists of a refrigerator that can be used in normal operation mode or as an incubator. In the first case, the built-in compressor and temperature controller are able to maintain a

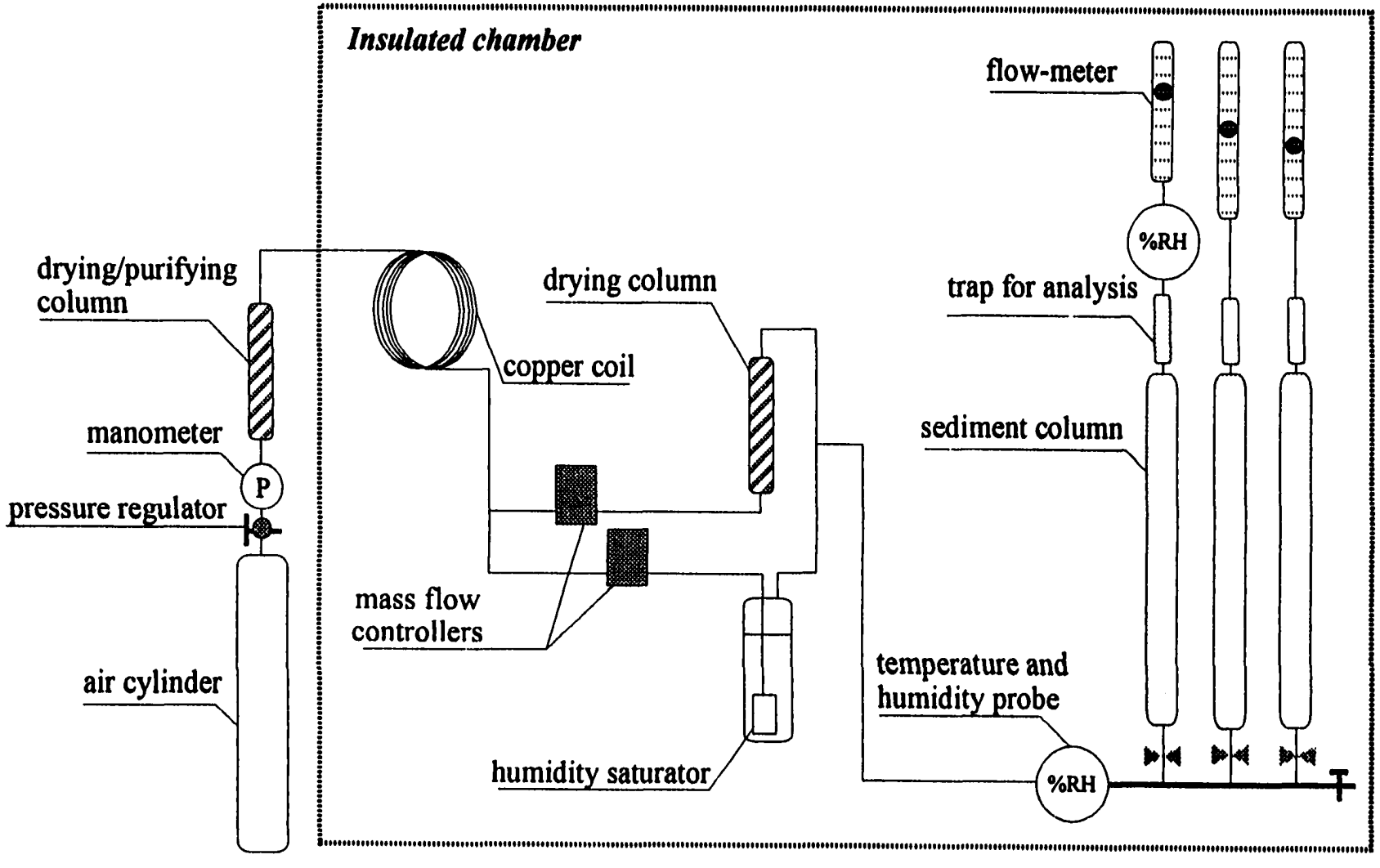

Figure 3.4 Schematic of the experimental set-up

temperature of 14.0±0.7°C for unlimited periods of time. In the second case, the refrigerator is switched off and the desired temperature is obtained by heating with a set of electrical resistors controlled by a differential temperature regulator. In the incubator configuration, temperatures of 25.0±0.7°C and 35.0±0.2°C can be maintained over extensive periods of time. A fan insures temperature uniformity inside the chamber.

3.3.1.2 Air phase preparation

Air from a cylinder (quality Zero 2.0™ from BOC gases) is passed through a drying column containing Drierite™ followed by an activated carbon cartridge. The air stream is then brought to the chamber temperature by passing through a 2-meter copper coil. The flow is subsequently split between two mass flow controllers. (Sierra Instruments, Model 810 Mass-Trak, 0-50 cm^3/min). One stream is sent to a drying column and the other to a gas-washing bottle filled with water. By mixing the dry and the water-saturated streams at different flow rates, an air stream at any desired humidity can be obtained. The mass flow controllers also ensure a steady flow rate to the air stream fed to the columns. The flow rate would otherwise be affected by pressure drop variations resulting from: (i) the decreasing water level in the humidifying column and (ii) possible changes in packed sediment porosity over the duration of an experiment. An electronic probe (Cole Parmer Cat. No. E-37950-10) monitored the temperature and the relative humidity of the stream before it is divided between a number of columns containing the contaminated sediment. Calibration of the probe is performed regularly with standard salt solutions. Their accuracy is specified by the manufacturer to be ±2% RH from 0 to 95% and ±3% RH from 95 to 99%. The probe is set in-line, using a specially designed glass holder minimizing dead volume. The relative humidity is monitored again at the column

outlet to ascertain that water exchange between the air stream and the sediment is negligible.

3.3.1.3 Columns

Columns made of thick wall borosilicate glass (diameter=3.5cm; length=40cm) were constructed in the Glass Blowing Shop of the College of Basic Sciences (Louisiana State University, Baton Rouge). One to six columns can be mounted on a glass manifold at a time. The flow to each column is controlled with a Teflon™ needle valve. At the bottom of each column, a bed of 3mm glass beads, about 6cm high, supports the sediment bed and ensures a uniform flow. A schematic representation of a column is given in Figure 3.5. The sediment is uniformly packed by using a vibrating carving device fitted with a rubber tip. At the outlet of each column the air stream is passed through analytical traps. A specially designed trap holder shown in Figure 3.6 minimizes losses by adsorption on structural parts and prevents air borne particles from getting into the trap.

3.3.1.4 Flow rates

Flow rates are measured by two sets of three flowmeters. The first set (Cole Parmer Cat No P-03210-00) covers the range 0.02-15ml/min. The second set (Cole Parmer Cat No P-03201-00) covers the range 1-280ml/min. Flow rates are measured at regular time intervals during an experiment. The flow rate profile over the experiment time length is subsequently integrated to obtain the total air volume passed through a column. As an example, in Figure 3.7, such profiles are shown for two experiments that were conducted at different flow rates. Columns A and B were monitored with the first flowmeters set (0.02-15ml/min). Columns D and E were monitored with the second set

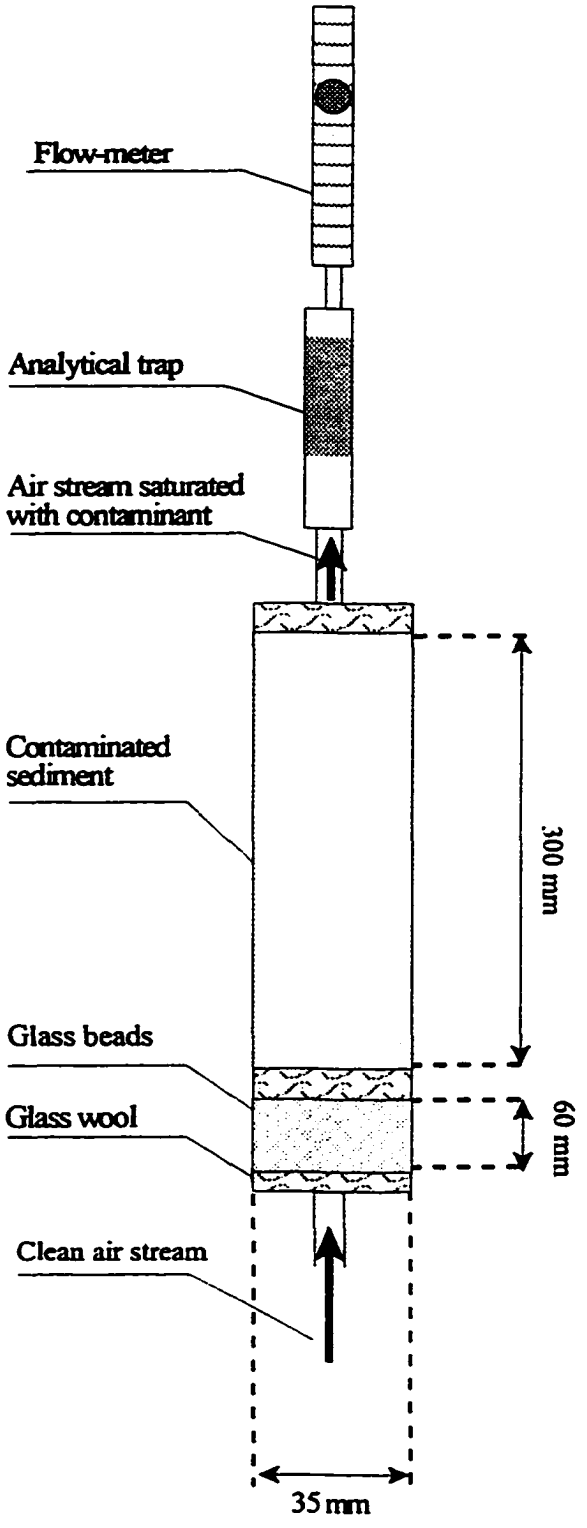

Figure 3.5 Schematic of a gas saturation column used to investigate the sediment/air partitioning of contaminants.

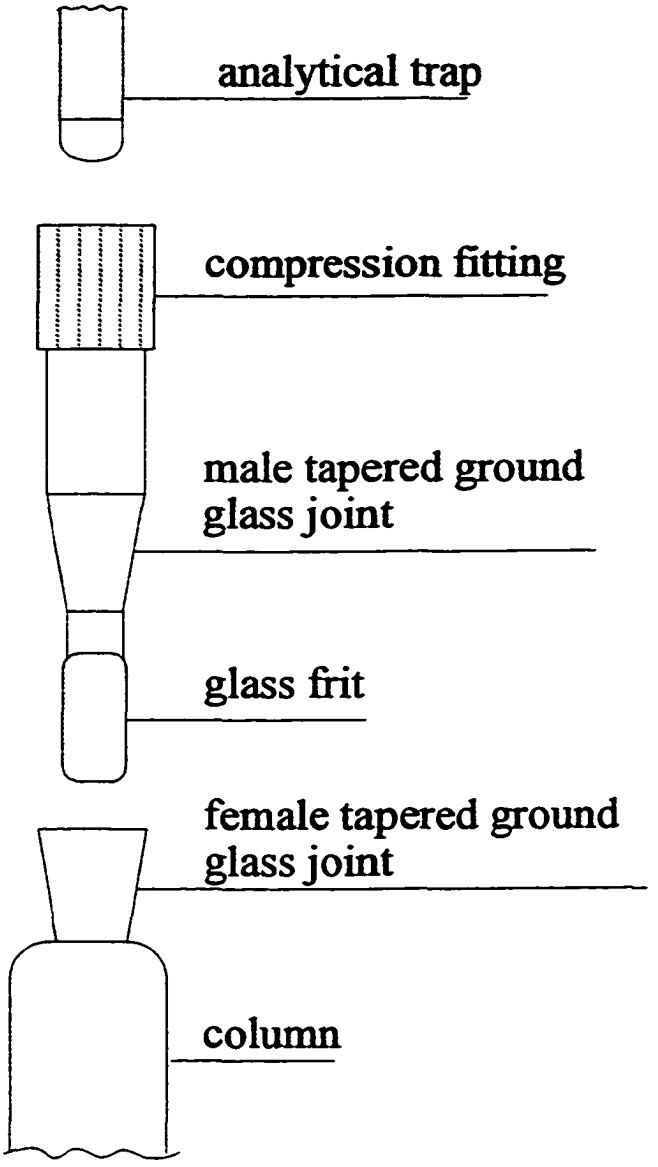

Figure 3.6 Schematic of the analytical trap holder fitted at the outlet of a gas saturation column.

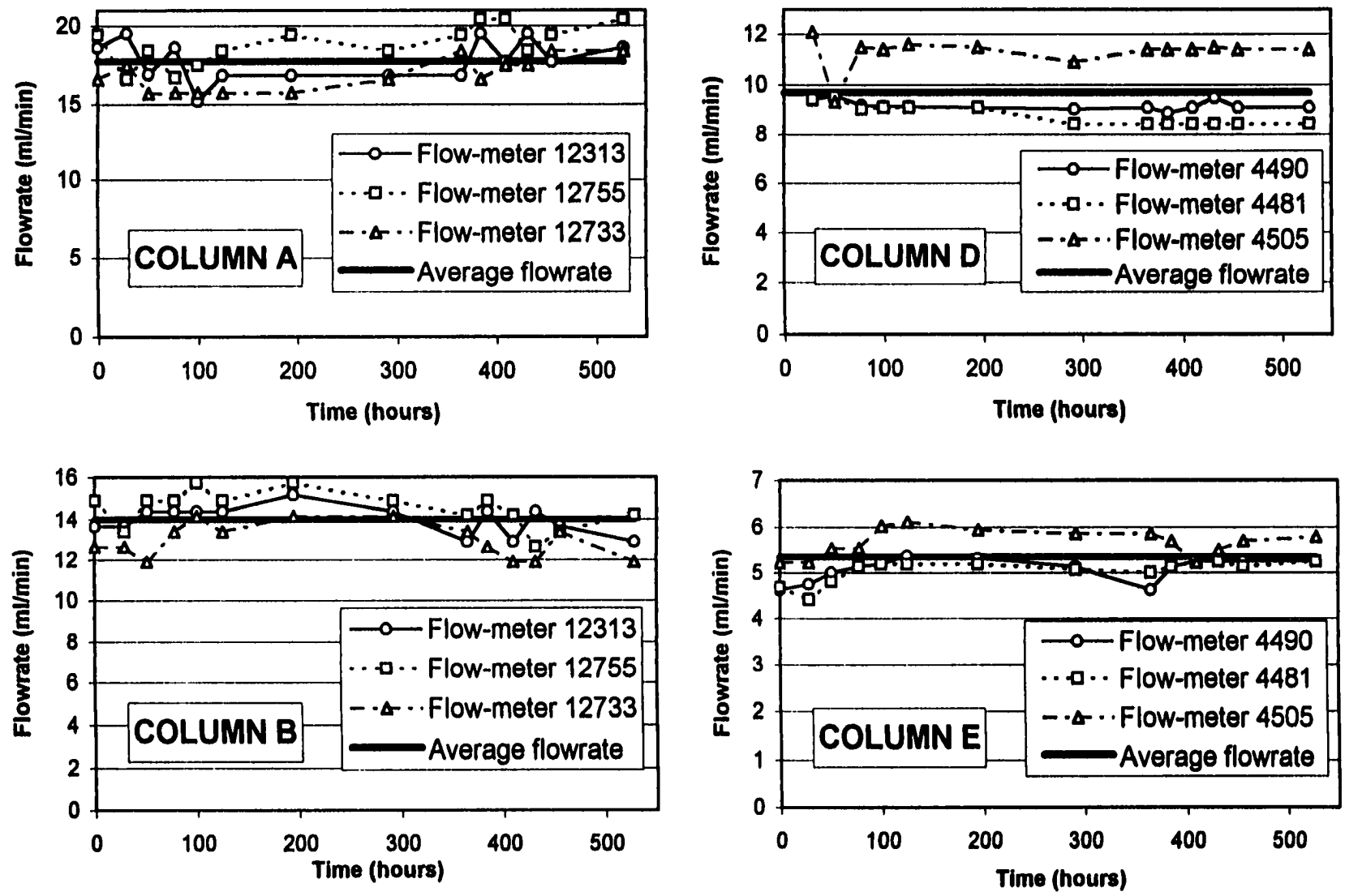

Figure 3.7 Profile of the air flowrate through sediment columns over the time of a desorption experiment.

(1-280ml/min). Reproducibility within each set of flow meter is good. Furthermore, flow rates can be kept steady even over long time experiments.

3.3.2 Vapor pressures determination

Some modifications were made to the set-up to conduct experiments aimed at determining saturated vapor pressures. Specific characteristics of the set up used for this purpose were the followings:

- Columns are 1.5cm in diameter and 20 cm in length. Crystals of the pure compound are supported by a bed of glass micro-beads (140-170μm in diameter). The length of this supporting bed can be varied in order to obtain the desired crystal bed length.
- An air stream at 0% RH is fed to the columns. Thus, only one mass-flow controller is required.

3.3.3 Water sorption isotherm

The modified set-up used to determine water sorption isotherms is shown in Figure 3.8. A stream of clean air is split into two streams. One is saturated to 100% relative humidity by passing through a gas-washing bottle filled with water; the other is dried to 0% RH by passing through a column filled with Drierite™. The dry and humid streams are then fed to two identical columns of sediment at a given moisture content to determine respectively the desorption and adsorption branches of the isotherm. The sediment bed is prepared in the same way as for partitioning experiments. Relative humidity and temperature are monitored at the outlet of the column using probes similar to the one described in 3.3.1.2.

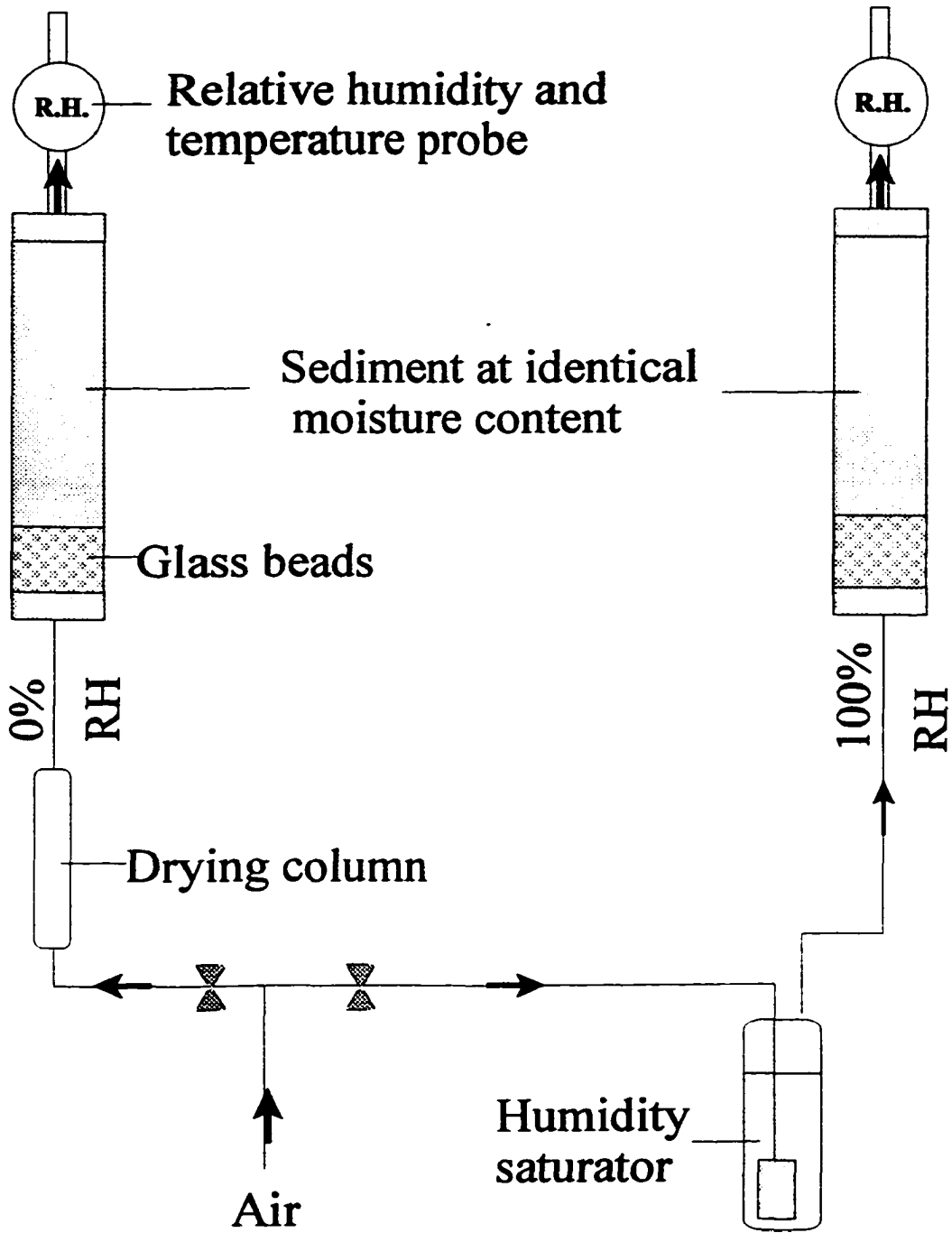

Figure 3.8 Schematic of the experimental setup used to determine the water sorption isotherm.

3.4 Sediment preparation

3.4.1 General preparation

Superficial layer sediment is collected from Campus Lake sediment (Louisiana State University, Baton Rouge) under about 4 feet of water. After collection, the sediment is coarse sieved through ¼ inch mesh to remove debris such as twigs, leaves and rocks. It is then passed through a 2 mm mesh sieve to leave only the sand, silt and clay fractions. GC-MS analysis of sediment extracts obtained by ultra-sonication do not show any trace of anthropogenic semi-volatile organic contaminant in this sediment.

3.4.2 Preparation of non-contaminated sediment

The sediment is dried on a tray at room temperature down to a moisture content of about 2.5%. It is then crushed and passed through a 1.68mm mesh sieve. In Appendix E, analysis of the data obtained by Puri et al., 1925 indicates that drying of a soil at a temperature as high as 130°C has no effect on its adsorptive properties. Thus, low moisture content sediment is prepared by drying under atmospheric pressure in an oven at 105°C for various periods of time. Higher moisture contents are reached by adding deionized water to the sediment. The moisture content is then homogenized by end-over-end tumbling in 2L polyethylene jars for at least 36 hours. Random sampling of sediment batches prepared in this fashion showed uniform moisture content.

3.4.3 Preparation of contaminated sediment

3.4.3.1 Choice of contamination characteristics

One objective of this project is to provide the data as input in volatilization models (Valsaraj et al., 1996, 1999). Thus, the characteristics of the sediment used in the present study were dictated by choices previously made in the volatilization project. The

compounds phenanthrene and dibenzofuran were selected. They are commonly found in contaminated sediments. Moreover, their vapor pressures are high enough to keep their experimental study practical. Contamination levels between about 10 and 150 mg/kg were chosen since this range of contamination is usually found in the field. Finally, the contaminants were spiked individually in different sediment batches. This does not correspond to field conditions. However, multiple contaminants could interact with one another and complicate the study of the mechanisms of sorption in sediments. For instance, Spencer and Cliath, 1972 observed that there was a small but detectable interaction between p,p'-DDT and o,p'-DDT sorbed in a soil.

3.4.3.2 Sterilization

The inoculated sediment batches had to be sterilized to prevent microbial degradation of the chemicals under study. Fletcher and Kaufman, 1980 studied the effect of several sterilization methods on the behavior of 3-chloroaniline in soil. They found that mercuric chloride addition, as opposed to other sterilization methods such as potassium azide did not enhance 3-chloroaniline volatilization from soils. Wolf et al., 1989 studied the effectiveness of various sterilization methods and their effect on soil physical and chemical properties. They showed that mercuric chloride, when added to soils at a loading of 500 mg/kg, totally eliminated microbial activity. Furthermore, mercuric chloride altered neither the specific surface area nor the cation exchange capacity of the soils studied. The pH increased by less than one pH unit. All these observations demonstrate that mercuric chloride is a potent antibiotic with minimal side effects. Thus, 500 mg/kg of mercuric chloride were added to inoculated sediment batches.

3.4.3.3 Inoculation

Researchers usually prepare dry contaminated sediment by adding the chemical dissolved in a volatile organic solvent (hexane) which is subsequently evaporated. This method was rejected in the present study for three reasons:

- The organic solvent may interact with the sediment organic matter and modify its physico-chemical properties.
- Organic solvents like hexane dissolve plasticizers, thus diminuating the use of plastic ware from the experimental protocol.
- In order to obtain dry sediment (moisture content lesser than 1%) the solvent evaporation should be done under dry atmosphere, which also complicates the preparation procedure.

Therefore, we developed a sediment inoculation method based on the procedure described by Thoma, 1994. The amount of contaminant required to reach the desired level of contamination is dissolved into a hexane solution and added to a clean 3.785L glass jar. While the jar is slowly rolled on its side, a nitrogen stream (Ultra pure Nitrogen, Grade 5.0 from BOC Gases) is directed into the jar to evaporate the hexane. When all of the hexane has evaporated, a thin coat of crystals is evenly distributed on the inner walls of the jar. Sediment slurry (about 50% moisture content) is then added in successive layers. The mercuric chloride solution is added in small increments between each layer. About 200 ml of headspace is left for mixing. The jar is finally sealed with Parafilm™ and duct tape and placed on a continuous axial tumbler for a period of four weeks. The sediment is subsequently dried on a tray at room temperature down to a moisture content

of about 2.5%. It is then crushed to pass a 1.68mm mesh sieve. High moisture content (wet) sediments are prepared in the same manner as uncontaminated sediments.

3.4.3.4 Drying

Low moisture contents (dry and damp sediments) are obtained by the following procedure. The sediment is mixed with Drierite™ chunks (4 mesh size) and tumbled end-over-end for about 48 hours. The Drierite™ is then sieved out and regenerated in an oven at 220°C for 5 hours, left to cool down in a dessicator and the procedure is repeated one more time. The Drierite™ is then left in the sediment for at least two weeks. The Drierite™ is sieved out at the time of sediment usage. By this method, sediment at moisture contents lower than 0.3% can be prepared. The method has the advantage of being very mild and simulates natural conditions causing sediment drying.

Sediment batches are protected from light while awaiting use to prevent photodegradation.

3.5 Sediment characterization

3.5.1 General characteristics

Methods used to determine the physical properties of the sediment are described in this section and summarized in Table 3.3.

3.5.1.1 Particle size distribution

Particle size analysis of the sediment was performed by the Wetland Biogeochemistry Institute of Louisiana State University, following the procedure described by Patrick, 1958. (The classification of soil minerals according to their size was presented in Table 2.1.)

Table 3.3 Properties of Campus Lake sediment crushed to pass a 1.68mm mesh sieve.

Property	Value
Bulk density (g/cm^3)[a]	2.66
Particle density (g/cm^3)[a]	1.19
Porosity[a]	0.55
Mineral fractions (%)[b]:	
Sand	20±4 (n=2)
Silt	61±4 (n=2)
Clay	18±0 (n=2)
Organic carbon fraction (%)[c]	3.0±0.1 (n=20)
CHN analysis[d]:	
Carbon (%)	2.26±0.2 (n=4)
Hydrogen (%)	0.49± 0.05 (n=4)
Nitrogen (%)	0.19±0.01 (n=4)

[a]by mercury porosimetry (section 3.5.3); [b]section 3.5.1.1; [c]by Residual ash method (section 3.5.1.2); [d]by CHN analyzer (section 3.5.1.2).

3.5.1.2 Organic carbon content

The organic carbon content of the sediment was determined by two different methods:

- Residual ash method. Cunningham, 1998 determined the organic carbon fraction of Campus Lake sediment by the residual ash method (Davis, 1974). Oven dried samples were placed in a furnace at 430°C for 24 hours. The weight loss is then divided by 1.724 (Van Bemmelen factor) to calculate the organic carbon fraction.
- CHN analyzer. The carbon, hydrogen and nitrogen content of the sediment were determined by the Department of Coastal Ecology of Louisiana State University,

using a Perkin Elmer 2400 Series II. The sediment samples were not treated with acid prior to analysis.

3.5.2 Specific surface area

The sediment surface area was determined by multi-point nitrogen adsorption following ASTM standard method D3663-92. This was conducted using an OMNISORB 360 BET apparatus (Coulter, Omicron Division, Hileah, FL). After calibration of the instrument, the surface area of ASTM standards # 8571 (alumina) and #8572 (silica-alumina) were measured. The values measured were respectively within 6 and 8% of the specified surface area.

Six samples dried overnight under vacuum (~10^{-2} torr) at temperatures ranging from 105°C to 330°C had a surface area of 7.9±1.1 m^2/g.

3.5.3 Mercury intrusion porosimetry

3.5.3.1 Pore volume distribution

The pore volume distribution was determined by mercury intrusion porosimetry by Micromeritics Laboratories (Norcross, Georgia) using an AutoPore III 9420 instrument. As seen in Figure 2.2, plate-like philosilicate particles, made of silica tetrahedra sheets, create slit-shaped pores when they stack up on one another. Thus, some authors (Gregg and Sing, 1982) have suggested that a parallel-wall pore model is appropriate to describe silicate materials. This suggests that the pore volume distribution should be reported as a function of pore width. However, in most cases, a cylinder-shaped pore of radius r will be equivalent to a slit-shaped pore of width w, provided that w=r. For instance, the two models predict identical observations with respect to the following three phenomena:

- According to Young-Laplace equation, the two shapes of pore require the same pressure to fill up with liquid. (Therefore, the two pore models can account for the same pore volume distribution).
- The two shapes also share the same volume over surface area ratio. (Therefore, the two pore models can also account for the same pore surface area distribution).
- Finally, according to Kelvin equation, capillary condensation occurs at the same partial pressure in both pores. (Therefore, the two pore models predict that capillary condensation in the sediment will occur at the same relative humidity).

Within the scope of this study, the two pore models are thus interchangeable. A cylindrical pore model is adopted here. The pore volume (cumulative and incremental) and pore surface area (cumulative) as a function of pore diameter are shown in Figure 3.9. The pore size distribution data is presented in Appendix F. Intrusion was stopped at a pressure of about 60000 psi, corresponding to pores having a diameter of 3nm. Only the larger micropores (diameter less than 4nm) are thus investigated by this method. Over the range of pore size considered, pores having diameter smaller than 50nm account for 91% of the surface area and 9% of the total pore volume. Pores having diameter smaller than 10nm account for 62% of the surface area and only 3% of the total pore volume. Thus, adsorption will be most important in mesopores (diameter between 4 and 100nm), especially at the lower end of the mesopore range. Given the trend of the surface area versus pore size distribution, we also expect adsorption to be significant in micropores. 60% of the total pore volume is found in macropores of 2 to 10μm diameter. In view of the particle size analysis of the sediment in Table 3.3, this volume certainly corresponds

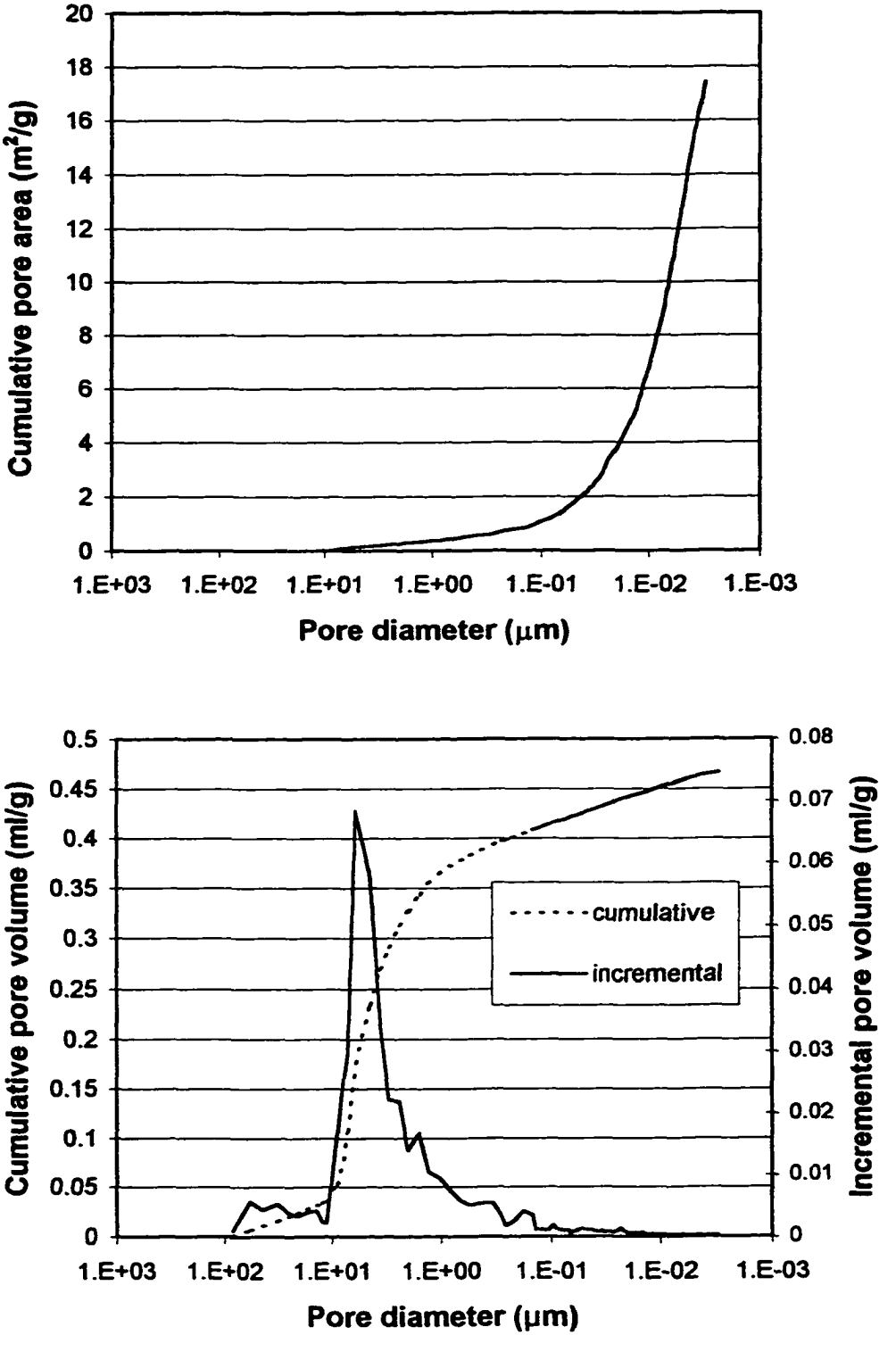

Figure 3.9 Pore volume distribution (bottom) and pore surface area distribution (top).

to inter-particle pores. The median pore diameter based on area is 7.6nm. The median pore diameter based on volume is 4.4 μm.

3.5.3.2 Surface area

By relating the work done to force a volume of mercury into the pore of a solid to the increase in mercury-solid interface, it is possible to calculate the solid surface area by integration of the mercury intrusion data. The surface area determined by mercury intrusion porosimetry is 17.4 m^2. This is higher than the nitrogen adsorption surface area. This result is not unusual and may be caused by either the presence of ink bottle pores or the sediment's compressibility (Rootare and Prenzlow, 1967).

3.6 Chemical analysis

Most of the analytical methods used in this project are described in the Quality Assurance Project Plan (Category IV) for the Project Entitled "Modeling Air Emissions of Volatile Organic Compounds from Contaminated Sediments and Dredged Materials" submitted to the Hazardous Substance Research Center, South/Southwest, Louisiana State University, May 1996. They are briefly recalled in this section along with analytical methods specific to the present study.

3.6.1 PAH analysis methods

3.6.1.1 Reagents

Reagents were purchased from Aldrich Chemical Company. Dibenzofuran 99+% (23 637-3), phenanthrene 98% (PI, 140-9) and pyrene 99% (18,551-5) were used as received for the following applications:

- Preparation of gas saturation columns used to determine saturated vapor pressures.
- Preparation of analytical standards.

- Sediment inoculation.

3.6.1.2 Equipment

Analyses were performed by liquid chromatography, using the equipment listed in Table 3.4.

Table 3.4 HPLC equipment.

Autosampler	Shimadzu Sil-9A
Liquid Chromatograph	Hewlett Packard 1090 L
Detector	Fluorescence Hewlett Packard 1046A
Precolumn	Phenomenex, Envirosep-pp 30mm x 3.20mm
Column	Phenomenex, Envirosep-pp 125mm x 3.20mm

3.6.1.3 Fluorescence detection

Optimal wavelengths for the detection of pyrene and phenanthrene by fluorescence are recommended by the manufacturer (Polynuclear Aromatic Hydrocarbons by HPLC, Application note, Hewlett Packard Co., 1993). Optimal wavelengths for the detection of dibenzofuran were determined in this study by the stop-flow method. Results are presented in Table 3.5.

Table 3.5 Optimal wavelengths for fluorescence detection..

	$\lambda_{excitation}$ (nm)	$\lambda_{emission}$ (nm)
Dibenzofuran	226	320
Phenanthrene	244	360
Pyrene	237	385

3.6.2 Air phase sample preparation

3.6.2.1 Analytical traps

At the outlet of a column, the gas stream containing the contaminant is passed through an analytical trap. Schematic of a trap is shown in Figure 3.10. The gas phase analysis method is based on NIOSH method 5506 (summarized in Supelco Bulletin 769F). The collection traps (tube Orbo-43 from Supelco) are filled with an adsorbent porous polymer designed for PAH analysis (Supelpak 20U (20/40)). The polymer bed in a trap is divided in a front (100mg) and back part (50mg). The front part traps the air contaminant and the back section is a control to make sure that no breakthrough occurred. The front section of a collection trap loaded with the contaminant is desorbed with 5 to 10ml of acetonitrile into a 20ml-scintillation vial. An aliquot of the extract is subsequently analyzed by liquid chromatography. The method features isocratic elution with the parameters summarized in Table 3.6.

Table 3.6 HPLC method used for the analysis of air phase samples.

Injected volume	25 µl
Eluent composition	Water: 20% Acetonitrile: 80%
Eluent flow rate	0.5 ml/min
Temperature	40°C

3.6.2.2 Control back traps

For each experiment, several back traps were selected for analysis to check for breakthrough. For experiments with sediment at moisture content higher than 1%, they always gave zero concentration. However, in the first experiment conducted with dry

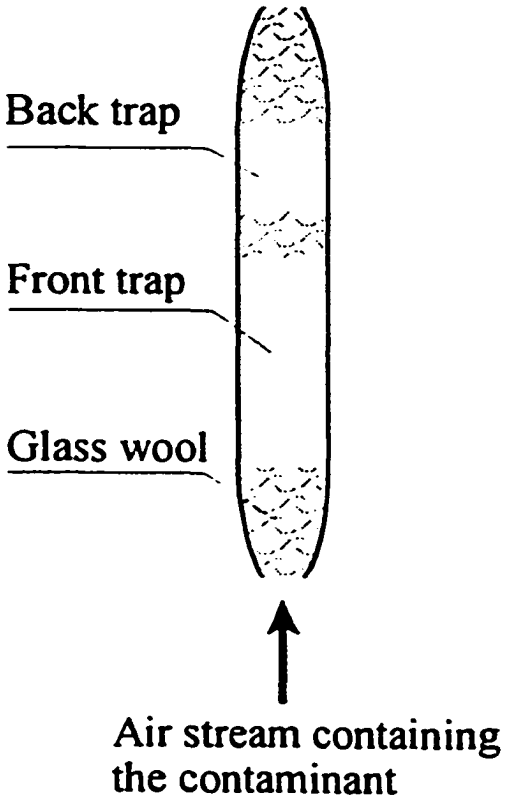

Figure 3.10 Schematic of a trap used for the determination of the air phase concentration.

sediment loaded with dibenzofuran, contamination of the back section of a few analytical traps was observed. This was probably caused by one or more of the following:

- Dibenzofuran vapor pressure is relatively high.
- The extensive duration of experiments conducted with dry sediment allows the contaminant to travel along the trap bed until it breaks through.

In order to overcome this problem, two traps were placed in series for all subsequent experiments conducted with dry sediment (involving dibenzofuran as well as phenanthrene). The back section of the second trap was analyzed separately and always gave zero concentration.

3.6.2.3 Desorption from traps

A. Recovery. A desorption recovery percentage was determined for each compound over the range of concentration of interest. Polymer beads from the front section of a trap were added to standard solutions containing the three analytes studied. After equilibration the supernatant was analyzed by HPLC. For each analyte, the ratio of the peak area obtained over the one obtained from the initial standard solution is the recovery factor. Results of the recovery test are summarized in Table 3.7.

Table 3.7 Desorption recovery of tubes ORBO 43.

Compound	Concentration range (ppb)	Recovery (%)	STDV (%)	n
Dibenzofuran	4-200	95	4	10
Phenanthrene	12-600	86	2	10
Pyrene	0.3-3	75	5	4

For each sample, the mass of chemical trapped was corrected using the recovery percentage.

B. Desorption time. Polymer beads from the front section of a trap were added to 9 vials filled with a mixed standard solution of each of the three analytes at about 15 ng/ml. Three sets of 3 samples were analyzed after equilibration times of respectively 30, 60 and 90 minutes. The recovery was identical each time. All samples were therefore desorbed for 30 minutes.

3.6.2.4 Trapping times and detection limits

An experiment must be pursued long enough so that an amount of PAH sufficient for quantitative analysis is trapped. The lowest air concentration measured in this study was 7 pg/L. This is the equilibrium concentration at 14°C of phenanthrene above a dry sediment contaminated at 127mg/kg. This particular experiment had to be carried out for 24 days in order to obtain a phenanthrene concentration in acetonitrile in the range of 0.15 to 0.6 ng/ml. The detector calibration chart for phenanthrene analysis in this range of concentration is shown in Figure 3.11. The response factor is plotted with its 95% confidence interval. The relative standard deviation on the slope of the response factor is 1.8%.

In an attempt to decrease the trapping time of experiments conducted with dry sediment, the set-up shown in Figure 3.12 was designed to concentrate the trap desorption solutions. The following procedure was tested on standard solutions and blank samples. A nitrogen stream from a cylinder (Ultra pure Nitrogen, Grade 5.0 from BOC Gases) is passed through an activated carbon cartridge and fed to an 8-port glass manifold. Needles fitted to each port of the manifold are punched in the Teflon™ septum of HPLC vials containing the solution to concentrate. A second needle ensures pressure equilibrium. After acetonitrile is evaporated down to about 1ml, vials can be directly

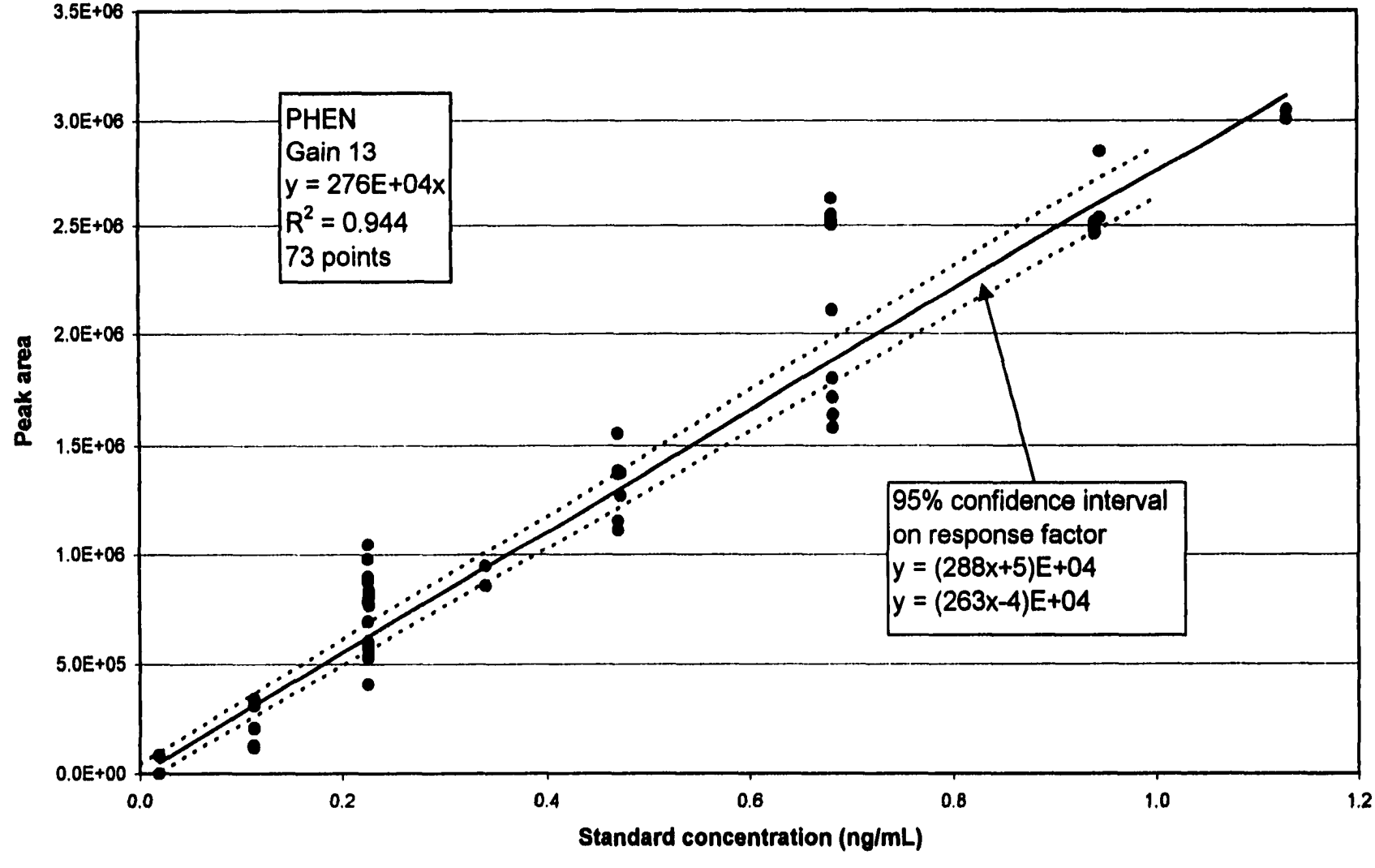

Figure 3.11 Calibration chart for phenanthrene fluorescence detection at gain 13.

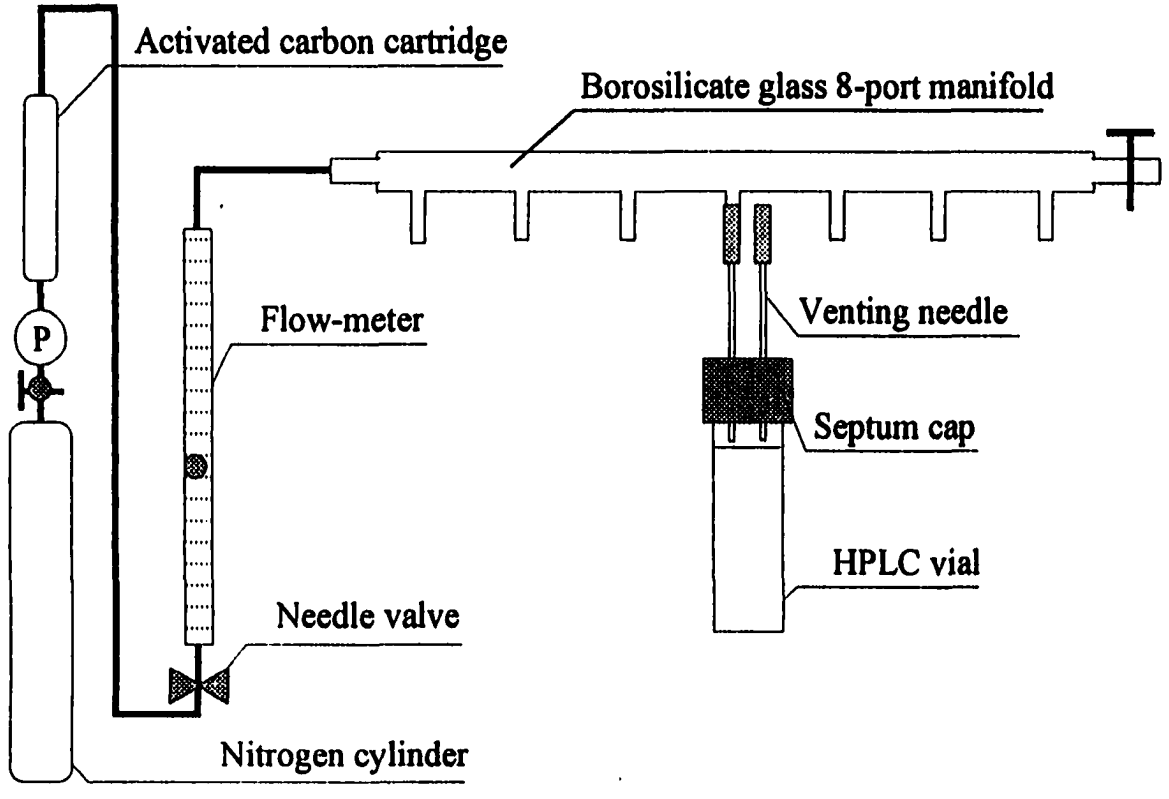

Figure 3.12 Schematic of the apparatus designed to concentrate extracts from the analytical traps.

placed in the HPLC autosampler, thus minimizing sample handling. The concentration factor is determined by weighing. Unfortunately, despite the precautions taken, this procedure introduced contamination in all the samples processed during the method test. The contamination introduced in blank acetonitrile samples corresponded to an initial phenanthrene concentration of 35 to 50 pg/mL. Although fairly low, this level of contamination defeated the purpose of the procedure, which was therefore never used. It is believed that contamination originated from the laboratory background concentration. In fact, a phenanthrene trace concentration was detected in the laboratory air (Ravikrishna, 1997). Furthermore, the hood in which the apparatus was set up had been previously used for tasks involving high concentrations of phenanthrene.

3.6.2.5 Reproducibility

In each experiment, the reproducibility of the air phase analysis was ascertained by doing the following things:

- Three or more identically prepared columns were run simultaneously.
- For each column, multiple samples of the air phase were taken over time.

3.6.2.6 Accuracy

Accuracy of the air phase analysis was ascertained by doing the following things:

- For each experiment, the effect on the air phase concentration of a change in bed length or air flow rate was monitored (see section 3.2.4.1).
- As a preliminary experiment, the vapor pressures of pyrene, phenanthrene and dibenzofuran were measured and compared to values found in the literature.

3.6.3 Sediment phase sample preparation

3.6.3.1 Moisture content

Several studies have demonstrated the ambiguity of the definition of a dry soil (Puri et al., 1925; Orchiston, 1953, 1954). It was observed in this work that the mass of crushed samples of Campus Lake sediment placed in an oven at 105°C stabilizes after about 100 hours. An example is shown in Figure 3.13. On the basis of this observation, samples moisture content was measured by drying at 105°C for exactly five days.

3.6.3.2 Contaminant

Pollutant concentration in the sediment was determined by ultrasonic extraction followed by HPLC separation and fluorescence detection. The extraction method was based on EPA SW-846 method 3550A. About 2g of sediment are mixed with roughly 20g of cleaned sodium sulfate in a 120ml glass jar. 60ml of a 50/50 mixture of acetone/hexanes are added to the jar, which is then sonicated (Cole Parmer 8852 sonicator) for 45 minutes. The jar is then stored in a refrigerator for about two days to allow particles to settle down. Finally, a 2ml aliquot of the extract is transferred to a test tube and the solvent is exchanged to acetonitrile by nitrogen blowdown.

The recovery of the method was assessed by processing spiked samples of clean sediment. Samples were prepared in the manner described above for sediment phase analysis, except that clean sediment was used and the 50/50 acetone/hexanes mixture was replaced by phenanthrene/dibenzofuran standards in 50/50 acetone/hexane. Four concentrations of phenanthrene and dibenzofuran were tested, in duplicates, corresponding to sediment concentrations of about 10, 30, 60 and 90 mg/kg. In order to assess the recovery of the nitrogen blow-down step alone, the same standard solutions in

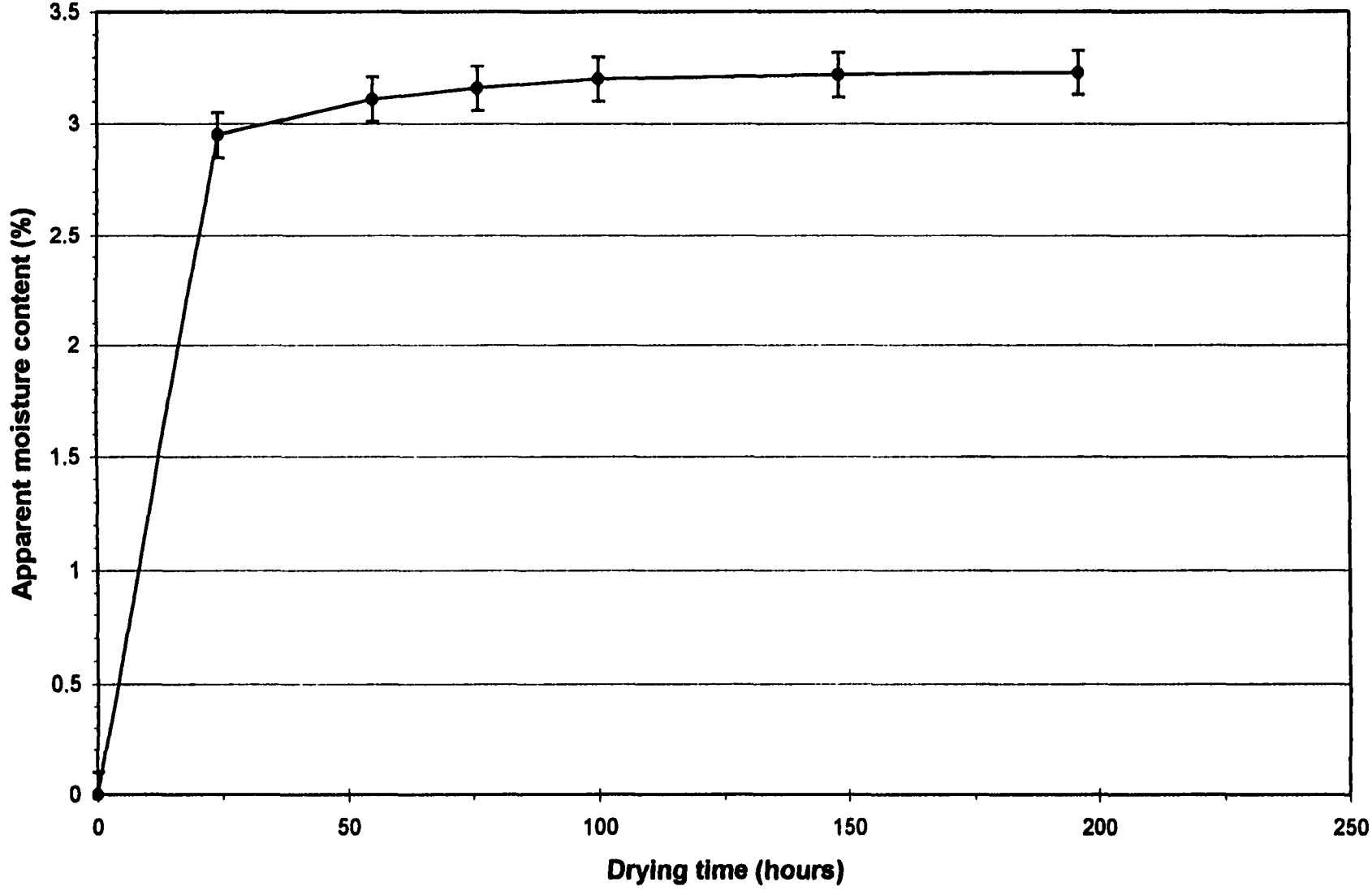

Figure 3.13 Apparent moisture content of Campus Lake sediment samples drying in an oven at 105°C.

hexane/acetone were exchanged to acetonitrile. The recovery percentage for both tests versus the initial acetone/hexane standard concentration is plotted in Figure 3.14. For both chemicals, the recovery of the extraction followed by the solvent exchange step is virtually identical to the recovery of the solvent exchange step alone. This indicates that the ultra-sonication extraction mobilizes virtually all the chemical present in the sediment. Losses occur during the nitrogen blow-down step alone. For dibenzofuran, the recovery of the whole procedure varies from 35±3% at the lowest concentration tested to 48±2% at the highest concentration. For phenanthrene, the recovery is 77±2% at the lowest concentration and 102±4% at higher concentrations. For each sample, the recovery factor was interpolated to calculate the initial sediment concentration.

The low value of the recovery factor of dibenzofuran and its sensitivity to the initial sediment concentration are problematic. They can harm the reproducibility of the analytical procedure. Thus, the solvent exchange step was eliminated. A 300 μL aliquot of the acetone/hexanes extract was diluted with acetonitrile to 3 mL and anlayzed directly by HPLC. Samples prepared in this fashion were 10 time less concentrated than solvent-exchanged samples but could be analyzed using the sensitive fluorescence detector.

All samples in acetonitrile were analyzed by HPLC using a concentration gradient. The method characteristics are listed in Table 3.8.

Samples of contaminated sediment were analyzed before loading the columns. After an experiment, two sediment samples from the top of each column were analyzed for pollutant content. Pollutant concentrations in these samples were always identical to the original sediment batches within experimental uncertainty.

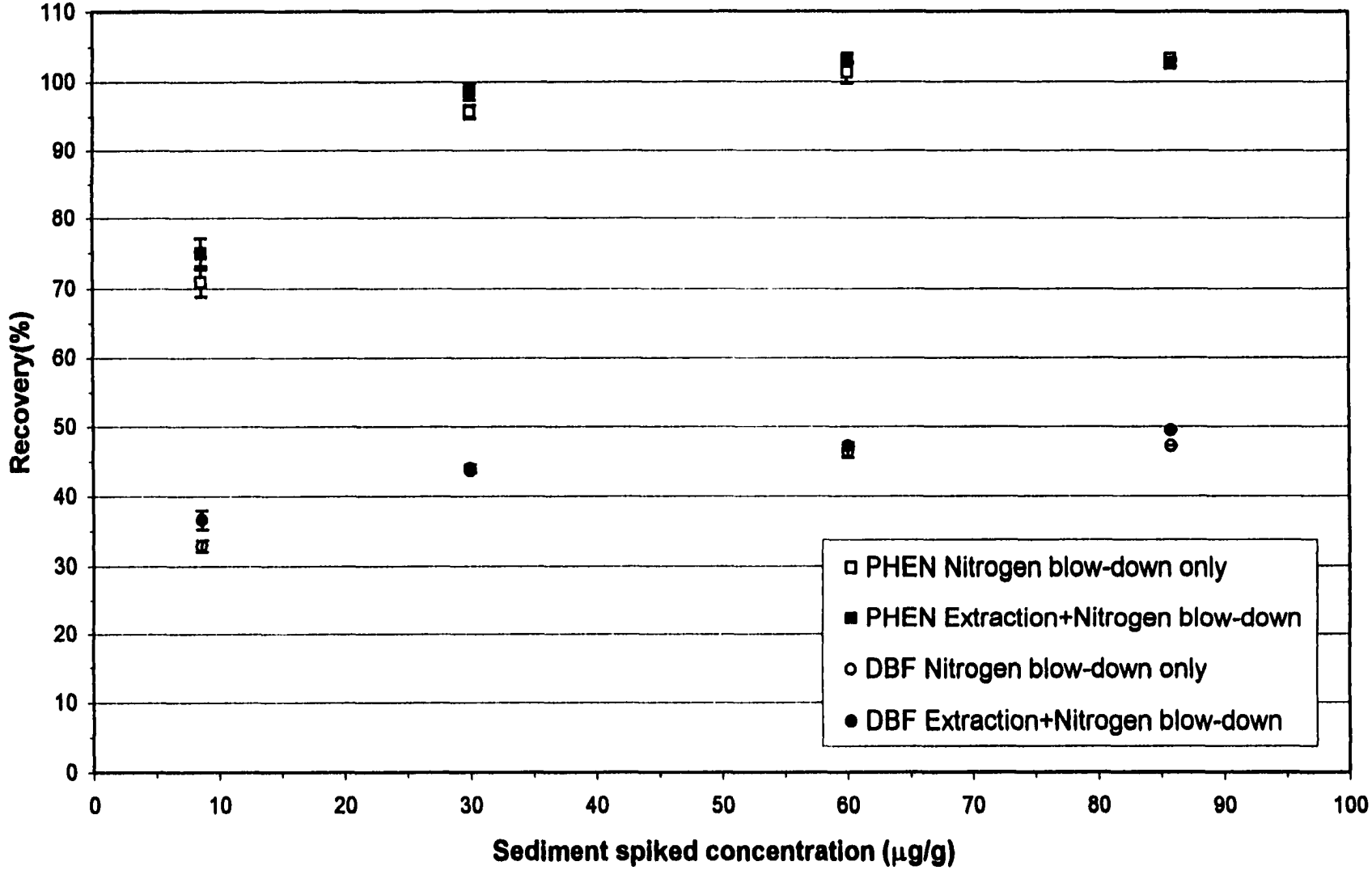

Figure 3.14 Recovery of the sediment extraction and the solvent exchange procedures.

Table 3.8 HPLC method used for the analysis of sediment phase samples.

Injection	25 µL
Temperature	40°C
Eluent composition	Acetonitrile/Water
Eluent Flowrate	0.5 mL/min
Concentration gradient	
Time (minutes)	Acetonitrile/Water
0	55/45
3	55/45
27	100/0

Chapter 4
Results and Discussion

In the first section of this chapter, the vapor pressures of pyrene, phenanthrene and dibenzofuran are measured. These experiments had two motivations:

- Values of the vapor pressures of semi-volatile organic compounds determined by different researchers often vary significantly, even when similar experimental techniques are used. Thus, it was necessary to determine values specific to the experimental method used in this study, to serve as references in the subsequent investigation of contaminated sediments.
- The comparison of the experimental values of vapor pressures and heat of sublimation to values reported in the literature provides a test of both the gas saturation apparatus and the analytical procedure.

Subsequently, in section 4.2 the isotherm of water sorption on Campus Lake sediment is determined. This was required for two reasons:

- In order to study the partitioning of contaminants in dry, damp and moist sediments, it was necessary to determine the moisture content corresponding to each region as well as the humidity of the air stream that would be in equilibrium in each case.
- In conjunction with the pore volume distribution, the sorption isotherm provides information on the physical state of water in the sediment. This information is required to assess the relative importance of the different mechanisms of contaminant sorption.

Finally, in section 4.3, the partial pressures of phenanthrene and dibenzofuran in equilibrium with contaminated sediments are measured. Different sediment moisture

contents and temperatures are investigated. A model for the partition coefficient is then proposed in section 4.4.

4.1 Saturated vapor pressures

4.1.1 Literature review

Delle Site, 1997 reviewed vapor pressure values found in the literature for phenanthrene and pyrene, among other environmentally significant organic chemicals. Also, the vapor pressure of phenanthrene obtained during an inter-laboratory evaluation of the gas saturation technique is reported in the ASTM method E 1194-87. The few available studies on dibenzofuran vapor pressures were also reviewed. Average values (± std) of vapor pressures obtained in experimental studies are presented in Table 4.1.

Table 4.1 Review of experimental values of the saturated vapor pressures at 25°C of dibenzofuran, phenanthrene and pyrene (mPa).

Reference/Review	method†	DBF	PHEN	PYR
Delle Site, 1997 (8 studies reviewed)	GS and E		31.3±28.8	
ASTM E 1194-87 Interlab Evaluation	GS		16.0±5.8	
Delle Site, 1997 (6 studies reviewed)	GS and E			1.07±1.00
Rodorf, 1989	GS	351		
Chirico et al., 1990	C	331		
Sato et al., 1986	GS	466±8		
Hansen and Eckert, 1986	GS	276±17		
Average of the 4 above studies.	GS and C	356±80		

†GS: Gas Saturation, E: Effusion, C: Calorimetry

The differences between the experimental studies reviewed lead to a fairly high degree of uncertainty on the average values of the vapor pressures. For instance, the relative standard deviation on the data reviewed by Delle Sitte, 1997 is almost 100% both for pyrene and for phenanthrene. This called for an independent experimental determination of the vapor pressures in the present study.

4.1.2 Experimental results

4.1.2.1 Validity of experimental results

For each compound, it was ensured that the outlet partial pressure was not affected when the superficial velocity varied by a factor of at least two. In addition, the effect of the crystal bed length was assessed in experiments with phenanthrene. Pyrene and dibenzofuran concentrations at 25°C in the column outlet air stream are plotted as a function of air superficial velocity in Figure 4.1. Phenanthrene concentration in the column outlet air stream is plotted as a function of air superficial velocity and for different bed lengths, at 14, 25 and 35°C in Figure 4.2. Sampling time did not affect the air concentrations, indicating that the outlet stream was equilibrated. Furthermore, it is apparent that:

- Phenanthrene outlet concentration is independent of the bed length.
- Air velocity shows no influence on the outlet concentration of the three chemicals within experimental uncertainty.

As explained in section 3.2.4.1, the first observation conclusively demonstrates that the measured concentration of phenanthrene is the saturated concentration. In the same section it was shown that the second observation is not as conclusive. However, according to ASTM method E 1194-87 it is enough to ascertain that the air stream has

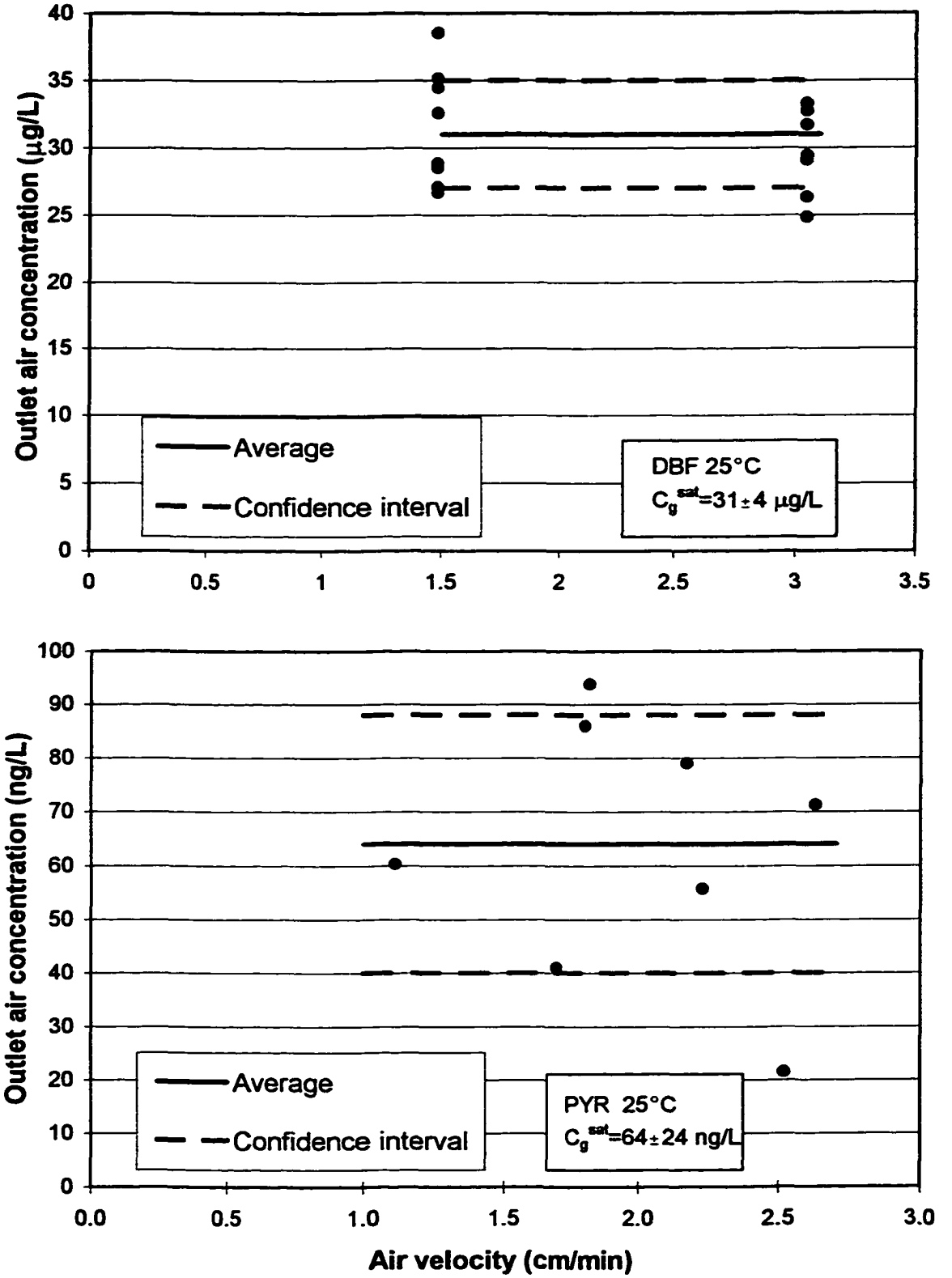

Figure 4.1 Assessment of the air phase equilibrium in dibenzofuran (top) and pyrene (bottom) saturated vapor pressure experiments.

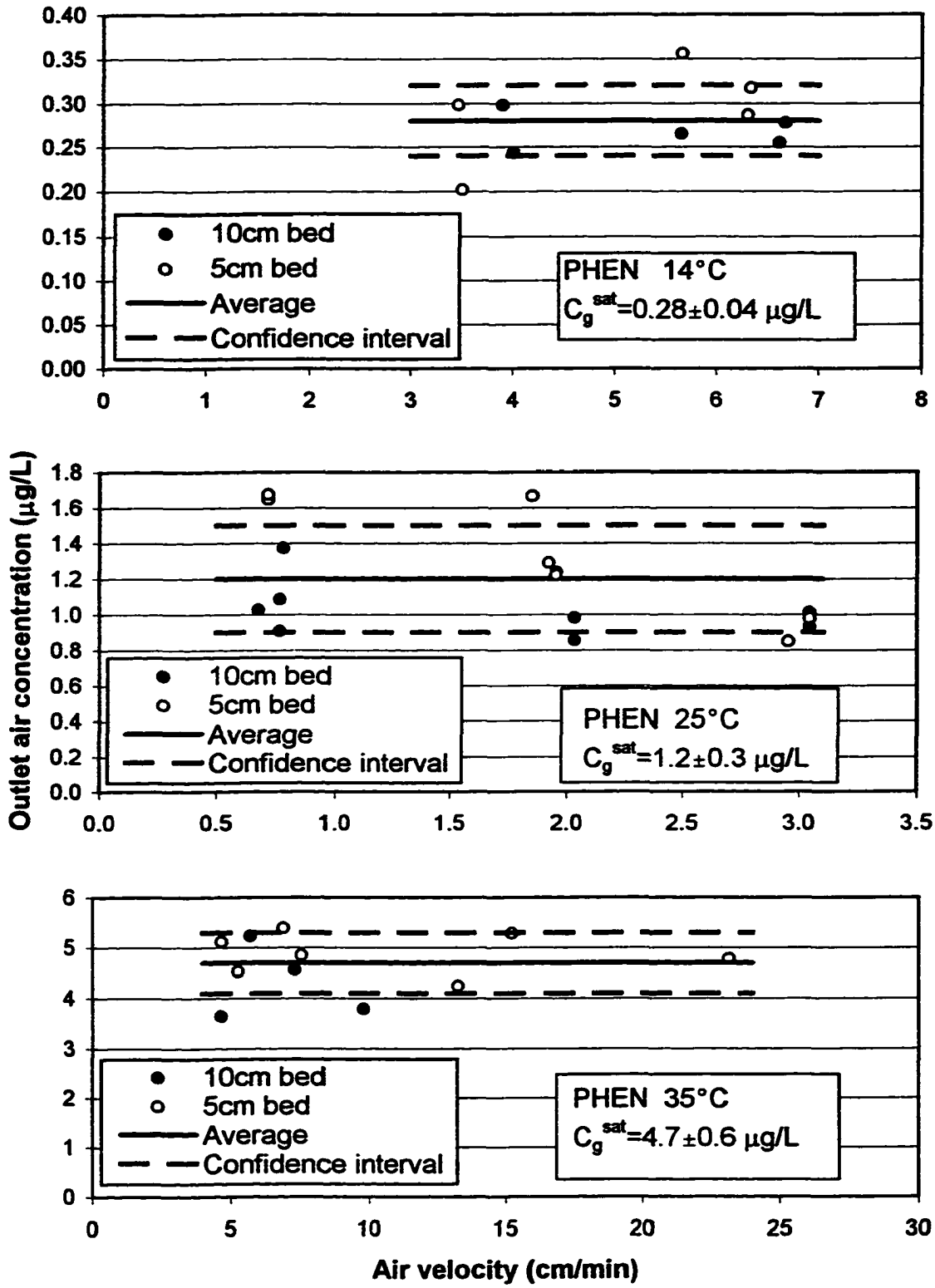

Figure 4.2 Assessment of the air phase equilibrium in phenanthrene saturated vapor pressure experiments.

reached saturation at the outlet of a gas saturation column. Furthermore, the experimental conditions were adequate to generate a saturated stream in the case of phenanthrene. The mass transfer coefficient, the axial dispersion coefficient and the porosity are expected to be similar whether a column is loaded with phenanthrene, pyrene or dibenzofuran crystals. Therefore, equation (3.12) predicts that, experimental conditions adequate to produce an air stream saturated with phenanthrene should also be adequate to generate air streams saturated with pyrene or dibenzofuran. The standard errors on the determinations of pyrene, phenanthrene and dibenzofuran saturated concentrations at 25°C were respectively: 37%, 25% and 13%. The high value obtained for pyrene has two causes:

- Pyrene saturated concentration is the lowest of the measured concentrations.
- The pyrene experiment was conducted before mass flow controllers were added to the setup. The regulation of the flow rate was thus not as accurate as in experiments conducted with the two other compounds.

4.1.2.2 Pyrene, phenanthrene and dibenzofuran vapor pressures at 25°C

Pyrene, phenanthrene and dibenzofuran saturated air concentrations were measured at 25.0±0.7°C. The results were converted into vapor pressures, using the ideal gas law. A summary of the experimental results is presented in Table 4.2. Experimental values determined in this study are in good agreement with values reported in Table 4.1. Furthermore, the estimated standard deviation within laboratories (average of the repeatability found in separate laboratories) on phenanthrene vapor pressure, determined during the inter-laboratory test reported in ASTM method E 1194-87, is 3.6 mPa. This is close to the standard deviation obtained in this study: 4.0 mPa.

Table 4.2 Experimental saturated vapor concentrations/pressures of dibenzofuran, phenanthrene, and pyrene.

	Saturated vapor concentration (ng/L)/pressure (mPa)									Enthalpy of sublimation	
	14°C			25°C			35°C			$\Delta H_{sublimation}$ (kJ/mol)	r^2
	C_g^{sat}(±std)	P^{sat}(±std)	n†	C_g^{sat}(±std)	P^{sat} (±std)	n	C_g^{sat}(±std)	P^{sat}(±std)	n		
DBF				31±4	429±54	16					
PHEN	0.28±0.04	3.75±0.5	14	1.2±0.3	16.3±4.0	16	4.7±0.6	67.5±8.6	11	101±3	0.971
PYR				0.06±0.02	0.73±0.33	8					

† n= number of replicates

The thermodynamic property of interest to model the adsorption of semi-volatile organic compounds is the subcooled vapor pressure, P_L^{sat} rather than the solid state vapor pressure, P_S^{sat} (see Appendix B). The two vapor pressures are related. Prausnitz et al., 1986 derived the relation linking the fugacity of the subcooled liquid to the fugacity of the solid phase. Making the simplifications that they suggest and replacing fugacities by partial pressures (which is acceptable for semi-volatile organic compounds), the following expression is obtained:

$$P_L^{sat} = P_s^{sat} \exp\left[\frac{\Delta H_{fus}}{RT_m}\left(\frac{T_m}{T} - 1\right)\right] \qquad (4.1)$$

Where:

- T_m is the melting temperature.
- ΔH_{fus} is the enthalpy of fusion at the melting temperature.

Using equation (4.1), subcooled vapor pressures values were calculated from the experimentally determined solid state vapor pressures. They are listed in Table 4.3.

Table 4.3 Calculation of subcooled liquid saturated vapor pressures.

	DBF	PHEN
P_S^{sat} (mPa)†	429	16
T_{melt}(°C)*	360	372
ΔH_{fus}(kJ/mol)*	20	16
P_L^{sat} (mPa)	1681	59

†Measured in this study
* Mackay et al., 1992

4.1.2.3 Phenanthrene heat of sublimation

Phenanthrene vapor pressure was determined at two other temperatures (14.0±0.7°C and 35.0±0.2°C). Results of these experiments are presented in Table 4.2. In Figure 4.3 the experimental results obtained in this study are plotted in the form of the Clausius-Clapeyron equation. On the same figure are plotted other experimental values determined with the gas saturation technique by various researchers. The experimental data fit the Clausius-Clapeyron equation very well (r^2 = 0.998), which allows the calculation of the heat of sublimation, $\Delta H_{sublimation}$: 101±4 kJ/mol. This compares well with the overall average heat of sublimation determined in the reviewed studies: 91±8 kJ/mol.

As explained in Appendix B, in adsorption studies of semi-volatile organic compounds, the heat of vaporization from the subcooled liquid is considered more useful than the heat of sublimation. The heat of vaporization from the subcooled liquid at 25°C may be calculated from a simple thermodynamic cycle: $\Delta H_{vaporization}(T) = \Delta H_{sublimation}(T) - [\Delta C_P (T_t - T)] - \Delta H_{fus}(T_t)$. Where T_t is the triple point temperature and ΔC_P is the difference of heat capacity between the solid and the subcooled liquid. ΔC_P is assumed constant betweeen T and T_t. Using values of the physical parameters recommended by Daubert and Danner, 1995, a heat of vaporization at 25°C of 84±3 kJ/mol is calculated from the experimental heat of sublimation. This is higher than the value of 77 kJ/mol compiled by the same authors for the heat of vaporization. However, the relative difference between the two values is similar to the relative difference between experimental and reviewed values of the heat of sublimation.

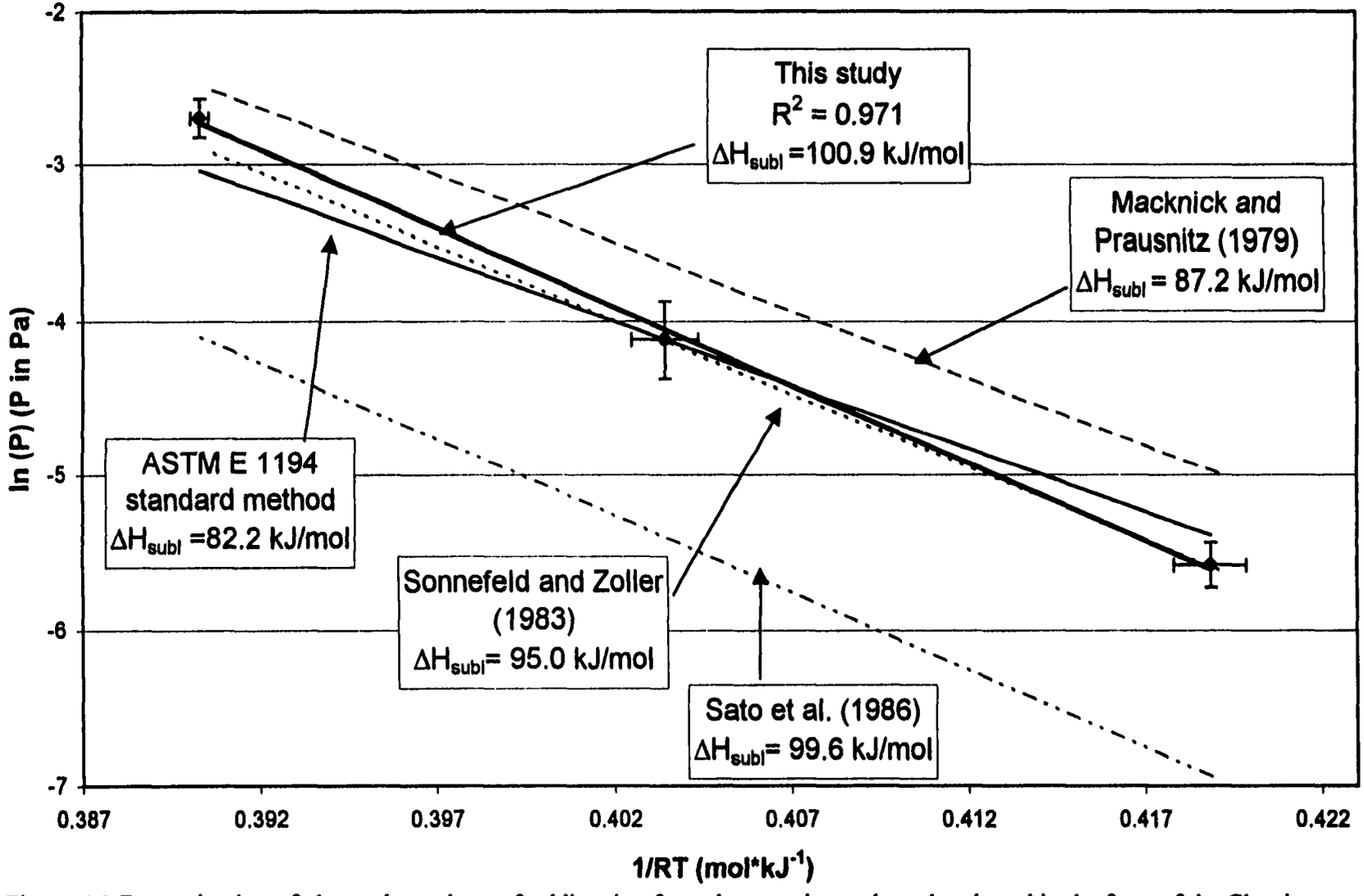

Figure 4.3 Determination of phenanthrene heat of sublimation from the experimental results plotted in the form of the Clausius-Clapeyron equation.

4.1.2.4 Summary

It was possible to generate and measure satisfactorily saturated vapor pressures in the range of 0.7 mPa to 430 mPa. The experimental protocol also permitted the accurate investigation of temperature effects.

4.2 Water sorption on sediment

4.2.1 Experimental results

4.2.1.1 Validation of experimental results

As detailed in section 3.2.4.2, investigation of the adsorption (or desorption) equilibrium of a fairly volatile compound (water) by the gas equilibration technique has associated concerns. The bed length and the air velocity must allow the relative humidity in the air phase to be in equilibrium with the sediment at the outlet of the column. Moreover, the progressive change of the sediment phase concentration eventually modifies the outlet air concentration. Thus, one must ensure that measurement is taken before breakthrough has occurred. Therefore, to ensure that the outlet air was truly at equilibrium, the stream was monitored over time.

As an example, Figure 4.4 shows the relative air humidity monitored over time at the outlet of two columns both filled with sediment at 1.8% moisture content and fed respectively with air at 0 and 99+% relative humidity. After a brief transitory period, corresponding to the replacement of the air in the top of the column and in the probe chamber, the air humidity becomes steady at the outlet of both columns. The steadiness of the humidity in the outlet air stream indicates that it is equilibrated with sediment moisture. The equilibrium value is maintained until breakthrough occurs. The horizontal

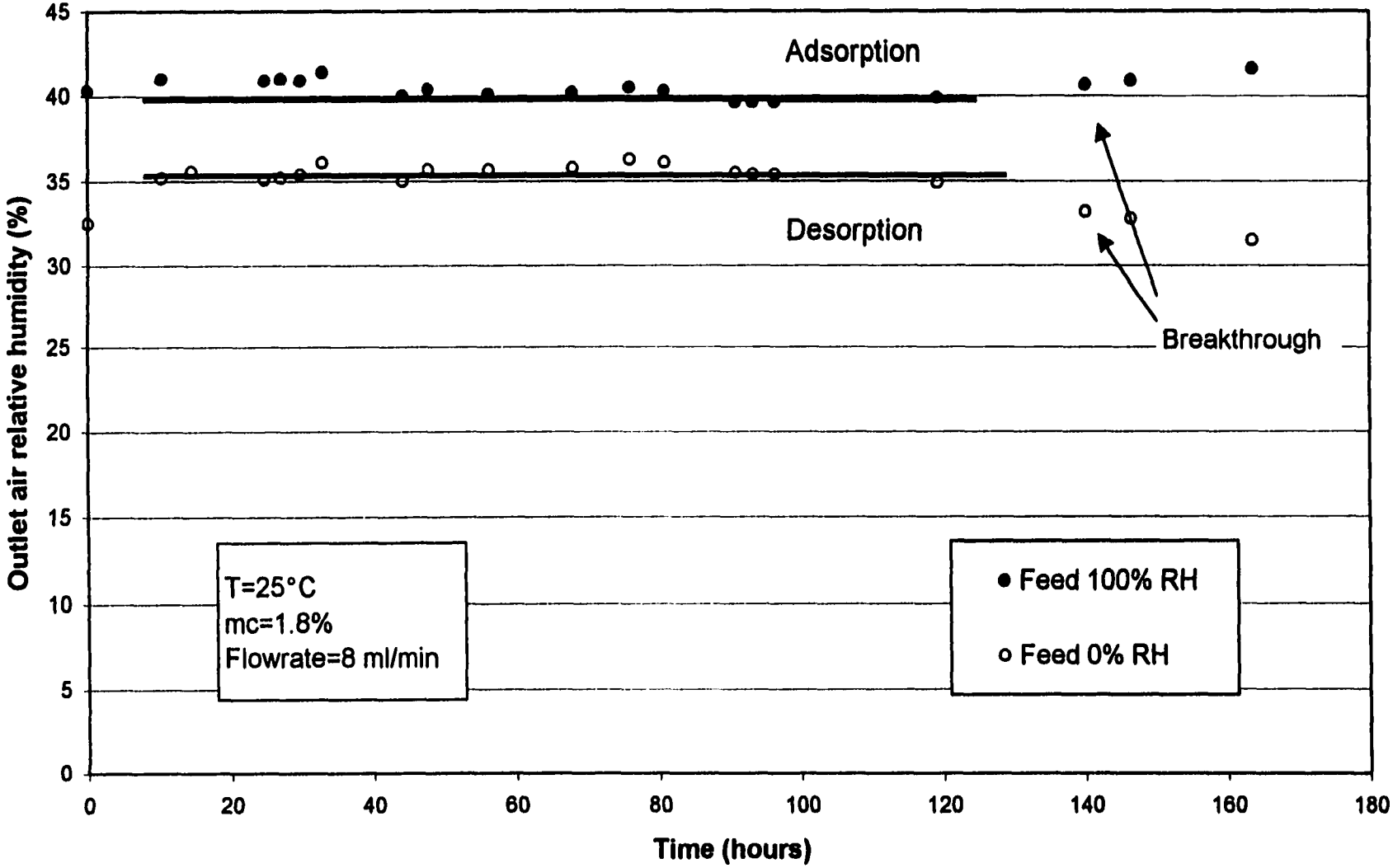

Figure 4.4 Evolution of the outlet air relative humidity over time during a water adsorption/desorption experiment.

lines define the plateau length over which the data is averaged to obtain the equilibrium air humidity.

Additionally, in some experiments, the air superficial velocity was varied in the range of 0.2 to 2 cm/min. This had no effect on the outlet air humidity.

Finally, the adsorption experiment with a sediment at 1.18% moisture content was conducted with two different bed lengths (15 and 30 cm). The two corresponding data points are indicated on the experimental isotherm of water sorption plotted in Figure 4.5. The outlet air humidity was virtually identical in both cases.

For the three mentioned reasons, it is safe to conclude that the values of the air humidity reported are equilibrium ones.

4.2.1.2 Experimental sorption isotherms

The experimental isotherms of water adsorption and desorption are plotted on Figure 4.5. (The error bars represent the accuracy of the RH probes specified in section 3.3.1.2.) It is to be noted that water sorption on the sediment exhibits hysteresis. Even though very narrow, the loop is clearly demonstrated in the three experiments that were carried out with two columns in parallel using the setup shown in Figure 3.9. The relative humidity of the air in equilibrium with a sediment at a given moisture content is lower when the equilibrium is reached by drying (feed at 0% RH) than when it is reached by wetting the sediment (feed at 99+% RH). This is equivalent to saying that the moisture content of sediment in equilibrium with air at a given relative humidity is higher when the equilibrium is reached by drying than when it is reached by wetting.

This hysteresis phenomenon has been observed by several authors, for water adsorption on sediments (Puri et al., 1925), clays (Orchiston, 1954) and silica gel (Naono

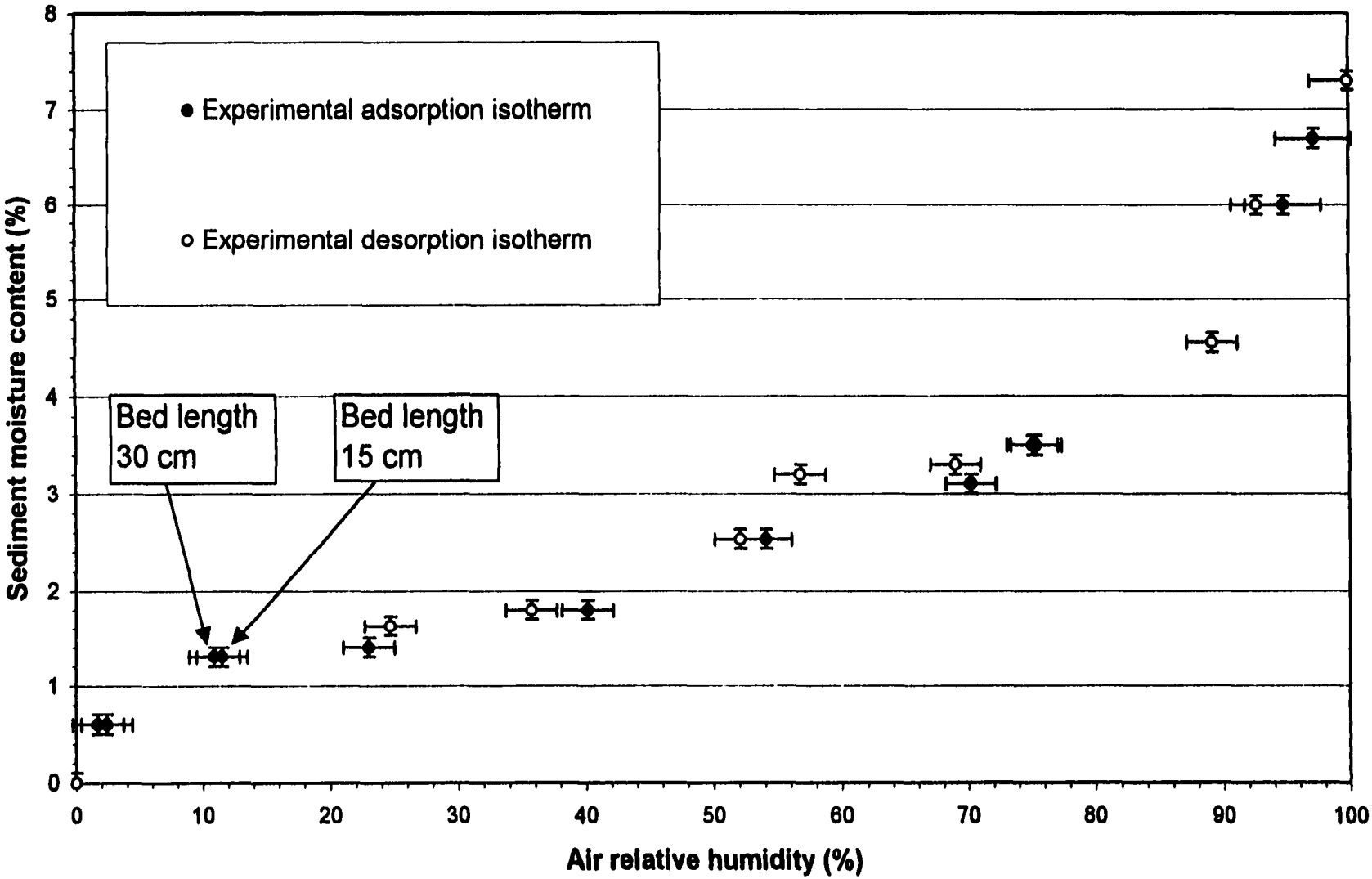

Figure 4.5 Experimental isotherms of water sorption on Campus Lake sediment.

and Hakuman, 1993). Gregg and Sing, 1982 reviewed several models of condensation/evaporation in pores of various shapes that support hysteresis. The general thought is that hysteresis results from condensation and evaporation not occurring as exact reverses of one another. Condensation occurs on the water film adsorbed on the pore walls when the pressure reaches the value given by Kelvin equation. The water film serves to nucleate the condensation process. On the other hand, evaporation is a continuous process. The condensed water phase is present from the beginning of the process and no nucleation step is involved.

4.2.2 Conventional BET model analysis

The conventional BET isotherm in the transformed form (Adamson, 1990) was applied for the region of relative humidity below 30%.

$$\frac{1}{mc}\left(\frac{RH}{1-RH}\right)=\frac{1}{B_w mc_m}+\frac{(B_w-1)}{B_w mc_m}RH \qquad (4.2)$$

Where:

- mc is the sediment moisture content expressed on a mass basis.
- mc_m is the moisture content corresponding to a monomolecular layer of water covering the entire surface area of the sediment.
- RH is the air relative humidity. $RH=P_w/P_w^\circ$, where P_w and P_w° are respectively the equilibrium partial pressure and the vapor pressure of water at the temperature of the experiment.
- $B_w=\exp[(\Delta H_{cond} - \Delta H_{adso})/RT]$, where ΔH_{cond} and ΔH_{adso} are respectively the enthalpy of condensation and the enthalpy of adsorption on the sediment surface of water.

Equation (4.2) is plotted in Figure 4.6. A good correlation is observed ($r^2 = 0.984$) and the two characteristic BET parameters are:

- B_w=53±30
- mc_m=1.24±0.09%.

For comparison, some values of B_w and mc_m reported in the literature are presented in Table 4.4.

Table 4.4 Values of the BET parameters for the adsorption of water on soils and soil components reported in the literature.

Soil or soil component	mc_m (%)	B_w	Reference
Campus Lake sediment	1.2	53	This work
Natural montmorillonite	1.3	21	Orchiston, 1954
Silty soil	1.17	37	Chiou and Shoup, 1985
5 different soils	0.6 -1.9	15-30	Calculated in Appendix E from data in Puri et al., 1925

The value of B_w determined in this study is slightly higher than those reviewed. However, differences from one study to another should be considered within the uncertainty inherent in the determination of this parameter.

The value of mc_m determined in this study is in the range of values reported in the literature.

The integral heat of adsorption of water on sediment, ΔH_{adso} can be calculated from the value of B_w: $\Delta H_{adso} = \Delta H_{cond} + RT\ln B_w$. Given that ΔH_{cond}= -37.8kJ/mol this equation gives ΔH_{adso}= -47.6±1.4kJ/mol. It is to be noticed that the relative standard error is much smaller than on B_w.

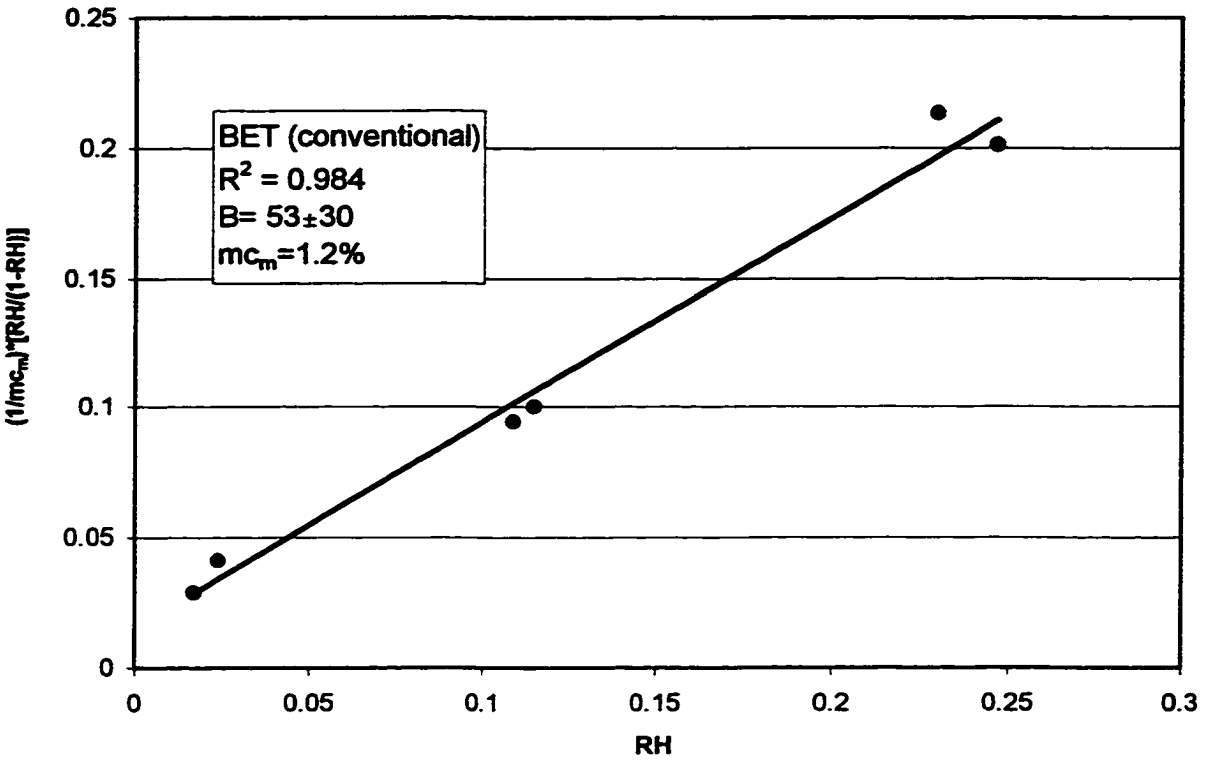

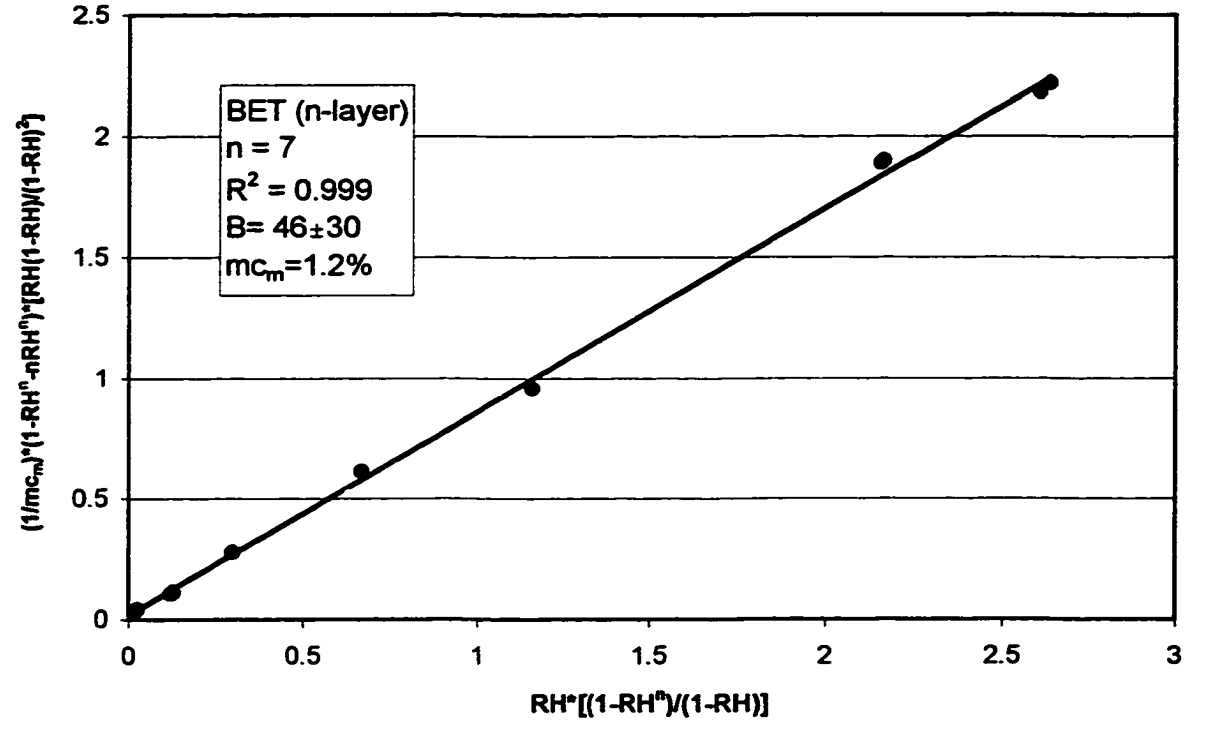

Fig 4.6 Conventional (top) and finite layer (bottom) BET plots of water adsorption onto Campus Lake sediment.

Literature values of the space occupied by a single adsorbed water molecule varies from $10.8 \times 10^{-20} m^2$ (Livingston 1949, Orchiston 1953) to $12.2 \times 10^{-20} m^2$ (Ferguson and Wade, 1967). This suggests a monolayer surface coverage of 40 to 45 m^2/g with mc_m=1.24%. This is higher than the surface areas determined by either nitrogen BET adsorption or mercury porosimetry. Such a result indicates that perhaps the sediment contains predominantly smectite clay (montmorillonite, illite). The smectite clays lattice has the property of being expandable as polar molecules (water) slip in between two tetrahedral silica sheets. Thus water adsorption would indicate a surface area much higher than the outer surface area of the clay crystal.

The water adsorption isotherm predicted by the BET model, using the two parameters calculated, is plotted in Figure 4.7 along with the experimental isotherm. The model over predicts the sediment moisture content for relative humidity >50%. This is expected since the model assumes adsorption on a non-porous surface, on which an infinite number of water layers can condense. In a porous solid like a sediment, however, the number of water layers is limited by the pores size, which results in a lower moisture content in the intermediate to high range of relative humidity (Jaycock and Parfitt, 1981; Adamson, 1990).

4.2.3 Finite layer BET model analysis

A simple way to take the sediment porosity into account is to use a modified BET model which assumes that, due to a lack of space, the number of water layers, n, that can adsorb on top of the monolayer is finite. The mathematical expression for the isotherm using this model is given in Appendix B (equation (B.1)). The linearized form of (B.1) is:

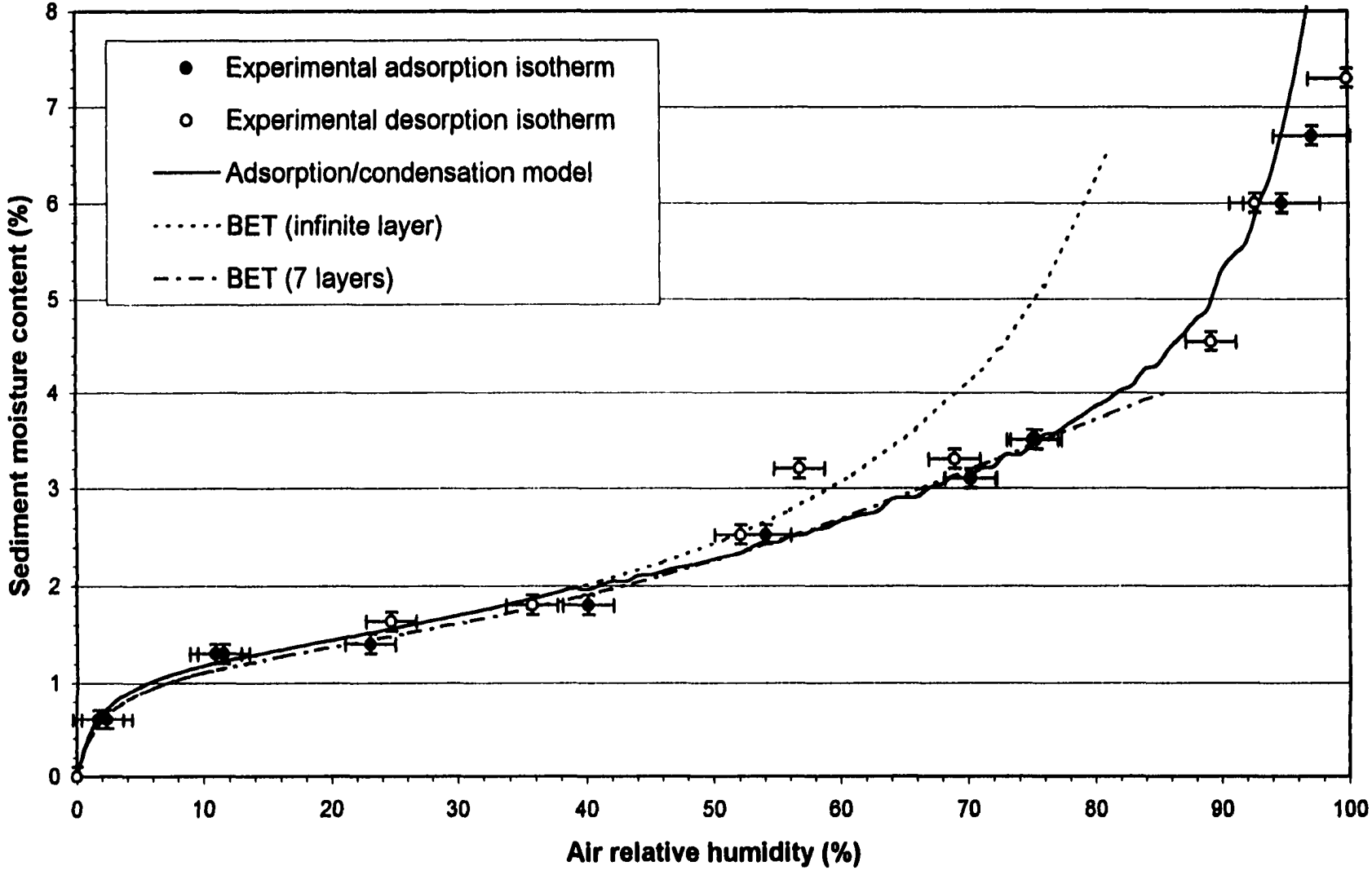

Figure 4.7 Isotherm models of water sorption on Campus Lake sediment.

$$\frac{Z}{mc} = \frac{1}{B_w mc_m} + \frac{Y}{mc_m} \tag{4.3}$$

Where:

$$Z = \frac{RH}{1-RH}\left[1 - RH^n - nRH^n(1-RH)\right] \tag{4.4}$$

and

$$Y = \frac{RH\left(1-RH^n\right)}{1-RH} \tag{4.5}$$

As shown in Figure 4.6, this model fits the experimental points below 70% RH very well ($r^2 = 0.999$). The three parameters obtained were:

- $B_w = 46 \pm 30$
- $mc_m = 1.19 \pm 0.03\%$
- $n = 7$

The fitted model curve is also plotted on Figure 4.7. The values of B_w and mc_m are similar to the ones obtained from the classical BET equation. This is expected since their physical meaning is identical in either one of the BET models. The parameter n gives insight on the sediment pore structure if the following assumptions are made:

- The sediment pore surface area accounts for the major fraction of the total surface area.
- All the pores have the shape of parallel walls slits of identical width and varying length.

With these assumptions the process of adsorption can be said to stop when pores are filled up, which happens when the thickness of the adsorbed water layer equals half the pore width. Thus, the value of n allows the calculation of the pore width: $w = 2n\delta$, where δ is the average thickness of a monomolecular water layer. Dividing the average volume of a water molecule in bulk liquid state by the surface area in the adsorbed state yields $\delta = 3x10^{-10}$ m, which is the value commonly used (Pashley, 1980, Hoff et al., 1993). Thus, a value $n = 7$ gives $w = 4.2$ nm. This agrees with the median pore width of 3.8 nm based on surface area determined by mercury intrusion (see section 3.5.3.1).

The fit of the three parameter BET model to experimental data points is good up to about 75% RH. Above this value, the sediment moisture content is severely under predicted by the model. This is the result of the assumption of a unique pore without consideration of larger pores. Mercury intrusion, however, reveals that pores of width larger than 1μm comprise 60% of the total sediment pore volume. At high relative humidity water condenses in the larger pores, which causes sediment moisture content to increase dramatically.

4.2.4 Development of an adsorption/condensation isotherm model

Neither of the BET models can account for the experimental water sorption isotherm over the whole range of relative humidity because they fail to account for the porous nature of the solid in a realistic manner. To overcome this limitation, an isotherm model was developed that simultaneously considers both adsorption and condensation of water. The calculations are based on analyses of the adsorption/condensation phenomena made by several authors in order to determine the pore size distribution from nitrogen

sorption isotherms. Gregg and Sing, 1982 have summarized these approaches. The "t-plot analysis" is one example of such analyses.

In the model developed here, adsorption is evaluated using the classical BET model. As condensation progresses the monolayer capacity of the soil is continuously adjusted to account for the surface area lost in pores filled with water. The pore volume distribution determined by mercury intrusion is used to evaluate condensation. More precisely, the isotherm is calculated step by step according to the following procedure:

Initially, the BET parameters characterizing the sediment surface, B_w and mc^0_m, are determined from experimental points at RH below 30%. Construction of the isotherm starts at RH=0%. For a small increase of relative humidity from RH^{i-1} to RH^i,

(i) The amount of adsorbed water, mc^i_{BET}, is calculated by the classical BET model.

(ii) The average statistical number of adsorbed water layers, θ^i is calculated by: $\theta^i = mc^i_{BET} / mc^{i-1}_m$

(iii) The critical capillary radius, r^i_K , for condensation to occur at RH^i is calculated from Kelvin equation: $r^i_K = -2\gamma V/RT\ln(RH^i)$ where γ is water surface tension and V the vapor phase molar volume. (The model could also assume parallel-wall pores).

(iv) The actual sediment pore radius in which condensation occurs, r^i_c , is obtained by adding to r^i_K the thickness of the adsorbed water layer: $r^i_c = r^i_K + \theta^i e$ where e is the thickness of one molecular layer of water.

(v) The total pore volume in which water has already condensed, when capillaries of radius r^i_c begin to fill up, is retrieved from the pore volume distribution data table. This gives the amount of condensed water: mc^i_{cond}

(vi) The surface area lost for adsorption because it is covered by condensed water is retrieved from the pore volume distribution data. This gives the surface still available for adsorption, A^i. The monolayer capacity can then be recalculated: $mc^i_m = mc^0_m(A^i/A^0)$ where A^0 is the water free sediment surface area.

(vii) The total sediment moisture content is calculated: $mc^i = mc^i_{BET} + mc^i_{cond}$

It is noted in section 4.2.2 that the surface areas determined by mercury intrusion and water adsorption do not match. Despite this discrepancy, in step (vii) we use the mercury intrusion data to calculate the reduction of surface area available for water adsorption caused by condensation. More precisely, we assume that the fraction of surface area lost to water adsorption, $F(r_c)$, when water condenses in pores of radius smaller than r_c is the same as the fraction of surface area determined to be in pores of radius smaller than r_c by mercury porosimetry. The new moisture content equivalent to an adsorbed monomolecular layer, mc^i_m, is then calculated as: $mc^i_m=[1-F(r_c)]\cdot mc^0_m$. This approximation is justified if the pore structure presents the two following characteristics:

- The pores accessible exclusively to water molecules open onto larger pores accessible to mercury.
- The water-accessible pore openings are uniformly located on the surface of mercury-accessible pores.

It is easy to imagine a pore model featuring these two characteristics. The simplified pore model represented in Figure 4.8 is an example. In this figure the walls of pores that are accessible only to water are represented by hatched lines. In such a pore structure, the water accessible surface is proportional to the mercury accessible surface.

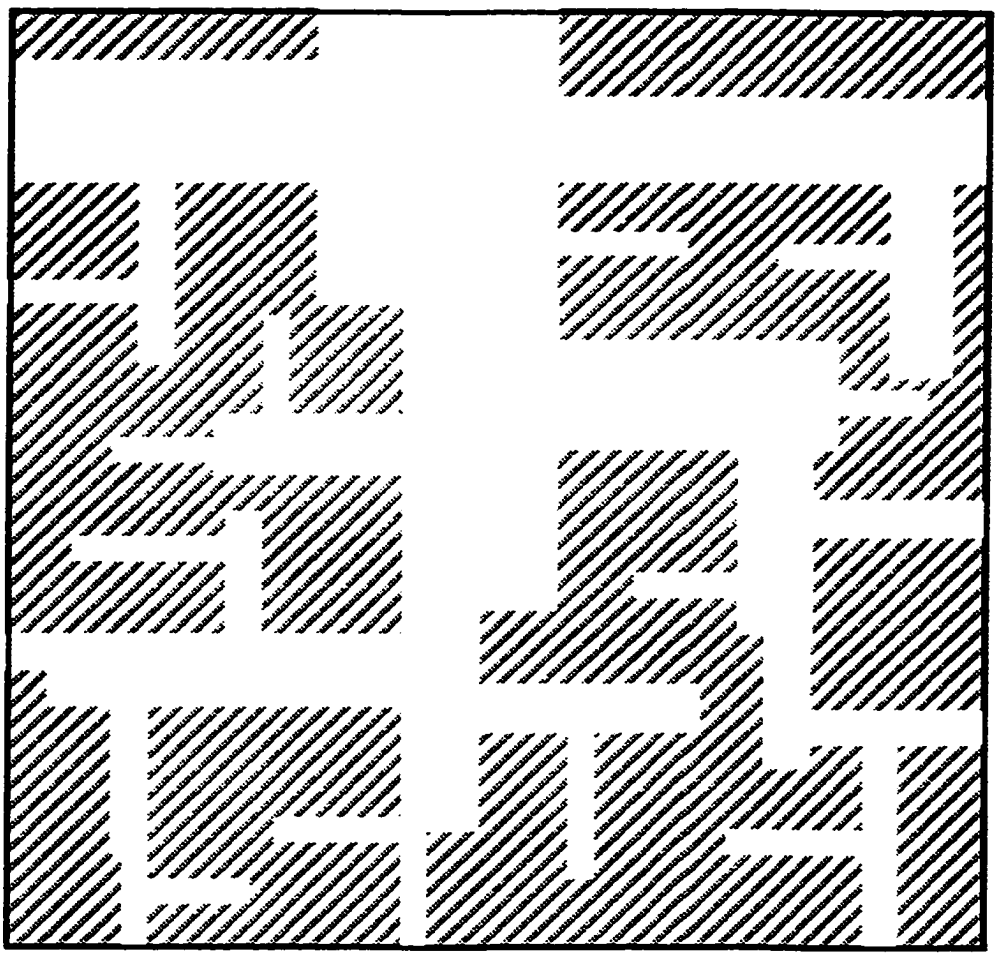

Figure 4.8 Hypothetical pore structure supporting the adsorption/condensation model.

The adsorption/condensation model is also plotted on Figure 4.7. The observed waviness of the curve is caused by the discrete nature of the pore volume distribution analysis. The model shows a remarkable agreement with the experimental sorption isotherm over virtually the whole range of relative humidity.

4.2.5 Nature and area of sediment exposed surfaces

The close agreement between the adsorption/condensation model and the experimental observations suggests that perhaps the physical phenomena invoked in its development are accurately described. In this case the unitary mechanisms which are summed up to calculate the total moisture content can be evaluated individually. It is thus possible to determine the water-free sediment surface area, the water film surface area and the condensed water volume, at any relative humidity. Estimation of these three quantities is valuable because they are needed to understand the mechanisms of contaminant uptake by the sediment.

- Condensed water is defined as the water found in pores of radius smaller than the critical condensation radius calculated by the Kelvin equation. The condensed water volume is directly calculated in the isotherm construction procedure.
- The condensation free sediment surface area is also calculated in the isotherm construction procedure.
- The fraction of surface area covered by adsorbed water can be calculated from the BET model by the formula established by Hill, 1946b:

$$1-\frac{A^0}{A}=\frac{B_w\left(\frac{mc}{mc_m}+1\right)-\left[\left(1-\frac{mc}{mc_m}\right)^2 B_w^{\,2}+4\frac{mc}{mc_m}B_w\right]^{\frac{1}{2}}}{2(B_w-1)} \qquad (4.6)$$

Where:

-A is the sediment surface area available for adsorption (condensation-free).

-A^0 is the water free sediment surface area.

The results of the computation are shown in Figure 4.9. The model predicts that the water free sediment surface area decreases dramatically between 0 and 10% RH. At 15% RH (corresponding to about 1.3% mc), 90% of the sediment surface area is covered by a water film. It is interesting to note that at 1.2% mc, which is the amount of water corresponding to uniform monolayer coverage of the sediment surface, more than 10% of the sediment surface area is actually still free of water. This discrepancy between statistical and actual sediment water coverage would be even wider for lower values of B_w that are commonly found in soils and sediments. The water film extends until about 35% RH (corresponding to about 1.8% mc), at which point capillary condensation begins and the film starts to shrink. The shrinkage continues until all pores are filled and the adsorbed water film ceases to exist when relative humidity approaches 100%.

From the same model the extent of the three moisture regimes can also be determined. Thibodeaux, 1996 defined a dry soil particle as a particle in which less than 5% of the adsorptive surface is covered by water. Between 5 and 95% of surface coverage the soil is considered damp and above 95% the soil is said wet. According to this scale, it appears from Figure 4.9 that Campus Lake sediment can only be considered dry below a tenth of a percent of moisture content. The damp region extends up to about 1.5% moisture content, corresponding to about 25% RH. From 1.5% moisture content, up to complete saturation, the sediment is wet.

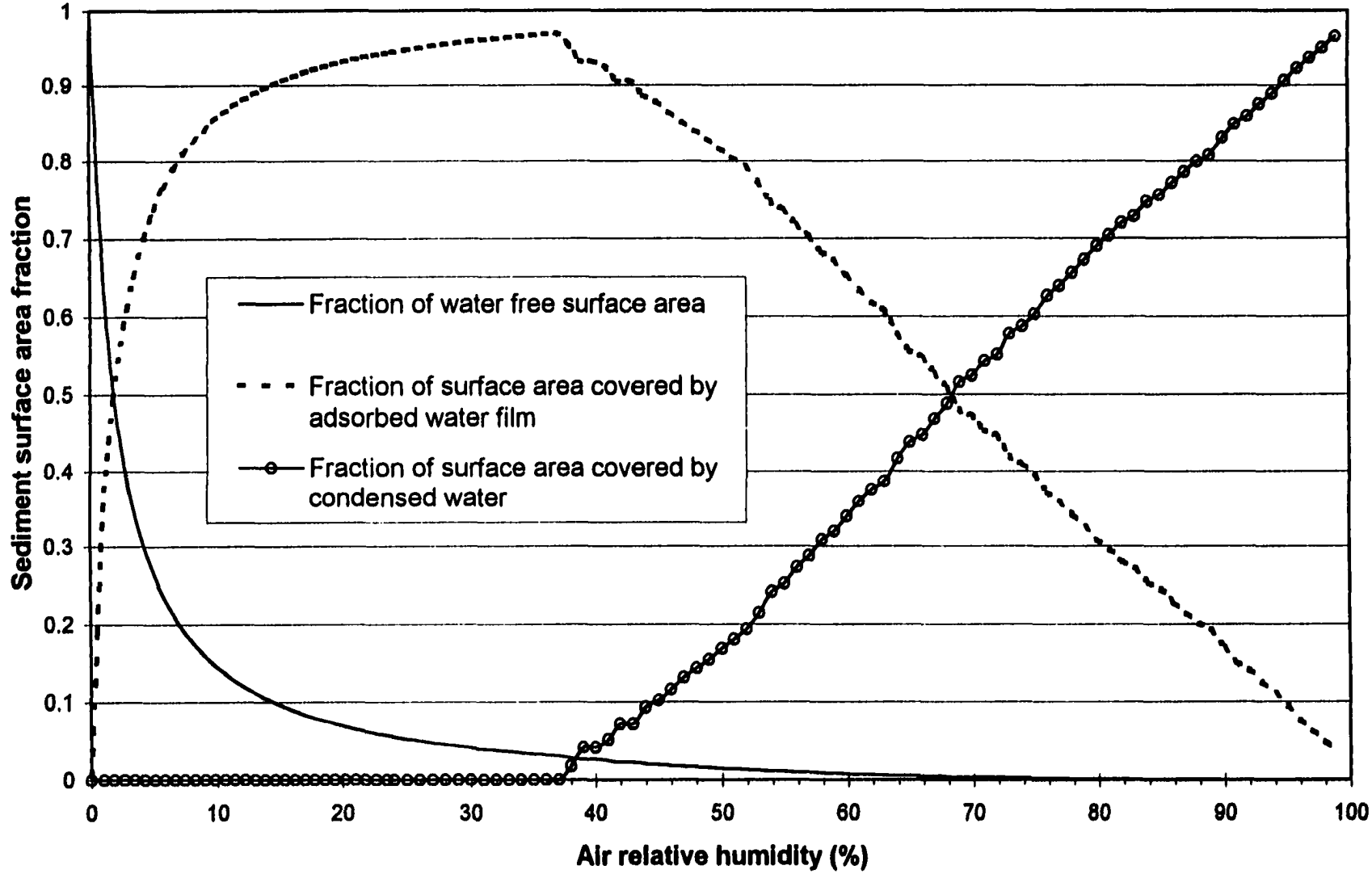

Figure 4.9 Model of the influence of air relative humidity on the nature and area of surfaces in the sediment matrix.

As it is very difficult to handle sediment at 0% moisture content, the driest sediment investigated in this study had a moisture content of 0.1%.

4.3 Contaminant partitioning experiments

4.3.1 Validation of experimental results

For each experiment, the outlet air concentration was measured at different values of air superficial velocity and for a few experiments, the effect of bed length was assessed as well. Individual charts of each experiment are gathered in Appendix G. They show that, for every experiment, the outlet air concentration was independent of air velocity or bed length. The outlet air was also independent of the time at which samples were taken.

This insures that the outlet air concentration measured were equilibrium concentrations.

4.3.2 Effect of moisture content on phenanthrene and dibenzofuran partitioning

4.3.2.1 Experimental results

Desorption equilibrium was studied for phenanthrene and dibenzofuran in different ranges of moisture content. The two extreme moisture content ranges investigated corresponded to sediment in equilibrium with very dry air (RH<3%) and with air close to water saturation (RH>93%). In terms of moisture content, "dry" sediments used for experiments contained less than 0.8% by mass of water and "wet" sediments had a moisture content above 6.0%. Sediments contaminated with phenanthrene were also studied at two intermediate moisture contents (1.5% and 3.0%). These sediment batches are referred to as "damp".

Experiments conducted on sediment contaminated with phenanthrene are summarized in Tables 4.5, 4.6 and 4.7, for the dry, damp and wet conditions,

respectively. Phenanthrene desorption isotherms are shown in Figures 4.10 and 4.11. Experiments with dibenzofuran sediments in the three moisture regions are summarized in Table 4.8. Dibenzofuran desorption isotherms are shown in Figure 4.12. In these three figures, the sediment-air partition coefficients obtained by linear regression on the data are also shown. The relatively poor correlation to straight lines of the data observed in Figure 4.10 through 4.12 may have several causes:

- Non-linearity of sorption isotherms.
- Sample to sample moisture content variations leading to different partition ratios within the same moisture range.
- Experimental artifacts.

These points are discussed in section 4.4.2.2.

Sediment moisture content has a tremendous effect on the partition coefficient. Dibenzofuran and phenanthrene estimated partitioning ratios vary respectively by a factor 200 and 1000 over the range of moisture content corresponding to a change of air relative humidity from 0% to 99+%. Furthermore, experiments conducted with phenanthrene contaminated sediment indicate that the decrease is particularly sharp when dry sediment remoisturizes. Phenanthrene partition coefficient is reduced by a factor of 500 when the air relative humidity increases from 0 to 60% (the sediment moisture content only changes from 0.2% to 2.7%). Such dramatic decreases of the partition coefficient have been reported in the literature. Chiou and Shoup, 1985 determined the sorption isotherms of m-dichlorobenzene and 1,2,4-trichlorobenzene on a soil at different humidites. From the isotherms it can be roughly estimated that the partition coefficient of these compounds decreased by a factor of more than 200 when the relative humidity varied

Table 4.5 Summary of the experiments conducted with dry sediment contaminated with phenanthrene.

	Sediment characteristics	*mc (%)*	0.7±0.1	0.5±0.0	0.2±0.1
		C_s *(± std) (mg/kg)*	16 ±3	37±3	127±13
Equilibrium air concentration	14°C	C_g^* *(± std) (pg/L)*			7±2
		Replicates			5
		Age (weeks)			32
	25°C	C_g^* *(±std) (pg/L)*	31±15	48±21	111±25
		Replicates	10	7	3
		Age (weeks)	42	41	26
	35°C	C_g^* *(± std) (pg/L)*			382±161
		Replicates			5
		Age (weeks)			20
	Enthalpy of adsorption	*ΔH (kJ/mol)*			-124±12
		r^2			0.906

Table 4.6 Summary of the experiments conducted with damp sediment contaminated with phenanthrene at 25°C.

Sediment characteristics	*mc (%)*	1.39±0.08	1.46±0.05	1.51±0.04	2.60±0.04	2.75±0.06
	C_s *(± std) (mg/kg)*	16±3	37±3	127±13	44±2	123±4
	Age(weeks)	48	50	46	58	52
Equilibrium air concentration	C_g^* *(± std) (ng/L)*	0.25±0.03	0.38±0.12	5.3±1.1	21±2	62±6
	Replicates	7	17	13	12	18

Table 4.7 Summary of the experiments conducted with wet sediment contaminated with phenanthrene.

	Sediment characteristics	*mc (%)*	7.2±0.1	6.0±0.2	6.7±0.1	7.4±0.2
		C_s (±std) (mg/kg)	12 ±1	26±4	58±2	133±7
Equilibrium air concentration	14°C	*C_g^* (±std) (ng/L)*	3±1	13±4	16±4	40±14
		Replicates	8	27	21	11
		Age (weeks)	14	13	10	10
	25°C	*C_g^* (±std) (ng/L)*	9±1	62±6	78±12	110±40
		Replicates	10	17	28	14
		Age (weeks)	12	9	9	15
	35°C	*C_g^* (±std) (ng/L)*	24±3	157±23	213±27	503±66
		Replicates	11	27	24	14
		Age (weeks)	15	13	12	14
	Enthalpy of partitioning	*ΔH (kJ/mol)*	-86±4	-88±3	-91±4	-93±5
		r^2	0.933	0.935	0.806	0.902

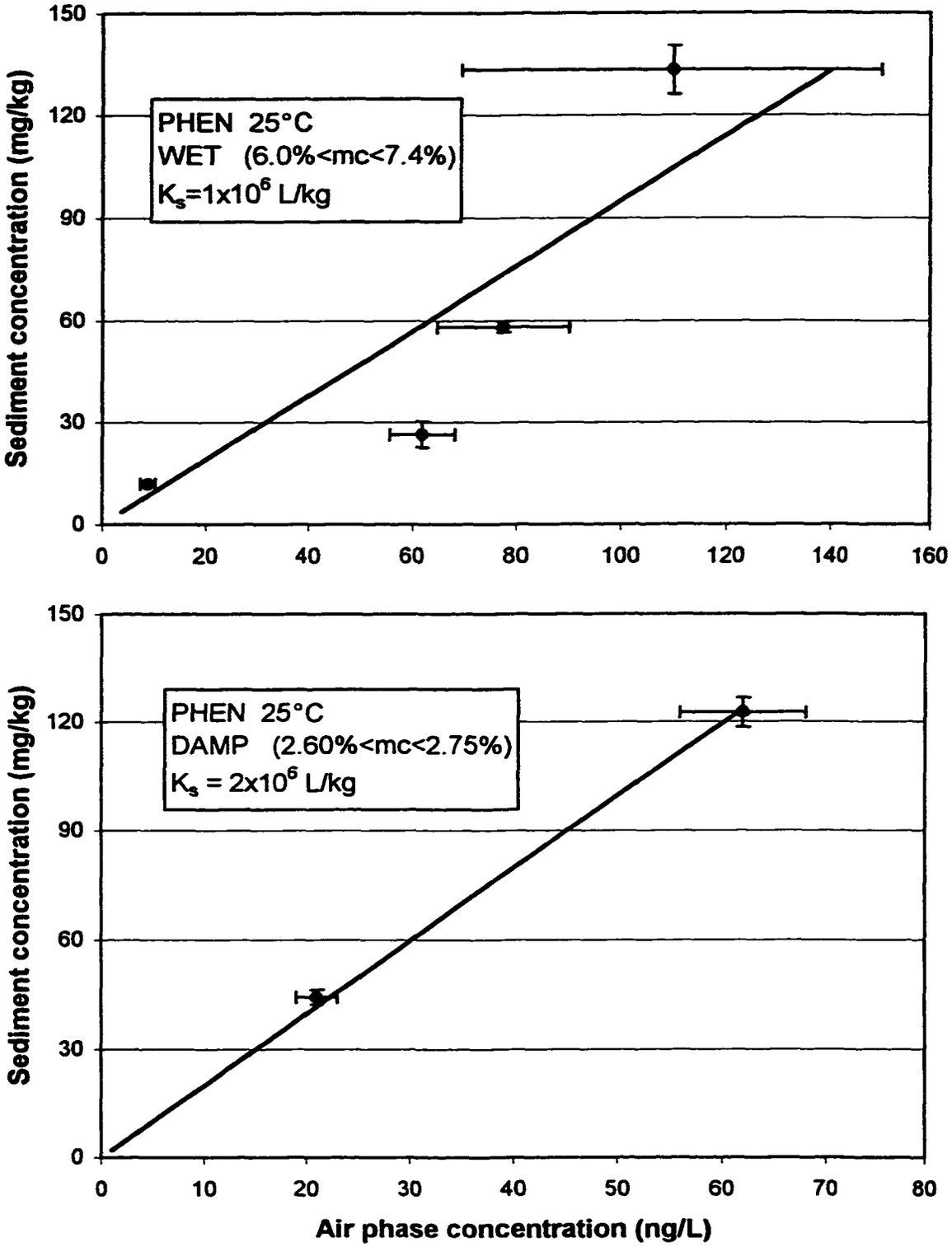

Figure 4.10 Phenanthrene partitioning coefficient at 25°C in wet and damp sediment.

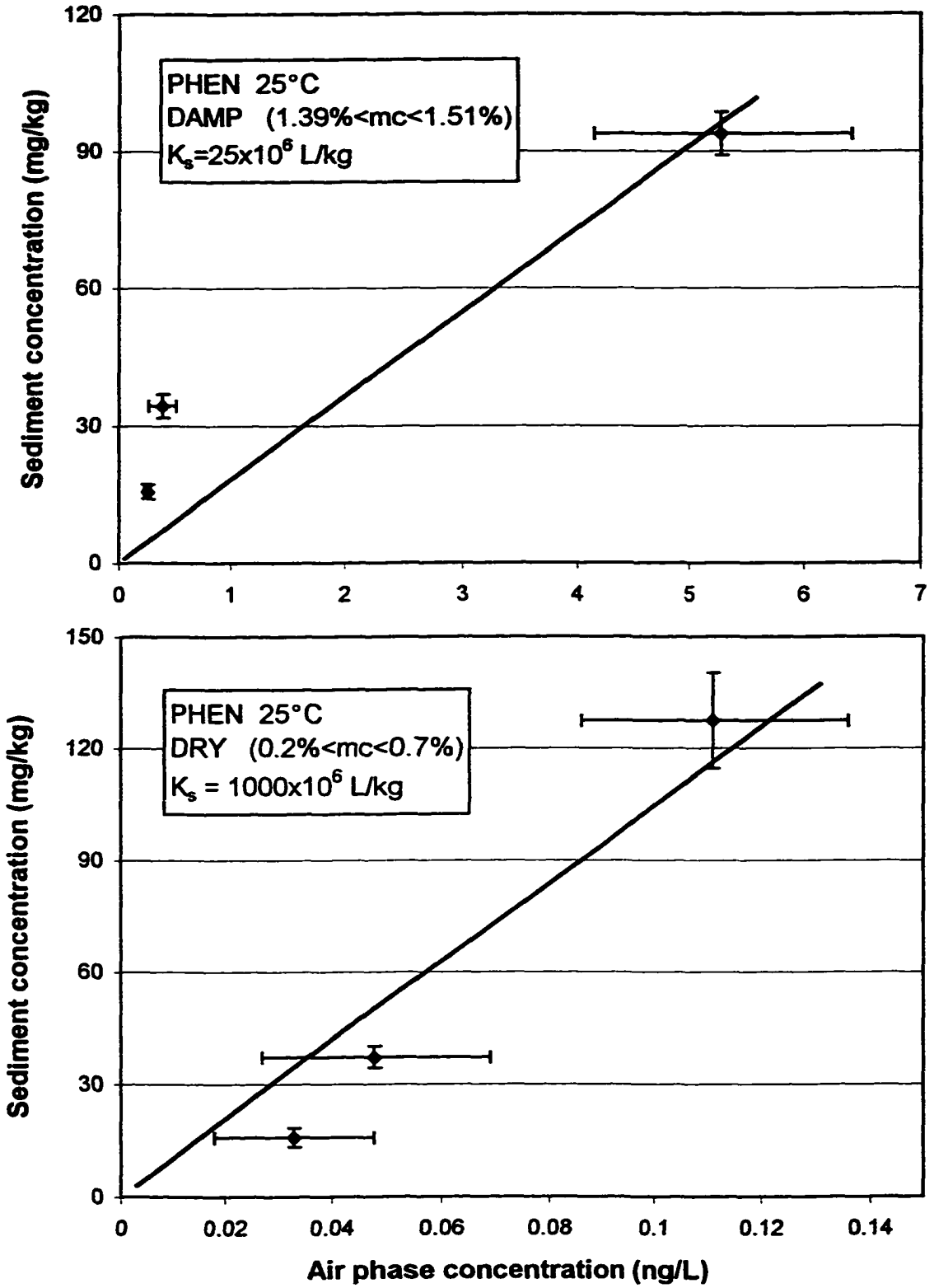

Figure 4.11 Phenanthrene partitioning coefficient at 25°C in dry and damp sediment.

Table 4.8 Summary of the experiments conducted with sediment contaminated with dibenzofuran at 25°C.

		Dry			Damp	Wet		
Sediment characteristics	*mc (%)*	0.27±0.05	0.30±0.03	0.77±0.05	1.07±0.03	6.5±0.1	7.0±0.1	6.2±0.10
	C_s (± std) (mg/kg)	9±1	24±3	13±2	28±3	10±2	43±7	92±6
	Age(weeks)	54	41	49	2	15	7	9
Equilibrium air concentration	*C_g^* (± std) (ng/L)*	3.0±1.0	1.3±0.5	0.19±0.04	3.1±0.5	67±8	614±89	646±97
	Replicates	14	12	10	12	17	24	21

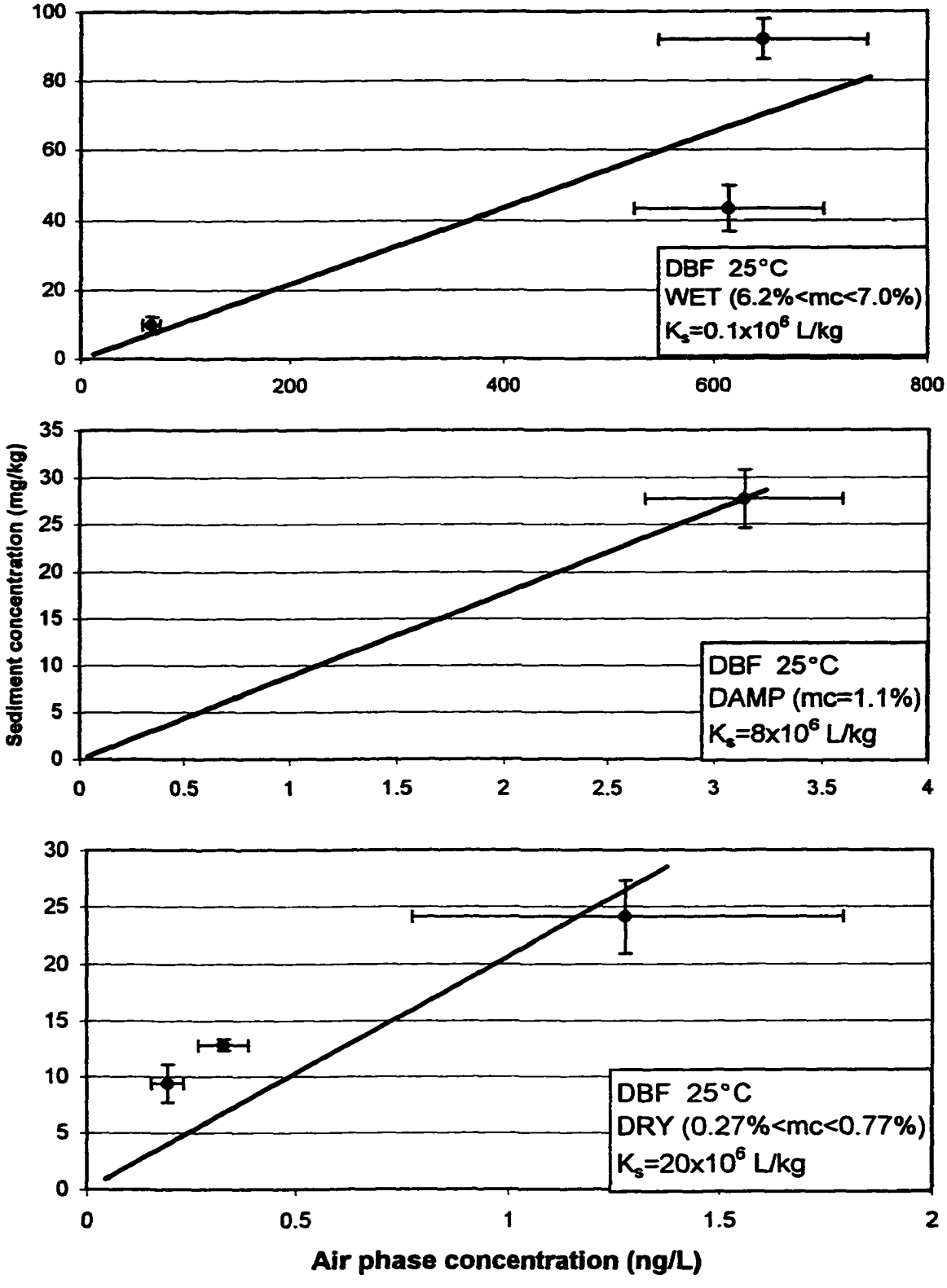

Figure 4.12 Dibenzofuran partitioning coefficient at 25°C in wet, damp, and dry sediment.

from 0 to 90%. Spencer and Cliath, 1974 report that the partition coefficient of the herbicide trifluralin was 3000 to 5000 greater in air-dried soil than in wet soil.

The partition coefficient of phenanthrene was estimated by linear regression on the results from the four experiments conducted with wet sediment. The value at 25°C, normalized for the soil organic content, is $3x10^7$ L/kg. Hippelein and McLachlan, 1998 measured the partition coefficient of phenanthrene at 21°C between air and a wet sandy soil from a single experiment. The value they report, normalized for the soil organic content and expressed in the units used in this study, is $10x10^7$ L/kg. The partition coefficient measured in this study, corrected for the temperature effect using the heat of sorption in wet sediment determined in section 4.3.3.2, is $5x10^7$ L/kg. This differs by a factor of 2 from the value reported by Hippelein and McLachlan, 1998. This variation can be explained by the uncertainty on the experimental measurements. Hippelein and McLachlan, 1998 calculated that the precision of their experimental method was about a factor two. In the present study, the partition coefficients calculated individually from each experiment vary by a factor three.

Cousins et al., 1998 measured the sediment-air partition coefficient of seven polychlorinated biphenyls and correlated the experimental values with the octanol-air partition coefficient. They found a linear relationship (r^2=0.92) between the logarithms of the two parameters. Using the value of the octanol-air partition coefficient of phenanthrene measured by Harner and Bidleman, 1998, the correlation predicts a value of $5x10^7$ L/kg (on an organic carbon basis) for the sediment-air partition coefficient. This is in good agreement with the value of $3x10^7$ L/kg that was determined in this study. The

logarithms of the experimental and calculated partition coefficients are respectively 7.48 and 7.70.

4.3.2.2 Investigation of an aging effect

Several studies have shown that aging of sediments modifies the sediment-air partitioning of hydrophobic organic contaminants. Considerations on this phenomenon are presented in Appendix H. The experiments conducted to determine the sediment-air partition coefficients at different sediment moisture contents spanned a long period of time. As a result, the age of a sediment batch used to determine a partition coefficient could vary significantly from one experiment to another. The age at the time of an experiment of batches of sediment contaminated with phenanthrene and dibenzofuran varied respectively from 9 to 58 weeks and from 7 to 54 weeks. Therefore, it was interesting to relate the experimental partition coefficients to the age of the sediment batches used in their determination. No correlation could be found indicating an aging effect. This has two possible meanings: (i) aging has no visible effect on the sediment-air partition coefficient (ii) The aging process involving phenanthrene or dibenzofuran had already reached equilibrium at the time of the first experiment.

Furthermore, the coefficient of partition between the organic matter and water, K_{oc} can be calculated from the sediment-air patition coefficient in wet sediment, using equation (2.14). The values of the Henry's constant for phenanthrene and dibenzofuran used in the calculation are reported in Table 4.9. $\log K_{oc}$ calculated from the experimental data is between 4.4 and 4.8 for phenanthrene and between 4.0 and 4.3 for dibenzofuran. These values are in good agreement with values reported in the literature (see table 4.9). Thus, there was no observable effect of aging on the sediment-air partition coefficient.

4.3.2.3 Use of K_s in volatilization models

Valsaraj et al., 1999 conducted experiments in a laboratory microcosm to investigate the effect of air relative humidity on the volatilization of contaminants from Campus Lake sediment. Air was passed over the sediment and variations in contaminant flux as a result of change in air relative humidity were measured. Ravikrishna, 1998 incorporated the sediment-air partition coefficients determined in this study into the volatilization model developed by Valsaraj et al., 1999 to predict the flux of phenanthrene and dibenzofuran in the microcosm. The experimental values along with the model predictions of the flux of phenanthrene and dibenzofuran are respectively shown in Figures 4.13 and 4.14. The model, using experimental values of K_s, accurately predicts the variations in flux resulting from a change in air relative humidity.

4.3.3 Effect of temperature on phenanthrene partitioning

Study of phenanthrene sorption equilibrium at different temperatures had several motivations:

- Allowing the prediction of phenanthrene partitioning ratio in a realistic range of environmental temperatures
- Validating experimental results by thermodynamic analysis
- Gaining insight on the sorption mechanisms
- Evaluating the heat of adsorption onto dry sediment, which is a required parameter in modeling the partitioning ratio.

4.3.3.1 Sorption isotherms

All experiments with wet sediment contaminated with phenanthrene were conducted at three different temperatures: 14.0±0.7°C, 25.0±0.7°C and 35.0±0.3°C. The

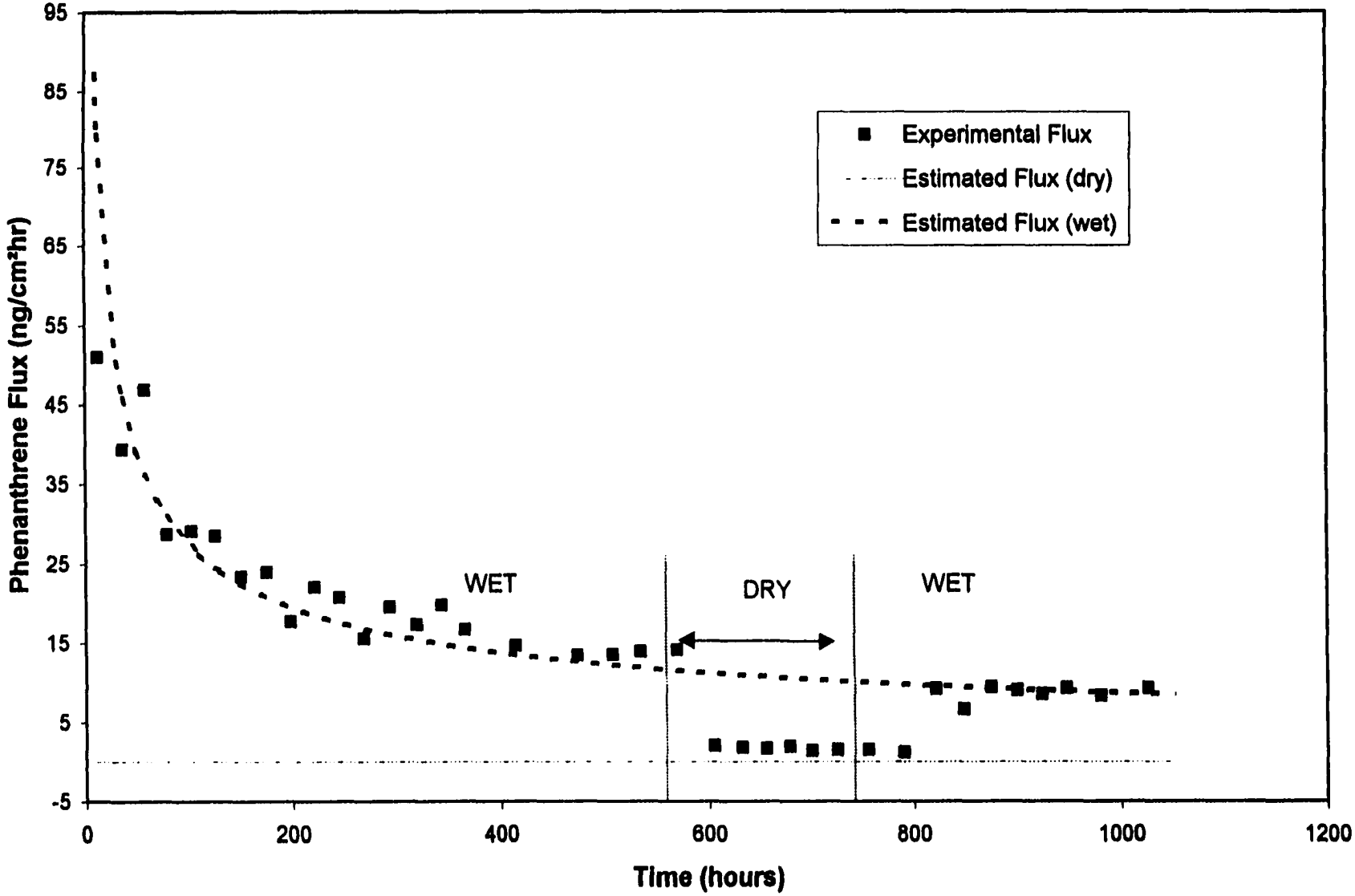

Figure 4.13 Flux of phenanthrene from exposed sediment observed and estimated using experimental values of K_s.

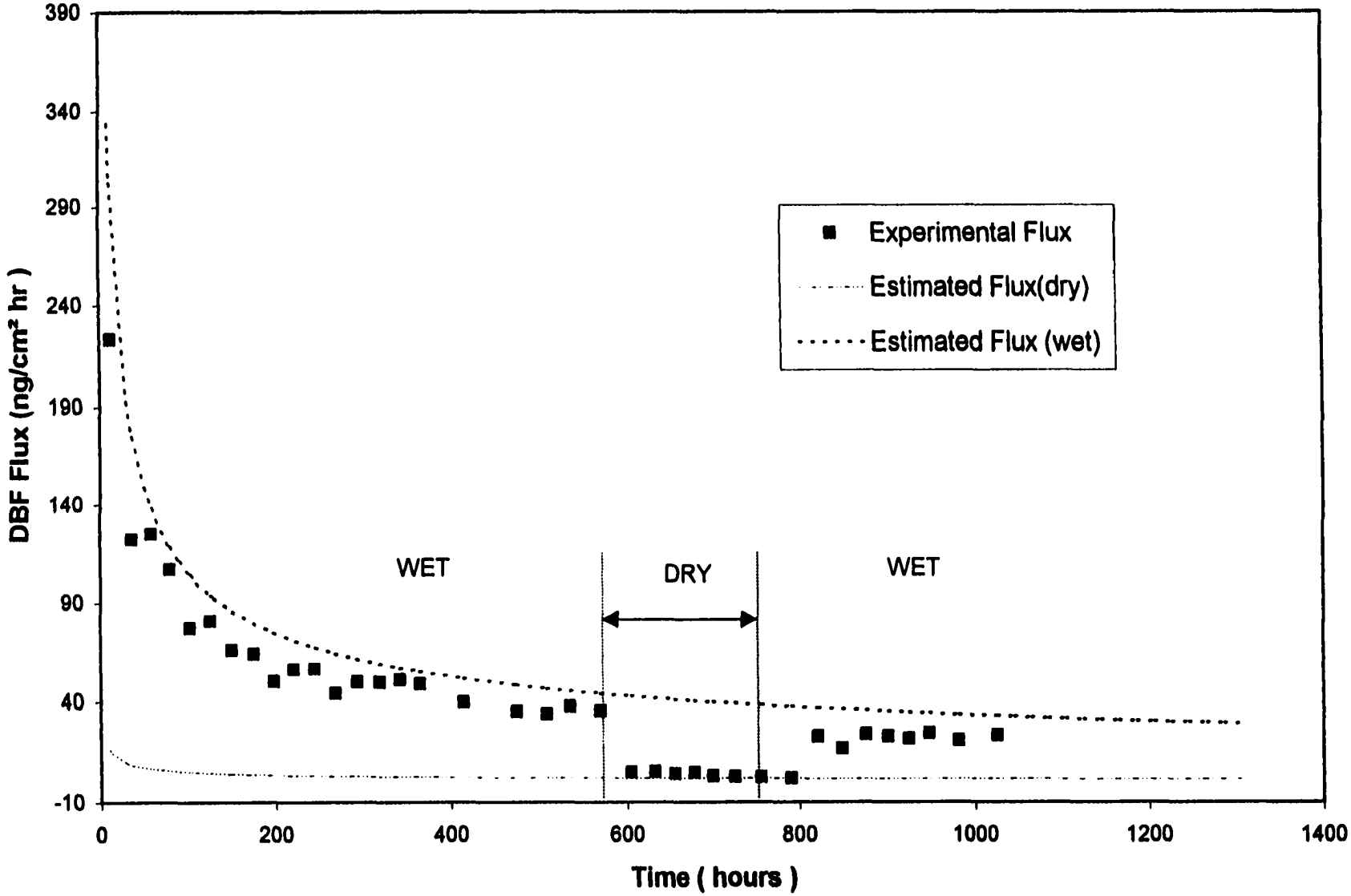

Figure 4.14 Flux of dibenzofuran from exposed sediment observed and estimated using experimintal values of K_s.

three isotherms are shown in Figure 4.15. Experimental conditions and results were summarized in Table 4.7. The isotherms at 14 and 35°C are fairly linear (r^2=0.964 and r^2=0.970, respectively). On the other hand, the isotherm at 25°C shows a poor linearity (r^2=0.752). This point is discussed in section 4.4.2.2. The partitioning of phenanthrene between wet sediment and air is fairly sensitive to temperature. The partition coefficient decreases by a factor 12 when the temperature increases from 14 to 35°C.

4.3.3.2 Heat of sorption in wet sediment

The partitioning of phenanthrene between air and a sediment at a given moisture content may be described by the reaction: $PHEN_{gas} \rightleftharpoons PHEN_{sediment}$. The equilibrium condition is the equality of phenanthrene fugacity in the gas and sediment phases: $f^{gas}=f^{sed}$.

The Gibbs-Helmoltz equation states that at constant composition, x and total pressure, P_T:

$$\left(\frac{d\ln f^{sed}}{dT}\right)_{P_T,x} = \frac{h_{sed}-h_{gas}}{RT^2} \qquad (4.7)$$

Where:

- h_{sed} is the partial molar enthalpy of phenanthrene in the sediment phase.
- h_{gas} is the molar enthalpy of pure phenanthrene in the ideal-gas state.

Phenanthrene in the gas phase may be considered as an ideal gas. Thus, the right term of the Gibbs-Helmoltz equation is the enthalpy of partitioning, $\Delta H_{partitioning}$. Furthermore, the phenanthrene gas phase fugacity can be approximated by its partial pressure, P and f^{sed} is thus equal to P. These substitutions result in:

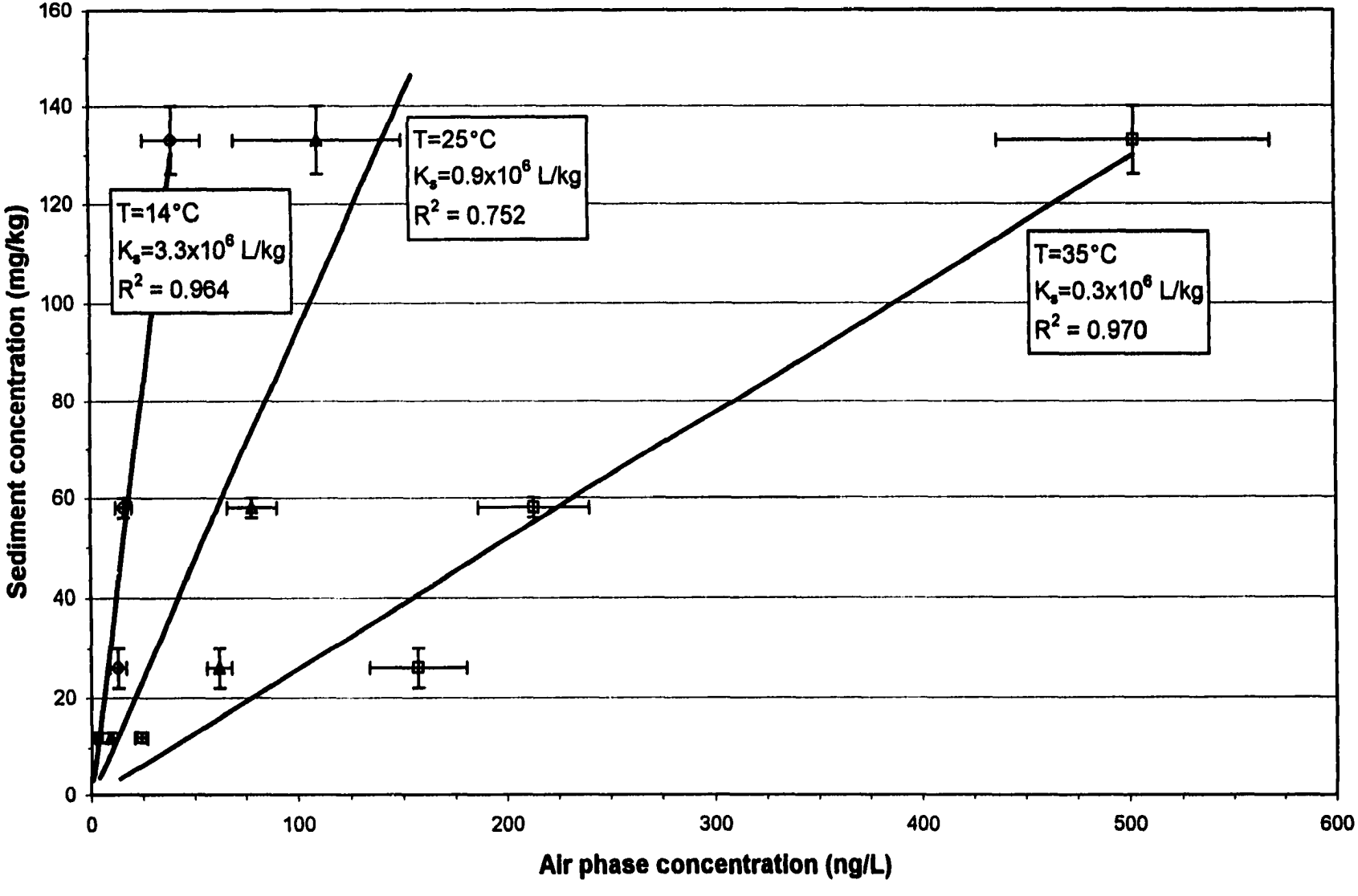

Figure 4.15 Influence of temperature on phenanthrene partitioning isotherm in wet sediment.

$$\left(\frac{d\ln P}{dT}\right)_{P_T,x} = \frac{\Delta H_{partitioning}}{RT^2} \tag{4.8}$$

Therfore, a plot of ln(P) as function of $1/RT^2$ should give a straight line provided that $\Delta H_{partitioning}$ is constant over the range of temperature. The slope of this line is $\Delta H_{partitioning}$.

Figure 4.16 shows plots of the Gibbs-Helmoltz equation applied to the four different sediments studied. At any sediment concentrations, data points at the three different temperatures fall on a straight line (r^2 coefficients were shown in Table 4.7). This allows the determination of $\Delta H_{partitioning}$. Values were summarized in Table 4.7. Within experimental uncertainty, enthalpy of phenanthrene partitioning in wet sediment appears independent of loading. This would be expected for the partitioning into a homogeneous medium.

Phenanthrene seems to be non-specifically sorbed into the wet sediment. This agrees with observations made by fluorescence spectroscopy reported in section 2.2.4. Pyrene molecules sorbed in organic matter are closely associated with it but keep their free motion. For comparison, Neue and Rudolph, 1993 measured that the isosteric heat of adsorption of pyrene on the surface of carbon soot was more exothermic by 20kJ/mol when the surface concentration increased by a factor 2 in the region of monolayer coverage. The average value of the heat of partitioning measured in this study is –90±4 kJ/mol. To gain insight on the mechanisms of partitioning, $\Delta H_{partitioning}$ should be compared to the heat of condensation of the subcooled liquid, $\Delta H_{condensation}$ rather than the

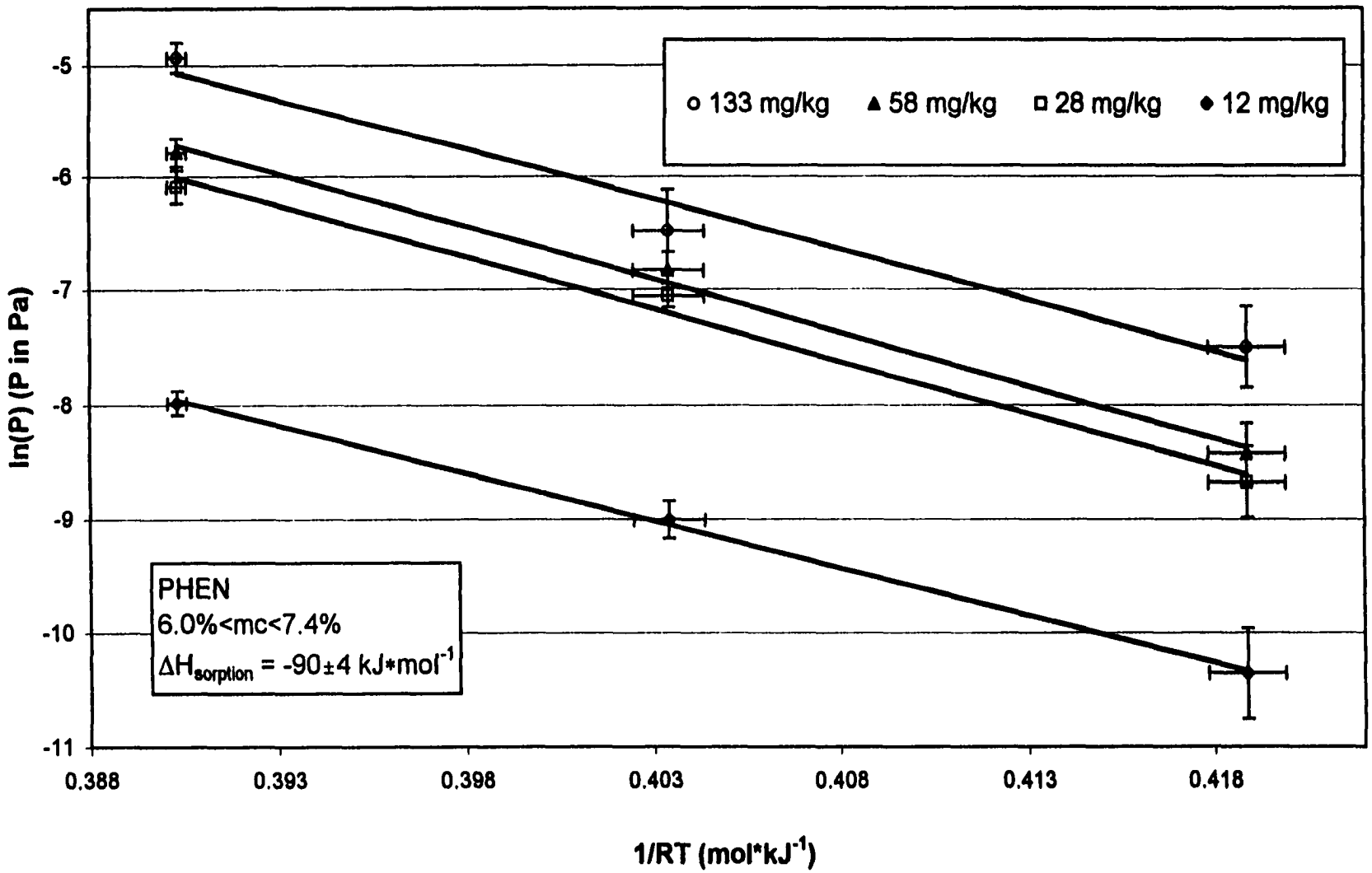

Figure 4.16 Determination of phenanthrene heat of sediment-air partitioning from the experimental results plotted in the form of the Gibbs-Helmoltz equation.

heat of condensation of solid phenanthrene. This will prevent taking into account structural effects. This point is discussed in Appendix B.

A heat of condensation of the subcooled liquid of –84±3 kJ/mol was calculated in section 4.1.2.3. Thus, within experimental uncertainty, the sorption process is energetically similar to the condensation of the subcooled liquid. This indicates that the strength of phenanthrene interactions with sediment organic polymers is of the same magnitude as the strength of intermolecular interactions in the pure (subcooled) liquid. This is compatible with fluorescence spectroscopy studies reported in section 2.2.4. Pyrene sorbed in soil slurries experiences an environment of polarity similar to the ones of benzene or cyclohexane.

4.3.3.3 Heat of adsorption on dry sediment

Desorption equilibrium of phenanthrene from a dry sediment (mc=0.21%) loaded at 127mg/kg was investigated at three different temperatures: 14±0.7°C, 25±0.7°C and 35±0.3°C. Experimental results were summarized in Table 4.5. As for pure phases transition, the Clausius-Clapeyron equation is applicable to pure gas adsorption equilibrium. However, in the case of adsorption, the equilibrium partial pressure depends not only on temperature but also on the adsorbate surface coverage, or sediment loading, C_s. Assuming that the gas phase is ideal and neglecting the adsorbate molar volume, the Clausius-Clapeyron equation is written:

$$\left(\frac{\partial \ln P}{\partial T}\right)_{C_s} = \frac{\Delta H_{adsorption}}{RT^2} \qquad (4.9)$$

Where $\Delta H_{adsorption}$ is the isosteric heat (or differential enthalpy) of adsorption of phenanthrene onto the sediment. Therfore a plot of ln(P) as a function of $1/RT^2$ should

give a straight line provided that $\Delta H_{adsorption}$ is constant over the range of temperature. The slope of this line is $\Delta H_{adsorption}$. Figure 4.17 shows the application of the Clausius-Clapeyron equation to experimental data. Data points at the three different temperatures fall on a straight line (r^2=0.909). This gives $\Delta H_{adsorption}$= -124±12 kJ/mol.

Such a value of $\Delta H_{adsorption}$ seems extremely high for a physical adsorption mechanism. The enthalpy change associated with physical adsorption is usually said to be less than 40 kJ/mol (Jaycock and Parfitt, 1981). However this remark concerns the adsorption of true gas and volatile compounds. For semi-volatile organic compounds, the difference between heat of sublimation and heat of desorption should be considered when evaluating the adsorption strength.

Phenanthrene heat of desorption from the sediment is larger than its experimentally determined heat of sublimation by 23 kJ/mol. This reveals that physical forces between phenanthrene molecules and adsorption sites on the sediment mineral surface are stronger than intermolecular binding forces in the crystal. The hydrogen bond involved in the adsorption of polynuclear aromatic compounds to silanol sites (see section 2.2.3.1) is in fact a strong physical bond. Its strength usually ranges from 8 to 40 kJ/mol (Prausnitz et al., 1986). Furthermore, the value of the heat of adsorption on sediment reveals that phenanthrene binds to more than one silanol site through hydrogen bonds. A similar conclusion is reached in fluorescence spectroscopy studies reported in section 2.2.3.1. More than one silanol group are involved in binding a pyrene molecule to the surface of silica gel or clay.

It is interesting to note that the heat of adsorption of water onto the sediment was determined to be - 48 kJ/mol. At first it may seem surprising that, having a lower heat of

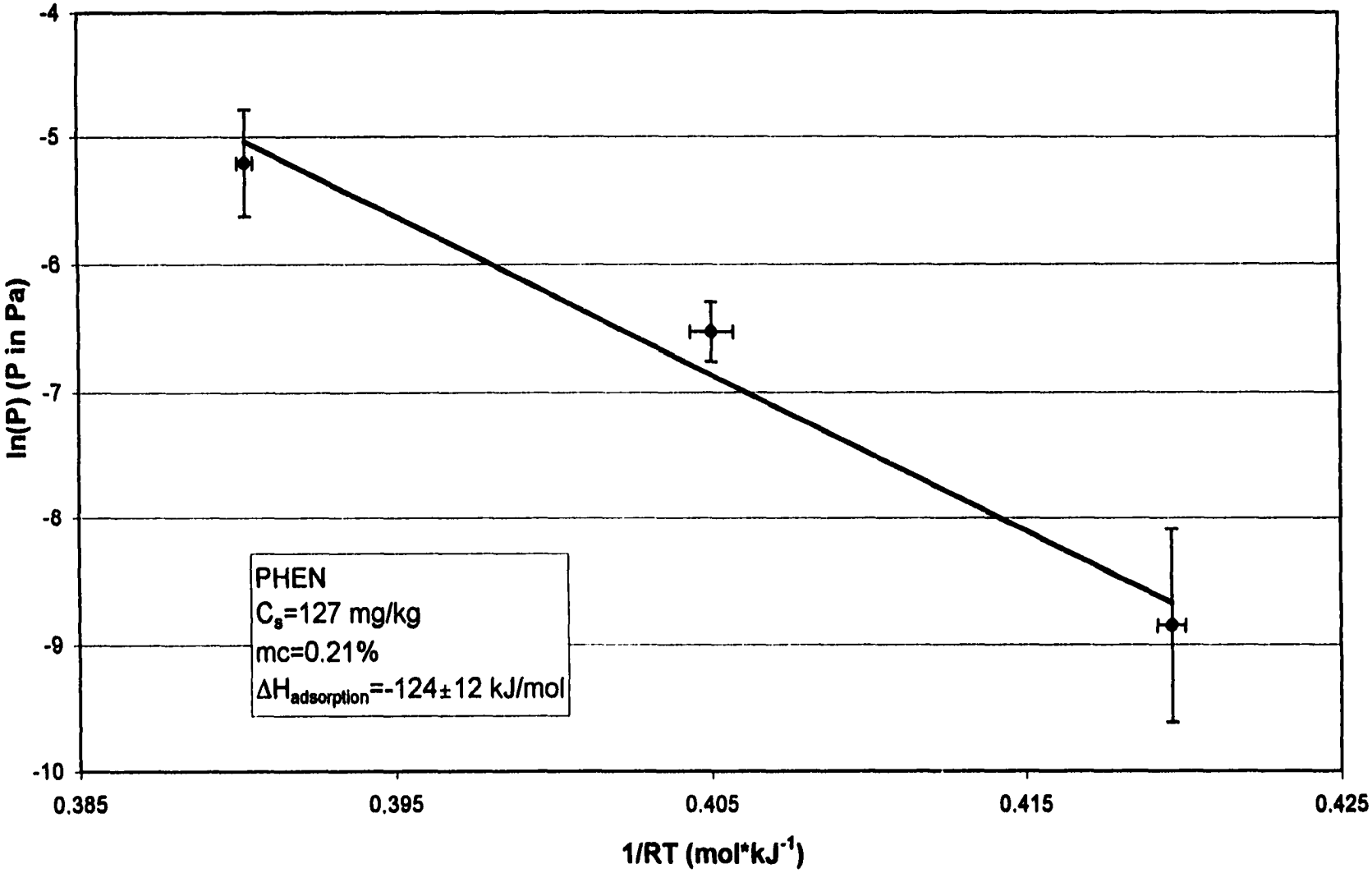

Figure 4.17 Determination of phenanthrene heat of adsorption on dry sediment from the experimental results plotted in the form of the Clausius-Clapeyron equation.

adsorption than phenanthrene, water is still capable of displacing phenanthrene from adsorption sites. Thiel, 1991 explained this apparent paradox when studying the competitive adsorption of water and cyclohexane on ruthenium crystal. She pointed out that "the only meaningful way to discuss the energetics of displacement is in terms of the energy change per unit area". The Van der Waals molecular surface area of phenanthrene is about 180 $Å^2$ (Daubert and Danner, 1995). The molecular surface area of water is reported to be 10.8 $Å^2$ (Livingston 1949, Orchiston 1953). Thus, on a surface area basis, the heat of adsorption of phenanthrene is about -100 mJ/m^2 whereas the one of water is about -740 mJ/m^2. Water adsorption onto the sediment mineral surface is energetically more favorable than phenanthrene adsorption by a factor of seven. In other words, on average, the bond between an adsorption site and a water molecule is 7 times stronger than for phenanthrene. Finally, it is easy to calculate that the replacement of phenanthrene by water at the sediment surface releases about 800 kJ per mole of phenanthrene displaced! This explains the dramatic decrease in the partition coefficient observed when a dry sediment is remoisturized even very slightly.

By considering the heat of adsorption per unit surface area, it is also possible to make the comparison with other volatile aromatic compounds. Rao et al., 1989 measured a isosteric heat of adsorption of -37 kJ/mol for the adsorption of toluene on an oven dried soil. Chiou and Shoup, 1985 obtained a value of -40 kJ/mol by analysis of the BET adsorption isotherm of benzene on an oven-dried soil. The value determined in this study for phenanthrene corresponds to a heat of adsorption of -41 kJ/mol per aromatic ring. This agrees very well with the values reported for benzene. It would be interesting to

obtain more experimental data to ascertain whether it is possible to predict the heat of adsorption, $\Delta H_{adsorption}$ of other polynuclear aromatic hydrocarbons by:

$$\Delta H_{adsorption} \approx -40 \cdot r \ kJ/mol \qquad (4.10)$$

where r is the number of aromatic rings of the PAH molecule.

4.4 Modeling the sediment-air partition coefficient

4.4.1 Contribution of individual sorption compartments

As described in section 2.3, different sorption mechanisms account for the uptake of organic contaminants by sediments. A model of the overall sediment-air partition coefficient is obtained by summing up the partition coefficients associated to each sediment compartment (equation (2.16)). In this section the contribution of each sediment compartment to the overall sorption is assessed.

Literature values of the physical parameters needed to quantify sorption mechanisms to each compartment are reviewed hereafter and summarized in Table 4.9.

Table 4.9 Physico-chemical properties of phenanthrene and dibenzofuran.

	PHEN	DBF
Molar mass	178.24	168.21
Water solubility (mg/L)†	1	10
H ($Pa.m^3/mol$)*	4.7	11.4
Log K_{oc}(K_{oc} in L/kg)		
Thoma, 1994	4.8	4.3
Literature average*	4.4±0.3 (n=8)	4.0±0.3 (n=2)

† Mackay et al., 1992
* see section 4.4.1.1 for reference

Saturated vapor pressures were reviewed in section 4.1.1.

4.4.1.1 Dissolution in water

Dissolution in water is estimated from expression (2.12) in which the sediment moisture content, mc is either measured or calculated as a function of the air relative humidity using the adsorption/condensation model developed in section 4.2.4.

Literature values of Henry's law constants for dibenzofuran and phenanthrene were reviewed.

- Dibenzofuran. Dibenzofuran experimental thermodynamic data are scarce. No experimental value of Henry's constant could be found in the literature. However, for sparingly soluble compounds such as dibenzofuran, Henry's constant is often approximated by the ratio of vapor pressure over solubility (Valsaraj, 1994). The three experimental solubility values compiled by Mackay et al., 1992 range from 4.2 to 10.0 mg/L. The average of these values is 6.3 mg/L. Value of the saturated vapor pressure measured in this study (Table 4.2) was used to calculate the value of Henry's constant reported in Table 4.9.
- Phenanthrene. Reviews of phenanthrene Henry's constant can be found in Mackay et al., 1992 and Montgomery et al., 1996. Reviews of experimental values are presented by Alaee et al., 1996 and de Maagd et al., 1998. The experimental values at 25°C reported by these 4 authors range from 2.4 to 5.6 ($Pa.m^3/mol$). Value by Alaee et al., 1996, is reported in Table 4.9.

Alaee et al.,1996 studied the effect of water salinity on naphthalene Henry's constant. They observed that H was about 50% larger in sea water than in deionized water. The solubility of non polar PAHs decrease with increasing ionic strength (salting

out effect), resulting in larger Henry's constant. In wet sediment, contaminant uptake is controlled by sorption in the organic fraction and the concentration in the air phase above the contaminated sediment is directly proportional to H. Thus, this increase in H should be taken into account when dealing with contaminated sediments in coastal CDFs.

4.4.1.2 Adsorption on water film

It is possible to obtain an estimate for the partition coefficient to the water film per unit mass of sediment, $K_{a/w}$ using equation (2.11):

$$K_{a/w} = A_{a/w}\kappa_{a/w} \tag{2.11}$$

Where:

- $A_{a/w}$ is the surface area of the water film per mass of sediment. The adsorption/condensation model developed in section 4.2.4 gives an estimate of $A_{a/w}$ as a function of relative humidity.
- $\kappa_{a/w}$ is the partitioning coefficient to the air/water interface per unit surface area of water film. Correlations to estimate $\kappa_{a/w}$ for phenanthrene and dibenzofuran as a function of relative humidity have been developed by different authors.

Goss, 1992 developed a model to determine the partition coefficient per unit surface area of non-polar volatile compounds:

$$\ln\kappa_{a/w} = A^{*} - [(\Delta H_s/R)(1/T - 1/323.15)] - C(100 - RH)$$

Where:

- ΔH_s is the heat of adsorption of the compound. ΔHs is correlated to the saturated vapor pressure at 25°C and the hydrogen bond acceptor, β.

- A^* is also correlated to the saturated vapor pressure, P^{sat}(25°C) and the hydrogen bond acceptor.
- C is correlated to the hydrogen bond acceptor, the molar refraction index, mR and the dipole momentum, μ.

Using correlations developed by Goss, 1992, Storey et al., 1995 and Pankow, 1996 (see section 2.3.3.2) the partition coefficient between the air/water interface and the air can be estimated. These correlations were developed to describe adsorption on a water film supported by a natural quartz surface. Although sediment mineral surfaces are likely to be different from quartz surfaces, correlations certainly give a fair estimate of $\kappa_{a/w}$. Values were calculated at two relative humidities, 30% and 100%, corresponding to adsorption on, respectively, the first monomolecular water layer and a bulk water surface. For dibenzofuran, parameters that could not be found in the literature (β and μ) were approximated by fluorene values (same molecular structure as dibenzofuran without the oxygen). Not taking into account the effect of the oxygen atom certainly introduces an error. Correlations by Storey et al., 1995 and Pankow, 1996, based solely on saturated vapor pressures, are limited to compounds within the PAH family. Thus, predictions for dibenzofuran have to be taken cautiously. Results as well as the parameters needed in the correlations are summarized in Table 4.10. Agreement between correlations from the three authors is very good. Thus, for each compound the four values calculated in Table 4.10 were used to evaluate the m and b coefficients in the linear relationship, $\log\kappa_{a/w}=mRH+b$. Values of m and b are reported in Table 4.10.

Table 4.10 Estimate of the coefficient of partitioning between the air/water interface and air for phenanthrene and dibenzofuran.

					log $\kappa_a^{a/w}$ ($\kappa_a^{a/w}$ in m)				log $\kappa_a^{a/w}$ = mRH + b	
					RH = 30%		RH = 100%		m	b
	P^{sat}_L (mPa)[a]	β[b]	mR[c]	μ[d]	Goss, 1992	Storey et al., 1995	Goss, 1992	Pankow, 1996		
Phenanthrene	59	0.2	61.74	0	-0.41	-0.01	-2.1	-1.8	-0.03	3.8
Dibenzofuran	1681	0.22†	53.42	0†	-1.5	-1.7	-3	-3.5	-0.02	2.1

a determined in this study, b Kamlet et al., 1988, c Weast and Aslte, 1981, d Reid et al., 1977.
† Fluorene value

4.4.1.3 Sorption in organic matter

Sorption in organic matter is estimated from expression (2.14). Literature values of the organic carbon-water partition constant, K_{oc} were reviewed.

Phenanthrene and dibenzofuran K_{oc} were measured by Thoma, 1994 for a sediment batch of the same origin as the sediment used in this study. Montgomery et al., 1996 and Mackay et al., 1992 have compiled a large number of K_{oc} values for phenanthrene. A range of values is also given for dibenzofuran in Montgomery et al., 1996. Average and standard deviation of values measured for soils and sediments are presented in Table 4.9 along with Thoma's values.

4.4.1.4 Adsorption on dry mineral surface

In section 2.2.3.3 studies were presented that demonstrated how water readily displaces pyrene from adsorption sites on mineral surfaces. Similarly, the magnitude of the estimated enthalpy gain associated with the substitution of phenanthrene by water molecules suggests that there is probably no competition for adsorption sites on a natural sediment surface. Instead, water adsorbs as if it was the only species present and phenanthrene occupies whatever sites remain uncovered by the water film. Thus, equation (2.10) seems adequate to model contaminant partitioning to the mineral surface. The key factor in (2.10) is the model used to describe water adsorption, $\Theta(mc)$. Expression (2.9) presented in section 2.3.3.1 assumes that water adsorbs on the sediment according to a Langmuir model i.e. $\Theta(mc)=1-(mc/mc_m)$. However, in section 4.2.4 it was shown that water sorption is accurately described by a different adsorption/condensation model. Thus, adsorption to the dry mineral surface is modeled here by:

$$K_m = \frac{BW_m}{P^{sat}} \Theta_{a/c}(mc) \qquad (4.11)$$

Where:

- $\Theta_{a/c}(mc)$ is the water-free surface area fraction calculated by the adsorption/condensation model developed in section 4.2.4.
- $B=\exp[(\Delta H_{cond} - \Delta H_{adso})/RT]$, where ΔH_{cond} and ΔH_{adso} are respectively the enthalpy of condensation and the enthalpy of adsorption on the dry sediment surface. For phenanthrene, B can be calculated from the heat of adsorption on dry sediment determined in section 4.3.3.3 and the heat of sublimation determined in section 4.1.2.3
- W_m is estimated by: $W_m=F \cdot M \cdot (A/\alpha N)$ where α is the surface area of an adsorbed molecule and the other parameters have the same meaning as in equation (2.5).

In equation (2.5), the parameter α is calculated from the liquid density by assuming spherical molecules. However, PAHs adsorb in a flat configuration. It is thus more accurate to use a different method to estimate α. In this study, the parameter α is approximated by the Van der Waals molecular surface area.

The parameter F is the fraction of the surface area, A, which is available to PAH adsorption. Some factors affecting F are discussed in Appendix I. It is possible to estimate F from experimental data by using equation (4.10). In the expression of K_m, all the parameters but F have been either experimentally determined or estimated. Thus, F can be calculated by replacing K_m in equation (4.10) by an experimental value. A fit of equation (4.10) to the experimental coefficients of partition obtained for dry sediments contaminated with phenanthrene gives a value of 0.1. However, values of F calculated in

Appendix I for the adsorption of non-polar VOCs on mineral surfaces or soils of low organic content are in the range of 0.6 to 1. The low value obtained in this study could be explained by various reasons:

- Fluorescence spectroscopy reveals that the adsorption sites of a PAH molecule such as pyrene on the surface of silica gel and clay are not homogeneously distributed but form clusters (see section 2.2.3.1). This results in portions of the surface being energetically unfavorable to adsorption i.e. a low value of F. Bauer et al., 1982 showed that a monomolecular layer of pyrene covers only 76% of the surface area of the silica gel on which it adsorbs (65% in the case of alumina).
- The review of two experimental studies presented in Appendix I indicates that the organic content of a soil decreases its surface area available for adsorption. From the correlation developed in the same appendix, it can be calculated that a soil having an organic content of 3% will have only half the available surface area of a similar soil with an organic content of 1%. Thus, the relatively high organic content (f_{oc}=3%) of Campus Lake sediment may in part explain the low value of F.

Numerical values of the parameters needed in the estimation of K_m are summarized in Table 4.11.

4.4.2 Model of the overall partition coefficient

4.4.2.1 Relative importance of the various sorption compartments

On the basis of the considerations developed above, estimates of phenanthrene partitioning to the various sediment compartments as a function of relative humidity were calculated. Results are shown in Figure 4.18.

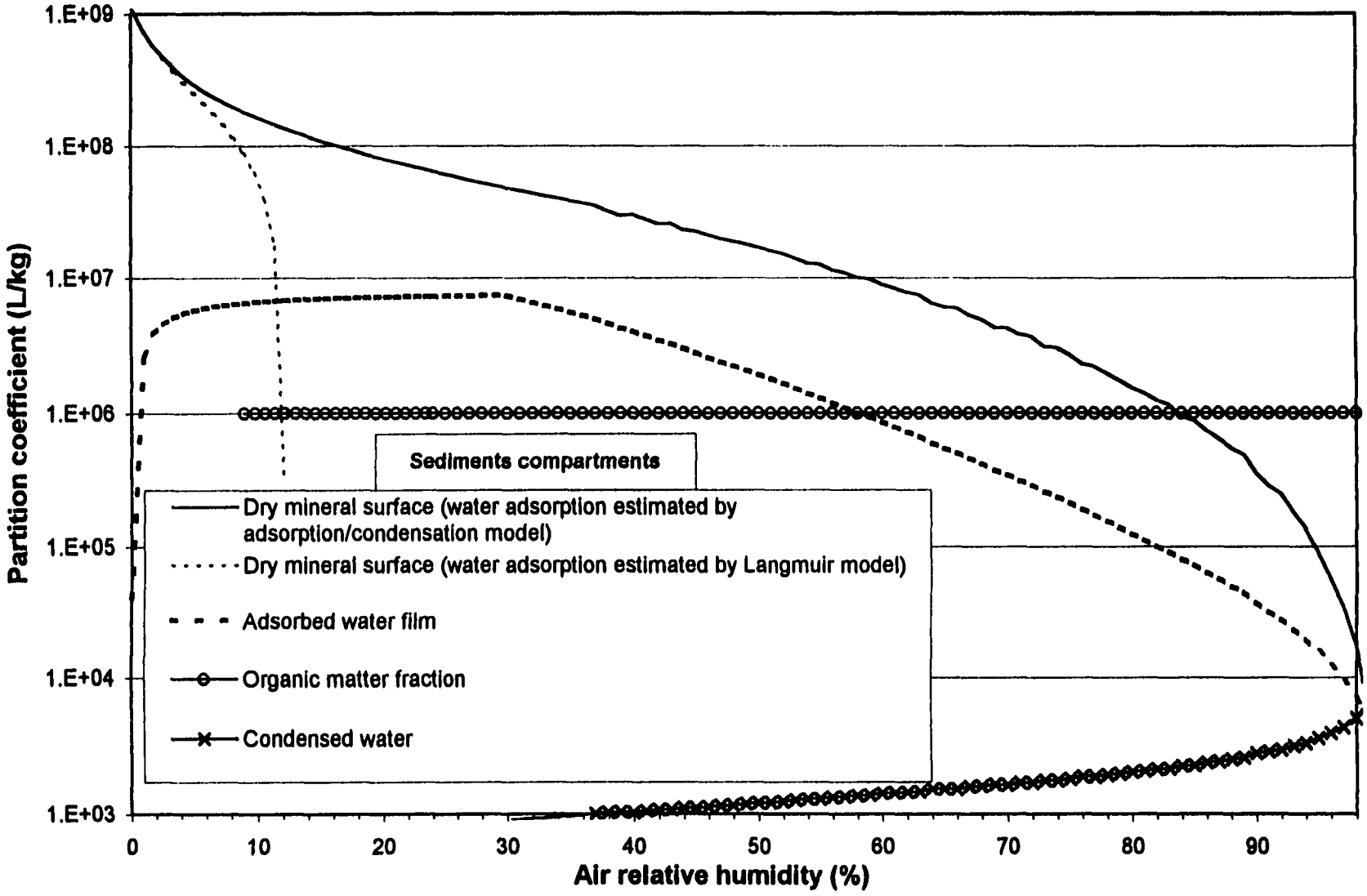

Figure 4.18 Models of the partition coefficients of phenanthrene between various sediment compartments and air.

Table 4.11 Parameters used in the calculation of K_m for phenanthrene and dibenzofuran

	PHEN	DBF
α (10^{-20} m^2)	190	180
F†	0.1	0.1
W_m(mg/m^2)	1.2	1.2
B* (RH=0.2%)	$11x10^4$	$11x10^4$
P_S^{sat} (mPa)	16	429
Log K_m (K_m in L/kg)	9.0	7.7

† Fitted to phenanthrene experimental data
* Experimentally determined for phenanthrene

For adsorption on the mineral surface, model (2.9) and (4.10), are both represented. Since it is based on the Langmuir model to predict water adsorption, equation (2.9) predicts that contaminant uptake by mineral surface falls to zero when mc $=mc_m$ (which is equivalent to the air relative humidity approaching 10%). On the other hand, equation (4.10) is based on the adsorption/condensation model, which predicts that a fraction of sediment surface area remains uncovered by water even at a high relative humidity (Figure 4.9). Therefore, model (4.10) predicts that adsorption on the mineral surface remains the most important uptake mechanism even at high relative humidity.

A realistic representation of contaminant adsorption onto mineral surfaces can probably be found in between these two approaches. Adsorption to the mineral surface remains an important mechanism even when the moisture content is higher than what is required for monolayer coverage because some dry surface is left for adsorption. However, water preferentially adsorbs onto the most energetic sites and the binding

capacity of the sites remaining on the water free surface is expected to decrease as moisture content increases. Consequently, the small fraction of dry surface area remaining at high relative humidity is not expected to play a significant role in contaminant adsorption. Thus, model (4.10) overestimates the uptake at high relative humidity. In conclusion, it seems realistic to account for adsorption to the mineral surface by model (4.10) only until about 95% of the surface is covered by water, which defines the lower limit of the "wet" range, as defined by Thibodeaux, 1996. This corresponds to a relative humidity of about 30% and a moisture content of about 1.6%.

The model predicts that adsorption at the air/water interface is an important mechanism of phenanthrene uptake. In fact, the water film has a larger capacity for phenanthrene than the sediment organic matter until the air relative humidity reaches about 50%.

Finally, the model shows that dissolution in the condensed water phase is not a significant mechanism in the range of moisture content investigated.

As a summary, maximum values of phenanthrene and dibenzofuran partition coefficients between air and the different sediment compartments were calculated. They are presented in Table 4.12. For phenanthrene these values correspond to the maximum of each curve plotted in Figure 4.18.

4.4.2.2 Overall partition coefficient

Different regions can be demarcated on Figure 4.18 depending on the dominant sorption mechanisms. In each region, the sediment-air partition coefficient model is obtained by summing the partition coefficient associated to the most important mechanisms. Three regions are demarcated:

- At low relative humidity (RH<30%, mc<1.6%) i.e. over the "dry" and "damp" ranges, sorption is caused by adsorption to mineral surfaces and to the water film.
- In the intermediate range, 30%<RH<85% or 1.6%<mc<4.5%, (which is the beginning of the "wet" range) the two most important sorption mechanisms are: (i) adsorption to the water film and (ii) partitioning into the organic matter.
- At higher humidity, partitioning into the organic matter is the sole sorption mechanism remaining. (Even in this region, dissolution into condensed water is not a significant uptake mechanism.)

Table 4.12 Estimates of the maximum of the partition coefficients between air and various sediment compartments for phenanthrene and dibenzofuran.

	log K (K in L/kg)	
	PHEN	DBF
Mineral surface (mc = 0.2%)	9.0	7.7
Water film (mc = 1.6%)	6.9	5.3
Organic matter (mc ≥ 1.6%)	6.0	5.1
Condensed water surface (mc = 8%)	4.0	2.5
Water bulk (mc = 8%)	3.6	3.2

In Figures 4.10 through 4.12, results of desorption experiments were presented by sets of sediment batches having similar moisture content. In order to assess precisely the influence of moisture content, a partition coefficient was calculated from each individual experiment. The partition coefficients obtained for phenanthrene and dibenzofuran are plotted as a function of moisture content in Figures 4.19 and 4.20, respectively. Partition coefficients calculated from the model are plotted on the same figures. The agreement with experimental data points is good. Two remarks can be made:

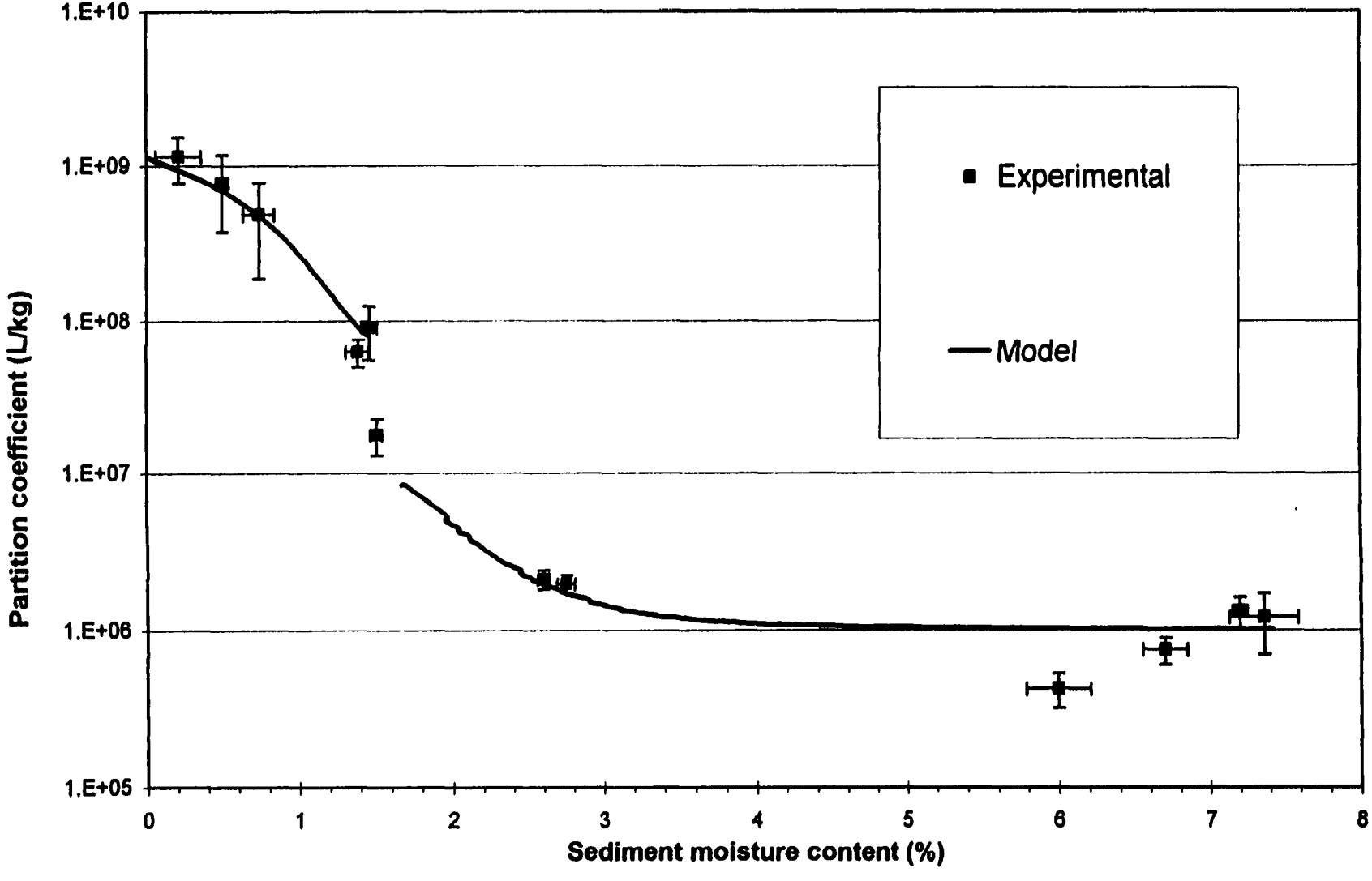

Figure 4.19 Influence of the moisture content on sediment/air partitioning of phenanthrene at 25°C.

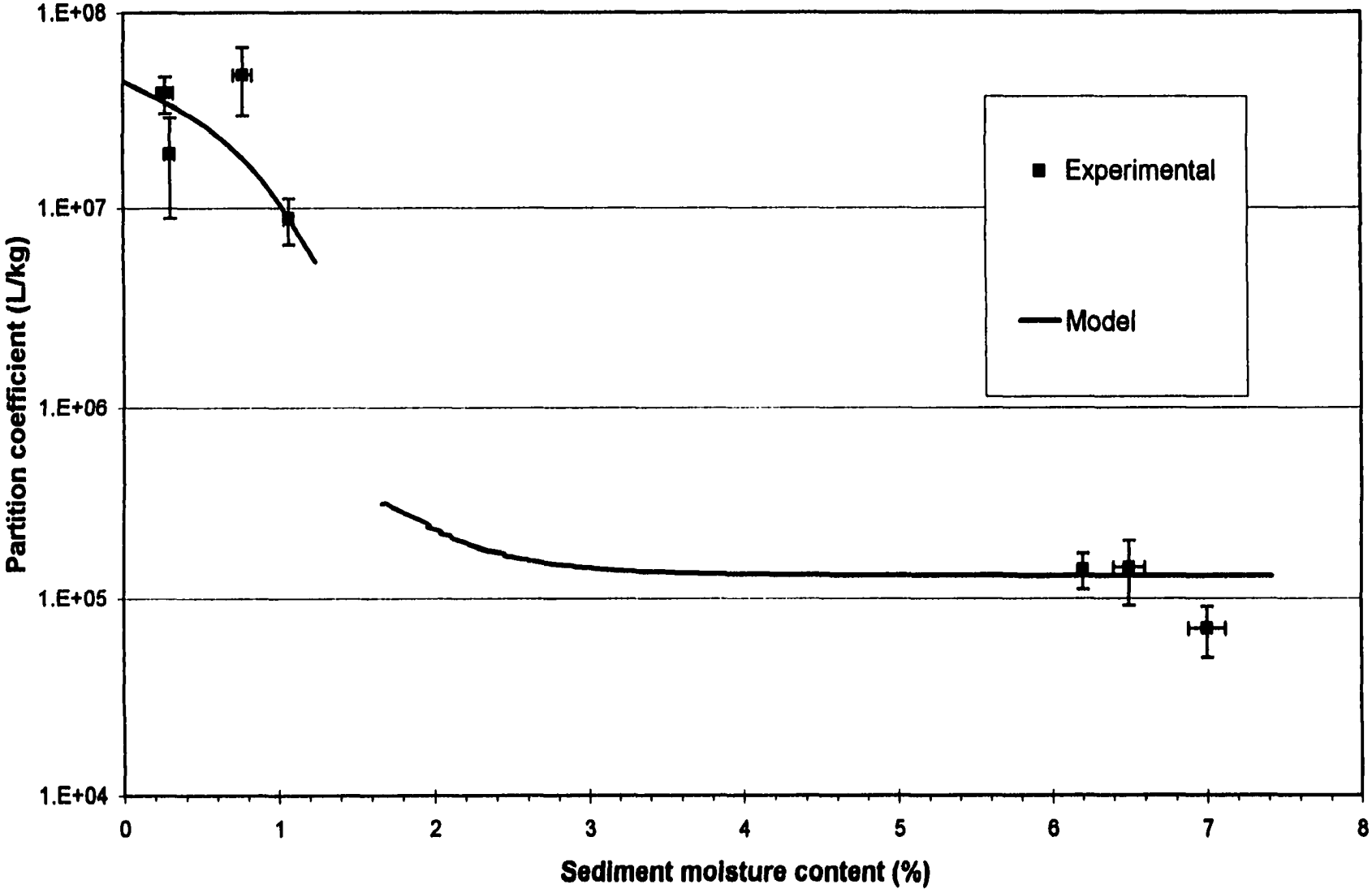

Figure 4.20 Influence of the moisture content on dibenzofuran sediment-air partitioning at 25°C.

- It is remarkable that, using the same value of F (the surface area fraction accessible to contaminant) the model fits both phenanthrene and dibenzofuran partition coefficients in the dry range.
- The partitioning to the air/water film has a significant contribution to the overall partition coefficient in the damp region. This is demonstrated by the upward curvature at the beginning of the second branch of both models. This uptake mechanism in the damp region is specific to semi-volatile organic compounds due to their low vapor pressures. For volatile compounds, this mechanism is expected to be negligible compared to sorption into the organic matter.

Observed deviations from the model. In the light of this model, it is interesting to reconsider the observations made in Figures 4.10 to 4.12 about the deviation of some experimental data points to the linear partitioning model.

For phenanthrene, agreement between the model and the experimental data obtained in the dry and damp range is good. This leads one to think that deviation from linearity of phenanthrene sorption isotherms in the dry and damp ranges observed in Figure 4.10 is caused by the slight sample to sample differences in moisture content, magnified by the high moisture sensitivity of the partition coefficient in this range.

The non-linearity observed for phenanthrene and dibenzofuran sorption isotherms at 25°C in wet sediments, however, is not explained by moisture content variations. (It is to be noted that the logarithmic scale magnifies the apparent amplitude of the deviation.) Phenanthrene adsorption isotherms at 14 and 35°C are much more linear and do not show any trend in curvature. This observation seems to indicate that the curvature observed in the adsorption isotherms at 25°C of phenanthrene and dibenzofuran does not reflect a true

non-linearity of the partitioning isotherm. The curvature is probably incidental, caused by experimental artifacts. Furthermore two different reasons lead to believe that the latter experimental artifacts do not originate from the determination of air phase concentrations:

- Saturated vapor pressures could be measured accurately following an experimental protocol similar to the one used to measure sediment-air partitioning
- Phenanthrene data were in good agreement with the Gibbs-Helmoltz equation. This shows that for a given sediment, measurements of the gas phase concentration are coherent.

Thus, non-linearity of phenanthrene and dibenzofuran adsorption isotherms on wet sediment at 25°C are likely to be caused by experimental artifacts specifically associated with the determination of the sediment phase concentrations. It was established in section 3.6.3.2 that the recovery of the concentration step involved in the sediment analysis was relatively low for the more dilute samples. The recovery factor was found reproducible. However, because of the low recovery, it is possible that variations from the experimental conditions in which the recovery test was conducted could modify the recovery factor. In fact, experimental parameters such as nitrogen flow rate or concentration time were subject to slight variations.

The random nature of the deviation from the model of dibenzofuran experimental data points in the dry range seems to indicate that it is caused by poor quality of the experimental data. Given the demonstrated reliability of the gas phase analysis technique, it is likely that these faulty measurements are caused by problems associated with the determination of sediment concentration. Losses caused by the concentration step are

especially high in the analysis of sediment samples contaminated with low concentrations of dibenzofuran (see Figure 3.14). Thus the hypothesis proposed to explain the non-linearity of the isotherms in wet sediment at 25°C is even more likely in this case.

Chapter 5
Conclusions and Recommendations

5.1 Project summary and conclusions

5.1.1 Experimental considerations

5.1.1.1 Experimental setup

An experimental method was developed in order to measure equilibrium partial pressures of organic contaminants in contact with polluted sediments or soils. The experimental setup allowed the measurement of equilibrium partial pressures of organic contaminants in the range of 10^{-7} to 10^{-2} Pa (7pg/L to 0.7μg/L). It was also possible to explore different conditions of temperature and humidity corresponding to various environmental conditions. The same setup permitted the determination of the sorption isotherm of water on the sediment.

5.1.1.2 Sediment inoculation

A new method for the laboratory preparation of dry sediments contaminated by semi-volatile organic compounds was developed. This method preserves the sediment nature and avoids the inconveniences associated with inoculation techniques previously reported in the literature.

5.1.2 Summary of results

5.1.2.1 Partitioning coefficient

The sediment-air partitioning of phenanthrene and dibenzofuran was studied. Changes in environmental conditions were found to have a large impact on the sorption of the two compounds in sediments. The partition coefficients at 25°C decreased respectively by a factor of 1000 and 200 when the moisture

content changed from about 0.1% to about 6%. Furthermore, phenanthrene partition coefficient in dry sediment decreased by a factor of about 55 when the temperature increased from 14 to 35°C. Over the same temperature range, K_s varied by a factor of 12 in wet sediment.

5.1.2.2 Heat of sorption

The heat of sorption of phenanthrene in sediments was determined. The respective values obtained for dry and wet sediments indicate that the sorption mechanisms involved in each case are fundamentally different. Furthermore, the magnitude of the heat of sorption in dry sediment is compatible with a mechanism of adsorption on the mineral surfaces by the establishment of hydrogen bonds between π-electrons of the aromatic rings and silanol groups of the surface. On the other hand, the magnitude of the heat of sorption determined in wet sediment is compatible with a mechanism of solvation in the organic matter.

The heat of adsorption on dry sediment per aromatic ring was in close agreement with values of the heat of adsorption of benzene on soils reported in the literature.

5.1.2.3 Water isotherm model

A new model for the sorption of water on a sediment was proposed. The model was able to capture the sorption isotherm of water on the studied sediment over virtually the entire range of relative humidity. The model is solely based on easily accessible physical parameters of the sediment, namely, the pore volume distribution and the two BET parameters (B_w, mc_m).

5.1.2.4 Model for the partition coefficient

The model for water adsorption/condensation in the sediment served as a basis for the modeling of the sediment-air partition coefficient of polynuclear aromatic hydrocarbons and heterocyclic hydrocarbons. Most of the additional parameters required in the model are easy to determine (f_{oc}) or available in the literature (P^{sat}). However, the fraction of surface area available to adsorption in dry sediments, F had to be estimated from the experimental data. This model accurately predicted the variations of the partition coefficients of phenanthrene and dibenzofuran over the entire range of air relative humidity.

5.2 Recommendations

5.2.1 Partition coefficient of SVOCs

No account of the study of the partition coefficient of PAHs in dry soils or sediments could be found in the literature. However, this parameter is required in the development of emission models from exposed soils and sediments. Thus, further experiments should be conducted in order to develop a database of partition coefficients allowing the assessment of emission models currently being developed. Compounds of interest include PAHs of high molecular mass (as they are prone to bioaccumulate and are often highly toxic) or other families of SVOCs usually found in contaminated sediments such as heterocyclic aromatic compounds or polychlorinated biphenyls.

5.2.2 Field sediments

5.2.2.1 Aging effect

Aging of the sediment is expected to cause part of the contaminant to become sequestrated. Elucidating the mechanisms of aging is thus a prerequisite to the modeling of toxic emissions from contaminated sediments by any of the possible release pathways. Aging effects on the partition coefficient of contaminants in wet sediment is expected to reflect the rule of the organic matter/water partition coefficient, K_{oc}. However, the sediment-air partition coefficient of contaminants in dry sediment is independent of K_{oc}. Thus, investigation of the aging effect on the sediment-air partitioning in dry conditions could give some insight on the mechanisms involved in the aging process.

5.2.2.2 Competitive adsorption

A wide range of semi-volatile organic compounds are likely to be present in field contaminated sediments. The partition coefficient between the organic matter of a sediment and water, K_{oc} of a given organic compound is not modified by the presence of other contaminants. Thus, the sediment-air partition coefficient in wet conditions determined in this study should remain valid for field sediments. However, in dry sediment, site specific adsorption accounts for the uptake of contaminant. It is thus expected that the various contaminant molecules compete for the adsorption sites. Interactions should, therefore, be observed between the different partition coefficients. In order to develop a realistic emission model for a given contaminant, its partition coefficient must take into account the presence in the sediment of other organic compounds. The effect of competitive adsorption

could be assessed by repeating the gas saturation experiments with sediment batches spiked with a set of compounds including phenanthrene and dibenzofuran.

5.2.3 Model of the partition coefficient

5.2.3.1 Water isotherm model

The model of water adsorption/condensation proposed in this study has a central role in the modeling of the sediment-air partitioning of organic contaminants. Therefore, it should be assessed for further use by comparing its predictions to experimental isotherm of water sorption in sediments or soils exhibiting various pore volume distributions or BET parameters.

5.2.3.2 Surface area available to adsorption

The fraction of the sediment surface area available to contaminant adsorption, F is the only parameter in the model of the partition coefficient that could not be independently estimated and had to be fitted to the experimental data. In other words, F is the only parameter precluding the obtention of a predictive model of the partition coefficient. Thus, factors likely to influence F such as the sediment organic fraction or the nature of the adsorbed molecule should be investigated.

5.2.3.3 Assesment of the model

The influence of the sediment moisture content on the partition coefficient of other PAHs, both heavier (pyrene) and lighter (naphtalene) than phenanthrene, should be investigated. This would provide a test of the model. Specifically, the proportionality of the BET parameter B to the number of aromatic rings in the

PAH molecule would be tested. Also, the contribution to the overall partition coefficient of the mechanism of adsorption on the water film in the intermediate range of relative humidity (20-50% RH) would be expected to be more significant for PAHs of high molecular mass.

5.2.4 Setup improvements

5.2.4.1 Measurement of the volume of the air phase

The total volume of the air phase that passed through the gas saturation column was determined by monitoring the air flow rate with flow-meters over the duration of an experiment. For the investigation of compounds having sediment-air partition coefficients higher than phenanthrene (and thus requiring long trapping times), it is recommended that electronic volume integrators be used instead of rotameters. This would not only simplify the experimental protocol but also improve the accuracy of the measurement.

5.2.4.2 Concentration of extracts from the analytical traps

In order to shorten the trapping time required for the determination of high partition coefficients, a method should be developed for the concentration of extracts from the analytical traps.

References

Aamot, E., E. Steinnes and R. Schmid. (1996) Polycyclic Aromatic Hydrocarbons in Norwegian Forest Soils: Impact of Long Range Atmospheric Transport. *Environment Pollution*. **92**(3), 275-280.

Abraham, M.H. (1993) Scales of Solute Hydrogen-bonding: Their Construction and Application to Physicochemical and Biochemical Processes. *Chemical Society Reviews*. **22**, 73-83.

Adamson, A.W. (1990) Physical Chemistry of Surfaces, Fifth Edition. *John Wiley & Sons, Inc.*

Alaee, M., R.M. Whittal, and W.M.J. Strachan. (1996) The Effect of Water Temperature and Compostion on Henry's Law Constant for Various PAHs. *Chemosphere*. **32**(6), 1153-1164.

Askari, M.D.F., M.P. Maskarinec, S.M. Smith, P.M. Beam and C.C. Travis. (1996) Effectiveness of Purge and Trap for Measurement of Volatile Organic Compounds in Aged Soils. *Analytical Chemistry*. **68**, 3431-3433.

Balogh, M. and P. Laszlo. (1993) Organic Chemistry Using Clays. *Springer-Verlag*.

Barlow, F. and A.B. Hadaway. (1956) Effect of Changes in Humidity on the Toxicity and Distribution of Insecticides Sorbed by Some Dried Soils. *Nature*. **178**, 1299-1300.

Barrer, R.M. and D.M. Macleod. (1954) Intercalation and Sorption by Montmorillonite. *Faraday Society Discussions*. **50**, 980.

Barrer, R.M., N. McKenzie, and J.S.S. Reay. (1956) Capillary Condensation in Single Pores. *Journal of Colloid Science*. **11**, 479-495.

Bauer, R. K., P. de Mayo, W.R. Ware, and K.C. Wu. (1982) Surface Photochemistry: The Photophysics of Pyrene Adsorbed on Silica Gel, Alumina and Calcium Fluoride. *Journal of Physical Chemistry*. **86**, 3781-3789.

Bauer, R.K., P. de Mayo, L.V. Natarajan, and W.R. Ware. (1984) Surface Photochemistry: The Effect of Surface Modification on the Photophysics of Naphthalene and Pyrene Adsorbed on Silica Gel. *Canadian Journal of Chemistry*. **62**, 1279-1286.

Bauer, R.K., P. de Mayo, K. Okada, W.R. Ware, and K.C. Wu. (1983) Surface Photochemistry: The Effects of Coadsorbed Molecules on Pyrene Luminescence and Acenaphthylene Dimerization on Silica Gel. *Journal of Physical Chemistry*. **87**, 460-466.

Bidleman, T. F. and W. T. Foreman. (1987) *Vapor-Particle Partitioning of Semivolatile Organic Compounds.* in Advances in Chemistry Series. Sources and Fates of Aquatic Pollutants. R. A. Hites and S. J. Eisenreich, editors.

Bird, R.B., W.E. Stewart and E.N. Lightfoot. (1960) Transport Phenomena. John Wiley and Sons.

Bohn, Hinrich L., G.K. Prosoki, and J.G. Eckhardt. (1980) Hydrocarbon Adsorption by Soils as the Stationary Phase of Gas-Solid Chromatography. *Journal of Environmental Quality.* **9**(4), 563-565.

Bridges, T.S., D.W. Moore, P. Landrum, J. Neff, and J. Cura. (1996) "Summary of a Workshop on Interpreting Bioaccumulation Data Collected During Regulatory Evaluations of Dredged Material," Miscellaneous Paper D-96-1, U.S. Army Engineer Waterways Experiment Station, Vicksburg, MS.

Brunauer, S., P.H. Emmett and E. Teller. (1983) Adsorption of Gases in Multimolecular Layers. *Journal of American Chemical Society.* **60**, 309-319.

Burgos, W.D., J.T. Novak, and D.F. Berry. (1996) Reversible Sorption and Irreversible Binding of Naphthalene and Alpha-Naphthol to Soil: Elucidation of Processes. *Environmental Science and Technology.* **30**, 1205-1211.

Cerfontain, H. (1968) Mechanistic Aspects in Aromatic Sulfonation and Desulfonation. Interscience Publishers.

Che, M. and G.C. Bond (eds). (1985) Adsorption and Catalysis on Oxide Surfaces. Elsevier. Chem Phys 1980, 51, p 61

Chin, Y. and P.M. Gschwend. (1991) The Abundance, Distribution, and Configuration of Porewater Organic Colloids in Recent Sediments. *Geochimica et Cosmochimica Acta.* **55**, 1309-1317.

Chiou, C.T. and D.W. Rutherford. (1992) Effect of Water Saturation in Soil Organic Matter on the Partition of Organic Compounds. *Environmental Science and Technology.* **26**, 965-970.

Chiou, C.T. and T.D. Shoup. (1985) Soil Sorption of Organic Vapors and Effects of Humidity on Sorptive Mechanism and Capacity. *Environmental Science and Technology.* **19**, 1196-1200.

Chirico, R.D., B.E. Gammon, S.E. Knipmeyer, A. Nguyen, M.M. Strube, C Tsonopoulos, and W.V. Steele. (1990) The Themodynamic Properties of Dibenzofuran. *Journal of Chemical Thermodynamics.* **22**, 1075-1096.

Chrisodoulatos, C. and M. Mohiuddinm. (1996) Generalized Models for Prediction of Pentachlorophenol Adsorption by Natural Soils. *Water Environment Research.* **68**(3), 370-378.

Chung, S.F. and C.Y Wen. (1968) Longitudinal Dispersion of Liquid Flowing Through Fixed and Fluidized Beds. *AIChE Journal*, **14**, 857.

Cohen, Y., P.A. Ryan. (1989) Chemical Transport in the Top Soil Zone – The Role of Moisture and Temperature Gradients. *Journal of Hazardous Materials*, **22**, 283-304

Cooper, W.T. and J.M. Hayes. (1984) Characterization of Adsorption at Kaolinite Surfaces by Heterogeneous Gas-Solid Chromatography. *Journal of Chromatography.* **314**, 111-125.

Cornelissen, G., P.C.M. van Noort, J.R. Parson, and H.R.J. Govers. (1997) Temperature Dependence of Slow Adsorption and Desorption Kinetics of Organic Compounds in Sediments. *Environmental Science and Technology.* **31**, 454-460.

Cousins, I.T., M.S. McLachlan, and K.C. Jones. (1998) Lack of an Aging Effect on the Soil- Air Partitioning of Polychlorinated Biphenyls. *Environmental Science and Technology.* **32**, 2734-2740.

Cunningham, B. (1998) Doctorate candidate. Louisiana State University. Department of Chemical Engineering. Personal Communication.

Daubert, T. E. and R.P. Danner. (1995) Physical and Thermodynamic Properties of Pure Chemicals; Data Compilation. *AIChE.*

Delle Site, A. (1997) The Vapor Pressure of Environmentally Significant Organic Chemicals: A review of Methods and Data at Ambient Temperature. *Journal of Physical Chemistry.* **26**(1), 157-193.

Delville, A. and S. Sokolowski. (1993) Adsorption of Vapor at a Solid Interface: A Molecular Model of Clay Wetting. *Journal of Physical Chemistry.* 97(23), 6261-6271.

Dong, D.C., and W.A. Winnik. (1982) The Py Scale of Solvent Polarities. Solvent Effects on the Vibronic Fine Structure of Pyrene Fluorescence and Empirical Correlations with E_T and Y values. *Photochemistry and Photobiology.* **35**, 17-21.

Dorris, G. M. and D. G. Gray. (1981) Adsorption of Hydrocarbons on Silica-Supported Water Surfaces. *Journal of Physical Chemistry.* **85**, 3628-3635.

Dupont, R.R. (1986) Evaluation of Air Emission Release Rate Model Prediction of Hazardous Organics from Land Treatment Facilities, *Environmental Programs.*, **5**, 197-202

Engebretson, R.R. and R. Wandruszka. (1994) Microorganization in Dissolved Humic Acids. *Environmental Science and Technology.* **28**, 1934-1941.

Everett, D.H., and J.C. Powl. (1975) Adsorption in Slit-like and Cylindrical Micropores in the Henry's Law Region. 619-636.

Farrell, J. and M. Reinhard. (1994) Desorption of Halogenated Organics from Model Solids, Sediments, and Soil under Unsaturated Conditions, 1. Isotherms. *Environmental Science and Technology* **28**, 53-62.

Farrell, J. and M. Reinhard. (1994) Desorption of Halogenated Organics from Model Solids, Sediments, and Soil under Unsaturated Conditions. 2. Kinetics. *Environmental Science and Technology*. **28**, 63-72.

Fletcher, C.L. and D.D. Kaufman. (1980) Effect of Sterialization Methods on 3-Chloroniline Behavior in Soil. *Journal of Agricultural Food Chemisty*. **28**, 667-671.

Francis, C., J. Lin, and L.A. Singer. (1983) Photophysical Studies of Pyrene on Oxide Supports: The Effect of Surface Modification on Probe Dispersion and Mobility. *Chemical Physics Letters*. **94**(2), 162-167.

Fu, G., A.T. Kan, and M. Tomson. (1994) Adsorption and Desorption Hysteresis of PAHs in Surface Sediment. *Environmental Technology and Chemistry*. **13**, 1559-1567.

Fujii, T. and E. Shimuzu. (1987) Photophysics on Solid Surfaces. Ground State Configuration of Dimeric Pyrene in the Adsorbed State on a Silica Gel Surface and Geometrical Relaxation for Excimer Formation. *Chemical Physics letters*. **137**(5), 448-452.

Fujii, T., E. Shimizu, and S. Suzuki. (1988) Photophysics at Solid Surfaces. *Journal of the Chemical Society*, **84**(12), 4387-4395.

Gan, Robert D. and R.R. DuPont. (1989) Multiphase and Multicompound Measurements of Batch Equilibrium Distribution Coefficients for Six Volatile Organic Compounds. *Hazardous Waste and Hazardous Materials*. **6**(4), 363-383.

Ganaye, V.A., K. Keiding, T.M. Vogel, M-L. Viriot, and J-C Block. (1997) Evaluation of Soil Organic Matter Polarity by Pyrene Fluorescence Spectrum Variations. *Environmental Science and Technology*, **31**(10), 2701-2706.

Gauthier, T.D., E.C. Shane, W.F. Guerin, W.R. Seitz, and C.L. Grant. (1986) Fluorescence Quenching Method for Determining Equilibrium Constans for Polycyclic Aromatic Hydrocarbons Binding to Dissolved Humic Materials. *Environmental Science and Technology*. **20**, 1162-1166.

Goss, K.-U. (1992), Effect of Temperature and Relative Humidity on the Sorption of Organic Vapors on Quartz Sand. *Environmental Science and Technology*. **26**, 2287-2294.

Goss, K.-U. (1993), Effect of Temperature and Relative Humidity on the Sorption of Organic Vapors on Clay Minerals. *Environmental Science and Technology*. **27**, 2127-2132.

Goss, K.-U. (1994), Adsorption of Organic Vapors on Polar Mineral Surfaces and on a Bulk Water Surface: Development of an Empirical Predictive Model. *Environmental Science and Technology*. **28**, 640-645.

Goss, K.-U. (1997), Conceptual Model for the Adsorption of Organic Compounds for the Gas Phase to Liquid and Solid Surfaces. *Environmental Science and Technology*. **31**, 3600-3605.

Goss, K.-U. and S.J. Eisenreich. (1996) Adsorption of VOCs from the Gas Phase to Different Minerals and a Mineral Mixture. *Environmental Science and Technology*., **30**, 2135-2142.

Grathwohl, P. and M. Reinhard. (1993) Desorption of Trichloroethylene in Aquifer material: Rate Limitation at the Grain Scale. *Environmental Science and Technology*. **27**, 2360-2366.

Gregg, S.J. and K.S.W. Sing. (1982) Adsorption, Surface Area, and Porosity Second Edition. *Academic Press*.

Handbook of Chemistry and Physics. (1981-82) Boca Raton, Florida: CRC Press, Inc.

Hansen, P.C. and C.A Eckert. (1986) An Improved Transpiration Method for the Measurement of Very Low Vapor Pressures. *Journal of Chemical Engineering Data*. **31**, 1-3.

Hara, K.,P. de Mayo, W.R. Ware, A.C. Weedon, G.S.K. Wong, and K.C. Wu. (1980) Biphasic Photochemistry: Time-Resolved Spectra of Adsorbed Hydrocarbons. *Chemical Physics Letters*., **69**(1), 105-108.

Harner, T. and T.F. Bidleman. (1998) Measurement of Octanol-Air Partition Coefficients for Polycyclic Aromatic Hydrocarbons and Polychlorinated Naphthalenes. *Journal of Chemical Engineering Data*. **43**, 40-46.

Harner, T. and D. Mackay. (1995) Measurement of Octanol-Air Partition Coefficients for Chlorobenzenes, PCBs, and DDT. *Environmental Science and Technology*. **29**, 1599-1606.

Harvey. R.G. (1991) Polycyclic Aromatic Hydrocarbons. Chemistry and Carcinogenicity. Cambridge University Press, Cambridge. 11-134.

Harvey, R.G. (1997) Polycylic Aromatic Hydrocarbons. New York: Wiley-VCH, 667p.

Henrich, V.E., & P.A. Cox. (1996) Molecular Adsorption on Oxides. The Surface Science of Metal Oxides. 247-282.

Hill, T.L. (1956) Statistical Mechanics: Principles and Selected Applications. New York: Dover Publications, Inc. 432 pp.

Hill, T. L. (1946a) Theory of Multimolecular Adsorption from a Mixture of Gases. *The Journal of Chemical Physics.* **14**(1), 46-47.

Hill, T. L. (1946b) Theory of Multimolecular Adsorption from a Mixture of Gases. *The Journal of Chemical Physics.* **14**(4), 268-275.

Hinckley, D.A., T.F. Bidleman, and W.T. Foreman. (1990) Determinatin of Vapor Pressures for Nonpolar and Semipolar Organic Compounds form Gas Chromatographic Retention Data. *Journal of Chemical Engineering Data.* **35**, 232-237.

Hippelein M, and M.S. Mclachlan. (1998) Soil/Air Partitioning of Semivolatile Organic Compounds. 1. Method Developtment and Influence of Physical-Chemical Properties. *Environmental Science and Technology.* **32**, 310-316.

Hoff, J.T., R.Gillham, D. Mackay, and W.Y. Shku. (1993) Sorption of Organic Vapors at the Air-Water Interface in a Sandy Aquifer Material. *Environmental Science and Technology.* **27**, 2789-2794.

Hougen, O.A. and W.R. Marshall. (1947) Adsorption From a Fluid Stream Flowing Through a Stationary Granualr Bed. *Chemical Engineering Progress.* **43**(4), 197-208.

Hunter, M.G., A.T. Kan, and M.B. Tomson. (1996) Development of a Surrogate Sediment to Study the Mechanisms Responsible for Adsorption/Desorption Hysteresis. *Environmental Science and Technology.* **30**, 2278-2285.

Inagaki, S., Y. Fukushima, K. Kuroda, and K. Kuroda. (1996) Adsorption Isotherm of Water Vapor and Its Large Hysteresis on Highly Ordered Mesoporous Silica. *Journal of Colloid and Interface Science.* **180**, 623-624.

Jaycock, M.J. and G.D. Parfitt. (1981) Chemistry of Interfaces. *John Wiley and Sons.*

Jepson, R., S. Borglin, W. Lick and D. L. Swackhamer. (1995) Parameters Affecting the Adsorption of Hexachlorobenzene to Natural Sediments. *Environmental Toxicology and Chemistry.* **14**(9), 1487-1497.

Johnston, C.T., T. Tipton, D.A. Stone, C. Erickson, and S.L. Trabue. (1991) Chemisorption of p-Dimethoxybenzene on Copper-Montmorillonite. *Langmuir.* **7**, 289-296.

Kan, A. T., G. Fu and M. B. Tomson. (1994) Adsorption/Desorption Hysteresis in Organic Pollutant and Soil/Sediment Interaction. *Environmental Science and Technology.* **28**(5), 859-867.

Kan, A.T., G. Fu, M. Hunter, W. Chen, C.H. Ward, and M.B. Tomson. (1998) Irreversible Sorption of Neutral Hydrocarbons to Sediments: Experimental Observations and Model Predictions. *Environmental Science and Technology*. **32**(7), 892-902.

Kan, A.T., G. Fu, M.A. Hunter, and M.B. Tomson. (1997) Irreversible Adsorption of Naphthalene and Tetrachlorobiphenyl to Lula and Surrogate Sediments. **31**, 2176-2185.

Kar, R. and S.K. Sanyal. (1990) A Study of Humic Acid Synthesised in Presence of Clay Catalyst. *Journal of Indian Chemical. Society*. **67**, 384-386.

Karger, B.L., R.C. Castells, P.A. Sewell, and A. Hartkopf. (1971) Study of the Adsorption of Insoluble and Sparingly Soluble Vapors at the Gas-Liquid Interface of Water by Gas Chromatography. *The Journal of Physical Chemistry*. **75**(25), 3870-3879.

Karimi-Lotfabad, S., M. A. Pickard and M. R. Gray. (1996) Reactions of Polynuclear Aromatic Hydrocarbons on Soil. *Environmental Science and Technology*. **30**(4), 1145-1151.

Krasnansky, R. and J.K. Thomas. (1994) Surveying the Silica Gel Surface with Excited States. *In* The Colloid Chemistry of Silica, Ed. *American Chemical Society*, 223-244.

Labbe, P. and G. Reverdy. (1988) Adsorption Characteristics of Polycylcic Aromatic Compounds on Clay: Pyrene as a Photophysical Probe on Laponite. *Langmuir*. **4**, 419-425.

Langer, A., A. Roethe, K.-P. Roethe, and D. Gelbin. (1978) Heat and Mass Transfer In Packed Beds—III. Axial Mass Dispersion. *International Journal of Heat and Mass Transfer*. **21**, 751-759.

Liang, C., J.F. Pankow, J.R. Odum, and J.H. Seinfeld. (1997) Gas/ Particle Partitioning of Semivolatile Organic Compounds to Model Inorganic, Organic, and Ambient Smog Aerosols. *Environmental Science and Technology*. **31**, 3086-3092.

Liu, S. Y, and W.R. Ware. (1993) Photophysics of Polycyclic Aromatic Hydrocarbons Adsorbed on Silica Gel Surfaces. 1. Fluorescence Lifetime Distribution Analysis: An Ill-Conditioned Problem. *Journal of Physical Chemistry*. **97**, 5980-5986.

Liu, X. and J.K. Thomas. (1991) Study of Surface, Properties of Clay Laponite using Pyrene as a Photophysical Probe Molecule. *Langmuir*. 7, 2808-2816.

Liu, X., K.-K. Iu, and J.K. Thomas. (1991) Studies of Surface Properties of Clay Laponite Using Pyrene as a Photophysical Probe Molecule. 2. Photoinduced Electron Transfer. *Langmuir*. **8**, 539-545.

Liu, Y.S., P. de Mayo, and W.R. Ware. (1993) Photophysics of Polycyclic Aromatic Hydrocarbons Adsorbed on Silica Gel Surfaces. 2. Lifetime Distribution and Symmetry. *Journal of Physical Chemistry*., **97**, 5987-5994.

Liu, Y.S., P. de Mayo, and W.R. Ware. (1993) Photophysics of Polycyclic Aromatic Hydrocarbons Adsorbed on Silica Gel Surfaces. 3. Fluorescence Quantum Yields and Radiative Decay Rate Constants Derived from Lifetime Distributions. *Journal of Physical Chemistry.*, **97**, 5995-6001.

Livingston, H.K. (1949) The Cross-Sectional Areas of Molecules Adsorbed on Solid Surfaces. *Journal of Colloid Science.* **4**(5), 447-458.

Lochmuller, C.H. and T.J. Wenzel. (1990) Spectroscopic Studies of Pyrene at Silica Interfaces. *Journal of Physical Chemistry.* **94**, 4230-4235.

Maagd De, G., Th. Ten Hulschner, H. Van den Heuvel, A. Opperhuizen, Dick Sijm. (1998) Physicochemical Properties of Polycyclic Aromatic Hydrocarbons: Aqueous Solubilities, n-octanol/water Partition Coefficients, and Henry's Law constants. *Environmental Toxicology and Chemisty*, **17**(2), 251-257.

Mackay, D., W.Y. Shiu, K.C. Ma. (1992) Illustrated Handbook of Physio-Chemical Properties and Environmental Fate for Organic Chemicals, Part 3. Lewis, Chelsea, MI, USA.

Mackay, D., W.Y. Shiu, R.P. Sutherland. (1979) Determination of Air-Water Henry's Law Constants for Hydrophobic Pollutants. *Environmental Science and Technology*, **13**, 333-337.

Mackay, D. and W.Y. Shiu. (1981) Henry's Law Constants for Organic Compounds. *Journal of Physical Chemistry*, **10**, 1189.

Macknick, A.B. and J.M. Prausnitz. (1979) Vapor Pressures of High-Molecuar-Weight Hydrocarbons. *Journal of Chemical and Engineering Data.* **24**(3), 175-178.

Matsui, K. and N. Usuki. (1990) Excimer Fluorescence of Pyrene in Sol-Gel Silica. Bull. *Chemical Society Jpn.* **63**, 3516-3520.

McClellan, A.L., and H.F. Harnsberger. (1967) Cross-Sectional Areas of Molecules Adsorbed on Solid Surfaces. *Journal of Colloid and Interface Science.* **23**, 577-599.

McGroddy, S.E. and J.W. Farrington. (1996) Comparison of the in Situ and Desorption Sediment-Water Partitioning of Polycyclic Aromatic Hydrocarbons and Polychlorinated Biphenyls. *Environmental Science and Technology.* **30**(1), 172-177.

McGroddy, S.E., and Farrington, J.W. (1995) Sediment Porewater Partitioning of Polycyclic Aromatic Hydrocarbons in Three Cores from Boston Harbor, Massachusetts. *Environmental Science and Technology.* **29**(6), 1542-1550.

Montgomery J. H. (1996) Groundwater Chemicals Desk Reference. Second Edition. Lewis.

Morra, M.J., et al. (1990) Fluorescence Quenching and Polarization Studies of Naphthalene and 1-Naphthol Interaction with Humic Acid. *Soil Science Society American Journal.* **54**, 1283-1289.

Muminov, S.Z., E.A. Aripov, and D.B. Gulyamova. (1992) Temperature Dependence of the Adsorption of Benzene Vapor on a Supporting Hydroxyaluminum Clay. *Zhurnal Prikladnoi Khimii.* **65**(6), 1292-1295.

Nam, K. and M. Alexander. (1998) Role of Nanoporosity and Hydrophobicity in Sequestration and Bioavailability: Tests with Model Solids. *Environmental Science and Technology.* **32**, 71-74.

Naono, Hiromitu and M. Hakuman. (1993) Analysis of Porous Texture by Means of Water Vapor Adsorption Isotherm with Particular Attention to Lower Limit of Hysteresis Loop. *Journal of Colloid and Interface Science.* **158**, 19-26.

Nawrocki, J. and B. Buszewski. (1988) Influence of Silica Surface Chemistry and Structure on the Properties, Structure and Coverage of Alkyl-Bonded Phases for High-Performance Liquid Chromatography. *Journal of Chromatography.* **449**, 1-24.

Neue, G. and F. Rudolph. (1993) A Method for Measuring the Vapor Pressures of PAH's Adsorbed on the Surface of Soot. *International Journal of Analytical Chemistry.* **52**, 229-236.

Niessner, R. and A. Krupp. (1991) Detection and Chemical Characterization of Polycyclic Aromatic Hydorcarbon Aerosols by Means of Laser Induced Fluorescence. *Part. Part. Syst. Charact.* **8**, 23-28.

Norman, R.O.C. and J.M. Coxon. (1993) Principles of Organic Synthesis Third Edition. *Educational Low-Priced Books Scheme with Chapman & Hall.*

Okamura, J. P. and D. T. Sawyer. (1973) Gas Chromatographic Studies of Sorptive Interactions of Normal and Halogenated Hydrocarbons with Water-Modified Soil, Silica, and Chromosorb W. *Analytical Chemistry.* **45**, 80-84.

Ollivon, D., B. Garban, and A. Chesterikoff. (1995) Analysis of the Distribution of Some Polycyclic Aromatic Hydrocarbons in Sediments and Suspended Matter in the River Seine (France). *Water, Air, Soil Pollution.*, **81**(1-2), 135-152.

Ong, S. K., T. B. Culver, L. W. Lion and C. A. Shoemaker. (1992) Effects of Soil Moisture and Physical-Chemical Properties of Organic Pollutants on Vapor-Phase Transport in the Vadose Zone. *Journal of Contaminant Hydrology.* **11**, 273-290.

Ong, S.K. and L.W. Lion. (1991) Mechanisms for Trichloroethylene Vapor Sorption onto Soil Minerals. *Journal of Environmental Quality.* **20**, 180-188.

Orchiston, H.D. (1953) Adsorption of Water Vapor: I. Soils at 25° C. *Soil Science.* **76**, 453-465.

Orchiston, H.D. (1954) Adsorption of Water Vapor: II. Clays at 25° C. *Soil Science*. **78**, 463-480.

Osborn, A.G. and D.R. Douslin. (1975) Vapor Pressures and Derived Enthalpies of Vaporization for Some Condensed-Ring Hydrocarbons. *Journal of Chemical and Engineering Data*. **20**(3), 229-231.

Oscik, J. (1982) Adsorption. Ellis Horwood Ltd., Chichester.

Pankow, J.F. (1991) Common y-Intercept and Single Compound Regressions of Gas-Particle Partitioning Data VS 1/T. *Atmospheric Environment*. **25A**, 2229-2239.

Pankow, J.F. (1994) An Absorption Model of Gas/Particle Partitioning of Organic Compounds in the Atmosphere. *Atmospheric Environment*. **28**, 185-188.

Pankow, J.F. (1998) Further Discussion of the Octanol/Air Partriton Coefficient Koa as a Correlating Parameter for Gas/Particle Partitioning Coeffiecients. *Atmospheric Environment*. **32**, 1493-1497.

Pankow, J.F. and T.F. Bidleman. (1991) Effects of Temperature, TSP and Per Cent Non-Exchangeable Material in Determining the Gas-Particle Partitioning of Organic Compounds. *Atmospheric Enviroment*. **25A**, 2241-2249.

Pankow, J.F. and T.F. Bidleman. (1992) Interdependence of the Slopes and Intercepts from Log-Log Correlations of Measured Gas-Particle Partitioning and Vapor Pressure-I. Theory and Analysis of Available Data. *Atmospheric Environment*. **26A**, 1071-1080.

Pankow, J.F. (1996) Partitioning of Semi-Volatile Organic Compounds to the Air/ Water Interface. *Atmospheric Environment*. **31**(6), 927-929.

Park, K.S., R.C. Sims, and R.R. Dupont. (1990) Transformation of PAHs in Soil Systems. *Journal of Environmental Engineering*. **116**(3), 632-640.

Pashley, R.M. (1980) Multilayer Adsorption of Water on Silica: An Analysis of Experimental Results. *Journal of Colloid and Interface Science*. **78**(1), 246-248.

Patrick, W.H. Jr. (1958) Modification of the Method of Particle Size Analysis. *Soil Science Society of America. Proceedings*. **22**, 366.

Pennel, K. D., R. D. Rhue, P. Suresh, C. Rao and C. T. Johnston. (1992) Vapor Phase Sorption of Para-Xylene and Water on Soils and Clay Minerals. *Journal of Environmental Quality*, **21**, 419-426.

Pohle, W. (1982) Infrared study of the Adsorption of Aromatic Molecules onto Silica and Chlorinated Silica. *Journal of Chemical Society, Faraday Transactions I*. **78**, 2101-2109.

Prausnitz, J.M., R.N. Lichtenthaler, and E.G. de Azevedo. (1986) Molecular Thermodynamics of Fluid-Phase Equilibria Second Edition. Prentice-Hall, Inc.

Puri, A.N., E.M. Crowther, and B.A. Keen. (1925) The Relation Between the Vapour Pressure and Water Content of Soils. *Journal of Agricultural Science*. **15**, 68-88.

Rao, P.S.C., R.A. Ogwada, and R.D. Rhue. (1989) Adsorption of Volatile Organic Compounds on Anhydrous and Hydrated Sorbents: Equilibrium Adsorption and Energetics. *Chemosphere*. **18**(11/12), 2177-2191.

Ravikrishna, R. (1997) Doctorate candidate. Louisiana State University. Department of Chemical Engineering. Personal Communication.

Ravikrishna, R. (1998) Doctorate candidate. Louisiana State University. Department of Chemical Engineering. Personal Communication.

Reid, R.C., J.M Prausnitz, and T.K. Sherwood. (1977) The Properties of Gases and Liquids Third Edition. MacGraw-Hill.

Rhue, R.D., K.D. Pennel, W.H. Reve, and A.G. Hornsby. (1993) Sorption of Para-Xylene Vapors on Salt-Treated Soils Measured by Flow-Equlibration and Gas Chromotography Methods. *Journal of Environmental Quality*. **22**, 521-527.

Rice, M.R. and H.S. Gold. (1984) Investigation of the surface of a polymeric adsorbent with pyrene as a fluorescence probe. *Analytical Chemistry Acta*. **164**, 111-118.

Rootare, H.M. and C.F. Prenzlow (1967) Surface Areas from Mercury Porosimeter Measurements. *Journal of Physical Chemistry*. **71**, 2733-2736.

Rordorf, B.F. (1986) Thermal Properties of Dioxins, Furans and Related Compounds. *Chemosphere*. **15**(9-12), 1325-1332.

Rordorf, B.F. (1989) Prediction of Vapor Pressures, Boiling Points and Enthalpies of Fusion for Twenty-Nine Halogentated Dibenzo-p-Dioxins and Fifty-Five Dibenzofurans by a Vapor Pressure Correlation Method. *Chemosphere*. **18**(1-6), 783-788.

Rodorf, B.F. (1985) Thermodynamic Properties of Polychlorinated Compounds: The Vapor Pressures and Enthalpies of Sublimation of Ten Dibenzo-para-dioxines. *Thermochimica Acta*, **85**, 435-438.

Rosen, J.B. (1952) Kinetics of a Fixed Bed System for Solid Diffusion into Spherical Particles. *Journal of Chemical Physics*. **20**(3), 387-394.

Ruiz, J., R. Bilbao, and M.B. Murillo. (1998) Adsorption of Different VO onto Soil Minerals from Gas Phase: Influence of Mineral, Type of VOC, and Air Humidity. *Evironmental Science and Technology*. **32**, 1079-1084.

Ruthven, D.M. (1984) Principles of Adsorption and Adsorption Processes. *John Wiley & Sons, Inc.*

Sabljic, A. (1987) On the Prediction of Soil Sorption Coefficients of Organic Pollutants from Molecular Structure: Application of Molecular Topology Model. *Environmental Science and Technology.* **21**, 358-366.

Sato, N., H. Inomata, K. Arai, and S. Saito. (1986) Measurement of Vapor Pressures for Coal-Related Aromatic Compounds by Gas Saturation Method. *Journal of Chemical Engineering of Japan.* **19**(2), 145-147.

Schulthess, C.P. and C.P. Huang. (1991) Humic and Fulvic Acid Adsorption by Silicon and Aluminum Oxide Surfaces on Clay Minerals. *Soil Science Society of America Journal.* **55**, 34-42.

Shonnard, D.R., R.L. Bell and A. P. Jackman. (1993) "Effect of Nonlinear Sorption on the Diffusion of Benzene and Dichloromethane from Two Air-Dry Soils". *Environmental Science and Technology.* **27**, 457-466.

Shonnard, D.R. and R.L. Bell. (1994) The Effects of Nonlinear Sorption on the Diffusion of Volatile Organic Compounds from Air-Dry Soils: A Theoretical Study. *Journal of Hazardous materials.* **37**, 397-414.

Smith, J.M. and H.C. Van Ness. (1959) Introduction to Chemical Engineering Thermodynamics. *McGraw-Hill, Inc.*

Socha, S.B. & R. Carpenter. (1987) Factors Affecting Pore Water Hydrocarbon Concentrations in Puget Sound Sediments. *Geochimica et Cosmochimica Acta.* **51**, 1273-1284.

Sokolowska, Z., G. Jozhaciuk, and A. Ourumova-Pesheva. (1993) Adsorption of Water Vapor by Soils: Investigations of the Influence of Organic Matter, Iron, and Aluminum on Energetic Heterogeneity of Soil Clays. *Clays and Clay Minerals.* **41**(3), 346-352.

Sonnefeld, W.J. and W.H. Zoller. (1983) Dynamic Coupled-Column Liquid Chromatographic Determination of Ambient Temperature Vapor Pressure of Polynuclear Aromatic Hydrocarbons. *Analytical Chemistry*, **55**, 275-280.

Spencer, W.F. and M.M. Cliath. (1970) Desorption of Lindane from Soil as Related to Vapor Density. *Soil Science Society of America, Proceedings.* **34**, 574-578.

Spencer, W.F. and M.M. Cliath. (1972) Volatility of DDT and Related Compounds. *Journal of Agricultural Food Chemistry,* **20**(3), 645-649.

Spencer, W.F. and M.M. Cliath. (1974) Factors Affecting Vapor Loss of Trifluralin from Soil. *Journal of Agricultural Food Chemistry.* **22** (6), 987-991.

Spencer, W.F. and M.M. Cliath. (1969) Vapor Density of Dieldrin. *Environmental Science and Technology.* **3**(7), 670-674.

Spencer, W.F., T.D. Shoup, M.M. Cliath, W.J. Farmer, R. Haque. (1979) Vapor Pressures and Relative Volatility of Ethyl and Methyl Parthion. *Journal of Agricultural Food Chemistry.* **27**(2), 273-278.

Spencer, W.F., M.M. Cliath, and W.J. Farmer. (1969) Vapor Density of Soil Applied Dieldrin as Related to Soil Water Content, Temperature and Dieldrin Concentration. *Soil Science Society of America, Proceedings.* **33**, 509-511.

Spencer, W.F. and M.M. Claith. (1970) Vapor Density and Apparent Vapor Pressure of Lindane (gamma-BHC). *Journal of Agricultural Food Chemistry.* **18**(3), 529-530.

Sposito, G. (1984) The Surface Chemistry of Soils. *Oxford University Press.*
Stahlberg, J., M. Almgren, and J. Alsins. (1988) Mobility of Pyrene on Chemically Modified Silica Surfaces. *Analytical Chemistry.*, **60**(22), 2487-2493.

Stapleton, J. M., J. R. Mihelcic and D. R. Lueking. (1994) Adsorption and Desorption of Pyrene onto a Great Lakes Sediment. *Journal of Great Lakes Research.* **20**(3), 561-568.

Stevenson, F.J. (1994) Humus Chemistry, Genesis, Composition, Reaction. 2nd edition. Wiley

Storey, J.M.E. and J.F. Pankow. (1992) Gas-Particle Partitioning of Semi-Volatile Organic Compounds to Model Atmospheric Particulate Materials- I. Sorption to Graphite, Sodium Chloride, Alumina, and Silica Particles Under Low Humidity Conditions. *Atmospheric Environment.* **26A**, 435-443.

Storey, John M.E., W. Luo, L.M. Isabelle, and J.F. Pankow. (1995) Gas/Solid Partitioning of Semivolatile Organic Compounds to Model Atmospheric Solid Surfaces as a Function of Relative Humidity. 1. Clean Quartz. *Environmental Science and Technology.* **29**, 2420-2428.

Thibaud, C., C. Erkey and A. Akgerman. (1992) Investigation of Adsorption Equilibria of Volatile Organics on Soil by Frontal Analysis Chromotography. *Environmental Science and Technology.* **26**, 1159-1164..

Thibaud, C., C. Erkey and A. Akgerman. (1993) Investigation of the Effect of Moisture on the Sorption and Desorption of Chlorobenzene and Toluene from Soil. *Environmental Science and Technology,* **27**, 2373-2380.

Thibaud-Erkey, C., Y. Guo, C. Erkey, and A. Akgerman. (1996) Mathematical Modeling of Adsorption and Desorption of Volatile Contaminants for Soil: Influence of Isotherm Shape on Adsoption and Desorption Profiles. *Environmental Science and Technology.* **30**, 2127-2134.

Thibaud-Erkey, C., J. F. Campagnolo and A. Akgerman. (1995) Adsorption of Volatile Organic Contaminants on Soil and Soil Constituents. *Separation and Purification Methods.* **24**(2), 129-194.

Thibodeaux, L.J. (1996) Environmental Chemodynamics. Second edition., John Wiley & Sons, New York, NY

Thiel, P.A. (1991) New Chemical Manifestaions of Hydrogen Bonding in Water Adlayers. *Accounts of Chemical Research.* **24**(2), 31-35.

Thoma, G.J. (1994) Studies on the Diffusive Transport of Hydrophobic Organic Chemicals in Bed Sediments. *Louisiana State University Ph.D. Dissertation.*

US EPA. (1996) EPA 905-R96-001. Estimating Contaminant Losses from Components of Remediation Alternatives for Contaminated Sediments. Assessment and Remediation of Contaminated Sediments (ARCS) Program.

Valsaraj, K.T., B. Choy, R. Ravikrishna, D.D. Reible, L.J. Thibodeaux, C.B. Price, J.M. Brannon and T.E. Myers. (1996) Air Emissions from Exposed, Contaminated Sediments and Dredged Materials 1. Experimental Data in Laboratory Microcosms and Mathematical Modeling. *Journal of Hazardous Materials.* **54**, 65-87.

Valsaraj, K.T., R. Ravikrishna, B. Choy, D.D. Reible, L.J. Thibodeaux, C.B. Price, S. Yost, J.M. Brannon, and T.E. Myers. (1999) Air Emissions from Exposed Contaminated Sediments and Dredged Material. *Environmental Science and Technology.* (Accepted, January issue)

Valsaraj, K.T. and L.J. Thibodeaux. (1988) Equilibrium Adsorption of Chemical Vapors on Surface Soils, Landfills and Landfarms—A Review. *Journal of Hazardous Materials*, **19**, 79-99.

Valsaraj, K.T. and L.J. Thibodeaux. (1988) Equilibrium Vapor Phase Adsorption of Volatile Organic Chemicals on Dry Solids. *Journal of Hazardous Materials*, **19**, 17-32.

Valsaraj, K.T. and L.J. Thibodeaux. (1988) Mathematical Modeling for Predicting Chemical Vapor Emissions From Landfills. *Journal of Hazardous Materials*, **19**, 101-118.

Valsaraj, K.T. and Thibodeaux, L. J. (1992) Equilibrium Adsorption of Chemical Vapors Onto Surface Soils: Model Predictions and Experimental Data. *In* Fate of Pesticides and Chemicals in the Environment. John Wiley & Sons, 155-173.

Valsaraj, K.T. (1988a) On the Physico-Chemical Aspects of Partitioning of Non-Polar Hydrophobic Organics at the Air-Water Interface. *Chemosphere.* **17**(5), 875-887.

Valsaraj, K.T. (1988b) Binding Constants for Non-Polar Hydrophoic Organics at the Air-Water Interface: Comparison of Experimental and Predicted Values. *Chemosphere.* **17**(10), 2049-2053.

Valsaraj, K.T. , L.J. Thibodeaux, and D.D. Reible. (1997) A Quasi-Steady-State Pollutant Flux Methodology for Determining Sediment Quality Criteria. *Environmental Toxicology and Chemistry.* **16**(3), 391-396.

Wandruszka, R. (1992) Luminescence of Micellar Solutions. *Critical Reviews in Analytical Chemistry.* **23**(3), 187-215.

Wang, H., and J.M. Harris. (1995) Origins of Bound-Probe Fluorescence Decay Heterogeneity in the Distribution of Binding Sites on Silica Surfaces. *Journal of Physical Chemistry.* **99**, 16999-17009.

Wang, Thomas S.C., S.W. Li, and Y. L. Ferng. (1978) Catalytic Polymerization of Phenolic Compounds by Clay Minerals. *Soil Science.* **126**, 15-21

Wasik, S.P., M.M. Miller, Y.B. Tewari, W.E. May, W.J. Sonnefeld, H. DeVoe, and W.H. Zoller. (1983) Determination of the Vapor Pressure, Aqueous Solubility and Octanol/Water Partition Coefficient of Hydrophobic Substances by Coupled Generator Column/Liquid Chromatographic Methods. *Residue Review.* **85**, 29-42.

Weber, W.J., P.M. McGinley, and L.E. Katz. (1992) A Distributed Reactivity Model for Sorption by Soils and Sediments. 1. Conceptual Basis and Equilibrium Assessments. *Environmental Science and Technology.* **26**, 1955-1962.

Wehner, J.F. and R.H. Wilhelm. (1956) Boundary Conditions of Flow Reactor. *Chemical Engineering Science.* **6**, 89-93.

Werth, C.J. and M. Reinhard. (1997) Effects of Temperature on Trichloroethylene Desorption from Silica Gel and Natural Sediments. 1. Isotherms. *Environmental Science and Technology.* **31**(3).

Werth, C.J. and M. Reinhard. (1997) Effects of Temperature on Trichloroethylene Desorption from Silica Gel and Natural Sediments. 2. Kinetics. *Environmental Science and Technology.* **31**, 697-703.

Werth, Charles J., J.A. Cunningham, P.V. Roberts, and M. Reinhard. (1997) Effects of Grain-Scale Mass Transfer on the Transport of Volatile Organics Through Sediments. 2. Column Results. *Water Resources Research.* **33**(12), 2727-2740.

Wild, S.R. and K.C. Jones. (1995) Polynuclear Aromatic Hydrocarbons in the United Kingdom Environment: A preliminary source inventory and budget. *Environment Pollution.* **88**(1), 91-108.

Wilke, C.R. and O.A. Hougen. (1945) Mass Transfer in the Flow of Gases Through Granular Solids Extended to Low Modified Reynolds Numbers. *Trans. Am. Inst. Chem. Eng.*, **41**, 445-451.

Wilkins, M.D., L.M. Abriola, and K. D. Pennell. (1995) An Experimental Investigation of Rate-Limited Nonaqueous Phase Liquid Volatilization in Unsaturated Porous Media: Steady State Mass Transfer. *Water Resources Research*. **31**, 2159-2172.

Wolf, D.C., T.H. Dao, H.D. Scott, T.L. Lavy. (1989) Influence of Sterialization Methods on Selected Soil Microbiological, Physical, and Chemical Properties. *Journal of Environmental Quality*. **18**, 39-44.

Wong, A.L. et al. (1990) Measurements of Energy Dispersion at Liquid-Solid Interfaces: Fluorescence Quenching of Pyrene Bound to Fumed to Silica. *Canadian Journal of Physics*. **68**, 1027-1034.

Yamasaki, H., K. Kuwata, and H. Miyamoto. (1982) Effects of Ambient Temperature on Aspects of Airborne Polycyclic Aromatic Hydrocarbons. *Environmental Science and Technology*. **16**(4), 189-194.

Appendix A
Principle of the Fluorescence Process

Fluorescence occurs in certain molecules containing systems of delocalized π-electrons such as PAHs or heterocyclic hydrocarbons. The fluorescence process can be illustrated by the electronic-state diagram shown in Figure A.1. The molecule in its energetic ground state, S_0, absorbs a photon of energy $h\nu_{ex}$ and reaches the excited state S_1'. The excited state S_1' has a finite life time (typically 10^{-8} to 10^{-9} seconds) during which the molecule is susceptible to interactions with its micro-environment. These interactions have three consequences:

- The energy of S_1' is partially dissipated and the molecule reaches a relaxed excited state, S_1, from which the fluorescence originates.
- Not all the chromophoric molecules excited to S_1' will return to the ground state S_0 by fluorescence emission. Some of them will lose their excess energy in collisions with non-chromophoric species present in the medium (quenching process). The fluorescence quantum yield (ratio of the number of photons emitted to the number of photons absorbed) is a measure of this phenomenon.
- The microenvironment of the molecule will affect the shape of its fluorescence emission spectrum.

Finally, the molecule in its excited state S_1 emits a photon of energy $h\nu_{em}$ and returns to its ground state S_0. The excited state decay kinetics also gives information on the molecular surroundings.

Some molecules are particularly sensitive to their environment during the fluorescence process. Therefore, they can be used as probes to obtain information on their

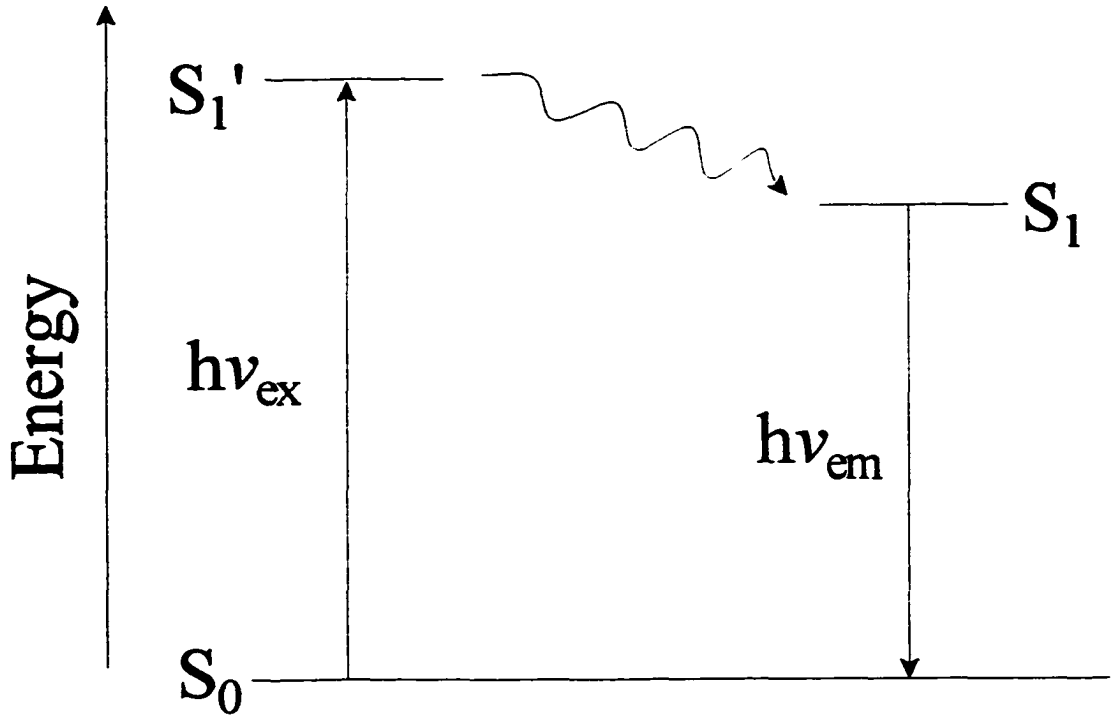

Figure A.1 Principle of the fluorescence process.

environment. A fluorescent probe must show strong fluorescence properties to allow for its detection, as well as structural characteristics susceptible to cause interactions with its environment.

Appendix B
Notes on the BET Isotherm Equation

B.1 BET model hypothesis

Presentations of the BET model, can be found in Adamson, 1990 and Hill, 1960. One of the main approximations made in deriving the model is the following: A first molecular layer of organic compound adsorbs on the solid with a heat of adsorption $\Delta H_{adsorption}$. Then, successive molecular layers of vapor condense on this first layer, all with the same heat of adsorption, equal to the energy of condensation of the compound, $\Delta H_{condensation}$. It is important to remark for what follows that Gibbs free energy of adsorption ($\Delta G_{adsorption}$) and condensation ($\Delta G_{condensation}$) should actually be used instead of the enthalpies. However, this approximation is of little consequences in comparison with the fundamentals assumptions made in the derivation of the model and the enthalpy of adsorption is easier to measure than the free enthalpy.

B.2 Expression of the BET isotherm

The most general equation of a BET isotherm is (Jaycock and Parfitt, 1981):

$$\frac{W}{W_m} = \frac{XB}{(1-X)}\left[\frac{1-(n+1)X^n + nX^{n+1}}{1+(B-1)X - BX^{n+1}}\right] \qquad (B.1)$$

Where:

- W is the amount of vapor of the compound adsorbed on the soil in equilibrium with a given partial pressure, P, in the air phase.
- X is the ratio of the partial pressure of the compound, P, over its saturated vapor pressure, P^{sat}.
- B is defined by:

$B=\exp[(\Delta H_{condensation}-\Delta H_{adsorption})/RT]$ (or $B=\exp[(\Delta G_{condensation}-\Delta G_{adsorption})/RT]$)

where $\Delta H_{condensation}$ and $\Delta H_{adsorption}$ are respectively the molar heat of condensation of the vapor on the pure compound and the molar heat of adsorption of the first layer onto the solid, ($\Delta H_{condensation} < 0$ and $\Delta H_{adsorption} < 0$)

- W_m is the solid monolayer adsorption capacity for the compound
- R is the gas constant and T the absolute temperature
- n is the maximum number of molecular layers that can be adsorbed. It is to be noticed that equation (B.1) reduces to the conventional BET isotherm for $n \to \infty$. On the other hand it reduces to Langmuir equation for n=1.

B.3 BET isotherms of type II and IV

Both isotherms of type II and IV occur when the heat of adsorption of the compound on the solid is greater than its heat of condensation. In this case B>1 which causes the characteristic knee shape of these isotherms. An isotherm of type II describes an adsorption which takes place on a homogeneous, non porous surface so that an infinite number of layers can be adsorbed ($n \to \infty$).

On the other hand, an isotherm of type IV describes adsorption taking place on a porous surface. The porosity has two effects:

- An excess of adsorption occurs at middle pressure due to capillary condensation in the mesopores of the surface.
- The adsorption is limited by the volume of the mesopores to a finite number of layers (n is finite) and reaches its maximum at a pressure less than the saturated vapor pressure.

B.4 Choice of a saturated vapor pressure below the triple point temperature

B.4.1 Statement of the problem

In the kinetics derivation of the conventional (infinite layers) BET equation, P^{sat} is introduced in order to normalize the expression. The argument that on a free surface the amount adsorbed at saturation is infinite allows the replacement in the equation of a group of unknown parameters by P^{sat}. As shown if Figure B.1, two situations can be envisioned when considering adsorption of environmental contaminants:

- The adsorption of the vapor takes place at a temperature above the triple point temperature, T_t. Then, when an infinite amount is adsorbed on the surface, the compound is in its liquid state and the pressure equals the saturated vapor pressure above the liquid, P_L^{sat}.
- On the other hand, if adsorption occurs at a temperature below the triple point of the compound, there are two vapor pressures to chose from, the one associated with the subcooled liquid, P_L^{sat} or the one associated with the crystallized solid, P_S^{sat}.

B.4.2 Interchangeability of P_L^{sat} and P_S^{sat}

The two vapor pressures are related. By definition, the relationship between the subcooled liquid fugacity and the one of the solid is:

$$f_L = f_S \exp\left[\frac{-\Delta G_{solid \rightarrow subcooled}}{RT}\right] \qquad (B.2)$$

Where $\Delta G_{solid \rightarrow subcooled}$ is the free enthalpy change when going from the solid to the subcooled liquid state at constant temperature. (This quantity has no physical meaning).

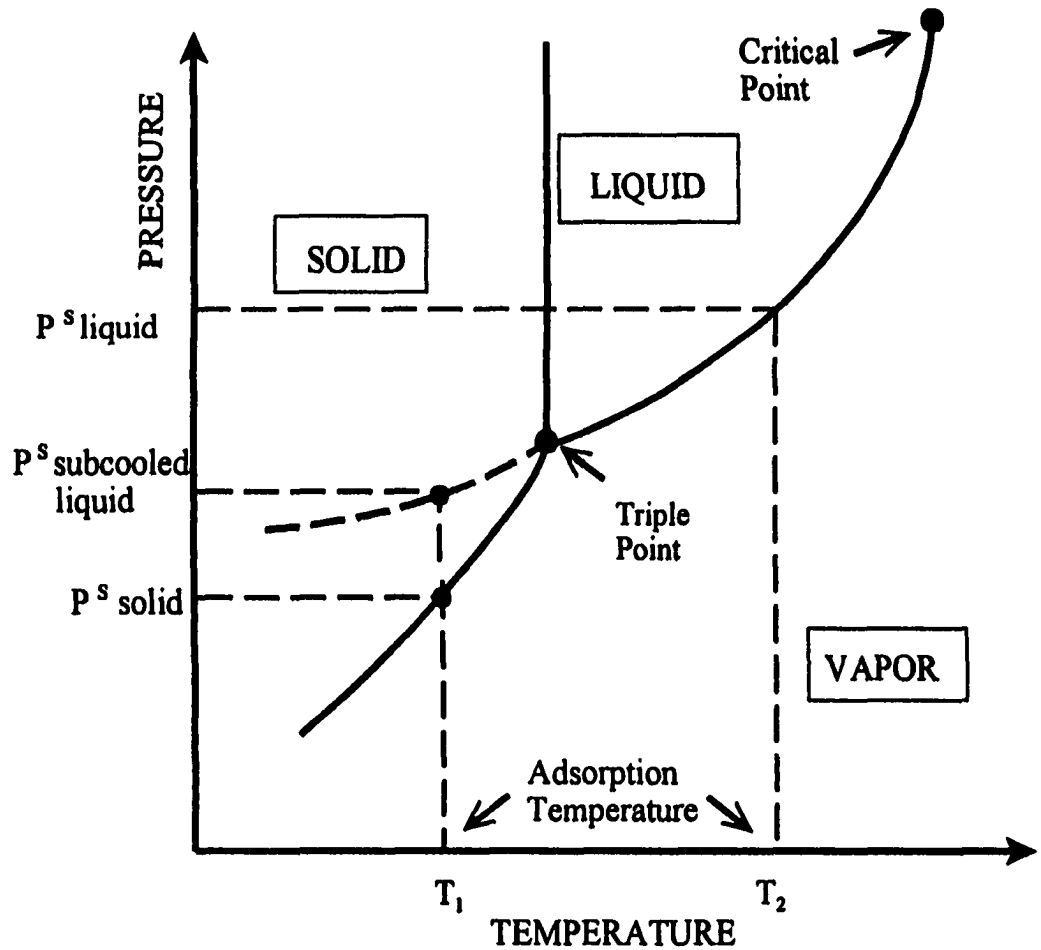

Figure B.1 Extrapolation of liquid vapor pressure on pressure-temperature diagram for a pure material.

Fugacities can be replaced by the corresponding pressures when dealing with low volatility compounds.

$$P_L^{sat} = P_S^{sat} \exp\left[\frac{-\Delta G_{solid \rightarrow subcooled}}{RT}\right] \qquad (B.3)$$

If both sides are multiplied by $\exp[(\Delta G_{adsorbed \rightarrow subcooled} + \Delta G_{vapor \rightarrow adsorbed})/RT]$, the equation becomes:

$$P_L^{sat} \exp\left[\frac{\Delta G_{subcooled \rightarrow vapor}}{RT}\right] = P_S^{sat} \exp\left[\frac{\Delta G_{solid \rightarrow vapor}}{RT}\right] \qquad (B.4)$$

Therefore, if free enthalpies instead of enthalpies are used in the definition of B, the ratio B/P^{sat} is independent of the choice of the vapor pressure. It is to be noted that this ratio is equal to the constant, L in Langmuir equation: $W/W_m=LP/(1+LP)$ (Pankow, 1987). Thus, it is sound that it does not depend on the choice of either one or the other of the heat of transition since Langmuir model does not take into account multilayer adsorption.

Consequently, when using the simplification of the BET (or Langmuir) equation (2.3) to model the partitioning coefficient between the air and a surface, the use of either vapor pressure is equivalent provided that the free enthalpy of adsorption on the successive layers after the first layer, is chosen coherently with the saturated vapor pressure. Choice of the subcooled liquid vapor pressure necessitates the use of the free enthalpy of condensation on the subcooled liquid at the considered temperature. Choice of the solid vapor pressure necessitates the use of the free enthalpy of deposition on the crystal.

B.4.3 Justification of the usual choice of P_L^{sat}

Authors studying the adsorption of SVOCs to environmental surfaces (Yamasaki et al., 1982; Pankow, 1987; Goss, 1992) have advocated the use of the subcooled liquid vapor pressure. The justification for this choice is that, within a family of similar compounds, logK shows a much better linear correlation to $\log P_L^{sat}$ than to $\log P_S^{sat}$ (Bidleman and Foreman, 1987). Pankow, 1991 showed that such a linear correlation is expected if:

- Adsorption is described by equation (2.3)
- There is a linear relationship between the free enthalpies of transition, $\Delta G_{vapor \rightarrow adsorbed}$ and $\Delta G_{vapor \rightarrow subcooled}$, valid for any compound of the family of interest.

It is reasonable to think that the second condition may be fulfilled because (i) the entropic difference between adsorption onto the subcooled liquid state and physical adsorption onto a solid is expected to be small and (ii) both $\Delta H_{vapor \rightarrow adsorbed}$ and $\Delta H_{vapor \rightarrow subcooled}$ measure physical forces involving the molecule in a fairly disordered state and a simple relationship between them can be expected to hold for similar compounds. On the contrary, such a linear correlation between $\Delta G_{vapor \rightarrow adsorbed}$ and $\Delta G_{vapor \rightarrow solid}$ is very unlikely. It would require that $\Delta G_{subcooled \rightarrow solid}$ be about constant within a family of similar compounds. However, $\Delta G_{subcooled \rightarrow solid}$ is determined by the energy of the crystal lattice and is dependent on the intimate structure of the molecule. $\Delta G_{subcooled \rightarrow solid}$ is thus highly variable, even between very similar compounds. Prausnitz et al., 1986 showed how such a difference in molecular structures causes phenanthrene to be about 25 times more soluble in benzene than its stereoisomer, anthracene. It is

therefore not surprising that logK shows a much better linear correlation to $\log P_L^{sat}$ than to $\log P_S^{sat}$.

B.4.4 Phenomenological model of SVOCs adsorption

In the general case it is easy to see from equation (B.1) that the two vapor pressures cannot be interchangeably used, even if the correct heat of transition to the condensed phase is used. This is of no consequence because the BET model is not valid to describe SVOCs adsorption after one monolayer. Neue and Rudolph, 1993 have shown that for fluoranthene and pyrene adsorption on carbon soot, the crystal phase is the stable thermodynamic phase after one monolayer is adsorbed. They support this statement by several observations:

- When more than one layer is adsorbed, NMR spectra of the adsorbed phase resemble the ones of the crystal.
- Adsorption follows Langmuir isotherm. After one monomolecular layer of pyrene or fluoranthene is adsorbed, the partial pressure stabilizes to the solid vapor pressure value and the mass adsorbed increases indefinitely.
- After one molecular layer covers the soot surface, pyrene isosteric heat of desorption falls steeply and become equal to the heat of sublimation.

Therefore, it seems that the best phenomenological description of SVOCs adsorption is provided by Langmuir model. After the first monomolecular layer, the adsorbed phase is similar to the crystal phase.

Appendix C
Calculation of the Concentration Profile of a SVOC in the Gas Saturation Column

In this appendix, the concentration profile of a semi-volatile organic compound in the gas saturation column is established. Calculations are performed using a Mathcad spreadsheet, based on the model presented in 3.2.2. (Notations are defined in the same section).

SYSTEM PARAMETERS

Sediment characteristics :

Specific surface area: $a = 21 \cdot 10^{6}$ /m

Porosity: $\varepsilon = 0.55$

Mean particle diameter: $dp = 2.10^{-6}$ m (conservative value)

Column characteristics:

Radius : $R = 0.0175$ m

Cross section surface area: $S = 3.14 \cdot R^{2}$

Bed Length: $L = 0.3$ m

Air diffusivity: $Dm = 6 \cdot 10^{-6}$ m2/s (value of phenanthrene diffusivity)

The dispersion coefficient is arbitrarily taken as 100 times the air diffusivity coefficient.

$D = 100 \cdot Dm$ m2/s

Wilkins et al., 1994 developed a correlation of the mass transfer coefficient, k for Non Aqueous Phase Liquids (NAPLs) evaporating from a soil packed in an experimental column. The mass transfer coefficient is taken here as one hundredth of the value predicted by this correlation in order to take into account the sediment-side mass transfer resistance. Moreover, the molecular diffusivity coefficient is used instead of the dispersion coefficient.

$$k(Q) := 0.01 \cdot \left[10^{-0.42} \cdot Dm^{0.38} \cdot dp^{0.44} \cdot \left(\frac{Q}{S \cdot \varepsilon} \right)^{0.62} \right] \quad /s$$

$$Pe(Q) := \frac{L \cdot \left(\frac{Q}{S} \right)}{D} \qquad Sh(Q) := \frac{L^2 \cdot k(Q) \cdot a}{D}$$

$$\beta := \frac{1 - \varepsilon}{\varepsilon} \qquad \gamma(Q) := \sqrt{1 + \frac{4 \cdot \beta \cdot Sh(Q)}{Pe(Q)^2}}$$

X is the dimensionless air concentration: X=Cg/Cg*

X is calculated for the limit values of Q: 0.5 ml/min (=8E-9m^3/s) and 20ml/min (=3E-7m^3/s)

$$X(Q,\zeta) := 1 - \exp(Pe(Q) \cdot (1 - \gamma(Q)) \cdot \zeta) \qquad \zeta := 0, 0.01 .. 1 \qquad (z = z/L)$$

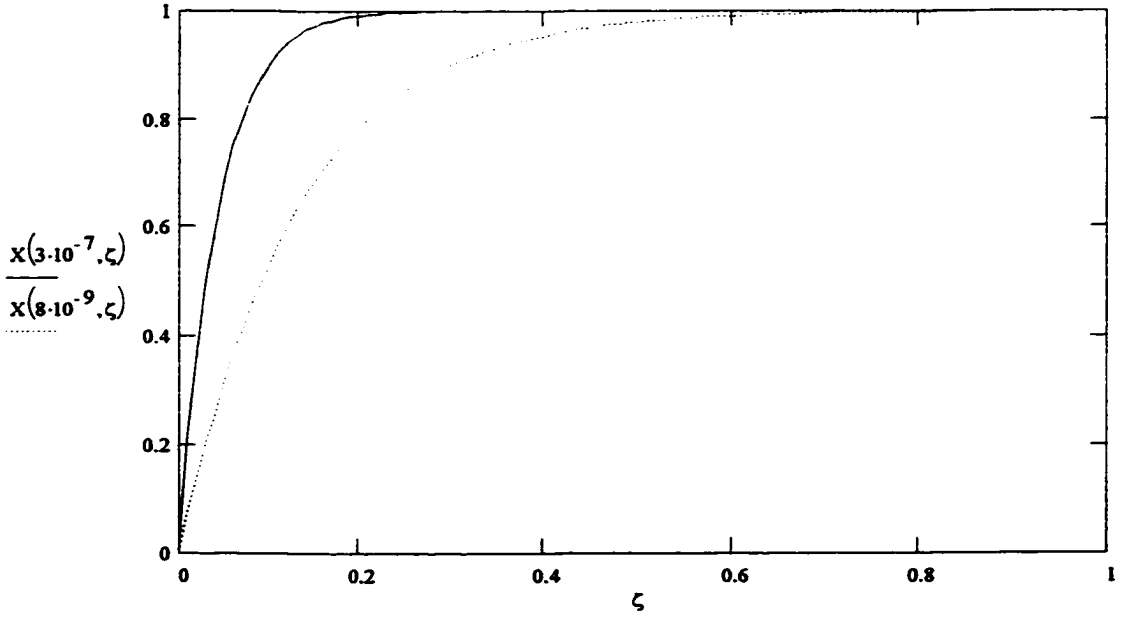

Appendix D
Calculation of the Concentration Profiles of Water in the Gas Saturation Column

In this appendix, the concentration profiles of water in the gas saturation column are calculated at different times. Using a Mathcad™ spreadsheet, the dimensionless profiles are calculated for the sediment bed and for the air phase of the column. Calculations are based on the model established in section 3.2.3.1. (Notations are defined in the same section). The dimensionless length of the sediment bed is chosen as 10.

Dimensionless concentration of the air stream:

$$X(\tau,\zeta) := \frac{1}{2\cdot\pi}\cdot\int_0^{\zeta}\int_0^{2\cdot\pi} \exp\left(2\cdot\sqrt{\tau\cdot z}\cdot\sin(\gamma) - \tau - z\right)\,d\gamma\,dz \qquad (3.34)$$

Dimensionless concentration of the sediment bed:

$$Y(\tau,\zeta) := 1 - \left(\frac{1}{2\cdot\pi}\cdot\int_0^{\tau}\int_0^{2\cdot\pi} \exp\left(2\cdot\sqrt{t\cdot\zeta}\cdot\sin(\gamma) - t - \zeta\right)\,d\gamma\,dt\right) \qquad (3.35)$$

D.1 Influence of bed length

τ=0

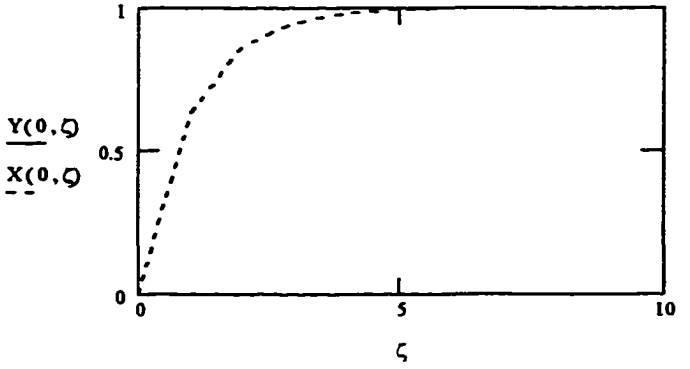

Concentration in the sediment is unchanged: Y=1

τ=1

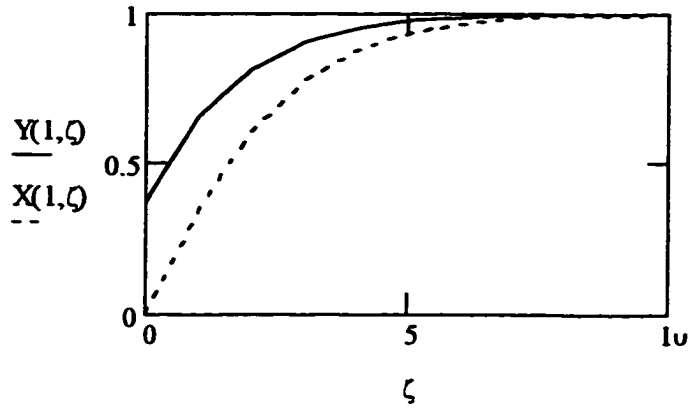

Depletion of the sediment starts at the inlet.

Equilibrium of the air stream is still reached at the column outlet.

τ=5

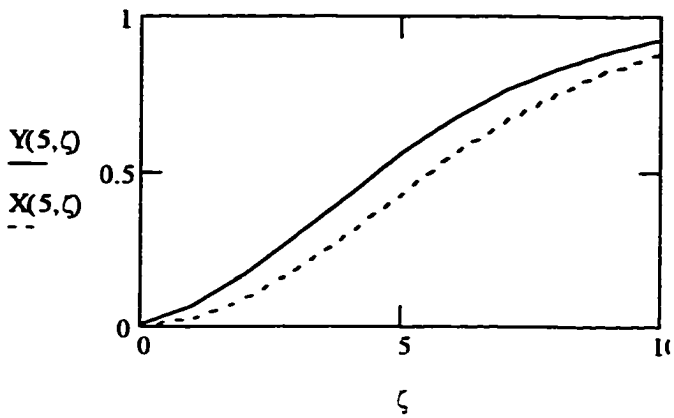

Depletion of the sediment reached the outlet.

Equilibrium of the air flow is no longer reached at the outlet.

τ=10

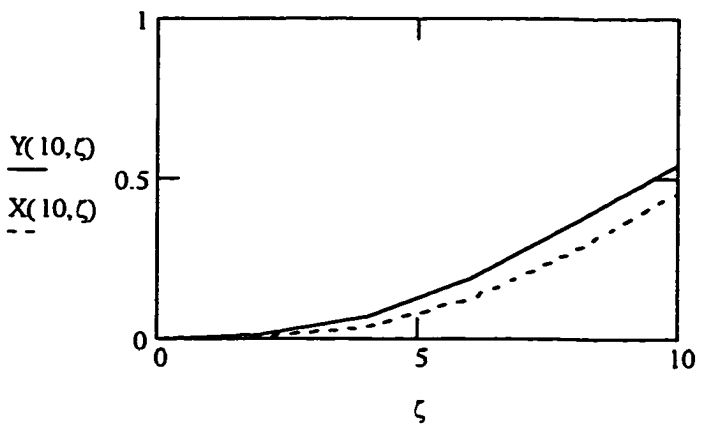

Depletion of the sediment progresses.

Gas concentration at the outlet decreases.

D.2 Influence of time

The air concentrations at the outlet (ζ=10) of the column was calculated as a function of time.

ζ=10

$\tau := 0, 0.5 .. 3$

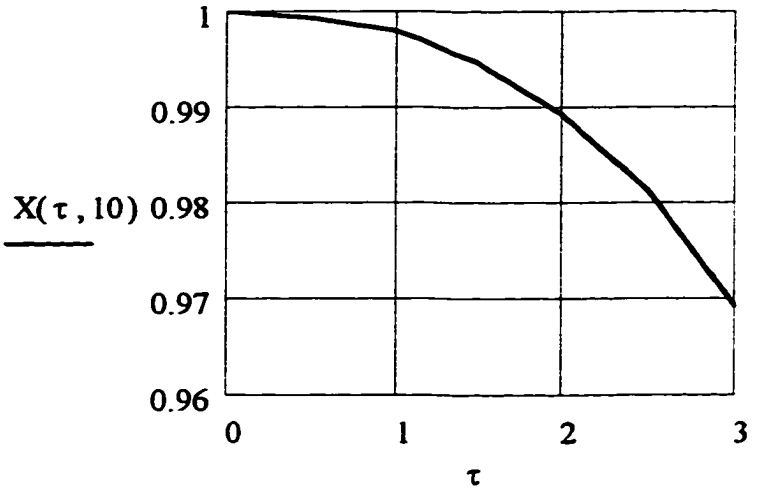

The air phase concentration at the outlet of the column decreases over time. The time after which the air concentration is less than a given percentage of the saturation concentration is referred to as the breakthrough time. For instance, if it is desired that the outlet air concentration be greater than 99% of the saturation value, the plot of X as a function of time indicates that the dimensionless breakthrough time is about 2.

Appendix E
Analysis of the Isotherms of Water Sorption from an Experimental Study

Thirteen years before Brunauer, Emmet and Teller presented their famous model of vapor adsorption on solids (Brunauer et al., 1938), Puri et al., 1925 studied the adsorption of water on soils. They determined the isotherms of water adsorption for a variety of soils and soil constituents and commented the different shapes they observed. As they provide comprehensive tables of their experimental data, it is possible to apply the BET theory to their results. This makes possible a more systematic study of some factors influencing the sorption of water vapor in soils. The two BET parameters, B_w and mc_m are obtained from the three first points of each isotherm (RH<0.20) using the linear form of the BET equation (equation (4.2)). The fit to this equation is good (r^2>0.99 in every case but one, for which r^2=0.98).

E.1 Influence of the different mineral fractions

E.1.1 Clay fraction

Puri et al., 1925 determined the isotherms of water adsorption for 6 different soils. The monolayer moisture content is calculated from each isotherm using equation (4.2). In Figure E.1, mc_m is plotted for each soil as a function of the respective clay fraction. As expected, the monolayer moisture content increases with the clay content. It is well known that clay particles display a high surface area for adsorption. (Since B_w is calculated from the first points of the adsorption isotherm, it reflects only the most energetic sites available. It is thus meaningless to study the influence of the clay content on B_w.)

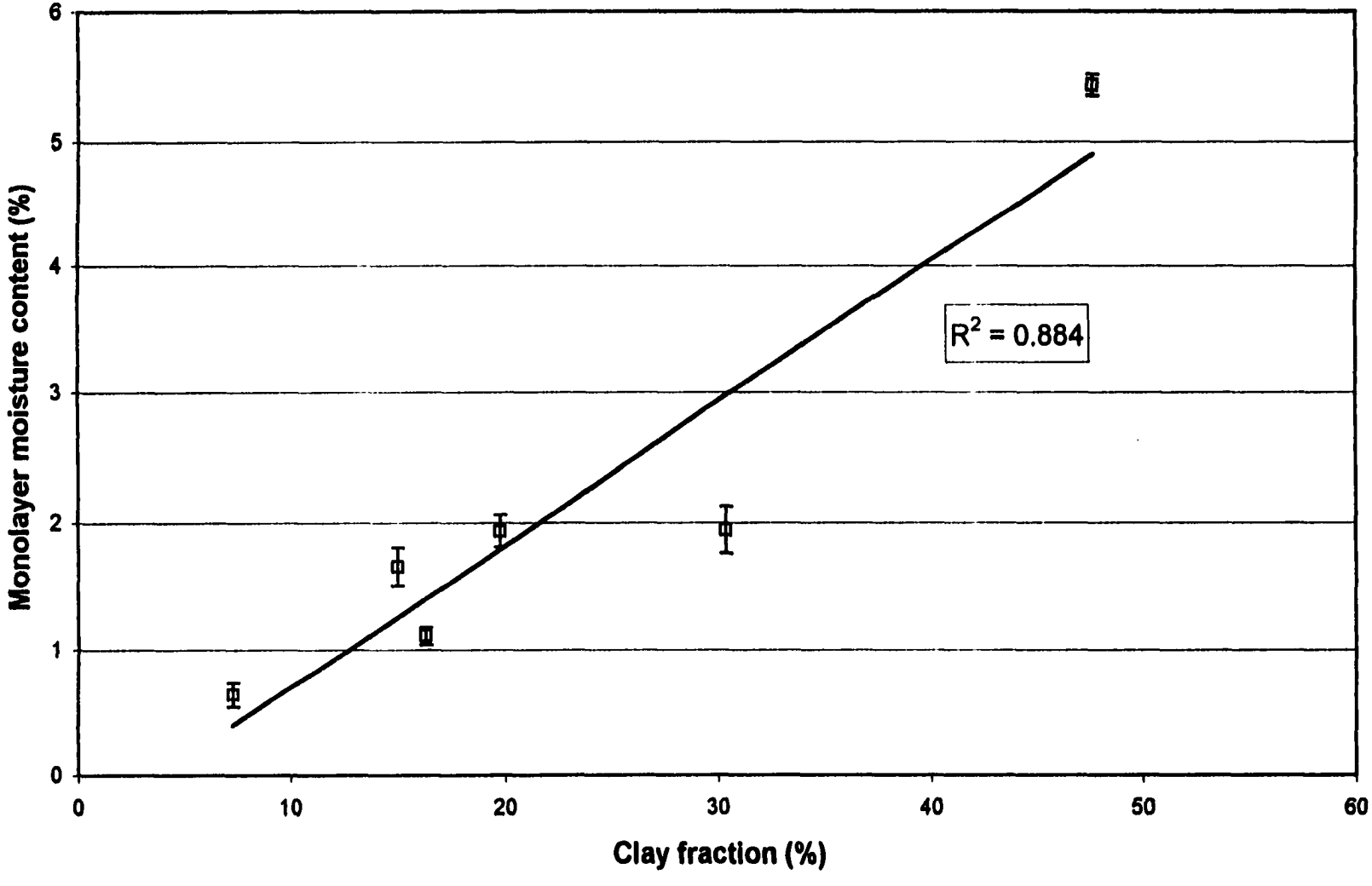

Figure E.1 Monolayer moisture content of different soils plotted as a function of their respective clay content.

E.1.2 Other particle-size fractions

The isotherms of water adsorption were also determined for different particle size. Four particle-size fractions were studied within the silt and clay fractions of a single soil. The two BET parameters calculated for each fraction are shown in Figure E.2. As expected, the monolayer moisture content is a decreasing function of particle size. (Smaller particles have a higher specific surface area). On the other hand, in the range investigated, the B_w parameter is independent of the particle size. This indicates that there is no correlation between the size of a particle and the most energetic adsorption sites found at its surface.

In conclusion, within the silt and clay fractions, the particle size distribution of a soil influences only its monolayer moisture content. The heat of adsorption of water at low surface coverage is independent of particle size.

E.2 Influence of the drying temperature

Finally, the isotherms of water adsorption were determined for several samples of a soil that had been dried at different temperatures. The sample dried at 25°C was placed in a dessicator containing sulfuric acid, samples dried at higher temperatures were placed in an oven. The two calculated BET parameters are plotted as a function of the temperature in Figure E.3. The drying temperature shows no influence on either parameter up to 130°C. On the other hand, drying at a temperature higher than 130°C has two effects:

- The parameter B_w increases. This indicates that the soil surface becomes energetically more favorable to water adsorption. This activation phenomenon is well known. Numerous studies (Krasnansky and Thomas, 1994) show that water physically

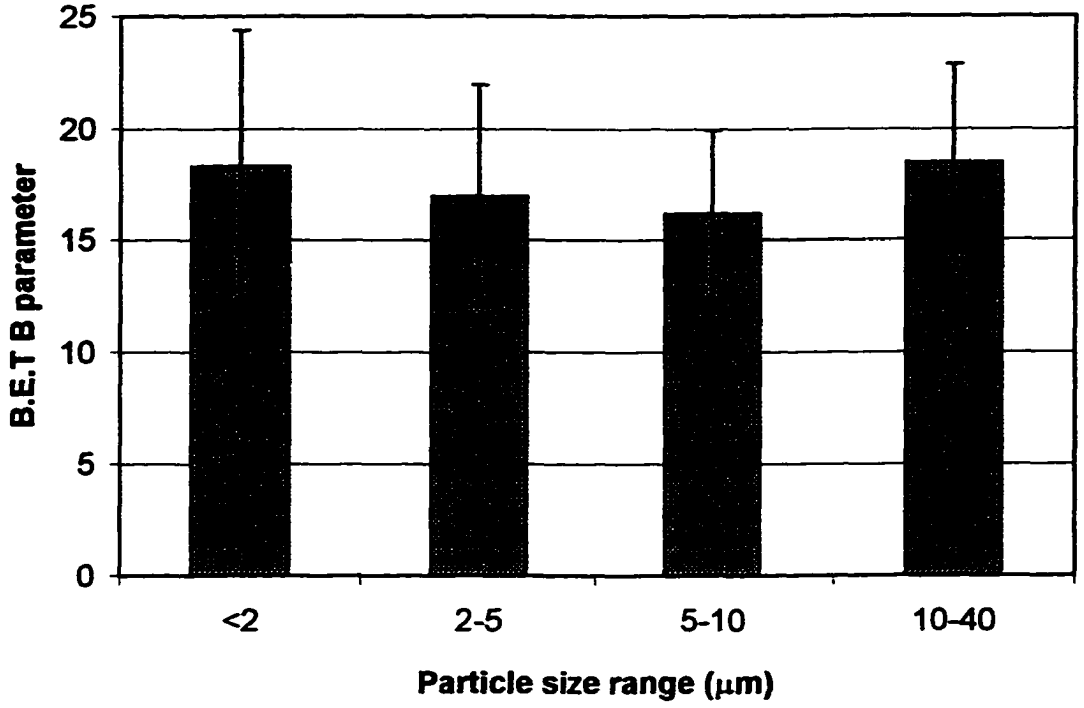

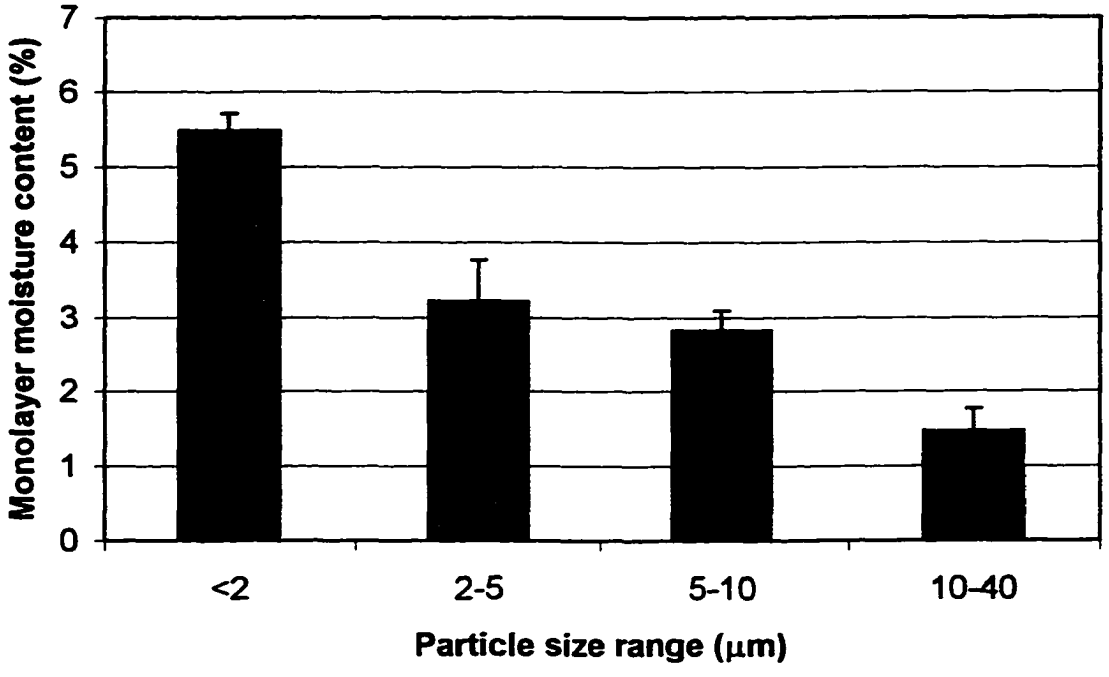

Figure E.2 B.E.T parameters of different particle size fractions of a single soil.

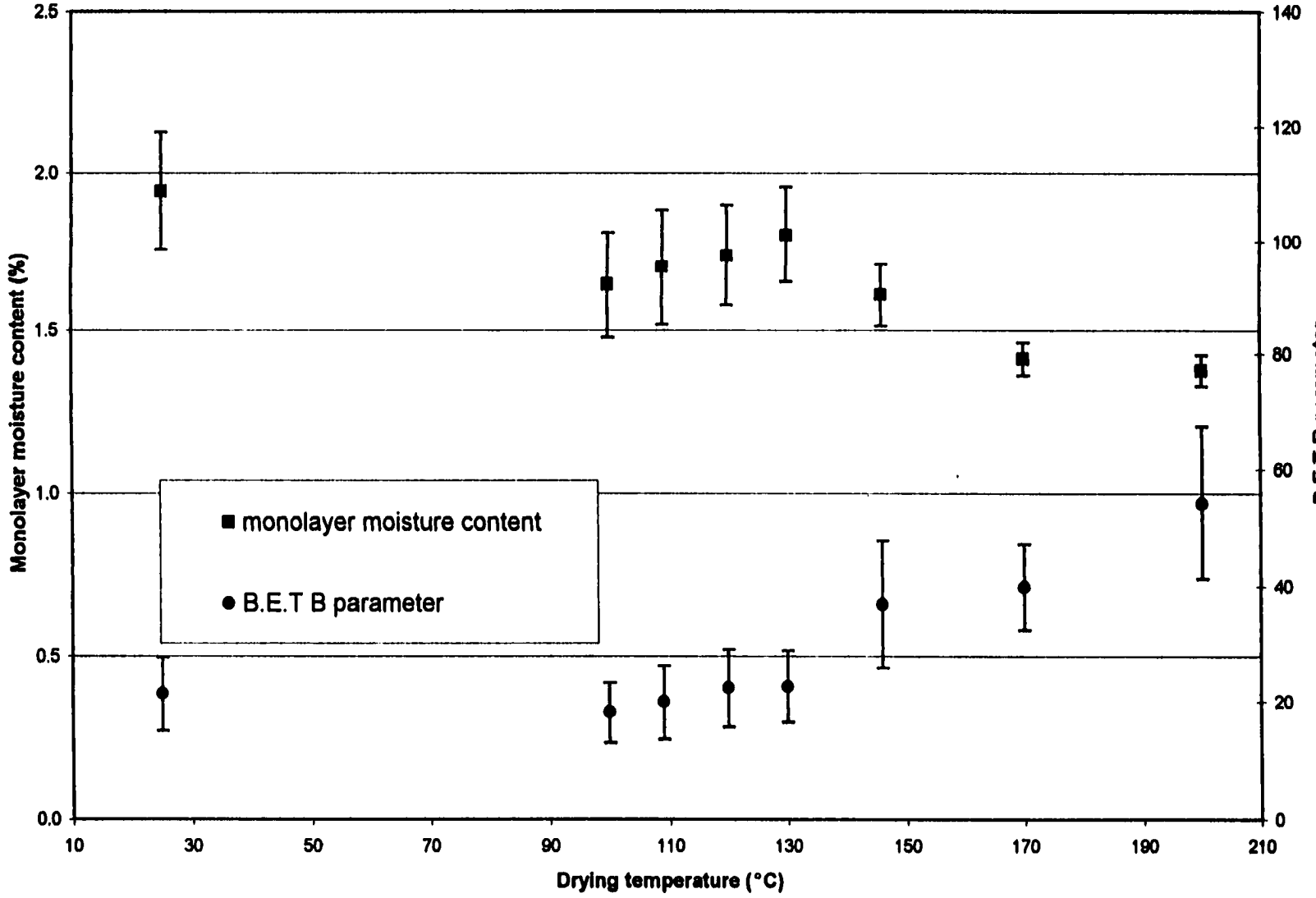

Figure E.3 Influence of the drying temperature on the B.E.T parameters of a soil.

adsorbed on silica gel is not released until the temperature reaches 120-130°C. When this range of temperature is reached, water desorbs from silanol groups. This creates adsorption sites of high energy.

- The monolayer capacity for water adsorption decreases. Gregg and Sing, 1982 cite several studies demonstrating that the concentration of silanol groups at the surface of silica gel depends on the dehydration temperature. The maximum concentration is observed for dehydration temperatures below about 125°C. Above this temperature the surface concentration of silanol groups decreases sharply. This phenomenon is compatible with the observed decrease in mc_m.

In conclusion, heating a soil at a temperature above about 130°C increases the strength of the surface adsorption sites but decreases their number.

Appendix F
Mercury Porosimetry Data

Pore volume and pore surface distributions for Campus Lake sediment. Analysis by Micromeritics, Norcross, GA.

Mercury Pressure (psia)	Pore Diameter (micrometers)	Incremental Pore Volume (mL/g)	Cumulative Pore Volume (mL/g)	Incremental Pore Surface (m^2/g)	Cumulative Pore Surface (m^2/g)
1.49	121.1502	0	0	0	0
2.16	83.8637	0.0009	0.0009	0	0
3.17	57.1248	0.0057	0.0066	0	0
4.14	43.6808	0.0043	0.0109	0	0
5.62	32.199	0.0053	0.0162	0.001	0.001
7.14	25.3383	0.0038	0.02	0.001	0.002
8.6	21.0251	0.0033	0.0233	0.001	0.003
10.61	17.0514	0.0039	0.0272	0.001	0.004
13.1	13.8017	0.0042	0.0314	0.001	0.005
14.78	12.2356	0.0024	0.0338	0.001	0.006
16.09	11.2423	0.0022	0.036	0.001	0.007
20.05	9.0206	0.0163	0.0523	0.006	0.013
23.06	7.8434	0.0257	0.078	0.012	0.025
25.03	7.2271	0.0294	0.1074	0.016	0.041
30.02	6.0257	0.0685	0.1759	0.041	0.082
40.45	4.4708	0.0583	0.2342	0.044	0.126
50.15	3.6067	0.0347	0.2689	0.034	0.16
60.07	3.0107	0.0223	0.2912	0.027	0.187
75.45	2.3971	0.0219	0.3131	0.032	0.219
89.71	2.0161	0.014	0.3271	0.025	0.244
114.89	1.5742	0.0169	0.344	0.038	0.282
139.77	1.294	0.0105	0.3545	0.029	0.311
174.86	1.0343	0.0095	0.364	0.033	0.344
219.12	0.8254	0.0076	0.3716	0.033	0.377
269.27	0.6717	0.0058	0.3774	0.031	0.408
328.61	0.5504	0.005	0.3824	0.032	0.44
418.28	0.4324	0.0054	0.3878	0.044	0.484
540.14	0.3348	0.0054	0.3932	0.056	0.54
638.38	0.2833	0.0033	0.3965	0.042	0.582
698.82	0.2588	0.0017	0.3982	0.024	0.606
798.12	0.2266	0.0024	0.4006	0.04	0.646
1000.38	0.1808	0.0041	0.4047	0.08	0.726
1225.75	0.1476	0.0035	0.4082	0.086	0.812
1308.11	0.1383	0.0011	0.4093	0.031	0.843
1405.11	0.1287	0.0011	0.4104	0.034	0.877

1506.17	0.1201	0.0012	0.4116	0.039	0.916
1600.85	0.113	0.001	0.4126	0.034	0.95
1697.76	0.1065	0.001	0.4136	0.038	0.988
1905.05	0.0949	0.0018	0.4154	0.071	1.059
2059.66	0.0878	0.0012	0.4166	0.054	1.113
2212.3	0.0818	0.0012	0.4178	0.059	1.172
2356.46	0.0768	0.0009	0.4187	0.046	1.218
2502.23	0.0723	0.0011	0.4198	0.058	1.276
2648.88	0.0683	0.001	0.4208	0.055	1.331
2703.83	0.0669	0.0004	0.4212	0.022	1.353
2850.99	0.0634	0.0009	0.4221	0.056	1.409
2996.47	0.0604	0.0008	0.4229	0.051	1.46
3251	0.0556	0.0013	0.4242	0.091	1.551
3495.54	0.0517	0.0013	0.4255	0.095	1.646
3740	0.0484	0.0012	0.4267	0.093	1.739
3980.91	0.0454	0.0011	0.4278	0.094	1.833
4282.06	0.0422	0.0011	0.4289	0.104	1.937
4525.56	0.04	0.0009	0.4298	0.086	2.023
4743	0.0381	0.0008	0.4306	0.085	2.108
4986.92	0.0363	0.0007	0.4313	0.077	2.185
5284.01	0.0342	0.001	0.4323	0.111	2.296
5483.62	0.033	0.0006	0.4329	0.073	2.369
5729.46	0.0316	0.0007	0.4336	0.089	2.458
5981.03	0.0302	0.0007	0.4343	0.092	2.55
6221.13	0.0291	0.0007	0.435	0.089	2.639
6467.69	0.028	0.0007	0.4357	0.1	2.739
6726.07	0.0269	0.0006	0.4363	0.088	2.827
6972.98	0.0259	0.0009	0.4372	0.134	2.961
7468.96	0.0242	0.001	0.4382	0.157	3.118
7968.88	0.0227	0.0014	0.4396	0.244	3.362
8502.85	0.0213	0.0008	0.4404	0.137	3.499
8980.55	0.0201	0.0007	0.4411	0.138	3.637
9306.31	0.0194	0.0005	0.4416	0.107	3.744
9600.53	0.0188	0.0005	0.4421	0.113	3.857
10049.92	0.018	0.0006	0.4427	0.12	3.977
10471.36	0.0173	0.0006	0.4433	0.14	4.117
10964.12	0.0165	0.0006	0.4439	0.142	4.259
11468.7	0.0158	0.0006	0.4445	0.149	4.408
11959.66	0.0151	0.0005	0.445	0.142	4.55
12569.96	0.0144	0.0007	0.4457	0.186	4.736
13081	0.0138	0.0005	0.4462	0.154	4.89
13600.63	0.0133	0.0005	0.4467	0.144	5.034
13968.67	0.0129	0.0004	0.4471	0.126	5.16
14287.62	0.0127	0.0004	0.4475	0.133	5.293
14562.13	0.0124	0.0003	0.4478	0.104	5.397
14970.31	0.0121	0.0005	0.4483	0.151	5.548
15392.83	0.0117	0.0005	0.4488	0.154	5.702
15757.29	0.0115	0.0004	0.4492	0.143	5.845
16146.83	0.0112	0.0004	0.4496	0.145	5.99
16657.51	0.0109	0.0004	0.45	0.159	6.149

16997.96	0.0106	0.0004	0.4504	0.137	6.286
17353.1	0.0104	0.0003	0.4507	0.096	6.382
17697.85	0.0102	0.0003	0.451	0.121	6.503
18101.73	0.01	0.0004	0.4514	0.14	6.643
18451.86	0.0098	0.0003	0.4517	0.126	6.769
18803.06	0.0096	0.0004	0.4521	0.152	6.921
19211.96	0.0094	0.0003	0.4524	0.126	7.047
19747	0.0092	0.0003	0.4527	0.141	7.188
20301.4	0.0089	0.0004	0.4531	0.169	7.357
20773.01	0.0087	0.0003	0.4534	0.156	7.513
21139.98	0.0086	0.0003	0.4537	0.144	7.657
21595.46	0.0084	0.0003	0.454	0.165	7.822
22009.74	0.0082	0.0003	0.4543	0.146	7.968
22601.76	0.008	0.0003	0.4546	0.159	8.127
23124.27	0.0078	0.0003	0.4549	0.171	8.298
23692.28	0.0076	0.0003	0.4552	0.141	8.439
24033.8	0.0075	0.0004	0.4556	0.199	8.638
24600.38	0.0074	0.0003	0.4559	0.178	8.816
24991.01	0.0072	0.0002	0.4561	0.11	8.926
25389.51	0.0071	0.0003	0.4564	0.173	9.099
25828.87	0.007	0.0003	0.4567	0.172	9.271
26393.66	0.0069	0.0003	0.457	0.193	9.464
26862.41	0.0067	0.0003	0.4573	0.176	9.64
27312.52	0.0066	0.0002	0.4575	0.148	9.788
27714.25	0.0065	0.0003	0.4578	0.157	9.945
28178.7	0.0064	0.0004	0.4582	0.221	10.166
28901.53	0.0063	0.0003	0.4585	0.161	10.327
29398.22	0.0062	0.0003	0.4588	0.192	10.519
29931.48	0.006	0.0003	0.4591	0.192	10.711
30519.92	0.0059	0.0003	0.4594	0.189	10.9
30900.86	0.0059	0.0002	0.4596	0.143	11.043
31318.01	0.0058	0.0002	0.4598	0.141	11.184
31802.52	0.0057	0.0002	0.46	0.174	11.358
32377.35	0.0056	0.0002	0.4602	0.166	11.524
32912.39	0.0055	0.0003	0.4605	0.215	11.739
33528.07	0.0054	0.0002	0.4607	0.127	11.866
33992.16	0.0053	0.0003	0.461	0.191	12.057
34645.1	0.0052	0.0003	0.4613	0.213	12.27
35466.48	0.0051	0.0002	0.4615	0.154	12.424
36198.63	0.005	0.0003	0.4618	0.26	12.684
36975.22	0.0049	0.0002	0.462	0.171	12.855
37606.3	0.0048	0.0002	0.4622	0.194	13.049
38431.63	0.0047	0.0002	0.4624	0.174	13.223
39167.72	0.0046	0.0003	0.4627	0.24	13.463
40024.22	0.0045	0.0003	0.463	0.231	13.694
40516.27	0.0045	0.0002	0.4632	0.135	13.829
41072.81	0.0044	0.0003	0.4635	0.23	14.059
42507.36	0.0043	0.0002	0.4637	0.226	14.285
43306.17	0.0042	0.0002	0.4639	0.214	14.499
43998.54	0.0041	0.0002	0.4641	0.234	14.733

44999.46	0.004	0.0002	0.4643	0.2	14.933
46460.53	0.0039	0.0002	0.4645	0.208	15.141
47990.77	0.0038	0.0003	0.4648	0.272	15.413
49476.93	0.0037	0.0002	0.465	0.236	15.649
50138.84	0.0036	0.0001	0.4651	0.164	15.813
52919.79	0.0034	0.0003	0.4654	0.364	16.177
54427.8	0.0033	0.0003	0.4657	0.355	16.532
55970.94	0.0032	0.0001	0.4658	0.166	16.698
57799.34	0.0031	0.0003	0.4661	0.433	17.131
59823.05	0.003	0.00002	0.4661	0.299	17.43

Appendix G
Assessment of the Air Phase Equilibrium

Control charts for the assessment of the equilibrium of the air phase at the outlet of the gas saturation column are gathered in this appendix. In each experiment conducted with contaminated sediment, the effect of flow rate variations on the concentration of the outlet stream was investigated. In the two experiments conducted with wet sediment contaminated with phenanthrene at respectively 58 mg/kg and 26 mg/kg, the influence of bed length was tested as well.

Charts of experiments conducted with phenanthrene are presented first, followed by the ones of dibenzofuran experiments. On each chart the average value of the experimental data points is plotted along with the 95% confidence interval.

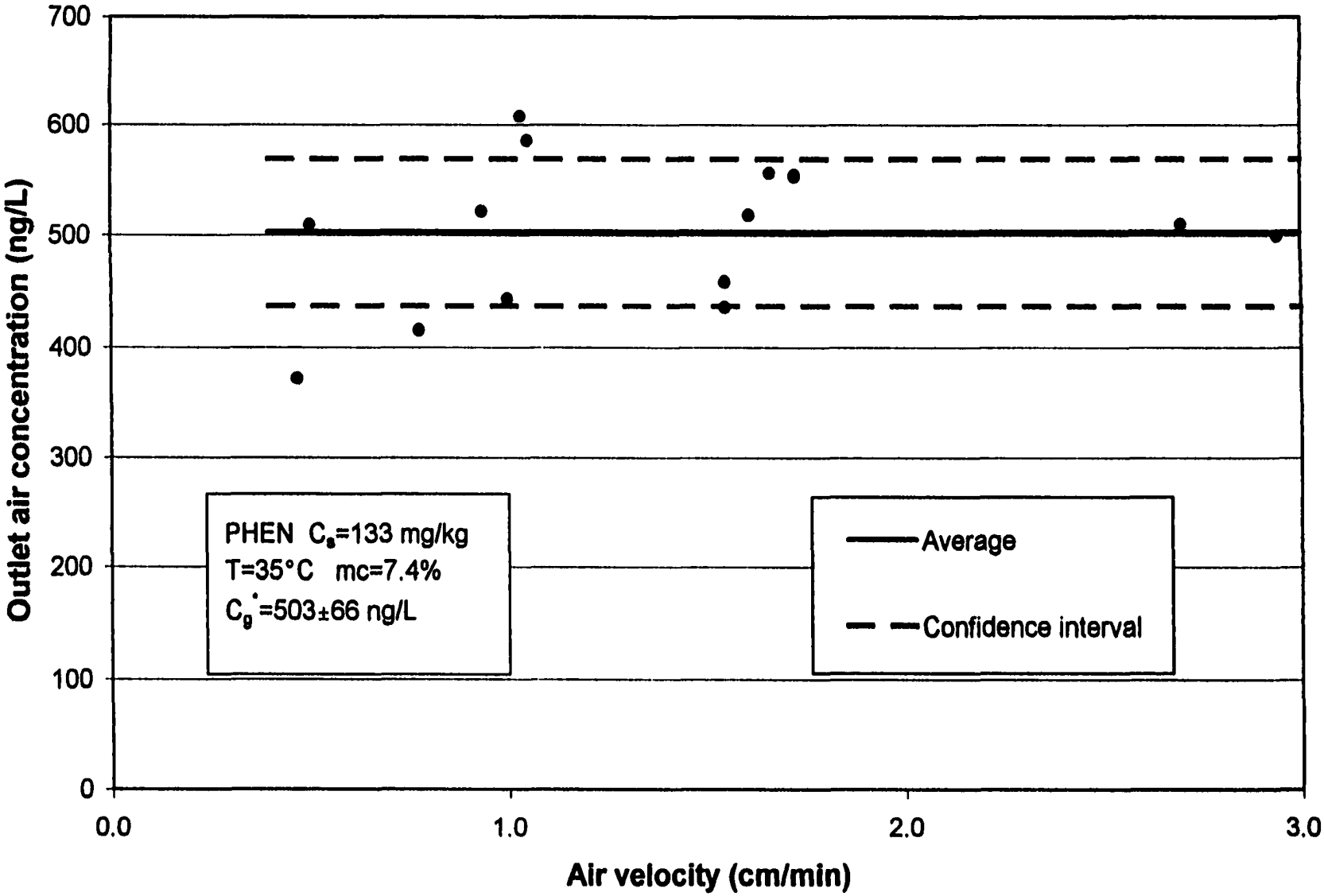

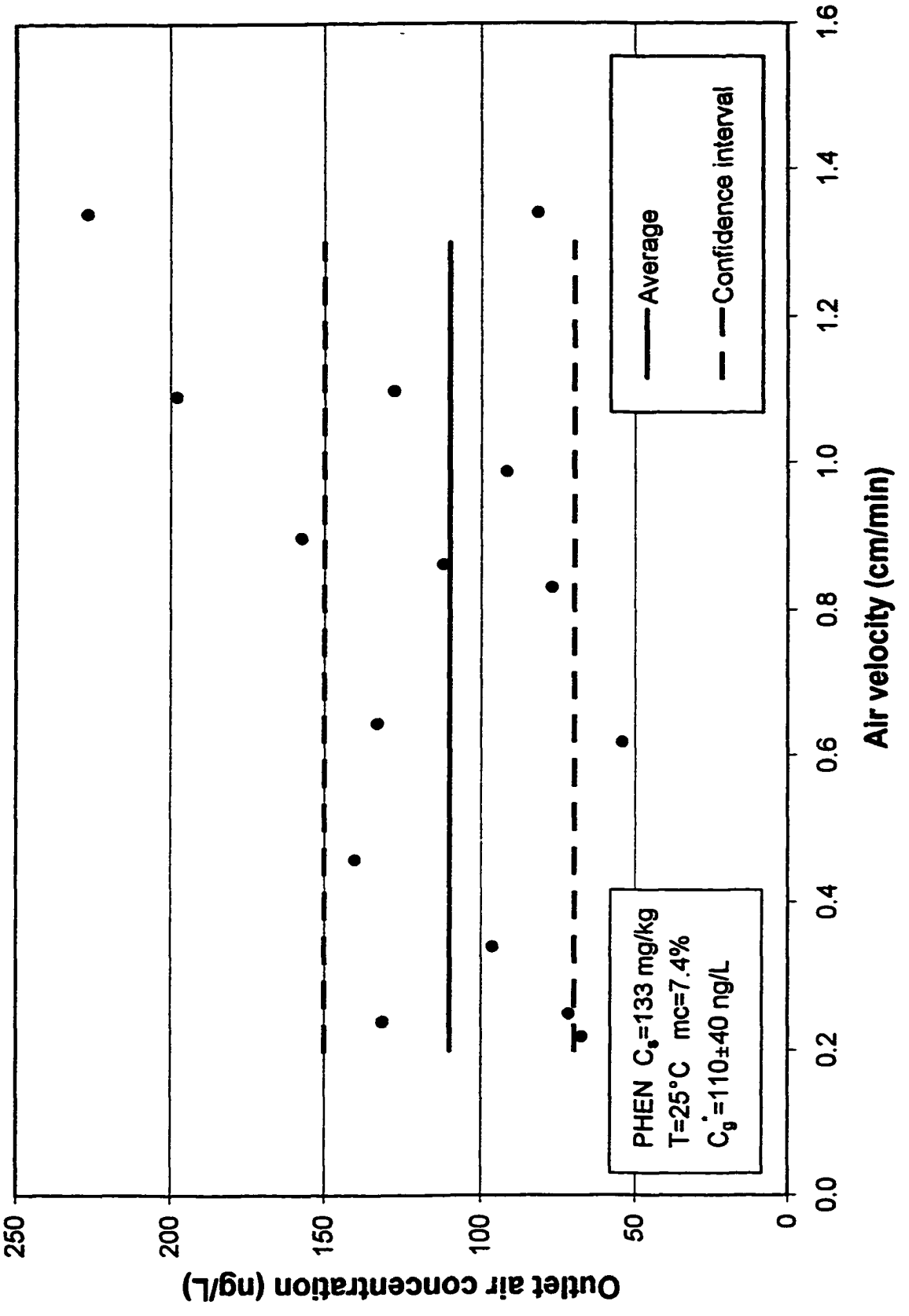

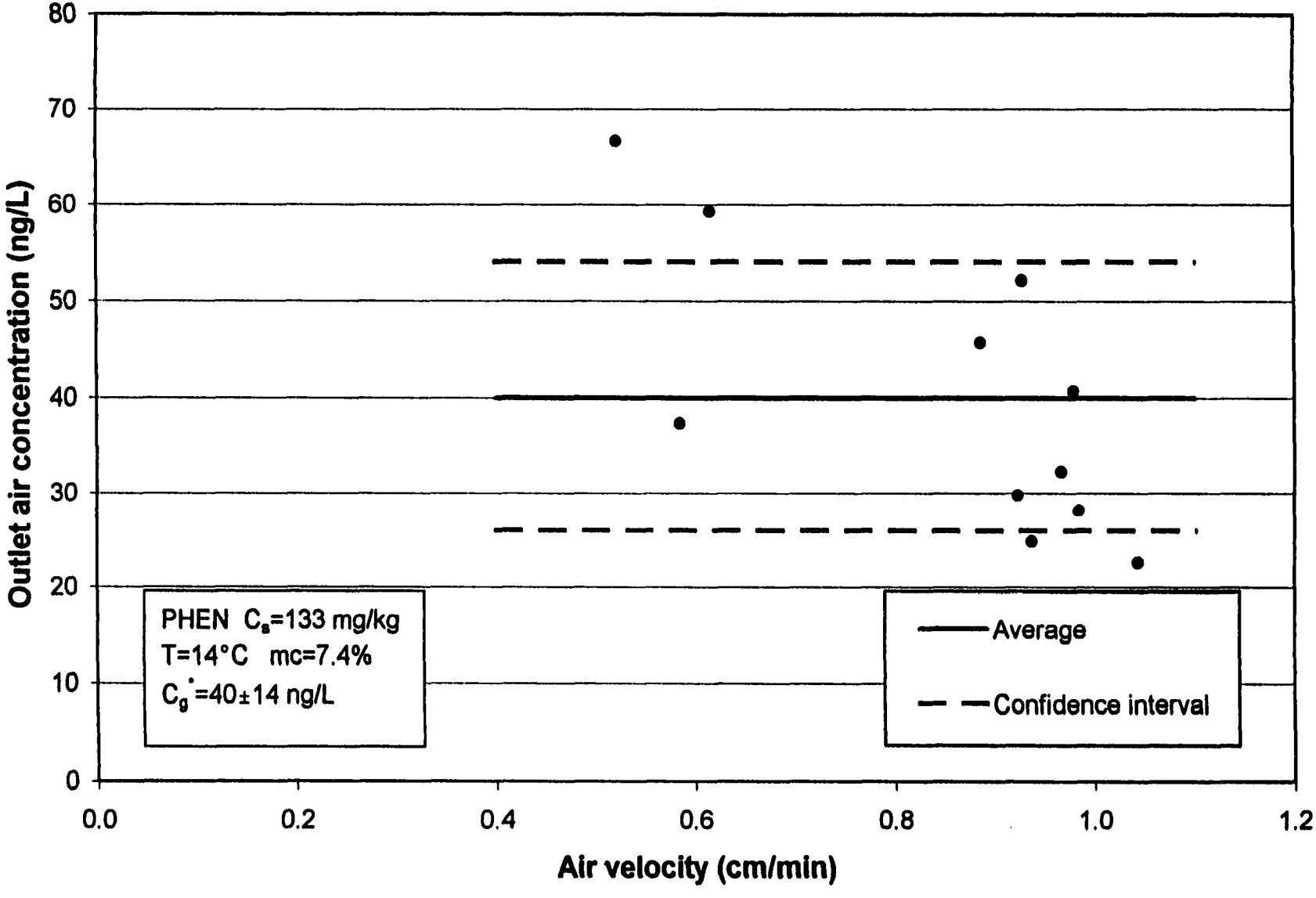

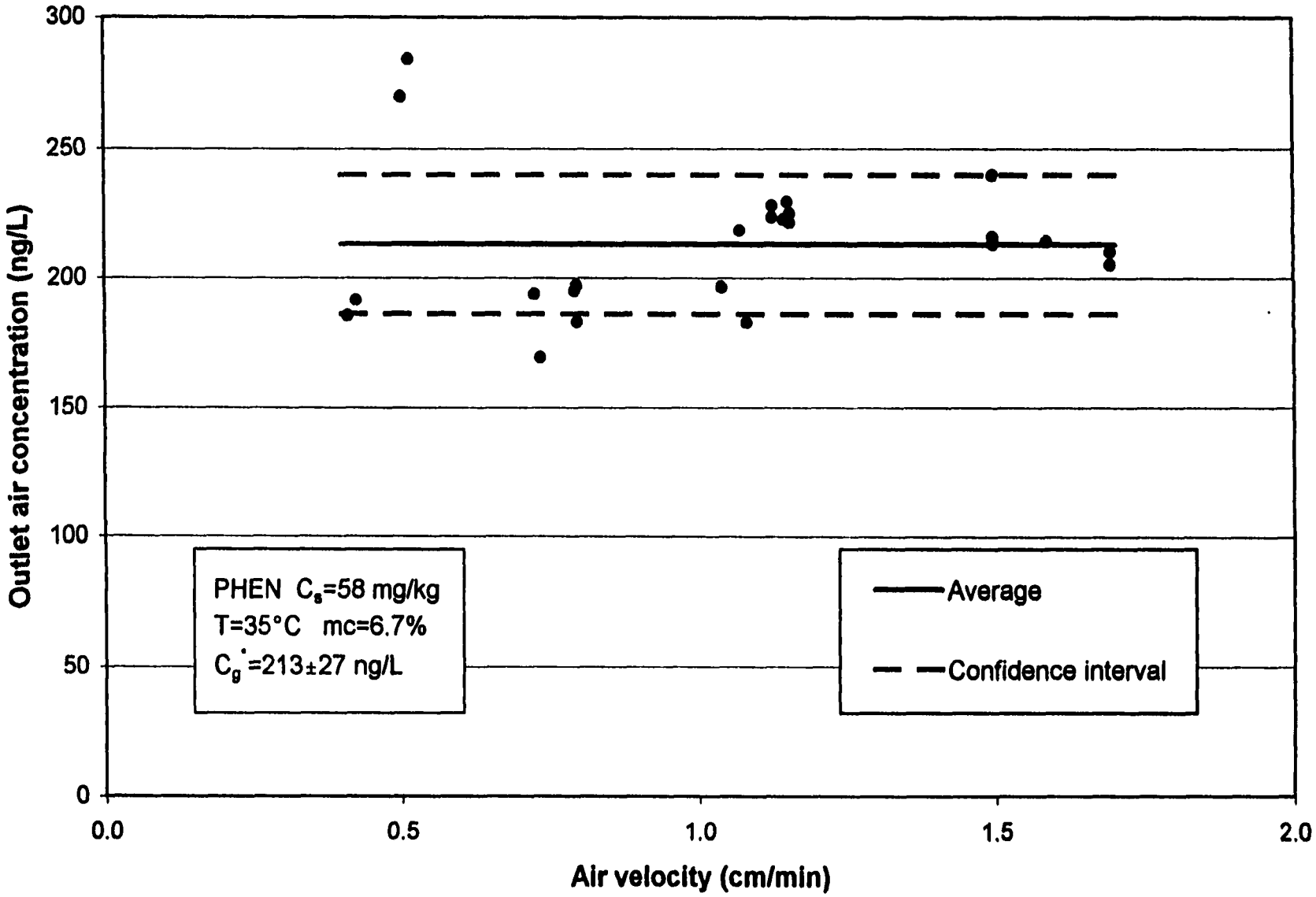

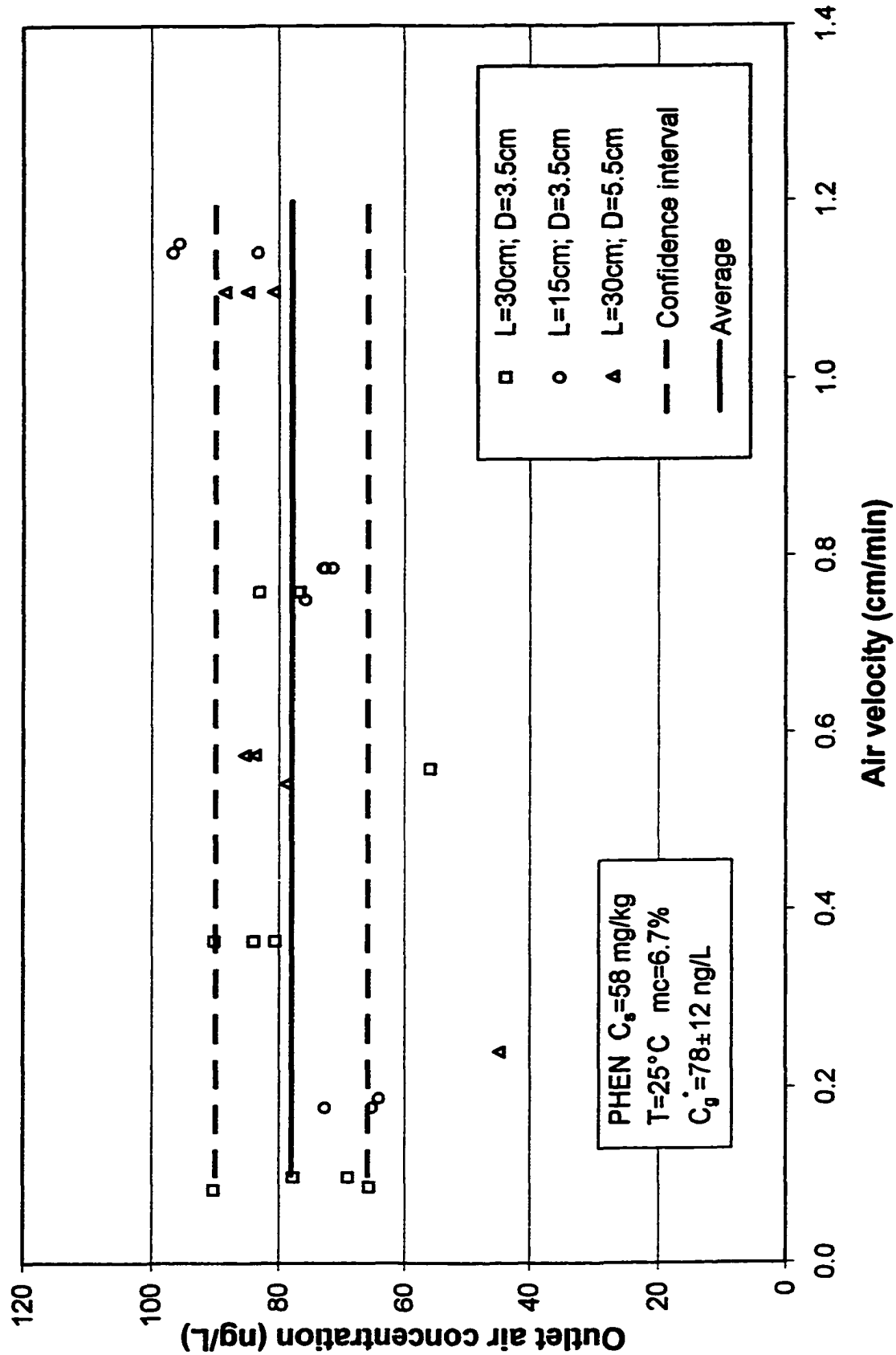

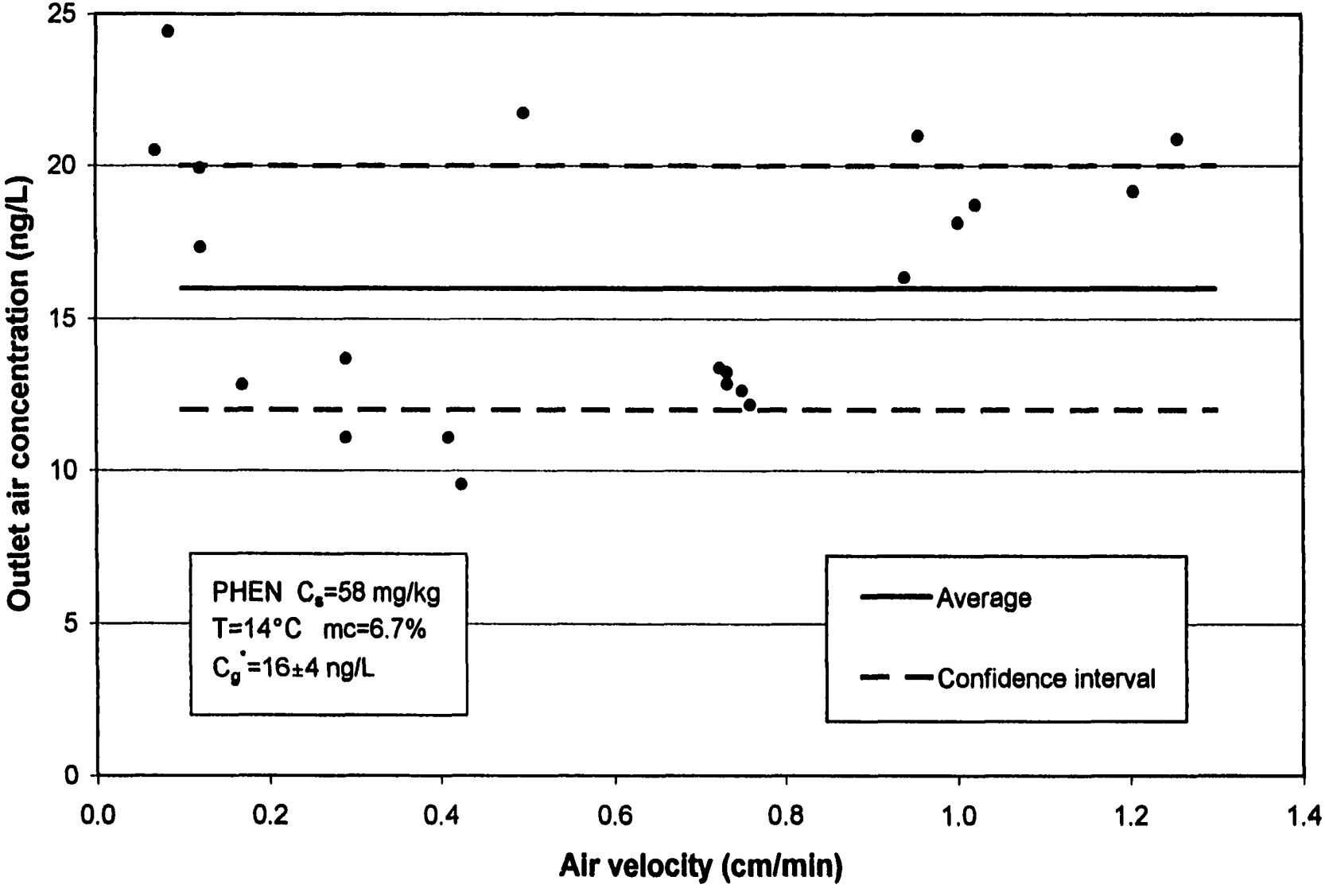

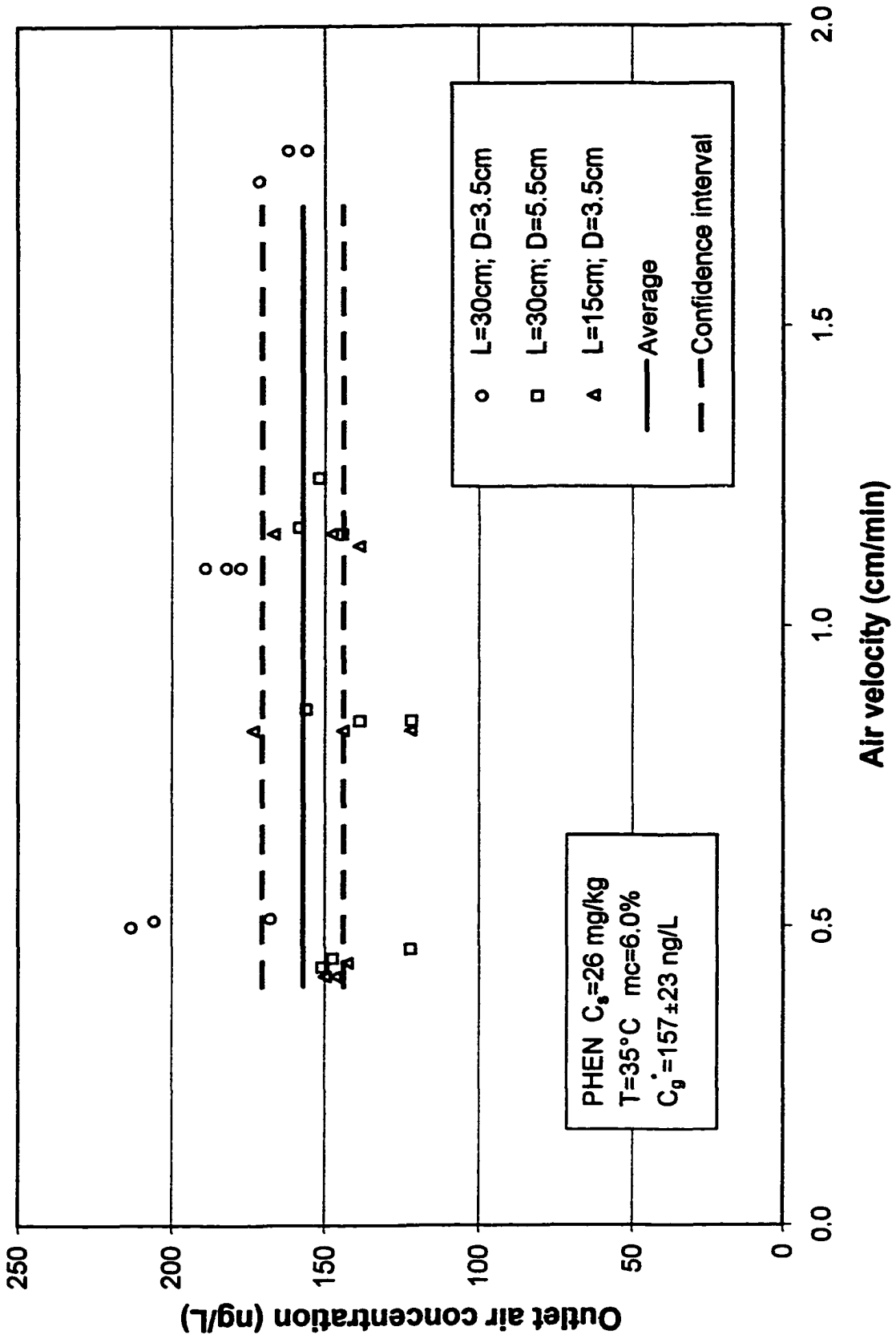

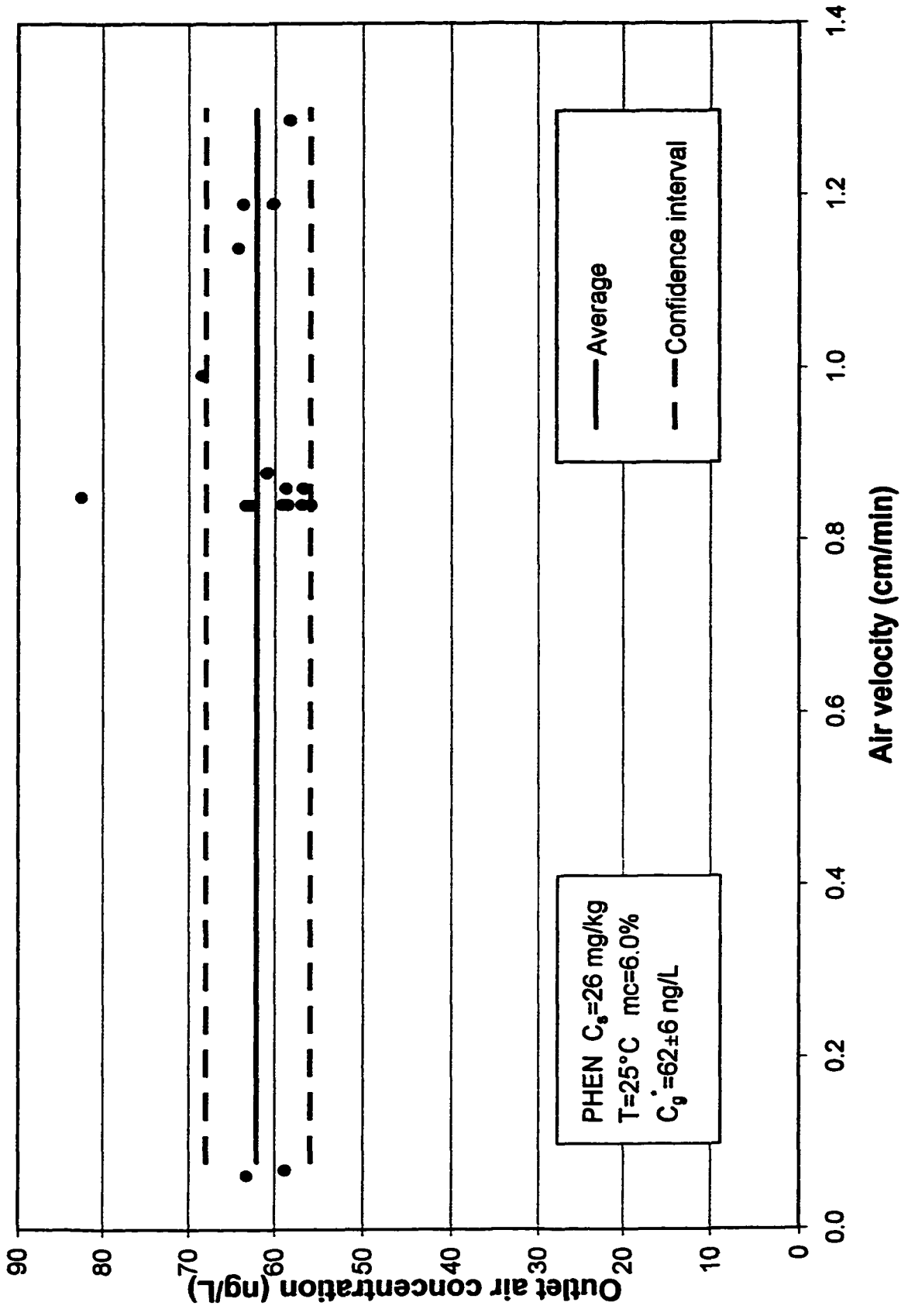

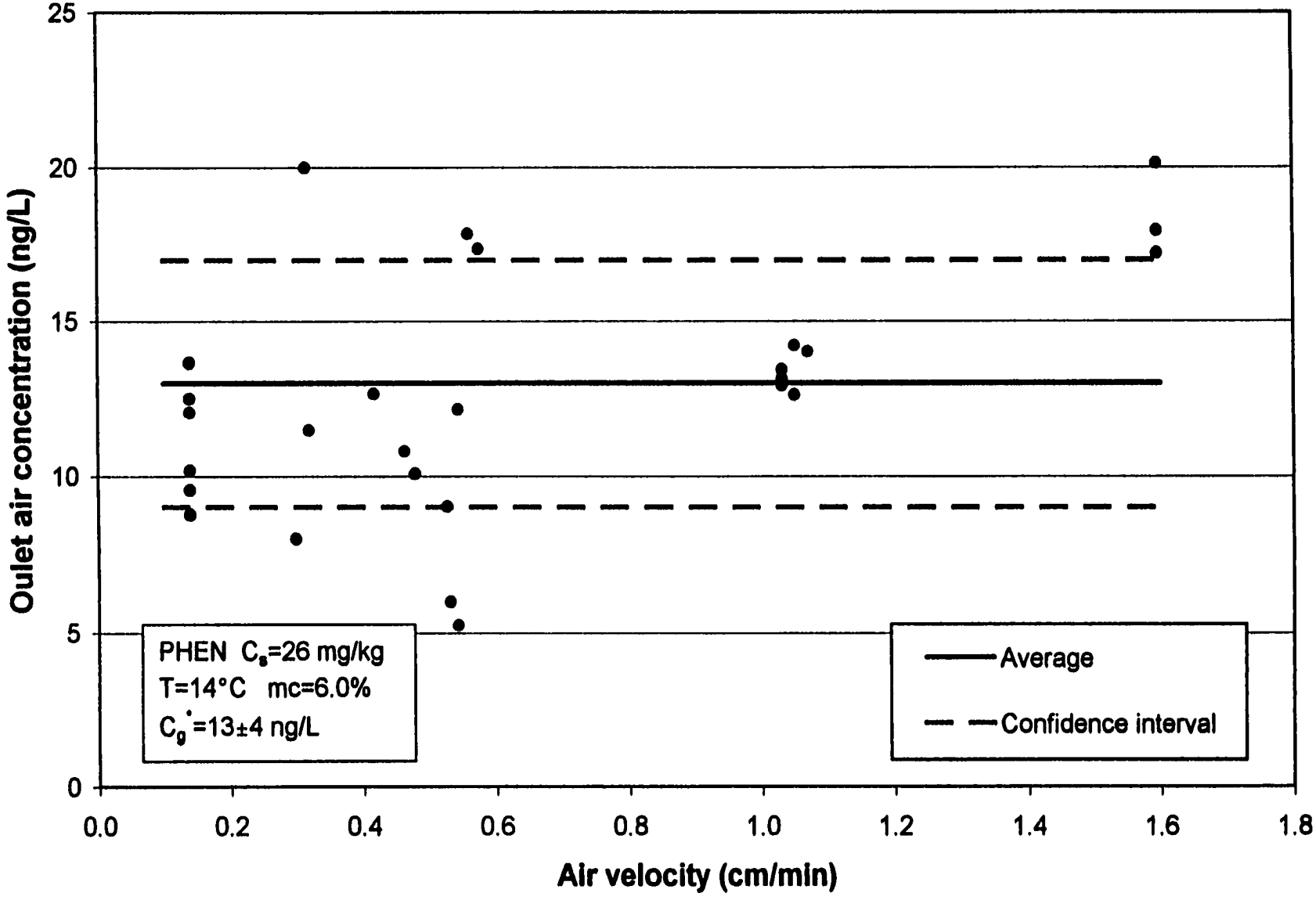

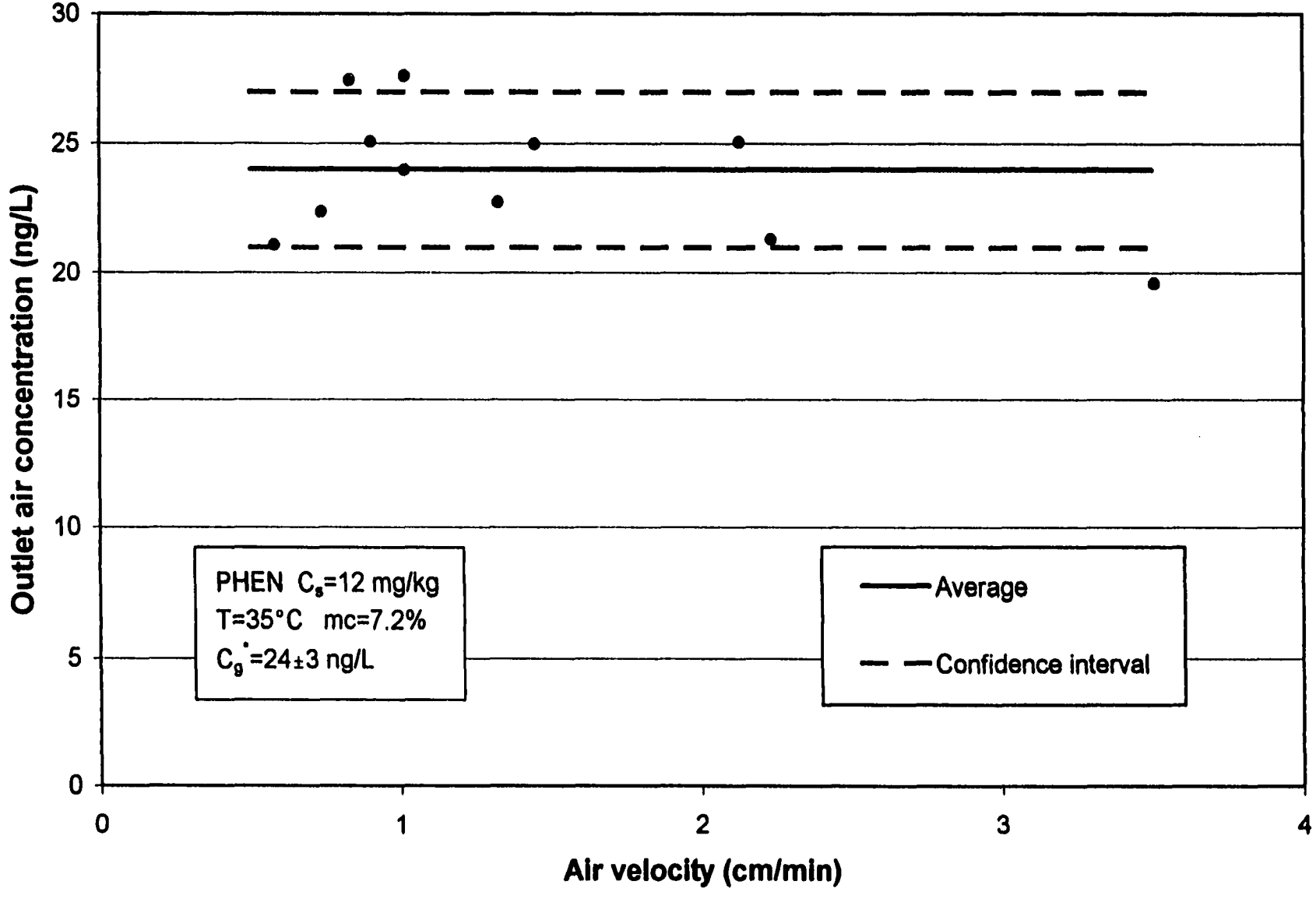

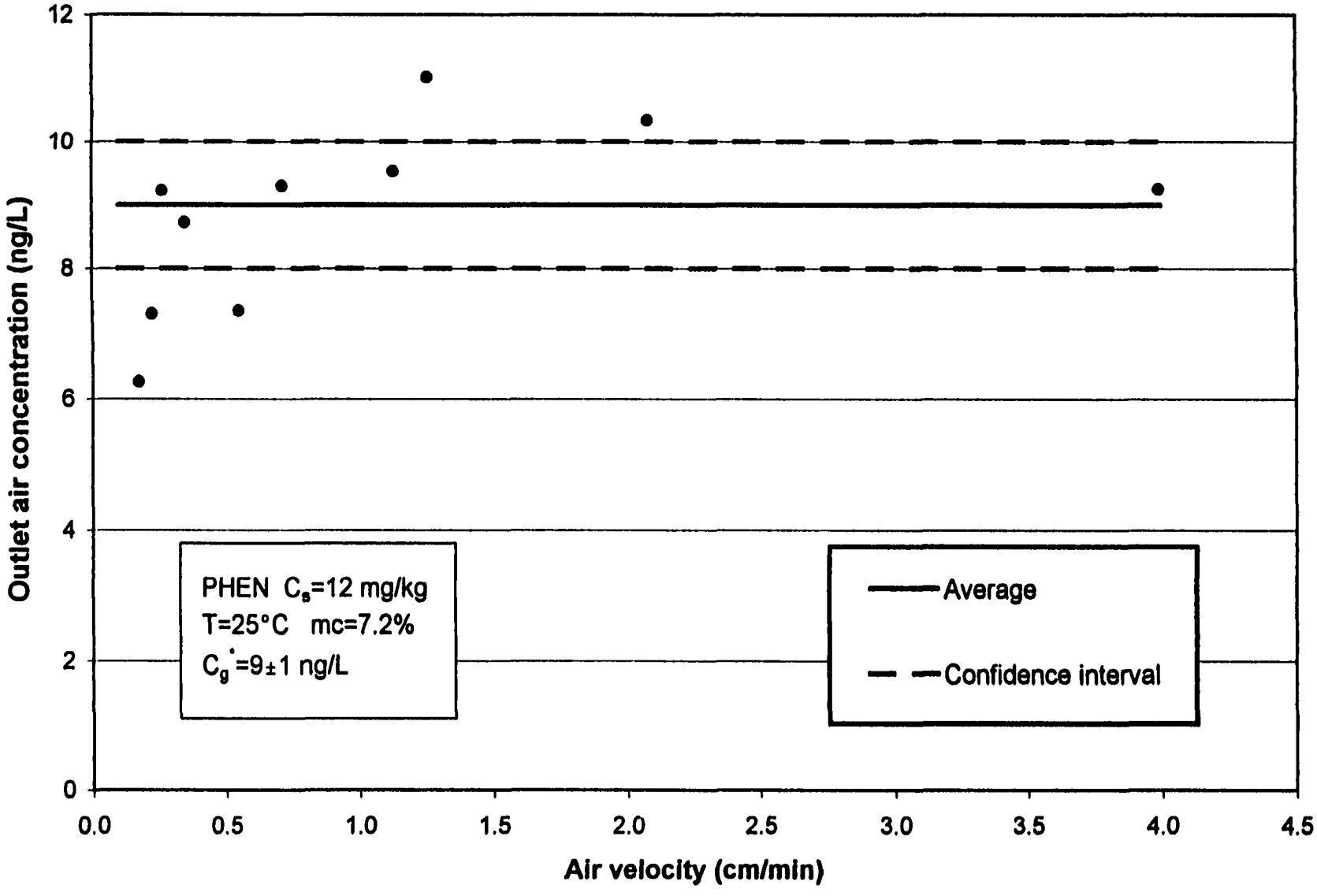

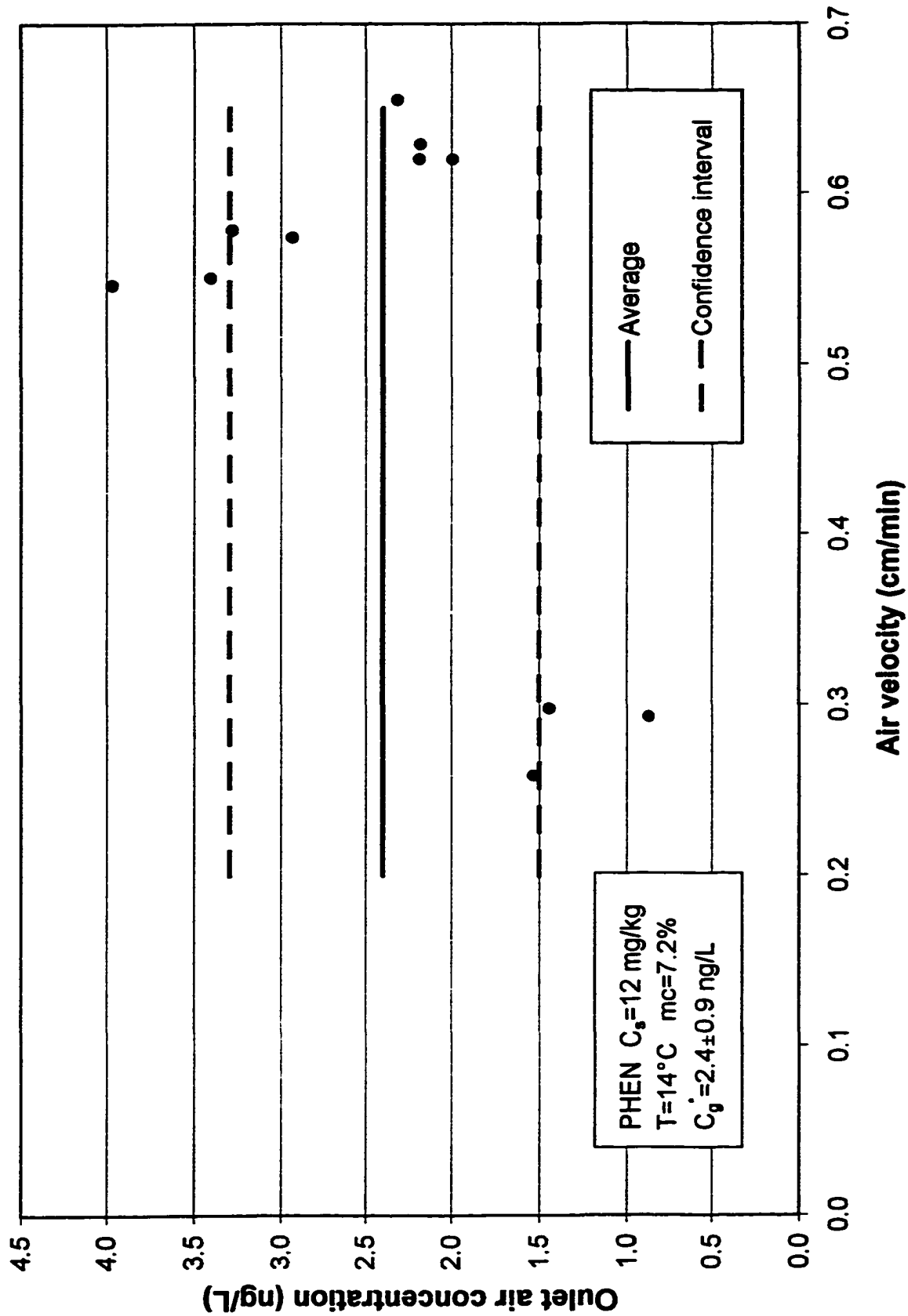

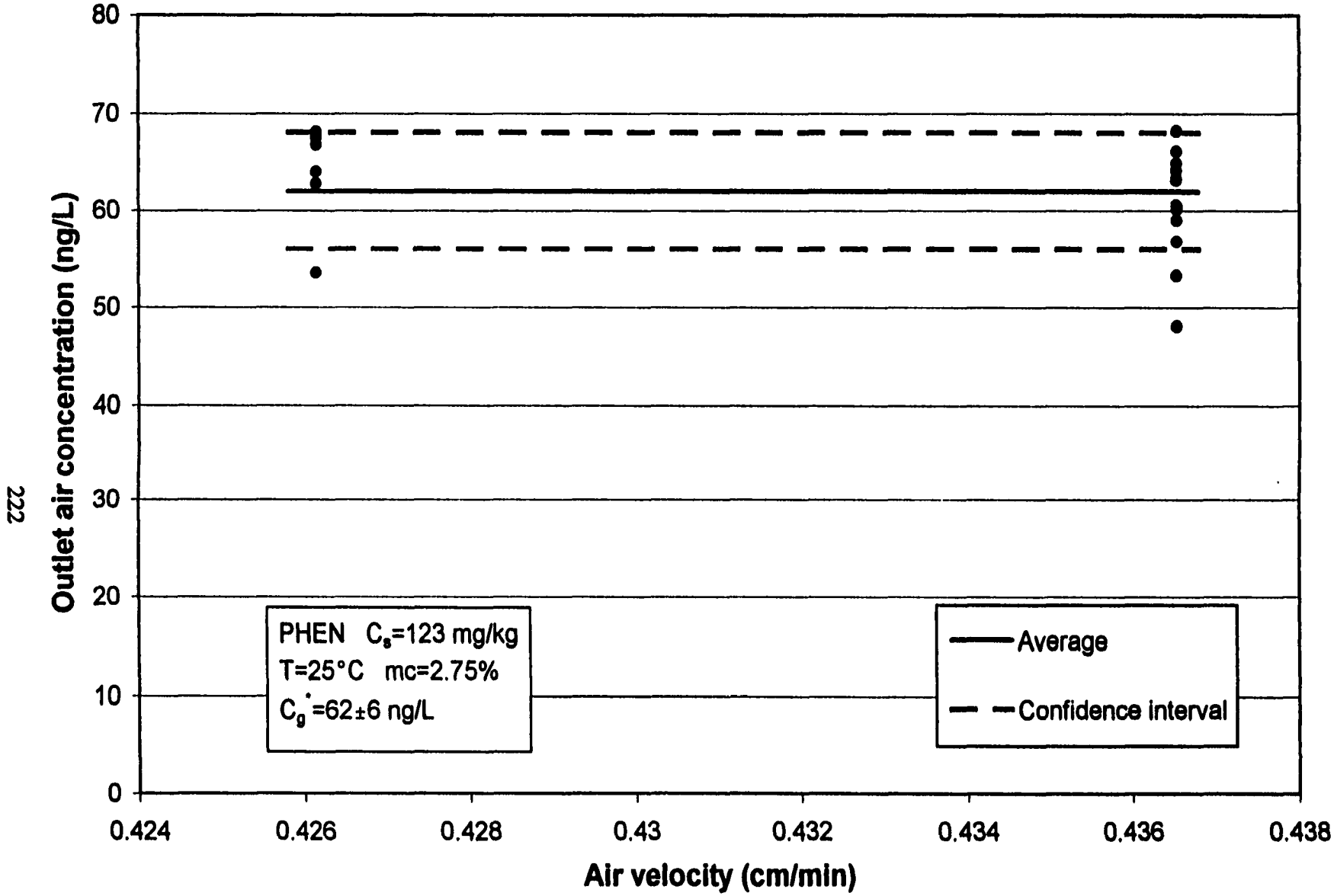

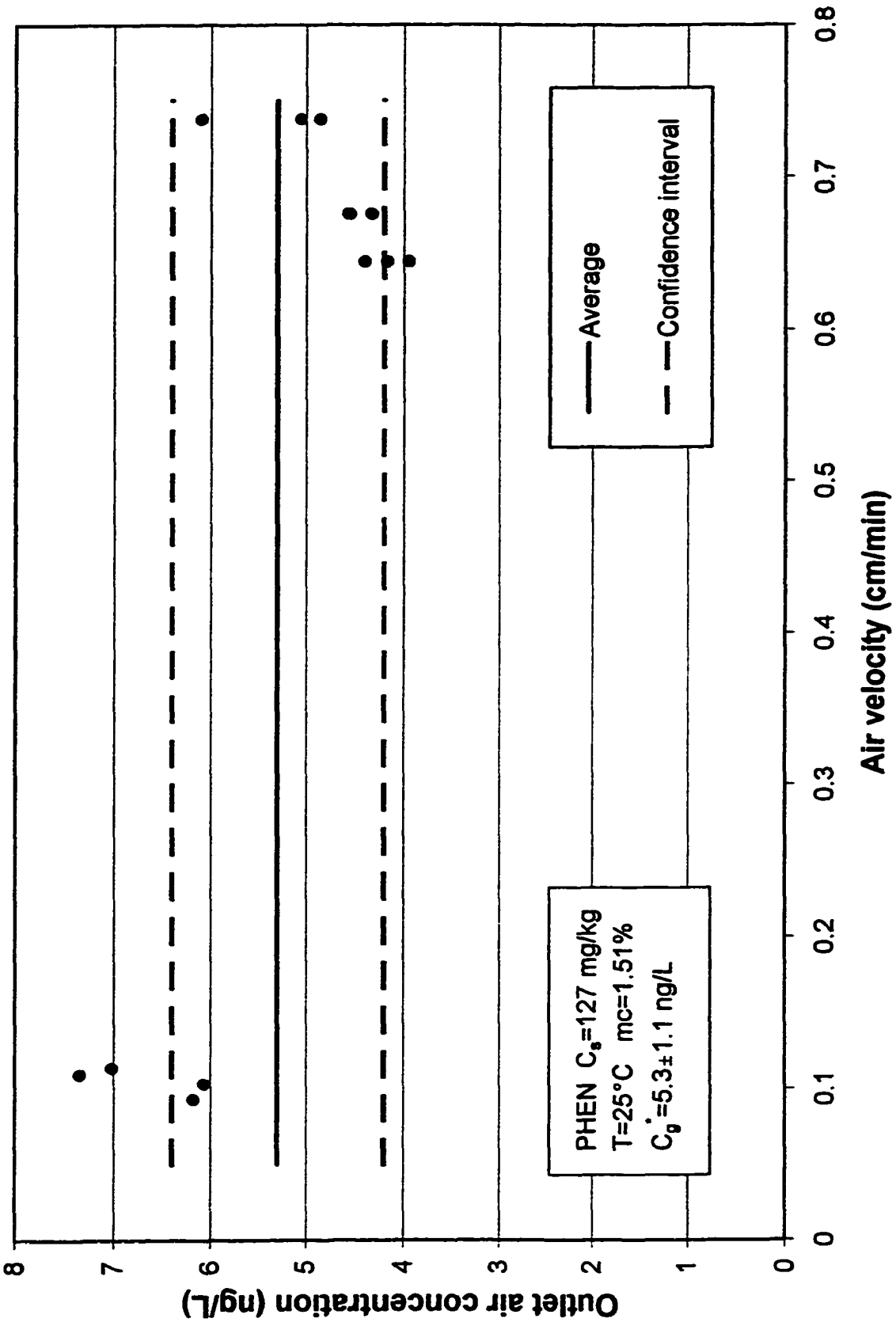

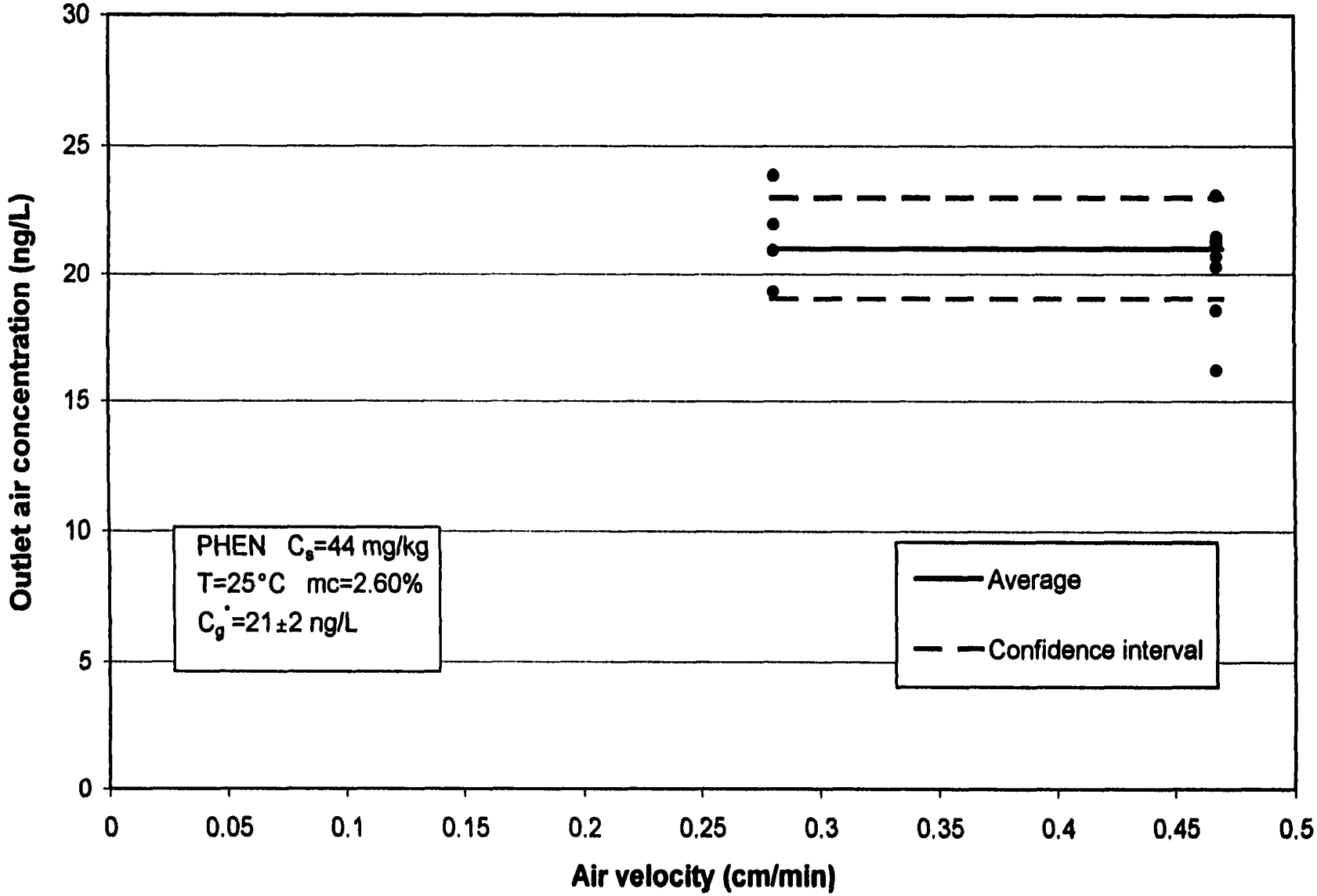

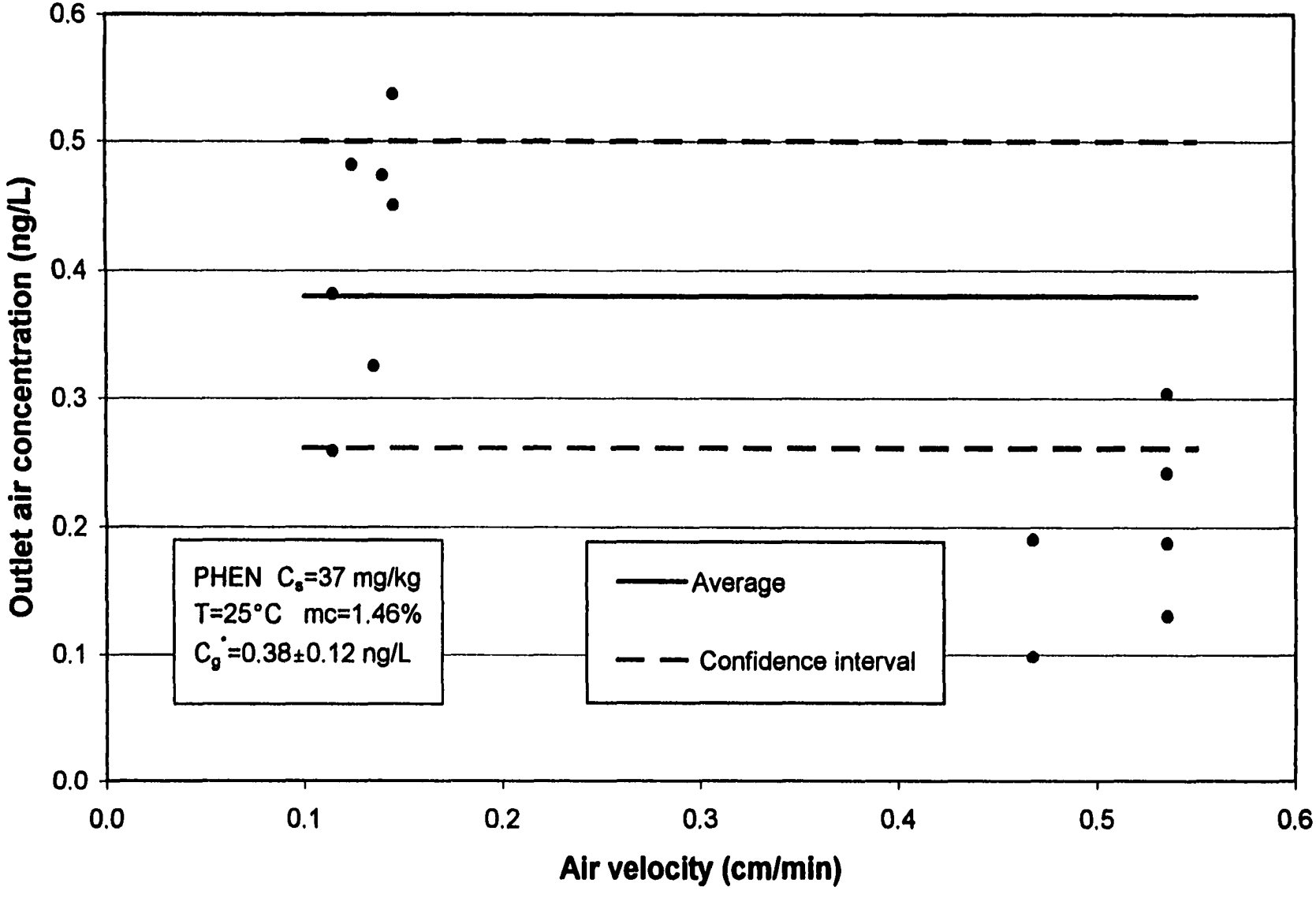

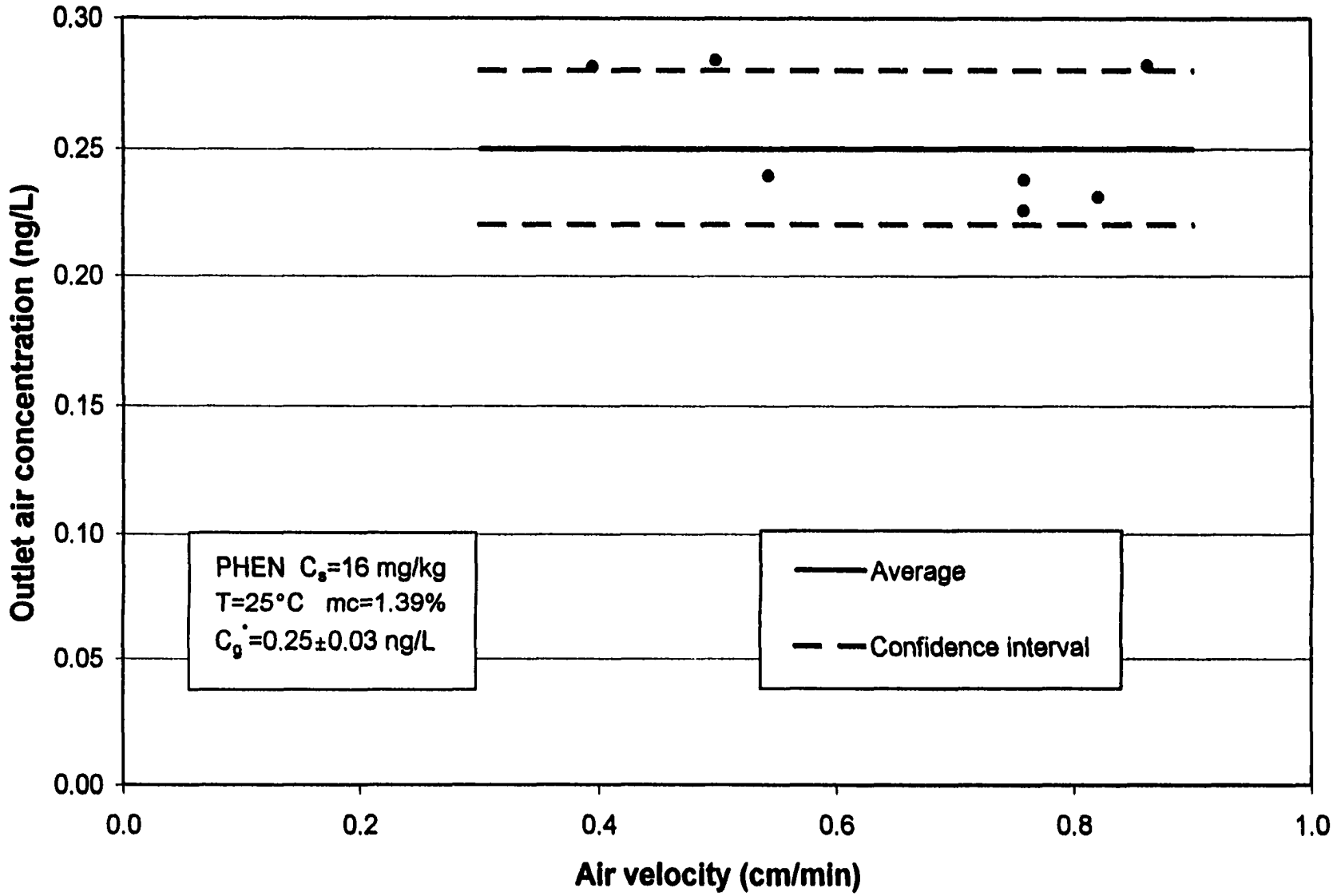

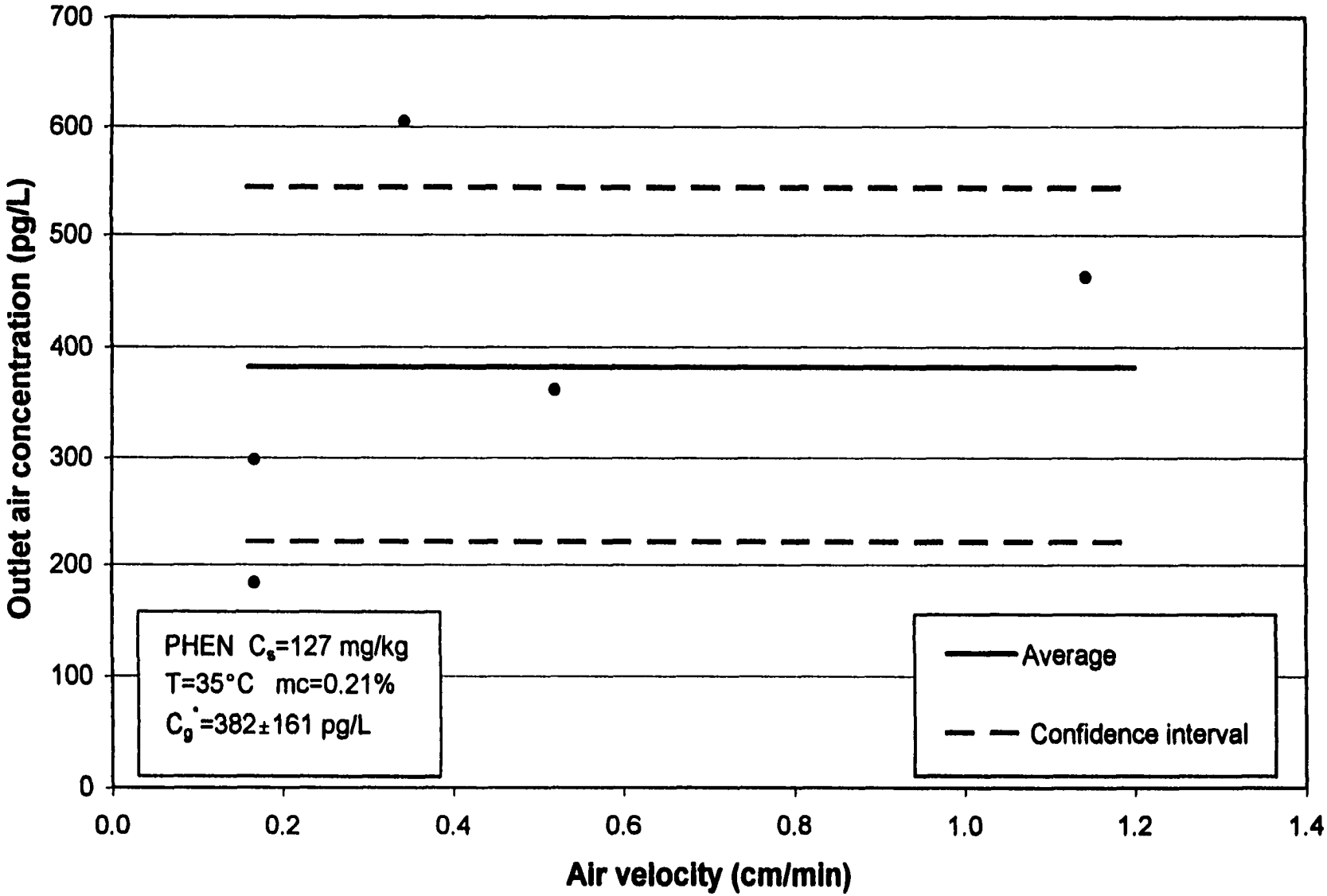

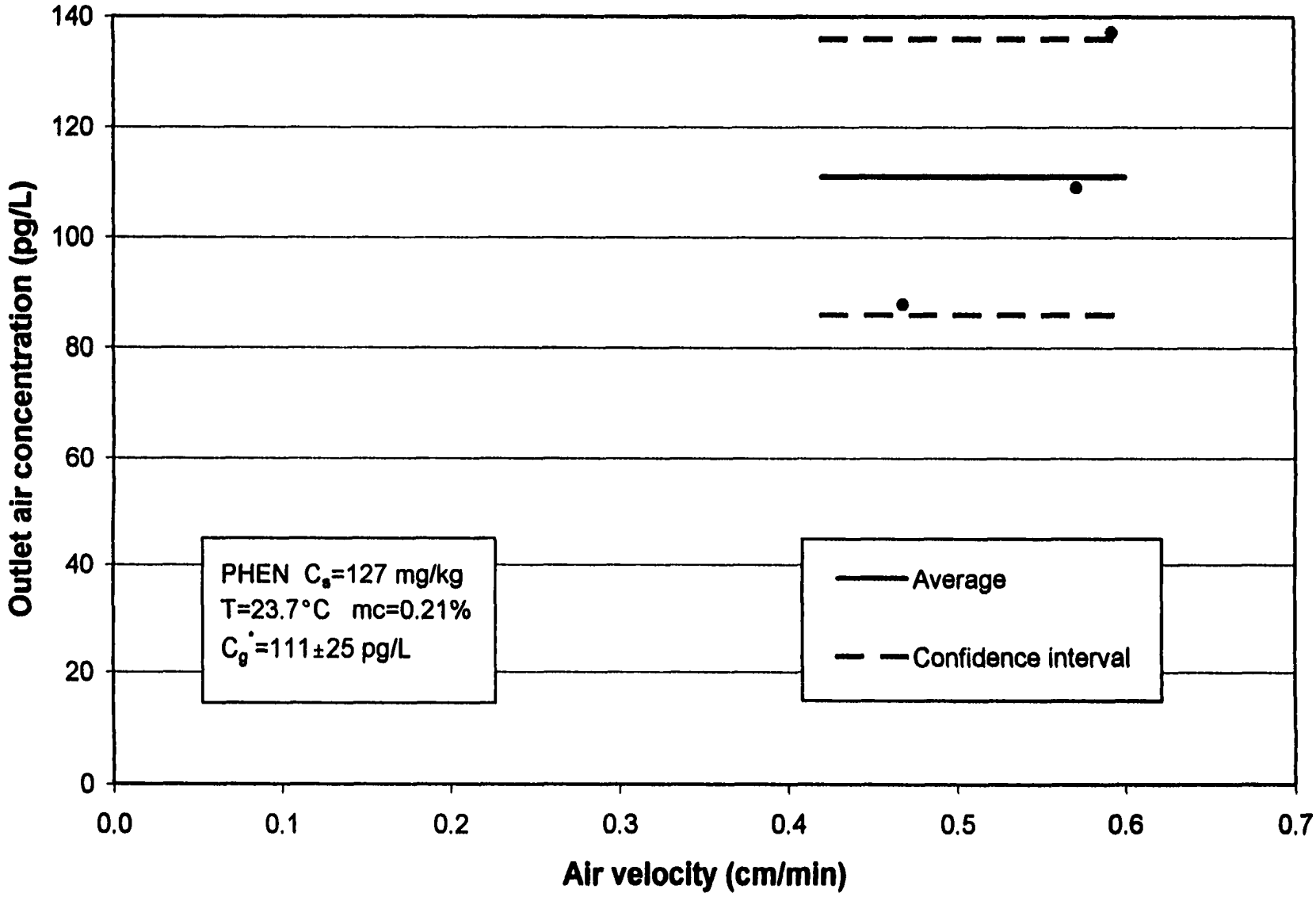

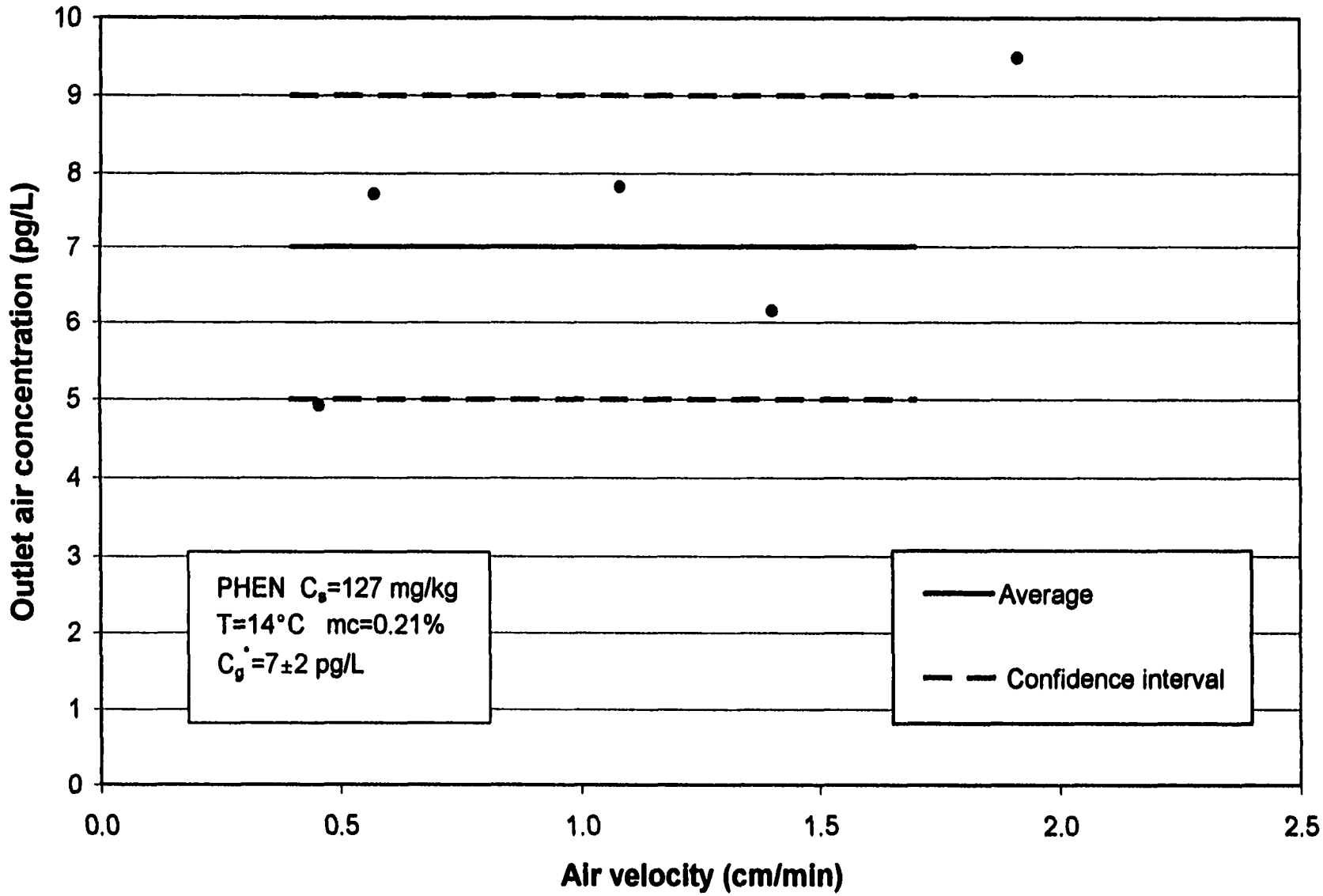

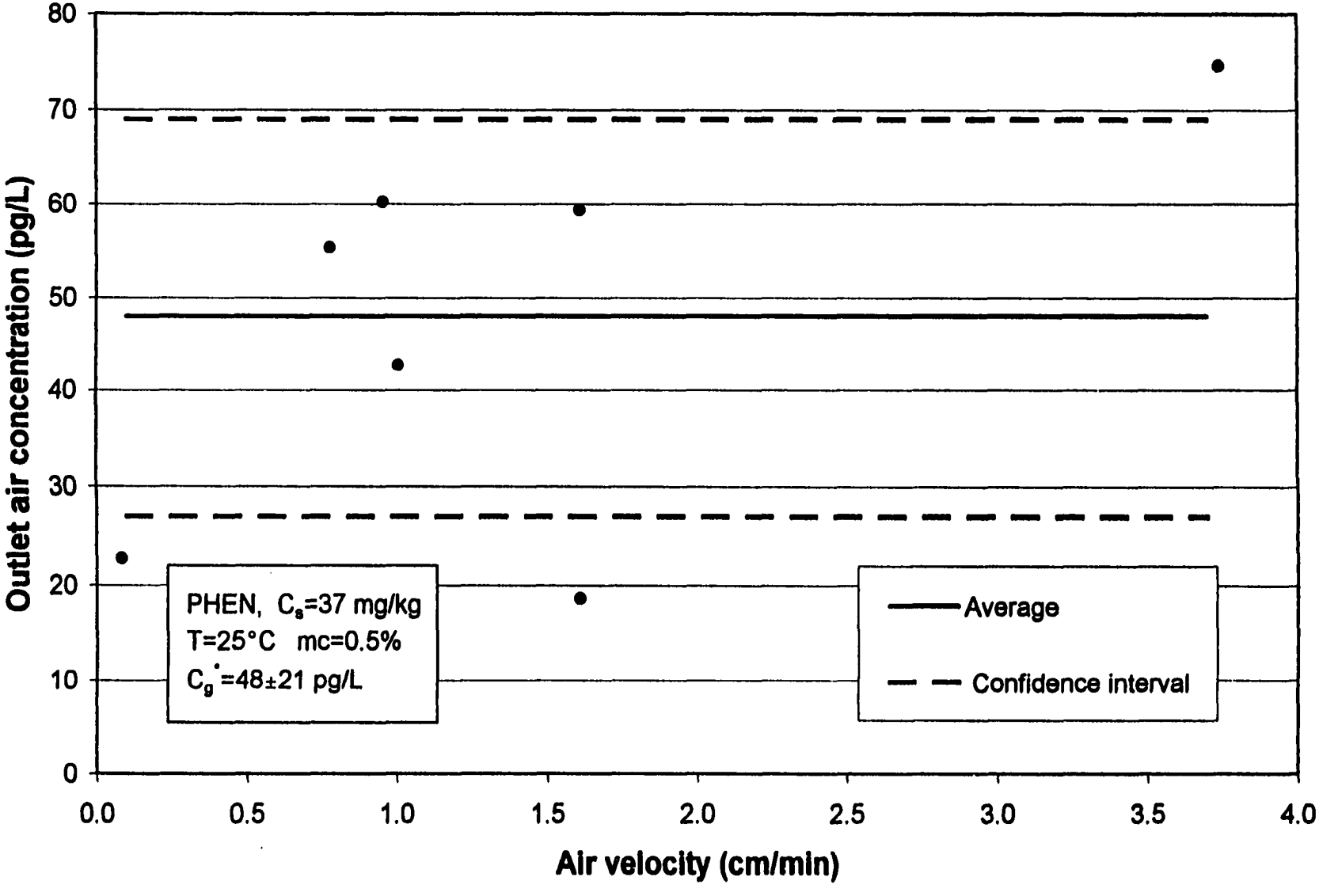

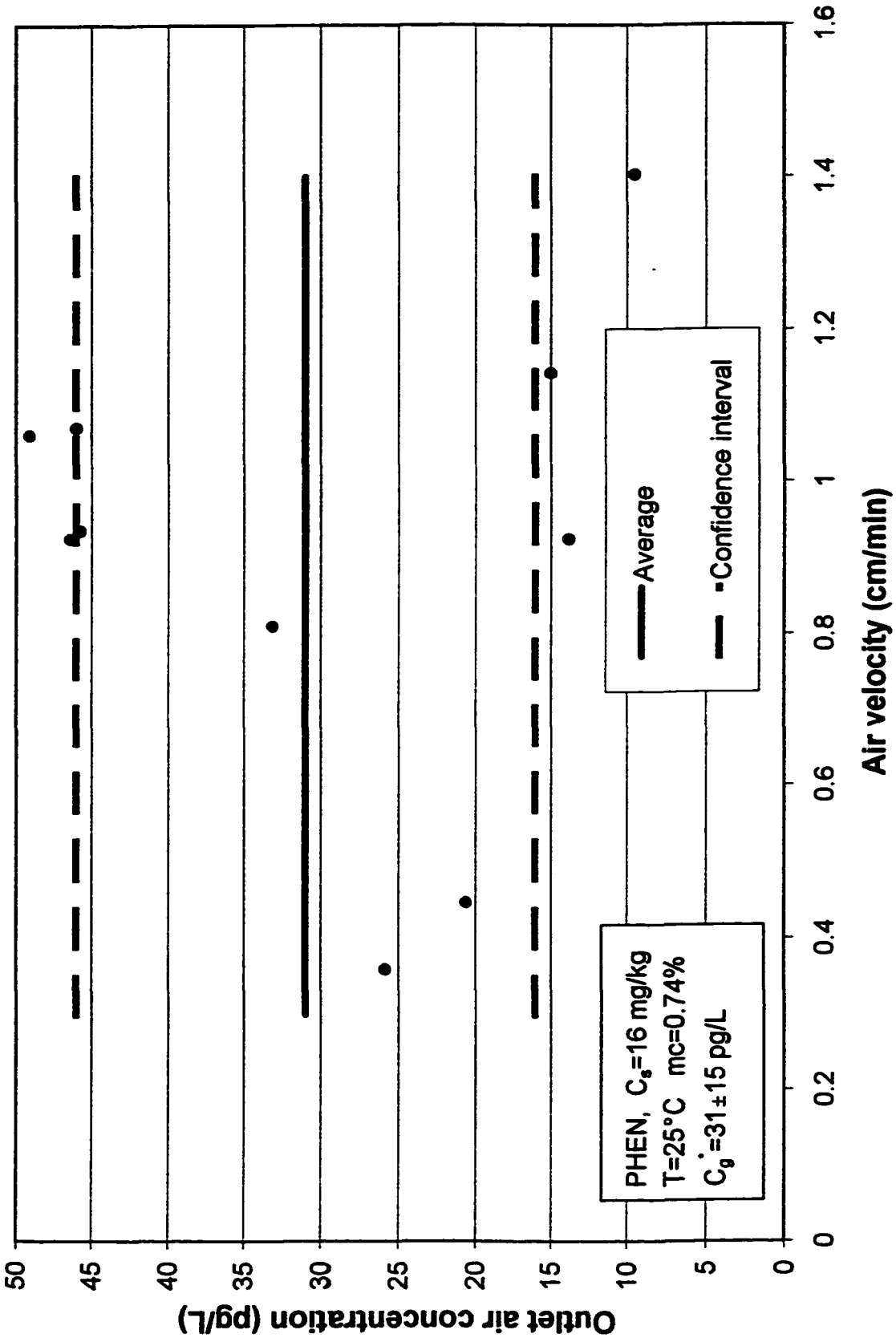

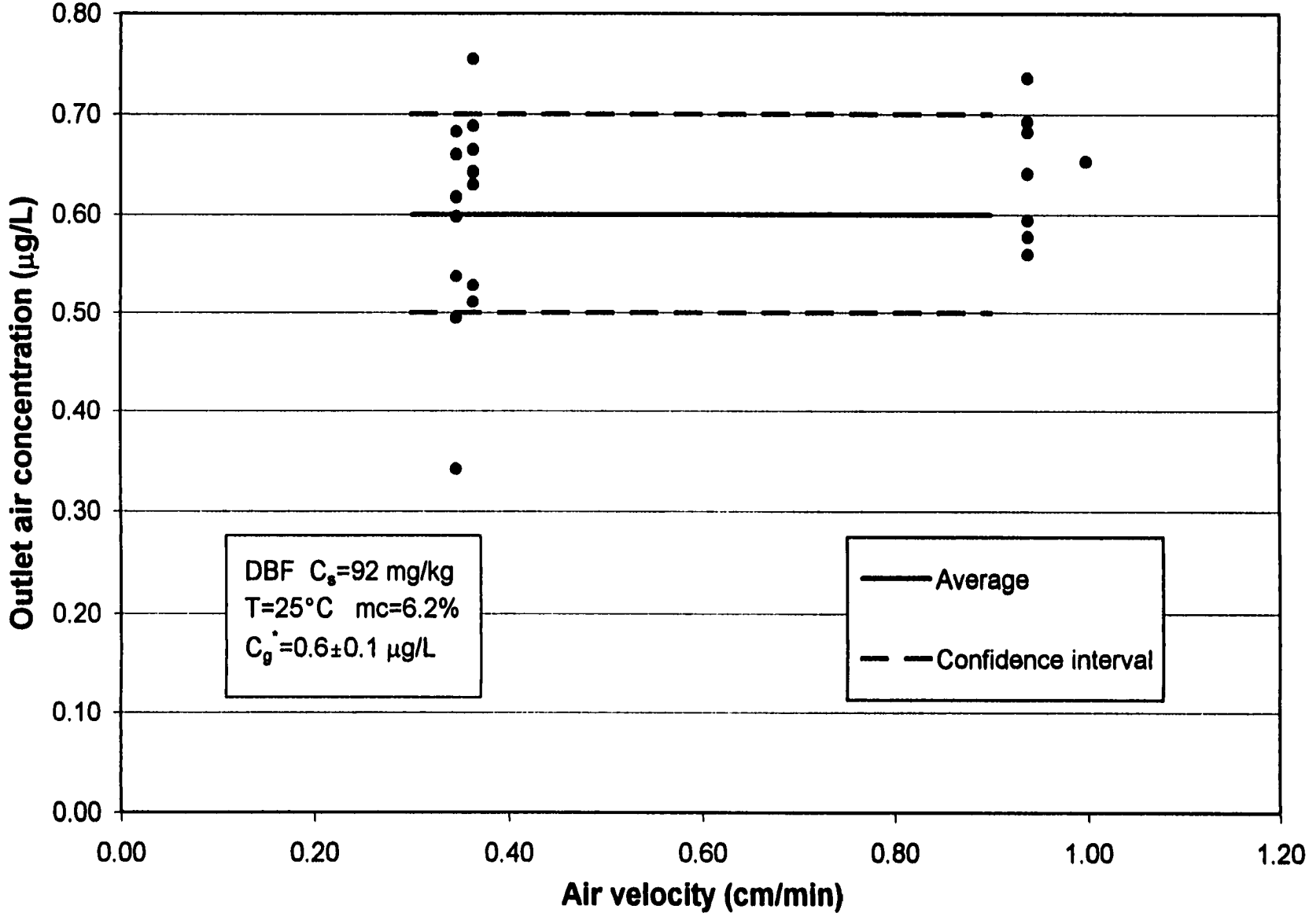

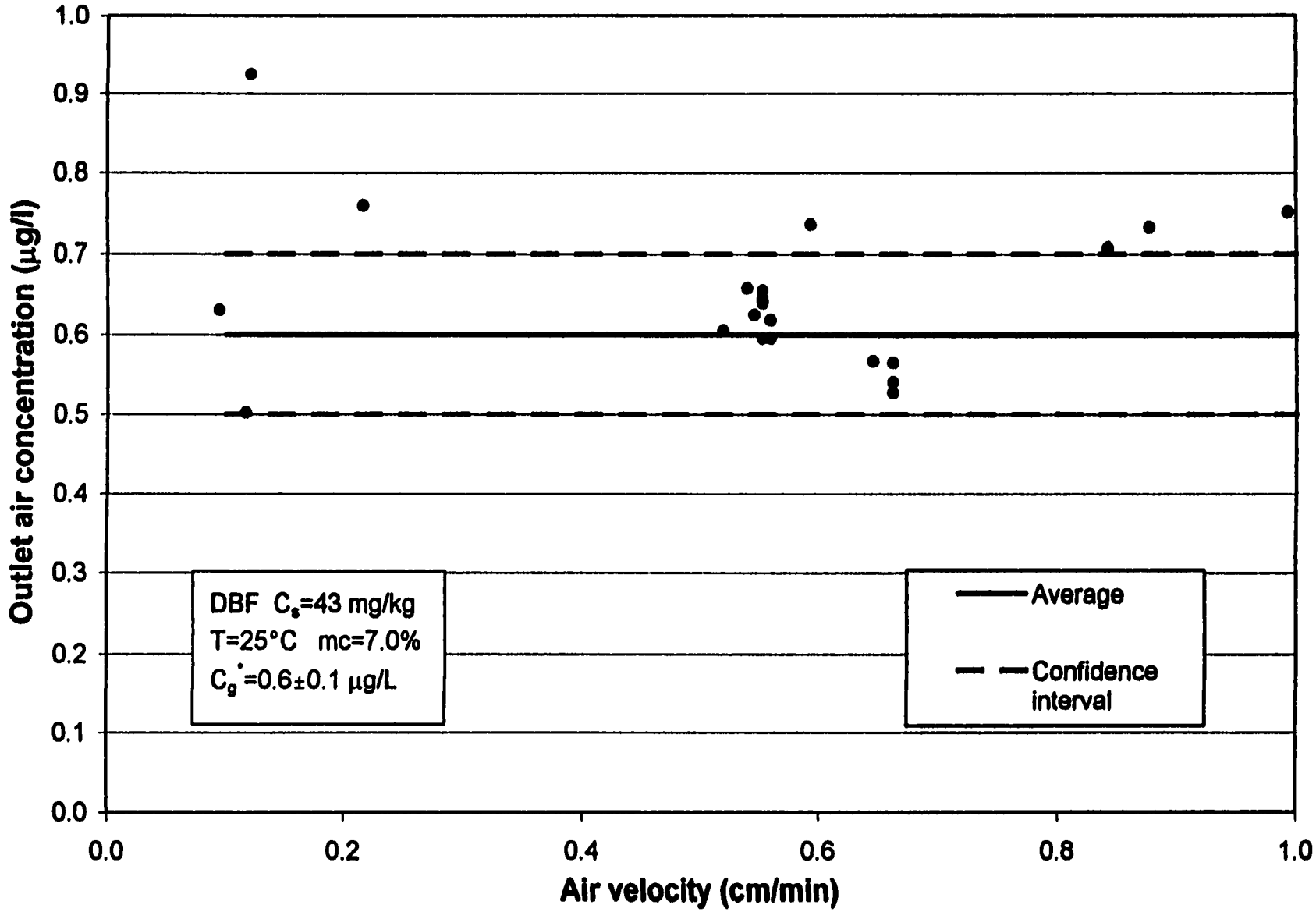

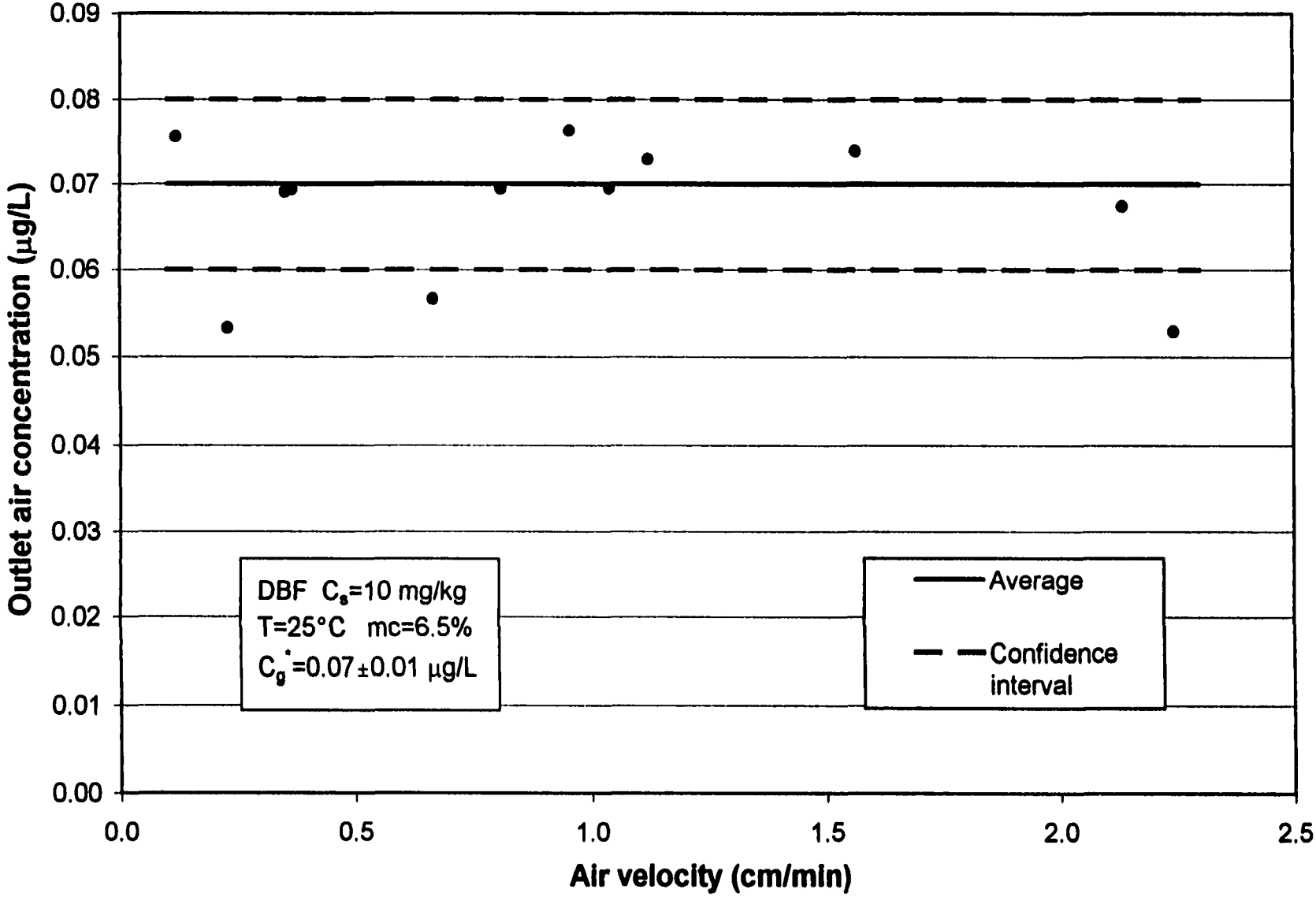

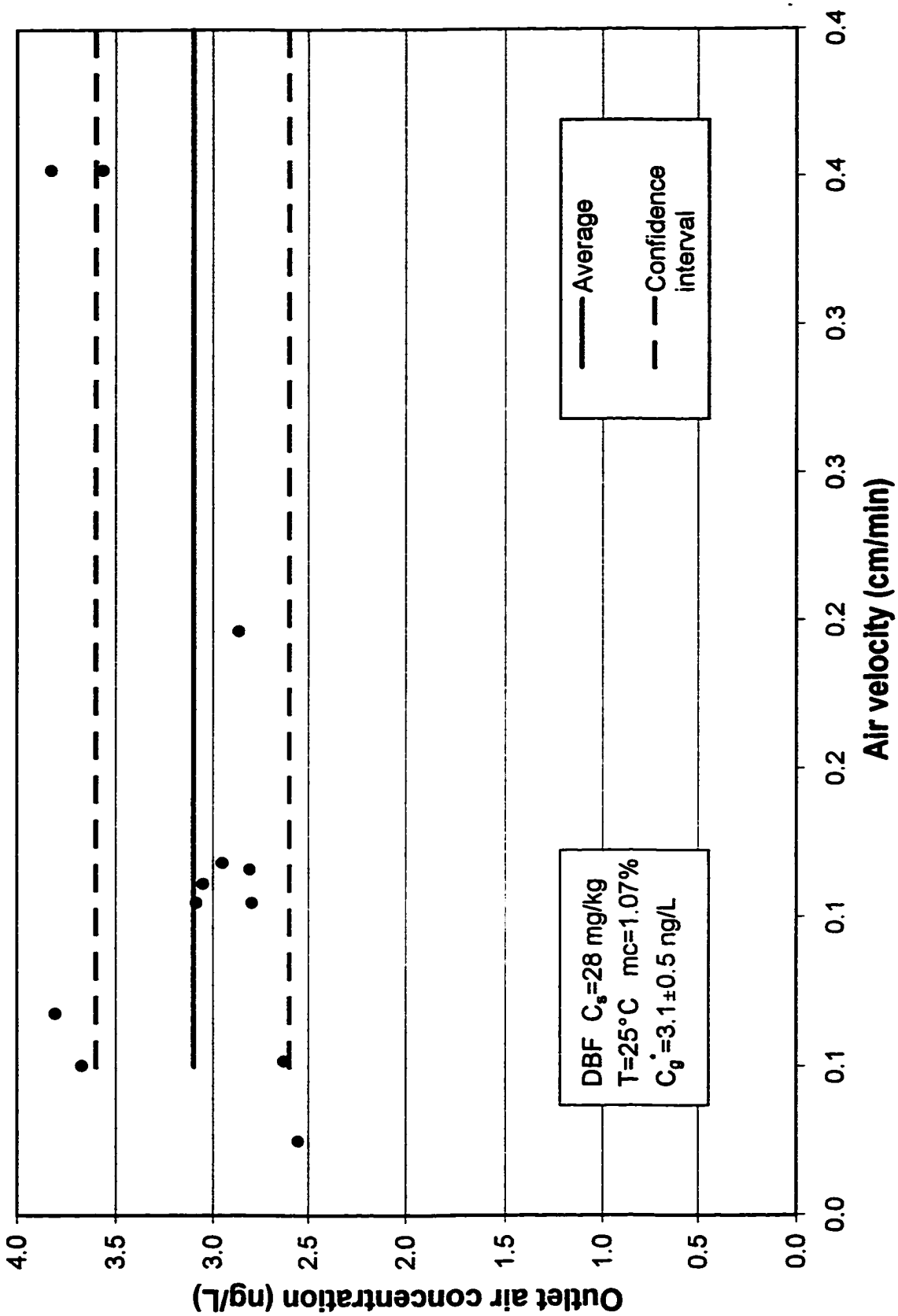

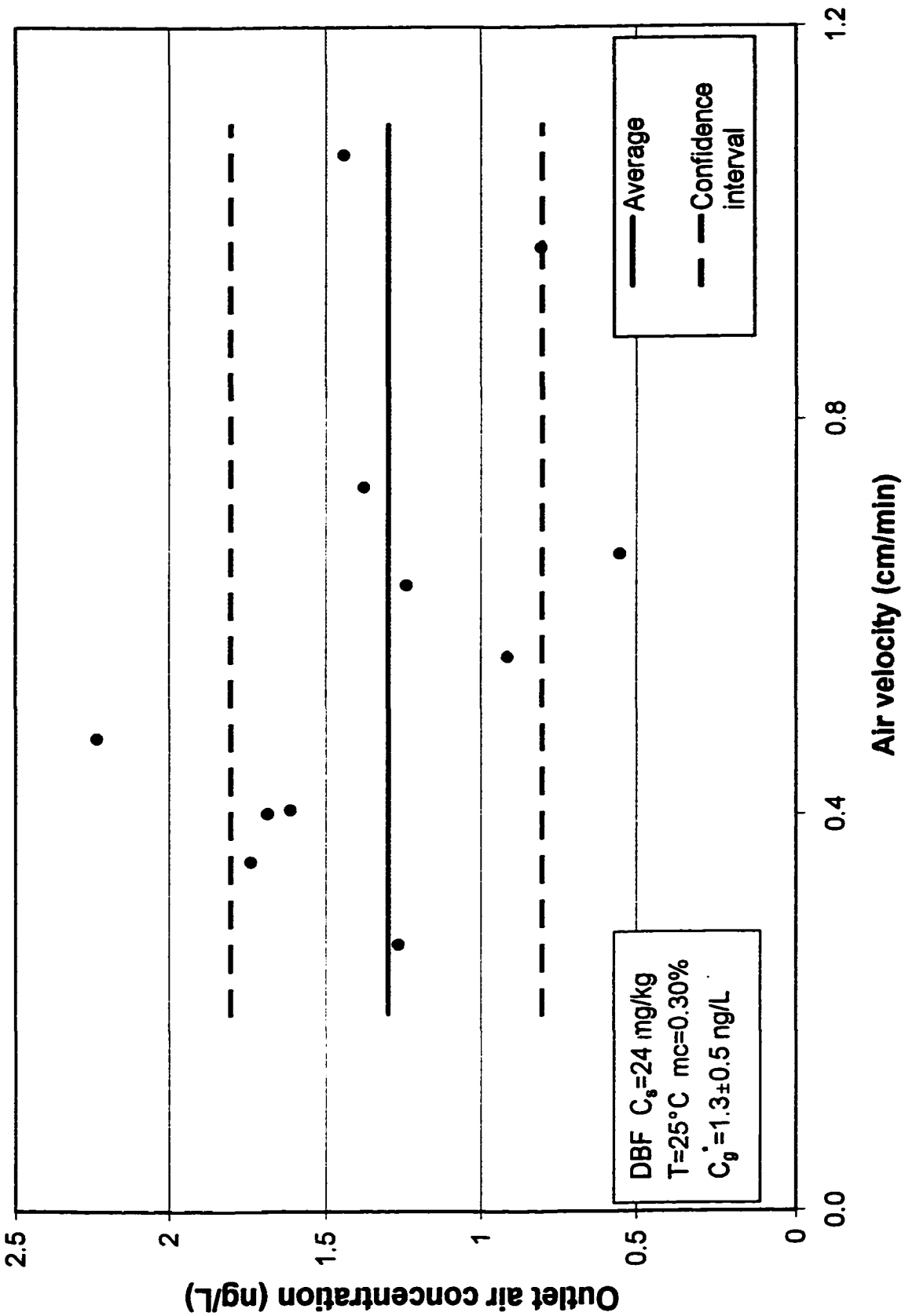

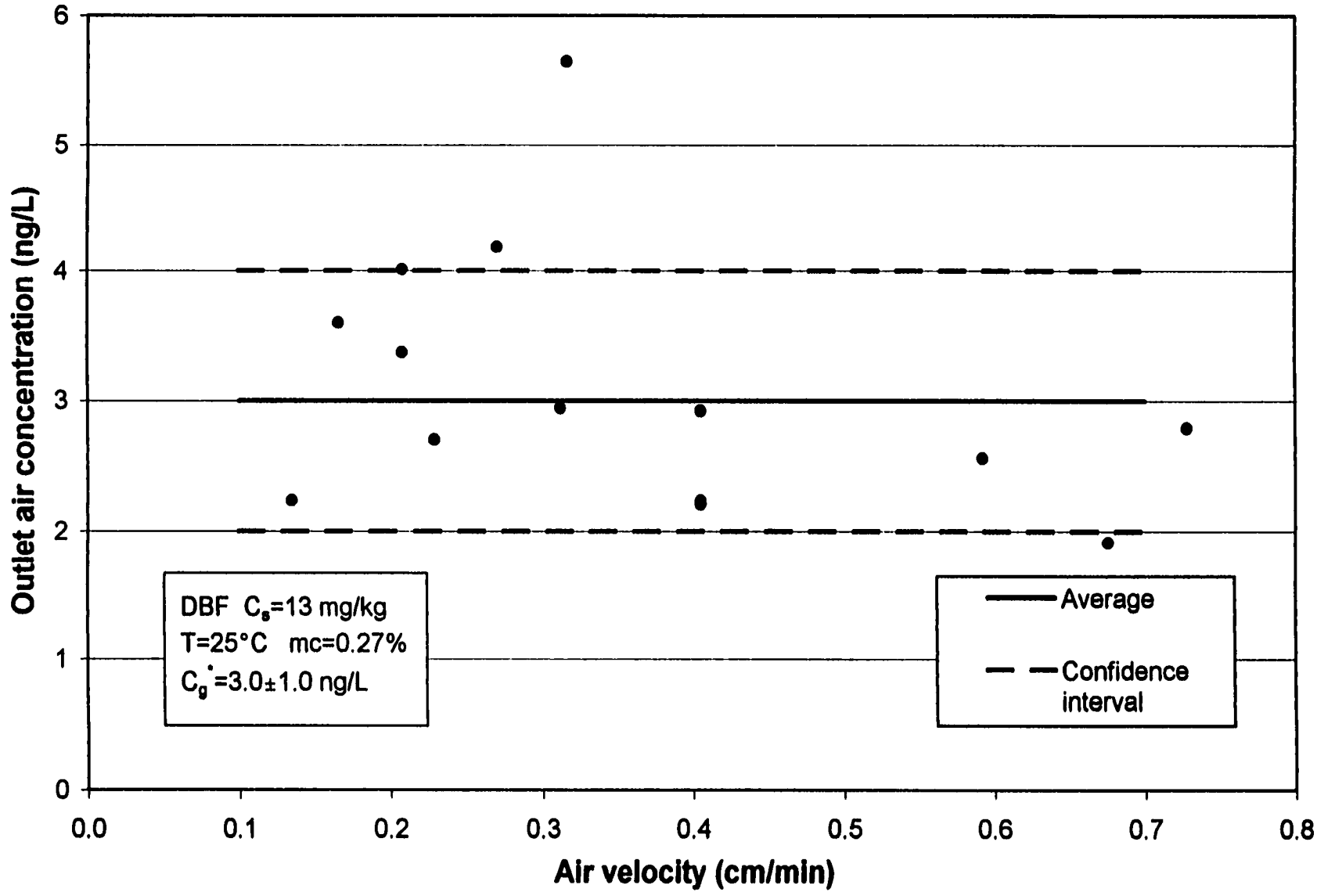

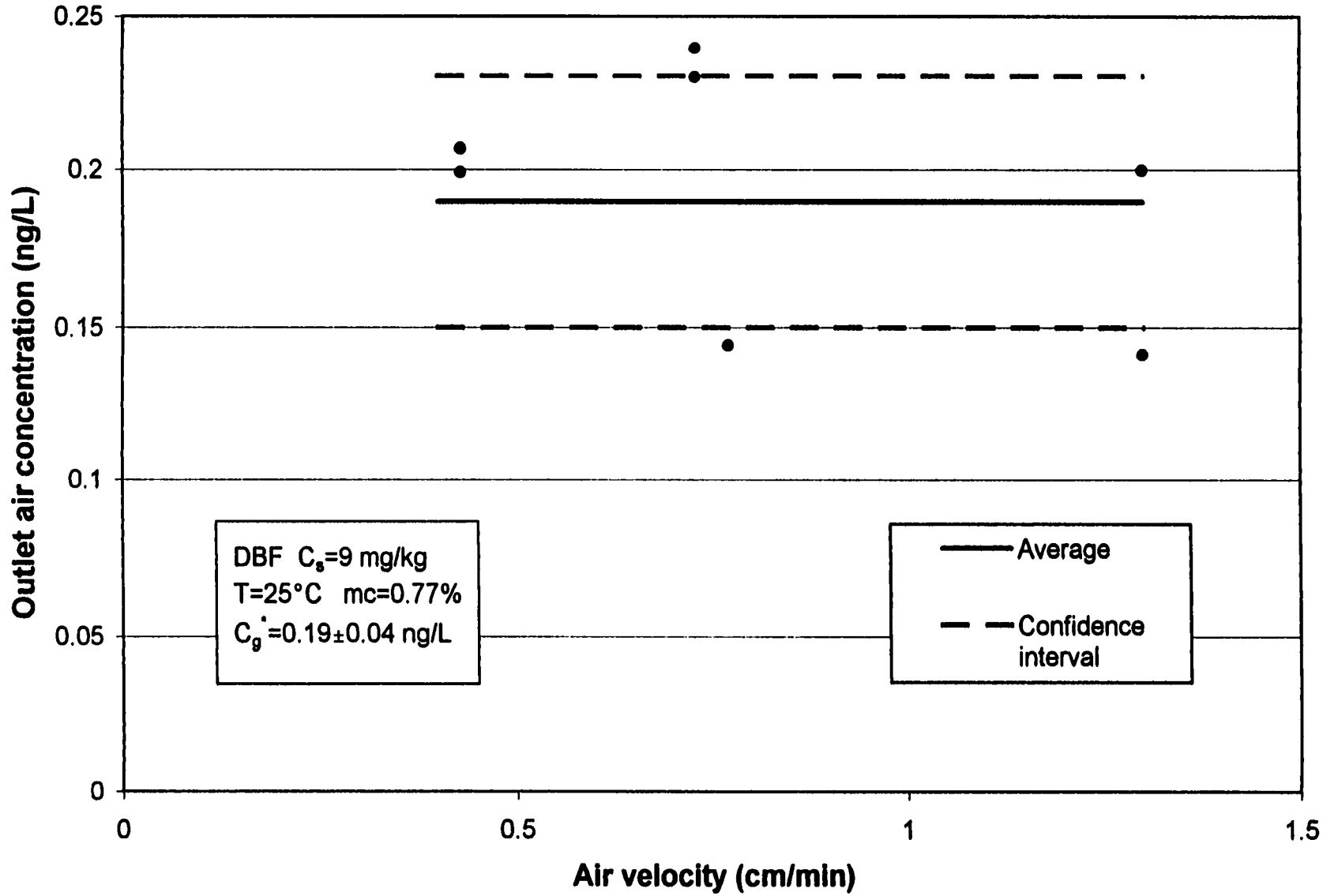

Appendix H
Effects of Aging on the Sorption of PAHs in Sediments

H.1 Observations and model of irreversible sorption

Numerous field (Socha and Carpenter, 1987; McGroddy and Farrington, 1995) and laboratory (Kan et al., 1994; Fu et al., 1994; Hunter et al., 1996) studies have shown that the PAH concentration in the pore water of aged sediments is much lower than the value predicted by the conventional linear isotherm ($C_w=C_s/f_{oc}K_{oc}$). In other words, a fraction of the contaminant becomes unavailable for desorption over time. Nonetheless, this fraction is still present in the sediment since it can be extracted by strong solvents (methylene chloride). Several theories have been proposed to explain the observed resistant desorption. For instance:

- Heterogeneous adsorption onto different types of sites (Socha and Carpenter, 1987; Weber and Huang, 1996)
- Slow diffusion rates (Cornelissen et al., 1997)
- Age of the organic carbon in the soil (Ball and Roberts, 1991)
- Conformational rearrangement of soil organic carbon (Kan et al., 1997)

However, Kan et al., 1997 showed that these two mechanisms alone cannot account for the whole fraction resistant to desorption. Based on their observations of the behavior of naphtalene and a tetrachlorinated biphenyl, they proposed a conceptual model of the phenomenon:

The contaminant in the organic matter of the sediment resides in two separate compartments. The first compartment contains the contaminant that is reversibly sorbed. The partitioning of this reversible fraction, q^{rev} is described by the conventional linear

isotherm of slope $f_{oc}K_{oc}$. The second compartment contains the remaining fraction of contaminant that is irreversibly bound to the sediment, q^{irr}. The concentration of the contaminant in the water in equilibrium with the irreversible compartment is very low. Furthermore, the capacity of this compartment is finite and the maximum capacity, q^{irr}_{max} is proportional to the soil organic content.

H.2 Hypothesis

H.2.1 Chemical reaction

The conceptual model proposed by Kan et al., 1998 is compatible with the hypothesis that the irreversible fraction of the PAH becomes bound to the soil organic matter, SOM by a reversible chemical reaction of equilibrium constant K:

PAH + SOM = PAH-SOM (K)

- The equilibrium constant depends on the nature of the solvent. Water does not stabilize the hydrophobic PAH, thus the equilibrium is displaced to the right in soils and sediments. However, in a non-polar solvent, the chemical potential of the PAH is lowered and the equilibrium is displaced to the left. The irreversible fraction is thus extractable in strong solvents.
- The reaction is limited by the amount of organic matter. Thus q^{irr}_{max} is proportional to the sediment organic content fraction (q^{irr}_{max}= [PAH-SOM]=K[PAH][SOM]).
- The kinetics of the reaction and thus the time to reach equilibrium are sensitive to temperature. In fact, Cornelissen et al., 1997 observed that the rate of desorption of the slow-desorbing fraction of PAH and PCB could be increased at elevated temperature.

Further experimental observations suggest a hypothesis on the nature of the reaction.

H.2.2 Electrophilic Aromatic Substitution

The mechanism of electrophilic aromatic substitution (EAS) is shown in Figure H.1. The substitution of an hydrogen atom occurs in two stages:

- The electrophilic reagent E^+ adds to one carbon atom of the aromatic ring, giving a carbocation in which the positive charge is delocalized over several carbons
- a proton is subsequently eliminated.

Several conditions for an EAS to occur between the soil organic matter and PAH are fulfilled.

H.2.2.1 Electrophilic reagent

Soil organic matter exhibits a variety of functional groups such as alcohols, esters, ethers, aldehydes and ketones (Stevenson, 1994) that are suitable electropilic reagents (E^+) (Norman and Coxon, 1993). An EAS between any of these functional groups and an aromatic molecule is a Friedel-Crafts alkylation. This is a reversible reaction. However, the reversibility usually requires more than a favorable solvent.

H.2.2.2 Catalyst

Alkylations involving alcohol, ester or ether functional groups are catalyzed by Lewis acids. The soil clay fraction is a potential Lewis acid catalyst:

- Clay minerals have been widely used as Lewis acid catalysts for EAS. Balogh and Laszlo, 1993 report the alkylation of phenanthrene by various alcohol catalyzed by 10% of active clay at 230°C. Yields of 19 to 46% were obtained in 1.5 hours.

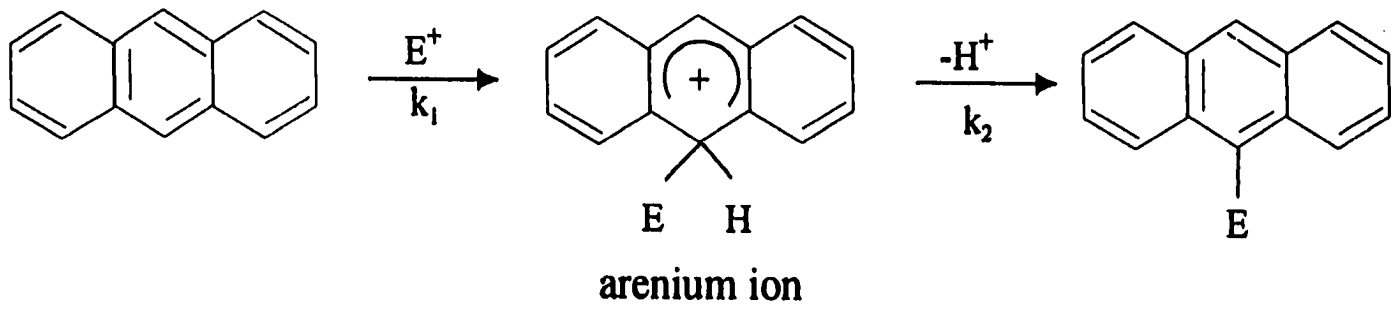

Figure H.1 The SE2 mechanism for electrophilic substitution of polynuclear aromatic hydrocarbons.

- The soil clay fraction is known to catalyze organic reactions. Wang et al., 1978 report the oxidative polymerization of phenolic compounds catalyzed by various natural clay. Karimi-Lotfabad et al., 1996 observed the polymerization of anthracene on a soil with a high clay content dried at 140°C. Liu and Thomas, 1991 and Liu et al., 1992 reported the formation of a pyrene cation on the surface of a synthetic clay (laponite). The phenomenon was dramatically increased by UV light and the activation of the clay. However, about 15% of the electron accepting sites, which ionize the pyrene molecules, were still active at 8.8% moisture content.

H.2.2.3 Heat of reaction

The standard Gibbs free energy of an EAS is expected to be low since the bonds created are similar to the ones dissociated. Kan et al., 1997 calculated the change in Gibbs free energy associated to the transition of naphthalene and 2,2',5,5'-tetrachlorobiphenyl from the reversible to the irreversible compartment. The respective values were –18 kJ/mol and –6 kJ/mol. Cornelissen et al., 1997 calculated from kinetics data the enthalpy change associated with contaminants going from the rapid to the slow desorbing fraction of a sediment. For 4 PAHs, the values were between –10 and –15 kJ/mol and for 4 chlorinated aromatic compounds the values were between –6 and –7 kJ/mol (the value for PCB-118 was +3kJ/mol). Values from the two studies are in very good agreement and compatible with the hypothesis of an equilibrated chemical reaction.

H.2.2.4 Selectivity of EAS

The delocalization of the positive charge in the transition state of an EAS is increased by the fusion of two or more benzene rings. All PAHs are therefore more reactive than benzene. In fact, compared to benzene, the partial rate factor in nitration at

the most reactive position is 500 for phenanthrene, 17000 for pyrene and 100000 for 3:4-benzopyrene (Norman and Coxon, 1995). On the other hand, substitution on benzene of one hydrogen by a Cl group, slightly destabilizes the reaction intermediate because of the electron-attracting inductive effect of the halogen atom. The intermediates formed in the reaction of polychlorinated benzenes and biphenyls are even more destabilized. For instance, the reactivity in sulfonation of p-dichlorobenzene relative to benzene is 0.063 (compared to 9 for naphtalene). This is compatible with the repeated observation that PCBs show little or no aging effect, even in conditions where PAHs are strongly affected by the phenomenon (McGroddy and Farrington, 1995; Cornelissen et al., 1997, Kan et al., 1997; Cousins et al., 1998).

Appendix I
Fraction of Surface Area Available to Adsorption

The parameter F is introduced in equation (2.5). F is simply defined as the fraction of surface area available to contaminant adsorption. Thus, different factors are susceptible to affect F. Some of them are reviewed hereafter.

I.1 Adsorption configuration

It is important to note that F has a value close to 1 only in the ideal case of spherical molecules adsorbing non-specifically (thus uniformly) on a totally accessible surface. In the case of specific adsorption, molecules bind to a finite number of surface groups. Thus, portions of the surface that are free of binding sites are inaccessible to the molecules and the calculated projection of the molecular surface area may be different from the actual surface area necessary to accommodate one molecule. F is thus expected to be less than 1. Bauer at al., 1982 measured from the adsorption isotherm that a full monolayer of pyrene adsorbed on a silica gel surface occupies only 76% of the total surface area (determined by nitrogen adsorption). The ratio even drops to 65% on alumina. Those two values should be taken with caution since they depend on the value attributed to pyrene molecular surface area. Nonetheless, it is of interest to notice that two surfaces of different nature give rise to different values of F. This is caused by different density of adsorption sites.

I.2 Natural surfaces

To gain insight on the parameter F associated to natural surfaces, results from experimental studies were reanalyzed.

I.2.1 Influence of the adsorbate nature on F

Ruiz et al., 1998 determined adsorption isotherms on dry mineral surfaces for a variety of non-polar VOCs. Data obtained for clay and sand are of special interest to this study. From the surface monolayer capacity, the occupied surface area can be calculated for each compound. The ratio F_N is then obtained by dividing this surface area by the one determined by nitrogen adsorption. Because of detection problems, only partial isotherms are presented for hexane. This compound is thus excluded from the present analysis. The calculated values of F_N for non-polar compounds are presented in Table I.1. One notices that, on each surface, the value of F_N is fairly constant among the set of non-polar VOCs.

Thibaud-Erkey et al., 1996 studied the adsorption of two non-polar VOCs on an oven-dried soil of low organic content (f_{oc}=0.8%). The values of F_N for n-hexane and toluene calculated from their results are respectively 0.8 and 1.1. This is in fair agreement with the study by Ruiz et al., 1998.

Poe et al., 1988 compared the apparent surface areas of four different soils calculated from the monolayer adsorption of five VOCs. Their results were analyzed in the same way as those from Ruiz et al., 1998. However, the soil surface areas were not measured by any conventional method in their study. Thus, instead of the soil available fraction, a factor F_C was calculated. F_C is the ratio of the determined available surface area (m^2/g_{soil}) over the soil clay content (g_{clay}/g_{soil}). Assuming that the clay fraction accounts for most of the surface area exhibited by the soils, F_C is the specific surface area available in the clay fraction of the soil. Results of the calculations are reported in Table I.2. Again, for non-polar compounds, F_C is constant for a given soil. However, values of

Table I.1 Fraction of surface area available to adsorption on sand and clay (from data by Ruiz et al, 1998).

		Sand (A^a=0.72m^2/g)			Clay (A=10.91m^2/g)		
Compound	s^b	W_m(mg/g)	S^c	$F_N{}^d$(%)	W_m(mg/g)	S	F_N(%)
n-heptane	63.1	1.46	0.55	76	2.25	8.53	78
n-octane	64.6	2.00	0.68	94	2.44	8.31	76
toluene	55.2	2.01	0.73	101	1.84	6.64	61
xylene	51.0	1.37	0.39	54	1.00	2.87	26
ethylbenzene	51.0	2.52	0.72	100	2.28	6.55	60
Average			0.7±0.1	90±20		7.5±1.1	60±20

a Surface area determined by nitrogen adsorption.
b Molecular surface area ($10^{-20}m^2$) (McClellan and Harnsberger, 1967)
c Available surface area (m^2/g)
d Fraction of available surface area (compared to nitrogen adsorption surface area)

Table I.2 Ratio of the surface available to adsorption over the soil clay content (F_C) for different soils (from data by Poe et al. 1988).

	Soil							
	Bernow		Parsons		Summit		Weller	
Compound	S†	F_C*	S	F_C	S	F_C	S	F_C
Ether	4	29	13	8	13	5	24	9
MCH[a]	5	36	13	8	10	4	22	8
Benzene	n/a	n/a	15	9	n/a	n/a	26	9
DCP[b]	2	14	15	9	13	5	19	7
Average		26±11		8±1		4±1		8±1
Methanol	n/a	n/a	38	0.23	42	0.16	62	0.22
Clay (%)	1.7		20.1		30.9		34.0	
Organic Content (%)	0.13		0.98		2.82		0.97	

a Methylcyclohexane
b 1,2-dichloropropane
† Available surface area (m^2/g)
* Available surface area normalized for the clay content (m^2/g),)

F_C calculated from methanol adsorption are significantly higher than for non-polar compounds. This point is discussed in the next section.

I.2.2 Effect of the soil organic content on F

I.2.2.1 Observations

Sokolowska et al., 1993 studied the influence of organic matter on the adsorption of water on soils. They determined the monolayer capacity for various soils before and after organic matter removal. In 4 of the 5 soils investigated, the surface area available to water adsorption was larger after organic matter removal. However, the gain of surface area was not correlated to the organic matter content.

More insight on the influence of soil organic matter on the surface area available for adsorption can be gained from the data by Poe at al., 1988. Figure I.1 shows the logarithm of the surface area of the clay fraction, F_C versus the logarithm of the soil organic carbon fraction, f_{oc}, for each soil they studied. Two sets of data are shown corresponding to (i) the average values of F_C for the four non-polar VOCs and (ii) the values of F_C calculated for methanol. A good correlation is observed in each case: r^2=0.999 for the non-polar VOCs and r^2=0.988 for methanol. Thus, in dry sediment, the organic matter decreases the surface available for adsorption of any contaminant, regardless of its polarity. Moreover, for both kinds of compounds F_C follows a similar decrease law: $F_C = b/f_{oc}^n$ with $n<1$. The exponent smaller than one indicates that the action of the organic matter is auto-inhibited. These observations suggest a qualitative model.

I.2.2.2 Model

Natural organic polymers cover adsorption sites, thus preventing contaminant adsorption. When the concentration of natural polymer at the soil surface is low, polymer

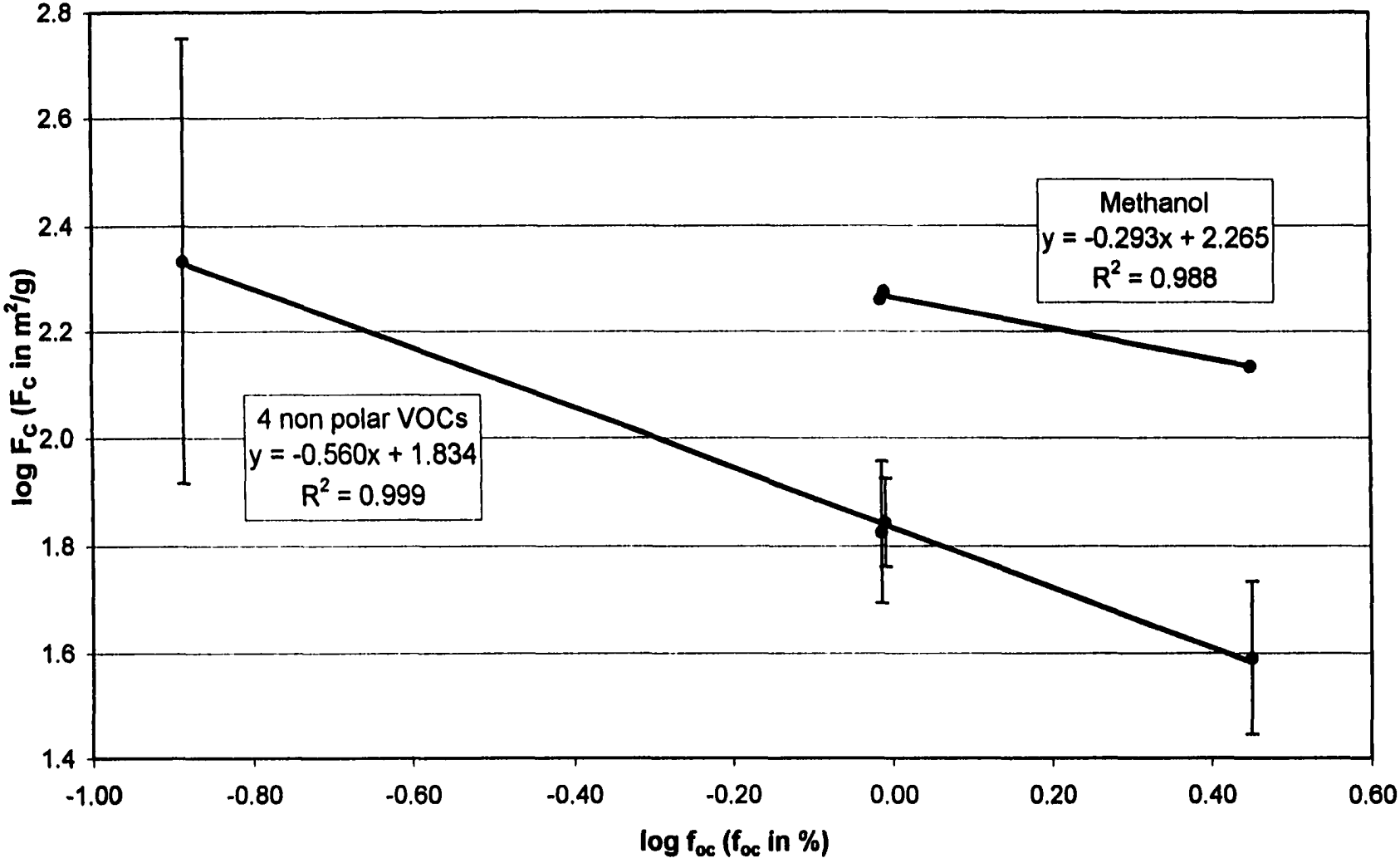

Figure I.1 Correlation between soil organic content and the fraction of surface area available for adsorption in various soils (calculated from Poe et al., 1988).

molecules can spread out and cover a relatively large surface area. At higher soil organic matter content, polymer molecules compete among themselves for adsorption sites. This supports the observed auto-inhibition of the organic matter effect on F_C. Molecules have less surface area available and adopt more compact configurations. For instance, a molecule may form an individual coil or tangle up with others. The behavior of natural polymer on soils surface is also enlightened by methanol adsorption characteristics. In any soil, the surface area available for adsorption is larger for methanol than for non-polar compounds. This may be explained by (i) the capacity that a small polar molecule like methanol has to penetrate in-between the silica layers of clay particles or (ii) the capacity to compete successively with natural organic polymers for adsorption sites. It is not possible to evaluate the relative importance of each mechanism. However, insight can be gained by comparing the slopes of the regression lines plotted in Figure I.1. The slope of methanol line is smaller than the non-polar VOCs one. This indicates that methanol is able to adsorb on the soil surface in the presence of organic matter more successfully than non-polar VOCs. This suggests that polar adsorption sites are involved in the binding of organic matter on soils surface.

I.2.3 Attempt to predict F

The correlation developed from the data obtained by of Poe et al., 1988 was tested against other studies. The ratio F_C was calculated for three non-polar VOCs from the data reported by Chiou and Shoup, 1985 and Thibaud-Erkey et al., 1996. Results of the calculations are presented in Table I.3.

The agreement between the experimental and the predicted values of $\log F_C$ is not very good. The experimental surface areas differ from the predictions by a factor of 0.4 to

2.6. However, this is not surprising considering that different experimental methods were used to determine the adsorption isotherms in the respective studies. The methods used to determine the organic matter content are not stated and may also have been different.

Table I.3 Comparison of the values of $\log F_C$ calculated from experimental studies to the ones predicted by the correlation developed from the data by Poe et al., 1988.

Author	Compound	$\log f_{oc}$	log F_C (measured)	$\log F_C$ (predicted)
Chiou and Shoup, 1985	Benzene	0.28	1.82	1.68
Thibaud-Erkey et al., 1996	Toluene	-0.10	1.48	1.89
	n-hexane	-0.10	1.63	1.89

The same correlation predicts that for Campus Lake sediment, the surface available to the adsorption of non-polar VOCs is 6.6m^2/g. This gives a value of F_N of 0.8 (on the basis of the surface area determined by nitrogen adsorption: 7.9 m^2/g).

I.2.4 Conclusion

For a given soil, the fraction of surface area available to adsorption, F is fairly constant among different non-polar VOCs. The results presented by Ruiz et al., 1998 and Thibaud-Erkey et al., 1996 indicate that, when the soil organic content is low, the surface area available to adsorb non-polar VOCs is at least half the one determined by BET nitrogen adsorption. However, the organic matter of a soil decreases F.

Vita

Guilhem de Seze was born in Paris, France, January 25, 1971. In the fall of 1991, he entered the Ecole Nationale Supérieure des Industries Chimiques, in Nancy, France, where he studied chemistry and chemical engineering for the next two years. In 1993/1994, he was an exchange student at Imperial College, London, U.K., in the master program of the Chemical Engineering department.

In October 1994, he was appointed by the Elf Aquitaine Company and came to Louisiana State University as a visiting Research Associate in the department of Chemistry. During a year and a half, he developed a treatment process for industrial hazardous waste. In the summer 1996, he enrolled in the graduate program of the Chemical Engineering department of Louisiana State University. His degree of Doctor of Philosophy will be awarded in May of 1999.

In January 1999, he will move to Brussels, Belgium, to start working as a Research Scientist for the Proctor and Gamble Company.

DOCTORAL EXAMINATION AND DISSERTATION REPORT

Candidate: Guilhem de Seze

Major Field: Chemical Engineering

Title of Dissertation: Sediment-Air Partitioning of Hydrophobic Organic Chemicals

Approved:

Major Professor and Chairman

Dean of the Graduate School

EXAMINING COMMITTEE:

Date of Examination:

December 17, 1998

IMAGE EVALUATION TEST TARGET (QA-3)

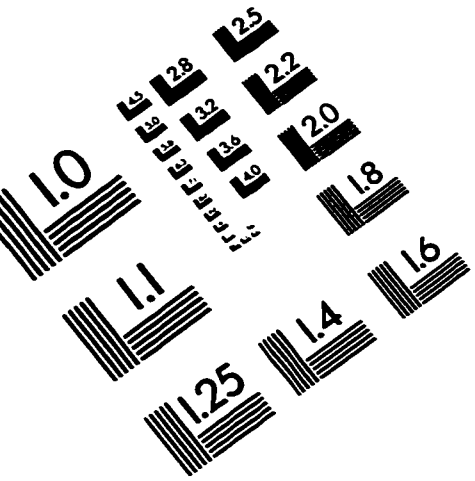

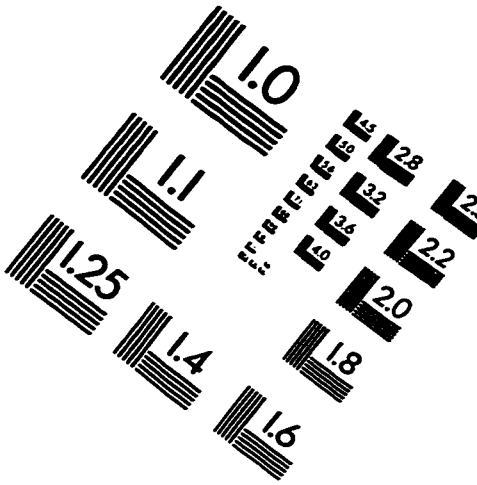

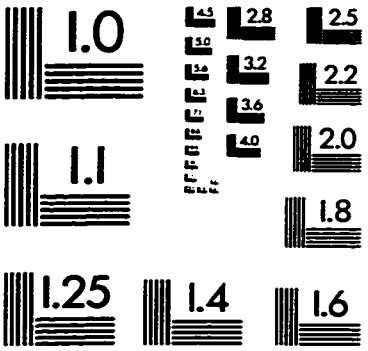

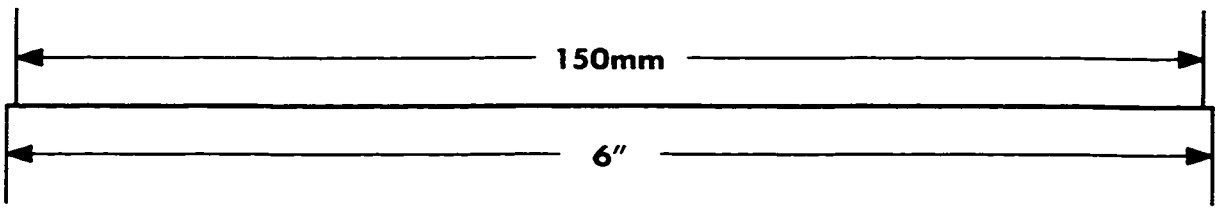

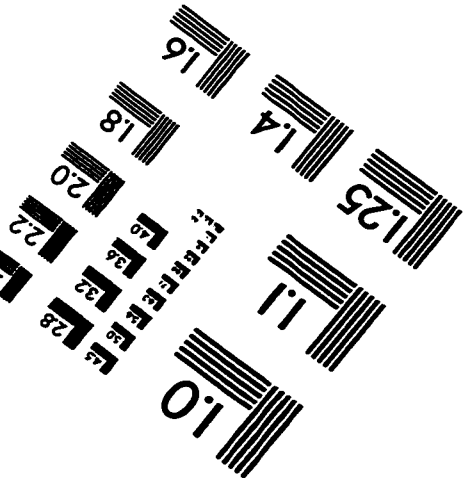

APPLIED IMAGE, Inc
1653 East Main Street
Rochester, NY 14609 USA
Phone: 716/482-0300
Fax: 716/288-5989